Three-Dimensional Monotonic and Cyclic Behaviour of Sand-Steel Interfaces: Testing and Modelling

Kazem Fakharian, B.Sc. Eng., M.Sc.

A Thesis
Submitted to the School of Graduate Studies and Research
Under the Supervision of

Dr. Erman Evgin

in partial fulfilment of the requirements for the degree of
Doctor of Philosophy in Civil Engineering

Department of Civil Engineering
University of Ottawa
Ottawa, Ontario
Canada K1N 6N5

May 1996

The Doctor of Philosophy in Civil Engineering is a joint program between Carleton University and the University of Ottawa, which is administered by the Ottawa-Carleton Institute for Civil Engineering

ISBN 0-612-15716-4

UNIVERSITÉ D'OTTAWA
UNIVERSITY OF OTTAWA

ACKNOWLEDGEMENTS

The author wishes to express his sincere thanks to his research supervisor, Dr. Erman Evgin, for his generous advice and continuous support during this research. He is particularly thanked for his efforts in providing the opportunity for the author to develop the new interface apparatus. The author also wishes to thank Dr. V. K. Garga and Dr. K. T. Law for their contributions as the member of various committees during this Ph.D. program.

The scholarship provided by the Ministry of Culture and Higher Education in Iran as well as the financial supports received from the University of Ottawa, the Natural Sciences and Engineering Research Council of Canada (NSERC), and the National Energy Board of Canada are gratefully acknowledged.

The technical assistance provided by the support staff, especially R. J. Moore, is gratefully acknowledged. Particular thanks are due to the workshop staff of the Department of Civil Engineering at the University of Ottawa, especially skill and dedication of C. Lavinge and B. Cotter, who were responsible for machining the components of the C3DSSI apparatus.

The author would like to thank his parents, parents-in-law, brother and sister, and brothers-in-law for their continuous encouragement and moral support in many ways. This work would not have been possible without the encouragement, patience, and overwhelming support of the author's wife, Giti. Finally, the patience of author's son, Amir, and author's daughter, Sarvenaz, during the lengthy period of this research are especially acknowledged.

ABSTRACT

The main objective of this thesis is to investigate the effects of various stress and displacement paths on the behaviour of sand-steel interface. The study includes three parts: (i) the development of a new automated interface testing apparatus, (ii) a comprehensive experimental program, and (iii) elasto-plastic modelling of the sand-steel interface behaviour.

The interface testing apparatus is capable of applying monotonic and cyclic forces in three perpendicular directions, simultaneously. Tests can be displacement or load controlled. Two computer-controlled stepper motors generate the desired tangential load or displacement paths on the interface plane, including rotational stress or displacement paths (circular or elliptical). Either a direct shear box or a simple shear box can be used as the soil container. In the direction normal to the interface plane, three boundary conditions, i.e. constant normal stress, constant normal stiffness, and constant volume can be imposed by using a pneumatic actuator which is operated by a computer-controlled system.

The results of more than 180 tests are reported for an interface between a Silica sand and a steel plate. Experiments include two-dimensional (2-D) monotonic and cyclic tests under constant normal stress conditions, to verify the performance of the new apparatus. A series of three-dimensional (3-D) monotonic and cyclic experiments are presented to show the coupling effects between two perpendicular shear stresses on the interface plane. A series of 2-D monotonic and cyclic experiments under constant normal stiffness condition are performed to study the variations in shear stress, normal stress, and volume change response under boundary conditions rather than the conventional constant normal stress.

The effects of various parameters such as surface roughness of steel, initial relative density of sand, magnitude of initial normal stress, rate of shearing, and type of sand are investigated. The 3-D circular and elliptical paths show that rotational paths affect the variations of the shear stress and normal displacement as well as peak and residual strengths of the interface. It is demonstrated that the shear stress, normal stress, and normal displacement variations of the interface are affected significantly if a constant normal stiffness is specified as the boundary condition. The phenomenon of the degradation of the shear stress in two-way displacement controlled cyclic tests under the

constant normal stiffness condition and its relation to degradation of shaft resistance of axially loaded piles are investigated.

An existing elasto-plastic constitutive model is used to make predictions for the interface behaviour. Comparisons show that the predictions for the monotonic 2-D and 3-D tests under constant normal stress and constant normal stiffness conditions agree well with their corresponding experimental results.

The results of this study may be used in the analyses of stability and load-deformation response of soil-structure systems such as piles, sheet piles, lined tunnels, offshore gravity structures, and retaining walls.

TABLE OF CONTENTS

LIST OF TABLES

LIST OF FIGURES

CHAPTER 1

INTRODUCTION

1.1 Statement of Problem

Behaviour of contact surfaces between two similar or dissimilar materials is an important topic in engineering mechanics. In geotechnical engineering, soil-structure interaction problems and the problems related to the mechanics of jointed rock involve contact surface behaviour. The contact zone between two bodies is normally referred to as *interface*. Interface is a thin layer thorough which stress is transferred from one medium to the other, therefore, exhibits localized and concentrated stress and strain. The response of soil-structure systems, such as shallow and deep foundations, lined tunnels, retaining walls, and reinforced earth, to monotonic and cyclic loads, is influenced by the existence of interfaces as well as dissimilarity of the mechanical properties of each continuum. Thus the strength parameters and load-displacement relations of interfaces significantly influence the load-deformation behaviour of such systems.

A number of devices have been employed in the past to study experimentally the behaviour of rock joints and interfaces between two different materials such as soil-steel, soil-concrete, and soil-geosynthetics. The most commonly used device is the direct shear type device (e.g., Potyondy 1961; Desai *et al.* 1985; Boulon and Plytas 1986). A ring torsion type device was used by Yoshimi and Kishida (1981) to overcome some of the disadvantages of the direct shear type apparatus such as non-uniformities of stresses and strains within the specimen. A simple shear type device was used for monotonic loading (Uesugi and Kishida 1986) and cyclic loading (Uesugi *et al.* 1989) of interfaces. The simple shear type device allows the measurement of sliding displacement between a structural material and soil as well as shear deformation of the soil mass. These studies have provided information on the influence of various parameters such as surface roughness of the structural material, composition and moisture content of soil, relative density, magnitude of normal stress, and boundary conditions in the direction normal to the interface plane, on shear strength parameters and stress-displacement characteristics of interfaces. The parameters affecting the cyclic behavior such as amplitude of shear displacement, frequency, and number of cycles have also been evaluated to some extent (e.g. Desai *et al.* 1985; Uesugi *et al.* 1989).

The interface in all aforementioned devices is subjected only to two-dimensional (2-D) loading. This kind of testing is appropriate for interfaces in 2-D soil-structure systems such as axially loaded piles. Many other practical systems, however, are subjected to three-dimensional (3-D) loading. For example, the wind, waves, ice, and ocean currents result in combined repeated uplift/compression and lateral loads on offshore gravity structures; power transmission lines are subjected to loads caused by wind and earthquake, resulting in repeated loads on their foundations; and highway bridges are subjected to a combination of a large dead load, repeated axial and lateral loads from traffic, and repeated lateral loads from wind (Turner and Kulhawy 1989). The solution of these problems require that the interface testing be in 3-D mode.

The load transfer from an axially-laterally loaded pile to soil is described here to show how the 3-D stress conditions are generated at the interface. Smith and Ray (1986) pointed out that a laterally loaded pile derives most of its resistance from frontal resistance, P_f, and from frictional resistance, P_s, as illustrated in Fig. 1.1*a*. At working loads, the frictional resistance provides the majority of the resistance. Briaud *et al.* (1982) reported that for a rigid concrete shaft at one half of the ultimate lateral load, frictional resistance contributed 43% to equilibrium. Based on the experimental data from an instrumented concrete pile, which was embedded in stiff clay and subjected to horizontal static loading, Smith and Ray (1986) calculated that at 1/8 of the ultimate lateral load, frictional resistance, P_s, contributed 84% to the soil reaction against the lateral loading. At a factor of safety of 1.2, close to the ultimate failure, the contribution from the frictional resistance dropped to 55%. Shear stress was mobilized very quickly and reached a peak at working load.

A typical infinitesimal interface element, e, on a pile shaft (Fig. 1.1*b*) is subjected to a normal stress, σ_n, resulting from the lateral pressure of the surrounding soil, a shear stress parallel to the axis of the pile, τ_{axi}, resulting from the axial load, and a second shear stress in the horizontal direction, τ_{lat}, induced by the external lateral load. The component of τ_{lat}, in the direction of the external lateral load, is the frictional resistance P_s illustrated in Fig. 1.1*a*. The interface zone in this problem is a very thin cylindrical shell and it can be idealized as a plane surface in the Cartesian coordinate system. Therefore, τ_{lat} and τ_{axi} are related to τ_x and τ_y, respectively, which are the shear stress components on the interface plane with a local *x-y-z* coordinate system as illustrated in Fig. 1.2*a*. In the absence of τ_y, the interface would only be subjected to 2-D stress condition as illustrated in Fig. 1.2*b*.

As a second example, the soil-structure systems subjected to cyclic rotational loading paths are described. Some approaches for anti-seismic design allow the sliding of structures or the relative displacements between soil and structure during earthquakes (Fujii *et al.* 1986, Kurimoto and Matsuda 1986). They have concluded that the displacement of a sliding structure depends on the coefficient of friction at its base. Since the direction of cyclic loads resulted from earthquake usually change during the response of the soil-structure systems, the interfaces may be subjected to rotational loads or rotational displacement paths. Ocean waves affecting the soil mass beneath the offshore structures also result in widespread change of principal stress values and directions, as demonstrated by *in situ* records (Figueroa *et al.* 1985; Ishihara *et al.* 1981).

Ishihara and Yamazaki (1980) studied the liquefaction behaviour of Toyoura sand by using a multi-directional simple shear apparatus. They showed that under undrained cyclic rotational (circular and elliptical) shear loading, the number of cycles required to cause liquefaction of sand was up to 35% less than that under uni-directional loading conditions. Wang *et al.* (1990) developed a hypoplastic bounding surface constitutive model for modelling the behaviour of sand subjected to rotational stresses. The behaviour of interfaces, however, under similar rotational shearing has not yet been studied.

Another significant aspect, affecting the behaviour of interfaces, is the boundary condition in the direction normal to the interface plane. There are practical problems where the normal stress acting on the interface does not remain constant during shearing. For example, for a typical interface between a pile shaft and the surrounding soil, the dilation in the interface zone is constrained by the soil beyond this zone. As a result, the normal stress acting on the interface varies during shearing. For this class of problems, it would be more realistic to use parameters obtained from representative stress path tests rather than using parameters from the conventional constant normal stress tests.

Failure of piles arising from cyclic degradation of shaft resistance is recognized to be predominant under axial two-way cyclic loading conditions (Poulos 1989). Uesugi *et al.* (1989) and Uesugi and Kishida (1991) stated that the dominant factor in the degradation of the frictional resistance at pile-soil interface is the sliding displacement at the interface. Poulos (1989) attributed the degradation in shaft resistance to the compressibility of the soil, which resulted in a large reduction in soil volume near the pile shaft due to cyclic loading. This volume reduction led to a reduction in normal stress, and consequently to a reduction or "degradation" of the shaft resistance. Airey *et al.* (1992) confirmed experimentally the above idea, expressed by Poulos, by conducting sand-to-sand two-way cyclic displacement controlled tests under constant normal stiffness condition by using a direct shear device. These investigations, however, are mostly focused on the calcareous sands because of their greater compressibility. Interface tests under the condition of constant normal stiffness are the proper way of measuring the frictional resistance between a pile and soil in the laboratory to recognize the degradation phenomena.

Constant normal stiffness tests in the laboratory have been performed by a number of researchers. However, the majority of the available results are from the investigations of the mechanical properties of rock joints (e.g. Obert *et al.* 1976; Lam and Johnston 1982; Leichnitz 1985; Ooi and Carter 1987; Saeb and Amade 1992; Mouchaorab and Benmakrance 1994). Boulon and Plytas (1986) developed a direct shear type device to investigate the behaviour of interfaces, subjected to monotonic shearing, under constant volume and constant normal stiffness test conditions. The results were used for the numerical modelling of the behaviour of a tension pile in sand. However, no experimental results have been reported for cyclically sheared interfaces between soil and structural materials under constant normal stiffness condition.

Two categories related to the behaviour of interfaces between soils and structural materials were identified for which no experimental study has been performed in the past. The first one was the coupling effects between two perpendicular shear stresses, acting simultaneously on the interface plane, i.e. the 3-D testing of the interface. The second category was the influence of the constant normal stiffness condition, in the direction normal to the interface plane, on the behaviour of interfaces subjected to cyclic shearing. The main objective of this dissertation is to study the influence of such stress paths on the behaviour of the interfaces between soil and structural materials.

A new automated apparatus for monotonic and cyclic testing of interfaces between soil and structural materials under 3-D stress conditions was developed. Direct shear type or simple shear type soil containers can be used in the new apparatus. For the first type, the apparatus is referred to as C3DI, i.e. Cyclic 3-D testing of Interfaces. In the second type, the testing apparatus is called C3DSSI, i.e. Cyclic 3-D Simple Shear testing of Interfaces. Simple shear soil container distinguishes the sliding displacement from the shear deformation of the soil mass.

The other feature of the new interface apparatus is the possibility of imposing the condition of constant (or variable) normal stiffness in the direction normal to the interface plane. The control and data-acquisition including the simulation of constant normal stiffness are performed by a closed-loop computer controlled system.

In fact the new testing apparatus facilitates the study of the mechanical behaviour of interfaces under various stress paths. The effect of various stress paths, both monotonic and cyclic or a combination of both, on the shear strength as well as stress-displacement relations of interfaces, are examined in this dissertation.

Constitutive models for simulating the behaviour of interfaces are normally required for the load-deformation analysis of the soil-structure systems. An elasto-plasticity based constitutive model, previously developed by Navayogarajah *et al.* (1992) for simulating the stress-displacement relations of interfaces between sand and structural materials, is expanded to 3-D. It is also formulated to model the condition of constant normal stiffness. The model parameters are obtained from the experimental results. Subsequently the model is used for prediction of the behaviour of interface subjected to some more sophisticated stress paths. The predicted results are then compared with the corresponding experimental results.

The Outline of the conducted research program is presented in Table 1.1.

1.2 Objectives

The main objectives of the thesis are as follows:

1. To determine the shear strength parameters and the stress-displacement relations of the sand-steel interfaces under 3-D monotonic and cyclic loading conditions.

2. To study the behaviour of interfaces between sand and steel under various normal boundary conditions, i.e. constant normal stress, constant volume, and constant normal stiffness, subjected to monotonic and cyclic shearing.

3. To develop an elasto-plastic constitutive model to account for 3-D as well as constant normal stiffness behaviour of the sand-steel interface.

1.3 Scope of Research

In order to achieve the above objectives, the scope of this research may be stated as follows:

1. Development of a new 3-D apparatus capable of applying monotonic and cyclic shear stresses and tangential displacements, in two orthogonal directions on the interface plane, and imposing various boundary conditions in the direction normal to the interface plane.

2. Verification of the performance of the apparatus by conducting a series of monotonic and cyclic tests similar to those available in the literature. The influence of several parameters including the magnitude of normal stress, initial relative density of sand, surface roughness, roundness of sand particles, and rate of shearing are evaluated under monotonic shearing of the sand-steel interfaces.

3. Conduct a series of tests under various stress paths between a crushed silica sand and a steel plate. The stress paths include: 3-D monotonic tests under constant normal stress and constant normal stiffness, 3-D cyclic rotational loading, monotonic under constant normal stiffness, and cyclic under constant normal stiffness.

4. Expand the elasto-plastic hierarchical single surface model, originaly developed by Professor C. S. Desai and co-workers for geomaterials, and recently employed by Navayogarajah *et al.* (1992) for interface behaviour, for 3-D and constant normal stiffness conditions. The model is simply used, however, for prediction of the monotonic test results mentioned in step 3. The model parameters are determined based on the results of step 2.

1.4 Outline of Thesis

Chapter 2 presents a review of literature on the devices employed for interface testing, observed interface behaviour, and constitutive models available for interface behaviour. The advantages and disadvantages of available devices are discussed.

Chapter 3 describes the 3-D interface apparatus developed for this research. The major mechanical components of the apparatus, data acquisition system, and constant (or variable) normal stiffness simulation methods are described.

Chapter 4 explains the testing procedure including the description of interface materials such as sand and steel, the specimen preparation and placement method, and the description of corrections required for measured loads and displacements.

Chapter 5 presents the results of 2-D monotonic and cyclic tests under constant normal stress. First some typical results are presented to verify the performance of the new testing apparatus. Then a series of monotonic test results are presented to study the influence of several parameters such as normal stress, relative density of sand, surface roughness, roundness of sand particles, and shearing rate effects. Several of 2-D displacement controlled cyclic test results are presented. Finally, a comparison is made between the direct shear and simple shear soil containers for interface testing.

Chapter 6 presents the 3-D monotonic and cyclic test results under the condition of constant normal stress. The monotonic tests include the stepwise and simultaneous shearing of the interfaces. The 3-D cyclic tests include cyclic shearing in one tangential direction with a constant shear stress in the orthogonal direction, and rotational displacement controlled shearing on the interface plane.

Chapter 7 describes 2-D monotonic and cyclic shearing under the condition of constant normal stiffness. In both monotonic and cyclic results, the influence of initial normal stress and the magnitude of constant normal stiffness on stress-displacement relations are studied. The results of a 3-D monotonic test under a constant normal stiffness condition is also presented.

Chapter 8 describes first the applicability of elasto-plasticity to interface behaviour. The analogies between solid materials and interfaces are pointed out. An existing elasto-plastic type constitutive model (described in Appendix A) is expanded and modified for modelling the stress-displacement relations of sand-steel interface under 3-D and constant normal stiffness conditions.

Chapter 9 presents the discussions and conclusions.

Appendix A describes an elasto-plastic constitutive model, developed by Navayogarajah *et al.* (1992) for modelling the monotonic and cyclic behaviour of 2-D interfaces between sand and construction materials. The determination of the model parameters from the results of this study are also described.

OUTLINE OF RESEARCH

Development of a New Interface Apparatus

Capabilities:

- 3-D Loading
- Monotonic and Cyclic
- Rotational Paths
- Various Boundary Conditions in the Normal Direction
- Simple Shear Soil Container

Comprehensive Testing Program

- 2-D Constant Normal Stress: (Verification of New Device)

  1. Monotonic
  2. Cyclic

- 3-D Constant Normal Stress:

  1. Monotonic
  2. Cyclic
  3. Rotational

- 2-D Constant Normal Stiffness:

  1. Monotonic
  2. Two-Way Cyclic Tangential-Displacement Controlled
  3. One-Way Cyclic Shear-Stress Controlled

Elasto-Plastic Modelling

- Single Surface Model of Desai
- Validation of the Model
- Expansion of Model to 3-D
- Normal Boundary Conditions:

  1. Constant Normal Stress
  2. Constant Volume
  3. Constant Normal Stiffness

Table 1.1. Outline of the research program

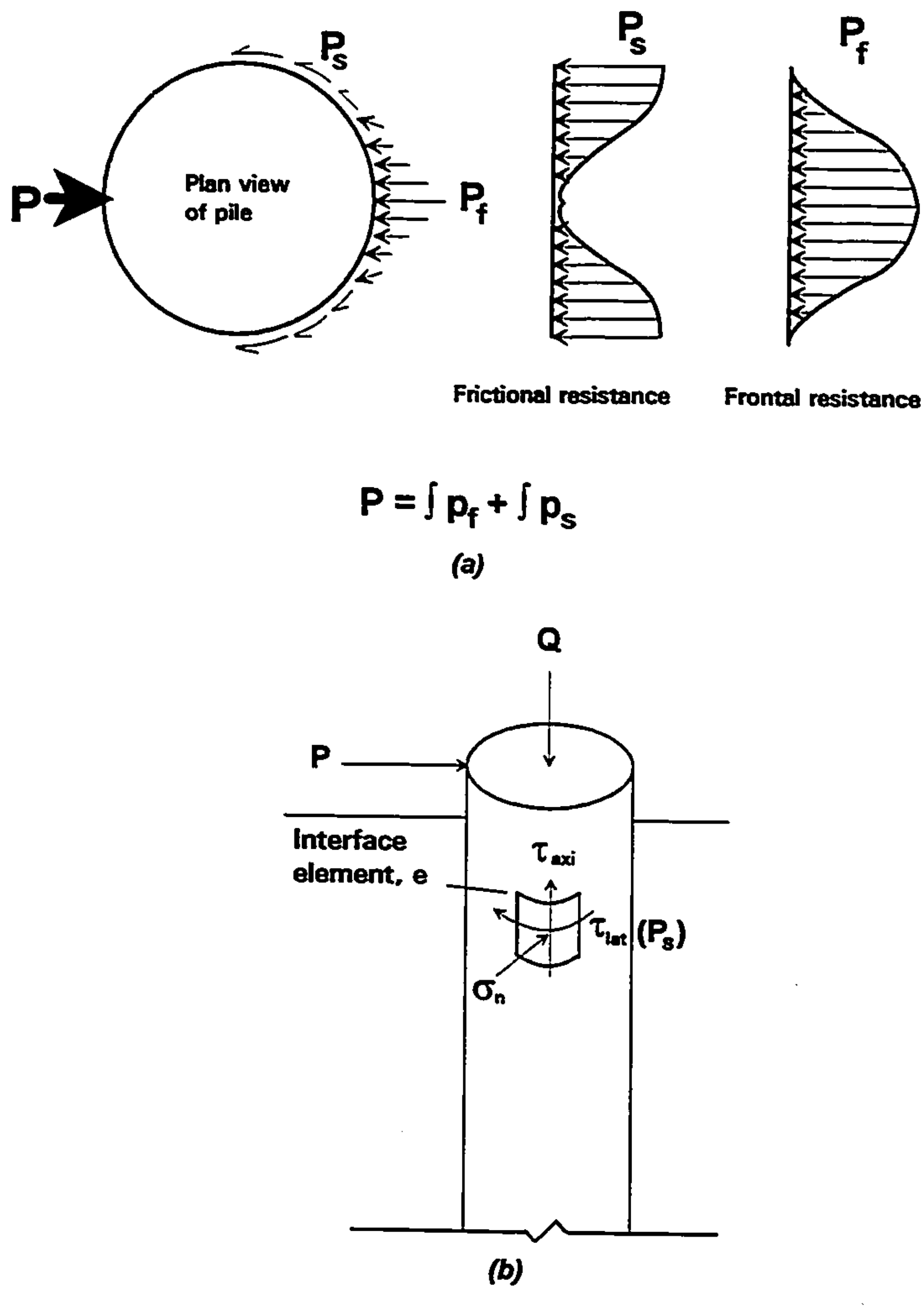

FIG. 1.1. Load transfer for an axially-laterally loaded pile: *(a)* Plan view (Modified after Smith and Ray 1986); *(b)* Stresses on an interface element on the shaft.

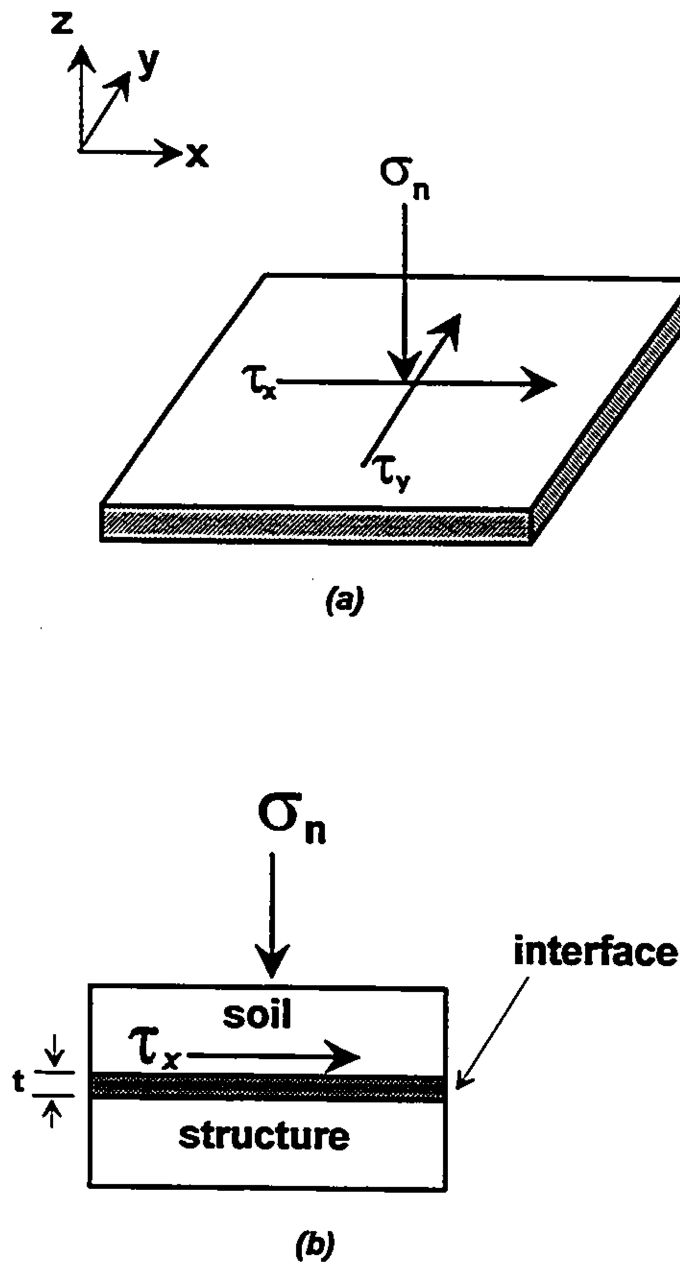

FIG. 1.2. Idealization of stresses and displacements: *(a)* 3-D; *(b)* 2-D.

CHAPTER 2

LITERATURE REVIEW

The review of literature is presented in three sections. The first section covers the experimental devices used for interface testing. Section two presents a summary of available test results for interface behaviour. Section three explains the constitutive models proposed for interface behaviour.

2.1 Devices Used for Interface Testing

2.1.1 Direct Shear Type Device

The direct shear testing of interfaces is similar to direct shear testing of soils. A hollow box, containing the soil specimen, rests on a constructional material such as steel, concrete, or wood (Fig. 2.1). A normal load is applied by a loading platen to the top of the soil specimen, and then a horizontal load is applied to shear the interface between the soil and the constructional material.

Potyondy (1961) used direct shear boxes to determine the skin friction between different types of soils and construction materials, both by strain controlled and stress controlled methods. For the strain controlled tests, the shear box had an area of 3600 mm^2. A box with an area of 8000 mm^2 was used for the stress controlled tests. The specimens of construction materials were placed in the lower portion of the box, and the soil was placed in the upper half.

Desai *et al.* (1985) have also used a shear box type device to study the friction between sand and steel/concrete under the conditions of repeated loading (Fig. 2.2*a*). The bottom half of the box had a square cross-section and was made from steel plates with inner dimensions of 410 × 410 mm. One of the materials such as concrete, ballast, and rock was inserted in the bottom half. The top part consisted of a square box (310 × 310 mm) and contained the other material. Thus, an interface of 310 × 310 mm was created at the junction (Fig. 2.2*b*).

2.1.2 Annular Shear Type Device

The annular shear device was used by Brummund and Leonards (1973) for experimental study of static and dynamic friction between sand and typical construction materials. The test configuration is shown schematically in Fig. 2.3*a*. It consists of a cylinder of sand encased in a rubber membrane with a 28.6 mm diameter, 356 mm long rod located along its axis. By evacuating air from within the membrane, a normal stress was applied to the sand-rod interface that ranged from 8.6 to 86 kPa. The rod was then caused to slip relative to the sand by gradually applying static forces to the rod in the axial direction. The dynamic test set-up, shown schematically in Fig. 2.3*b*, used the same rods as in the static tests. The dynamic force, *F*, was applied using a shock tube. The coefficient of friction between sand and different materials such as steel, Teflon, cement mortar, and graphite was measured using this apparatus.

2.1.3 Ring Torsion Type Device

Yoshimi and Kishida (1981*a*, *b*) used a ring torsion apparatus shown in Fig. 2.4. Dry sand was rained into an annular container lined with 0.3 mm thick rubber membrane, and the top surface of the sand was levelled with a suction device. Then a ring shaped metal specimen was placed on the sand as the construction material. A static torque was applied to shear the interface under a constant normal load applied with weights. In addition to measurements of circumferential and vertical displacements of the metal ring, the deformation of the sand and slippage at the soil-metal contact were measured in some tests using x-ray radiography.

Compared with a direct shear device the ring torsion apparatus has the following advantages (Yoshimi and Kishida 1981):

1. The stresses and strains within the specimen are nearly uniform.
2. Because the specimen is endless, it is free from progressive failure that would initiate at the ends of a direct shear device.
3. Unlimited circumferential displacement can be applied.

2.1.4 Simple Shear Type Device

Uesugi and Kishida (1986*a*) developed a simple shear type device which was capable of measuring both sliding displacement between steel and soil as well as shear deformation of soil mass. Fig. 2.5 shows the simple shear apparatus. The contact surface between steel and sand was originally 400 mm in length and 100 mm in breath. The area of friction surface remained constant during a test even if sliding occurred, since the steel plate was longer than the friction surface. Normal and tangential loads were applied by the vertical and horizontal hydraulic actuators. The container of sand specimen was a stack of rectangular 2 mm thick aluminium plates with 400 × 100 mm space in the middle. The surface of each plate was lubricated to allow the container to follow the shearing deformation of sand with minimum friction resistance.

Uesugi and Kishida (1986*b*) used another apparatus in which the samples had a contact surface of 100 × 40 mm. This apparatus was also used for one-way and two-way repeated loading of interfaces between sand-steel and sand-concrete (Uesugi *et al.* 1989, 1990).

2.1.5 Advantages and Disadvantages of each Device

Four types of devices for testing the interface behaviour between soil and construction materials were described. Each type of device has advantages as well as disadvantages both in performance and also reliability of results.

The direct shear device is the simplest system in sample preparation and test procedure. The direct shear device for soil testing is available in most of the geotechnical labs which may easily be employed for interface testing with some modifications. The stress concentration at the ends and also the impossibility of separating the sliding displacement and displacement due to soil deformation are the major disadvantages of this type of device. The simple shear type apparatus has overcome the problem of separation between sliding displacement and shear deformation of sand. But it still has the disadvantage of stress concentration at the ends. The ring torsion apparatus was used to avoid the non-uniformities of normal and shear stresses at the contact surface and within the soil specimen. It also has the advantage of distinguishing between sliding displacement and displacement due to shear deformation. However, the ring torsion apparatus is a complicated system in terms of sample preparation and measurement of shear displacements. Annular shear type apparatus is geometrically identical to shaft resistance of pile shafts and also frictional resistance of steel reinforcement elements. The disadvantages with this system are the unknown normal stress on the interface and stress concentration at all ends.

A summary of advantages and disadvantages of interface testing devices is presented in a table by Kishida and Uesugi (1987) which is shown in Table 2.1 with some modifications.

Type	Example	Advantage	Disadvantage
Direct Shear	Potyondy (1961) Desai *et al.* (1985) Boulon & Plytas (1986)	Commonly available Simple system Simple preparation Simple procedure	Displacement factors unable to be separated (sliding displ. and displ. due to sand def.) Stress concentration at ends
Annular Shear	Brummund & Leonard (1973)	Geometrically similar to skin friction of piles and friction of steel reinforcements	Normal stress on interface unknown Stress concentration at ends
Ring Torsion	Yoshimi & Kishida (1981)	Endless ring interface No stress concent. at ends Constant interface area Large displ. possible	Complicated system Difficult to prepare uniform sand mass in a ring shape Difficult to finish surface roughness of metal ring uniformly
Simple Shear	Kishida & Uesugi (1987)	Constant interface area Simple preparation Simple procedure Displacement factors measured separately Reliable cyclic test results	Stress concentration at ends

Table 2.1. Advantages and disadvantages of existing interface testing devices.

The common feature of all described interface devices is that they operate in a 2-D space, i.e. tangential and normal stresses and corresponding displacements are located in the same plane.

Annular shear and ring torsion apparatus are not suitable for expanding to 3-D. Annular shear device may simulate the 3-D condition by applying a torque, in addition to the axial force, to the rod surrounded by soil. However, distinguishing between shear deformation of soil and slip at the interface is not possible. There is no practical way to modify or expand the ring torsion type device to operate in 3-D mode.

Direct shear type and simple shear type devices seem to be feasible to operate in 3-D space. Direct shear box is simpler and faster to use, but simple shear type is more accurately simulating the behaviour of interfaces because of separating the sliding displacement from shear deformation of sand mass. The apparatus developed in this research is capable of both direct shear and simple shear testing in 3-D space.

2.1.6 Constant Volume and Constant Normal Stiffness Testing

The stiffness of the surrounding soil (or rock), in the direction normal to the interface plane, is usually denoted by K and is defined as the ratio of variations of the normal stress to the variations of the normal displacement (compression or dilation), i.e. $K = d\sigma_n / dv$.

Constant normal stiffness tests in the laboratory have been performed by a number of researchers. However, the majority of the available results are from the investigations of the mechanical properties of rock joints (e.g. Obert et al. 1976; Lam and Johnston 1982; Leichnitz 1985; Ooi and Carter 1987; Saeb and Amade 1992; Mouchaorab and Benmakrance 1994). Boulon and Plytas (1986) developed a direct shear type of device to investigate the behaviour of interfaces under constant volume and constant normal stiffness test conditions. The results were used for the numerical modelling of the behaviour of a tension pile in sand.

In most of the available interface devices a simply supported reaction beam provides the constant normal stiffness condition. The desired stiffness may be achieved by varying the span or moment of inertia of the beam. Leichnitz (1985) described a computer-controlled direct shear device capable of applying constant normal stiffness for investigation of rock discontinuities. A servo-valve and a hydraulic jack were used for simulation of the constant normal stiffness condition.

2.2 Typical Test Results

Depending on the application requirements, either shear strength parameters or stress-displacement relations of the interface might be of interest. Shear strength parameters include adhesion, denoted by C_a, and angle of friction between soil and structural material, denoted by δ. These parameters are normally required for instability investigation of practical engineering problems such as retaining walls, foundations, and piles. However, for rigorous and realistic analysis of soil-structure systems, the stress-displacement relations are essential.

Subsections 2.2.1 and 2.2.2 present the influence of various parameters on the shear strength coefficients and stress-displacement relations, respectively.

Subsection 2.2.3 presents the stress-displacement relations under various boundary conditions in the normal direction such as constant volume and constant normal stiffness. Typical test results on the interface between two materials under the conditions of cyclic loading are presented in 2.2.4.

2.2.1 Shear strength coefficients

Coulomb's law of friction has been widely used in physics and engineering. If a material, such as soil is in contact with another material like a steel plate (Fig. 2.1), Coulomb's law of friction is stated by the following equation:

$$f = \mu . N \qquad 2.1$$

in which f is the tangential or frictional force required to induce relative displacement at the contact surface, μ is the coefficient of friction, and N is the normal load between the two materials. The adhesion between soil and plate is neglected in Eq. 2.1. Assuming that the angle of friction between the steel plate and soil is δ, and the normal load and shear force be divided by the contact surface area to convert them to normal stress, σ_n, and shear stress, τ_f, respectively, and adhesion between soil and plate be denoted by C_a, therefore:

$$\tau_f = C_a + (\sigma_n)_f \tan\delta \qquad 2.2$$

The Mohr-Coulomb failure criterion is represented in Fig. 2.6 in which δ is the slope of the failure envelope and C_a is the intercept between the failure envelope and the τ axis.

Parameters influencing the shear strength of the interface under the conditions of constant normal stress and monotonic shearing are as follows:

1. Type of surface material (steel, concrete, wood, etc.)
2. Roughness of surface, R_{max} (smooth, medium, rough)
3. Composition of soil (sand, clay, mixtures)
4. Relative density of sand
5. Grain size distribution of soil
6. Moisture content of soil
7. Magnitude of normal stress
8. Rate of shearing

The first elaborate study to recognize the importance of these parameters was conducted by Potyondy (1961). Based on a series of tests between different soils (sand and clay) and construction materials, he found that four major factors determine the skin friction; the moisture content of soils, the roughness of surface, the composition of soils, and the intensity of normal load.

Based on a series of tests by direct shear device, Acar *et al.* (1981) concluded that relative density of sand and normal stress influence the angle of friction between sand and structural materials such as steel, wood, and concrete. Angle of friction was high for low normal stress and high relative densities as depicted in Fig. 2.7. They concluded that such effects are negligible for practical purposes.

By employing an annular shear type device, Brummund and Leonards (1973) found that the coefficient of friction increases with the surface roughness and angularity of the sand grains. They also found that in the case of unlubricated surfaces, the dynamic coefficient of friction is about 20 percent greater than the static coefficient.

The importance of the influence of surface roughness on the frictional resistance was also pointed out by Yoshimi and Kishida (1981*a*, *b*), Uesugi and Kishida (1986*a*) and others.

On the basis of a series of tests between different types of dry sand and steel plates by simple shear type device, Uesugi and Kishida (1986*a*, *b*) concluded that the type of sand and the surface roughness of steel had significant influence on the coefficient of friction. The influence of the normal stress (98 kPa to 980 kPa) and the mean grain size of sand (0.55 to 0.62 mm and 0.15 to 0.19 mm) were not so significant.

2.2.2 Stress-Displacement Relations

Four parameters are normally measured during an interface testing, i.e. normal stress, σ_n, shear stress, τ, volume change or normal displacement, v, and shear displacement, u. For the common case of constant normal stress, shear stress and normal displacement variations are usually plotted versus shear displacement.

Yoshimi and Kishida (1981) reported some test results between steel and Tonegawa sand as shown in Fig. 2.8. A ring torsion apparatus was used in these experiments. Uesugi and Kishida (1986*a*) reported similar results for the interfaces between steel and Toyoura sand, obtained from a simple shear type device, as shown in Fig. 2.9. The results from both test sets indicate that the surface roughness significantly influences the peak and residual shear strengths. A more pronounced peak is observed for rough surfaces followed by strain softening until the shear stress levels off at the residual shear strength.

Volume change (or normal displacement) results indicated some initial compression for smooth surfaces, whereas rough surfaces exhibited a substantial dilation after the initial compression (Figs. 2.8 and 2.9).

As explained earlier, one of the advantages of both simple shear type and ring torsion devices is the possibility of distinguishing between sliding displacement and shear deformation of soil at the interface. Separation of shear deformation of sand and sliding displacements are shown in Figs. 2.10*a* and 2.10*b*, respectively, for the results of Fig. 2.9.

2.2.3 Constant volume, constant normal stiffness

Some researchers have employed the direct shear type device for testing interfaces between two materials under various boundary conditions in normal direction to the interface surface, other than constant normal stress, such as constant normal stiffness and constant volume. The definition of such conditions is given in Section 3.6.

Boulon and Nova (1990) reported the results of some tests under the condition of constant normal stress and constant volume which are presented in Fig. 8.2 and explained in Section 8.2.

Leichnitz (1985) reported two series of test results for dilatant interfaces between two rock surfaces under the conditions of constant normal stress as well as constant normal stiffness at various initial normal stresses. Variations of shear stress, normal stress, and normal displacement are plotted against shear displacements in Figs. 2.11*a* and 2.11*b*. The normalized results of the same figures are shown in Figs. 2.11*c* and 2.11*d*. These results indicate that, although the peak shear stress and the shapes of the shear stress versus shear displacement curves depended on which type of loading condition was employed, the ratio of shear stress to normal stress at peak and at residual were functions of only normal stress and shear displacement. Thus he provided evidence that the shear stress-shear displacement relations and the dilatancy are functions of only normal stress and shear displacement, irrespective of stress path, throughout the entire monotonic shear test. No such results are available for soil-structure interfaces.

2.2.4 Cyclic loading

The other parameters influencing the cyclic behaviour of interfaces in addition to those mentioned in Subsection 2.2.1 are:

1. Amplitude of shear displacement (or shear stress)
2. Frequency
3. Number of cycles, N
4. Soil container type (Direct shear or simple shear)

Desai *et al.* (1985) reported cyclic test results by employing direct shear type device between Ottawa sand and concrete as shown in Figs. 2.12 and 2.13 for different number of cycles, N, and different normal stresses, σ_n, respectively. Figure 2.12 indicates that the peak or mobilized shear stress increased with N for both densities, i.e. loose and dense. However, the increase for higher density was not as rapid as that for the lower density. This implies that, in general, for cohesionless soils the interface response stiffens or hardens with number of cycles and the rate of such hardening decreases with increasing N. Figure 2.13 indicates that the interface exhibited increased stiffness as the normal stress increased.

On the bases of a series of cyclic tests on interfaces between sand-steel and sand-concrete, Uesugi *et al.* (1989) and Uesugi *et al.* (1990) presented some very interesting results by application of simple shear apparatus. Figure 2.14 shows the relationships between the shear stress ratio and the slip at the interface during cyclic test. In the first stage, Fig. 2.14*a*, the peak shear stress is not yet reached. The mobilized maximum shear stress increased with the increase in the number of loading cycles. Eventually, however, when the peak value of shear stress was reached, in Fig. 2.14*b*, the maximum shear stress ratio started decreasing with the number of loading cycles. After a certain number of loading cycles, the hysteresis curves converged to a loop shown in Fig. 2.14*c*.

Although some cyclic test results under the conditions of constant normal stiffness have been reported (Ooi and Carter 1987; Mouchaorab and Benmokrane 1994), it seems that more experimental results are required to understand the effect of stress path on the behaviour of interfaces. Airey *et al.* (1992) presented some sand-to-sand cyclic two-way displacement controlled tests, under the condition of constant normal stiffness, and assumed that similar results would be obtained from interface testing in such conditions. No experimental study, however, has been reported in literature for *cyclic* behaviour of interfaces between *soil and structural materials* under normal boundary conditions other than constant normal stress.

2.3 Constitutive Models for Interface Behaviour

2.3.1 Mohr-Coulomb type models

The Mohr-Coulomb failure criterion can be applied to interfaces similar to that of soils. The shear behaviour of the interface before failure is considered as rigid (Fig. 2.15*a*) or elastic (Fig. 2.15*b*) for practical applications. u is the shear displacement of the interface. This is the simplest, yet frequently used model for behaviour of interfaces.

The rigid-plastic model does not account for shear and normal displacements before failure or slip occurs. The elastic-perfectly plastic models consider the shear displacement, but lack the possibility of considering the non-recoverable (plastic) deformations before failure. Both models are poor in terms of modelling the normal displacements and post-peak behaviour of interfaces. The major advantage of such models is simplicity and applicability to some conditions like those without hardening effects. But they are not suitable for granular materials in which work hardening, non-recoverable displacements before failure, non-linearity, and post-peak softening are common.

2.3.2 Non-linear elastic models

In order to account for non-linearity involved in interface behaviour, non-linear elastic models have been used for interface modelling. The hyperbolic simulation is a common practice both in soil and interface modelling. Ramberg and Osgood (1943) proposed a curve fitting procedure for description of stress-strain curves by three parameters. Streeter *et al.* (1974) used the Ramberg-Osgood model for defining cyclic behaviour of soils, and Idriss *et al.* (1978) used it for cohesive soils. The same model with some modifications was applied for interfaces subjected to cyclic loads by Desai *et al.* (1985). The Ramberg-Osgood model simulates the interface behaviour as piece wise non-linear elastic. As a result, although unloading and reloading are included, inelastic deformations are not included in the sense of the theory of plasticity. The model also lacks the ability of considering the normal displacements at the contact surface.

2.3.3 Direction Type Model

A direction dependent constitutive relation was proposed by Boulon and Plytas (1986). This 2-D model was developed on the basis of the experimental results from direct shear tests with constant normal stress or constant volume testing conditions. A path dependent interpolation rule was applied and the incremental shear and normal stresses of the interface were related to the incremental shear and normal displacements:

$$\begin{pmatrix} \dot{w} \\ \dot{u} \end{pmatrix} = \begin{bmatrix} \dfrac{\partial \dot{w}}{\partial \dot{\tau}} & \dfrac{\partial \dot{w}}{\partial \dot{\sigma}_n} \\ \dfrac{\partial \dot{u}}{\partial \dot{\tau}} & \dfrac{\partial \dot{u}}{\partial \dot{\sigma}_n} \end{bmatrix} \begin{pmatrix} \dot{\tau} \\ \dot{\sigma}_n \end{pmatrix} \qquad 2.3$$

in which w and u are shear and normal displacement increments and τ and σ_n are shear and normal stress increments, respectively.

The coupling between normal and shear behaviour was derived automatically from the interpolation function. This model has been employed for the analysis of soil-structure interaction problems such as axially loaded piles by Boulon and Plytas (1986).

2.3.4 Elasto-plasticity Based Models

Except the direction type model explained in 2.3.3, all other constitutive models for interface behaviour disregard the normal response of the interface, thus ignore the coupling effects of shear and normal displacements. In order to account for the coupling between normal and shear behaviour and also establishing a meaningful framework for the behaviour of interfaces, the concept of theory of plasticity has been applied. The first attempt towards application of theory of plasticity for interface modelling was made by Ghaboussi and Wilson (1973). They applied the cap plastic model to joints in rock which uses a perfectly plastic yield surface to limit shear stresses and a strain hardening cap to control dilatancy. Therefore, the components of normal strain, ε_n, and shear strain, ε_s, can be divided into elastic and plastic parts.

An elasto-plastic constitutive model was developed by Fishman and Desai (1987) and Desai and Fishman (1991) for hardening behaviour of rock joints with associative and non-associative flow rules. The basic formulation of this model was the same as the one used for frictional materials by Desai (1980), Desai and Faruque (1984), and Desai *et al.* (1986). The same model was modified by Navayogarajah (1990) and Navayogarajah *et al.* (1992) for monotonic and cyclic behaviour of interfaces between sand-steel and sand-concrete. The properties of the model were described from the experimental results of the simple shear type device which was explained in 2.1.4. This model is described in more details in Appendix *A*.

Boulon and Nova (1990) also applied an elasto-plastic model for interfaces between dry sand and rough surfaces.

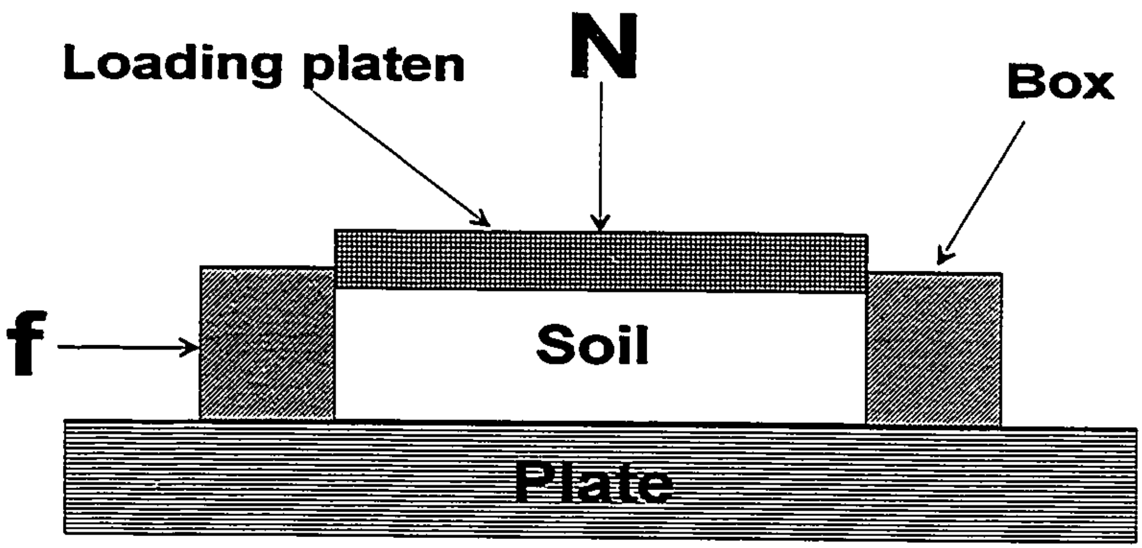

FIG. 2.1. A typical direct shear type device for interface testing

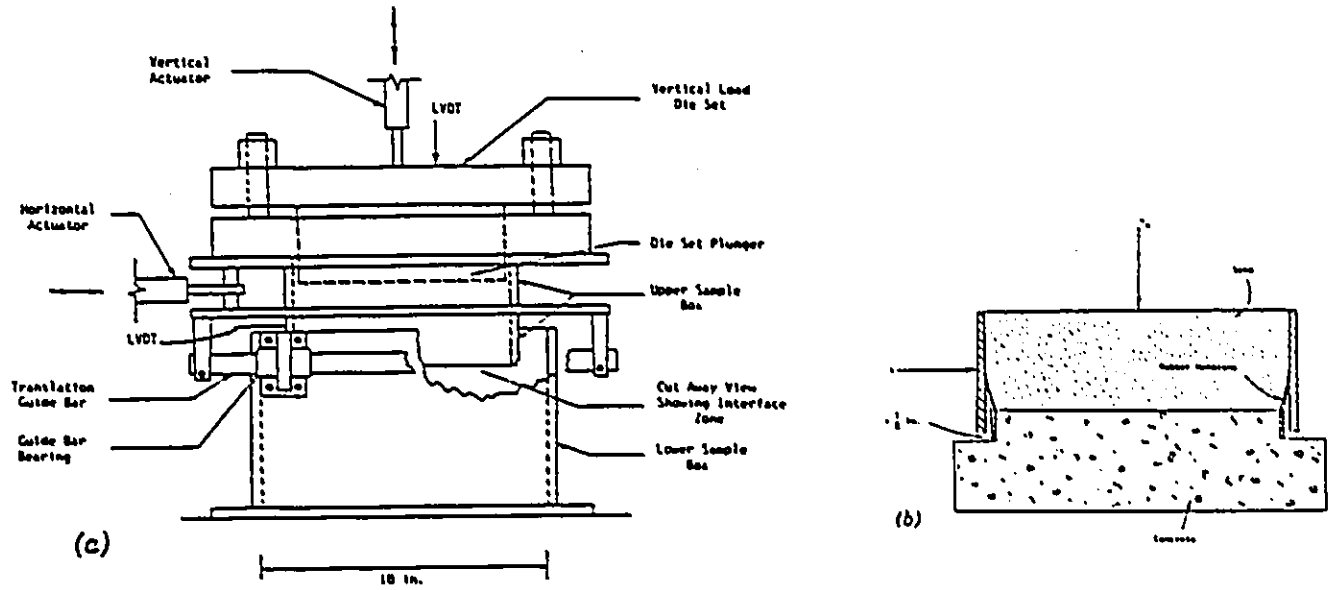

FIG. 2.2. Desai's direct shear type device: *(a)* Test box; *(b)* Schematic of the membrane arrangement

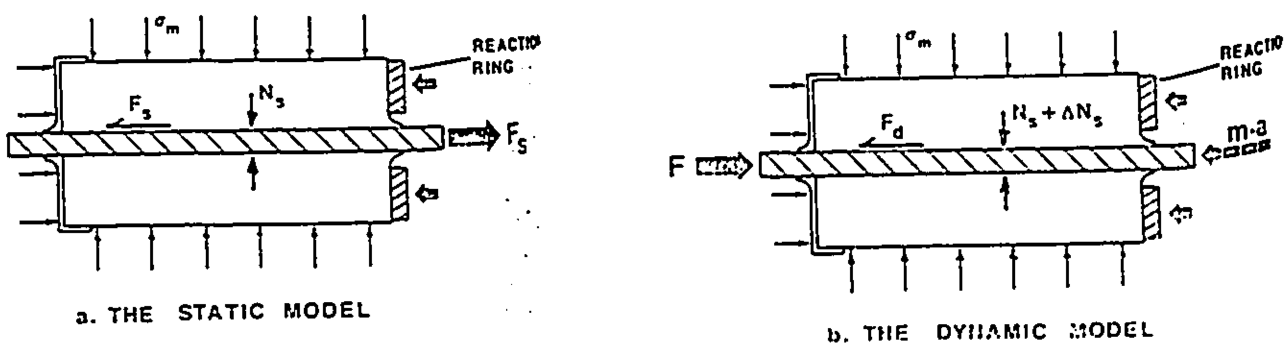

FIG. 2.3. Annular shear type device (After Brummund and Leonards 1973)

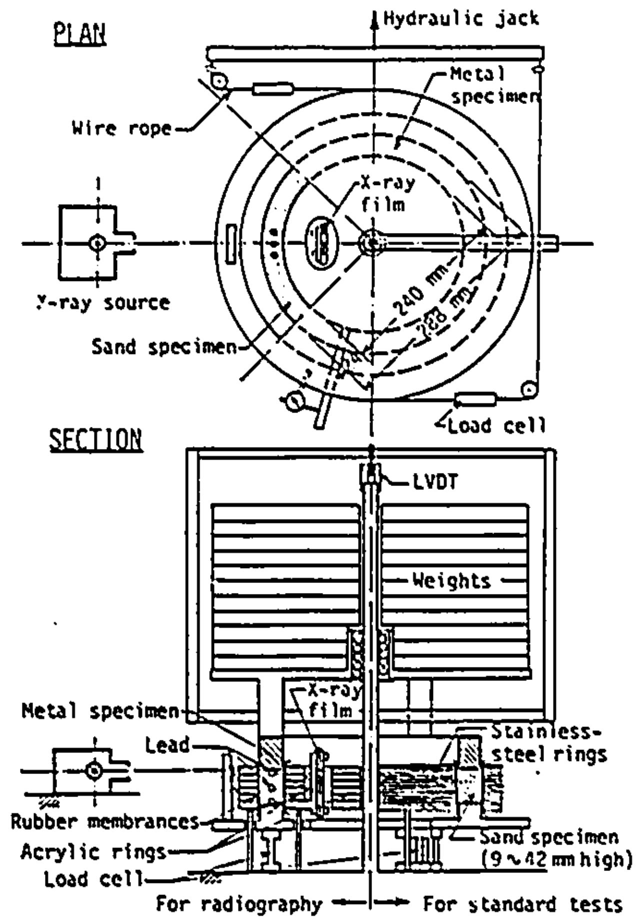

FIG. 2.4. Ring torsion apparatus (After Yoshimi and Kishida 1981)

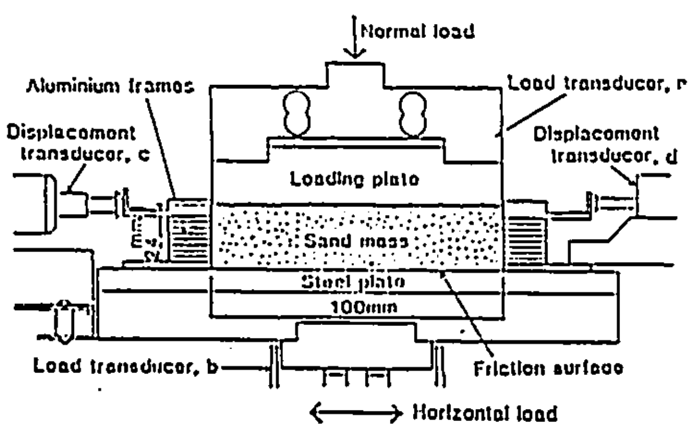

FIG. 2.5. Simple shear type apparatus (After Uesugi and Kishida 1986*b*)

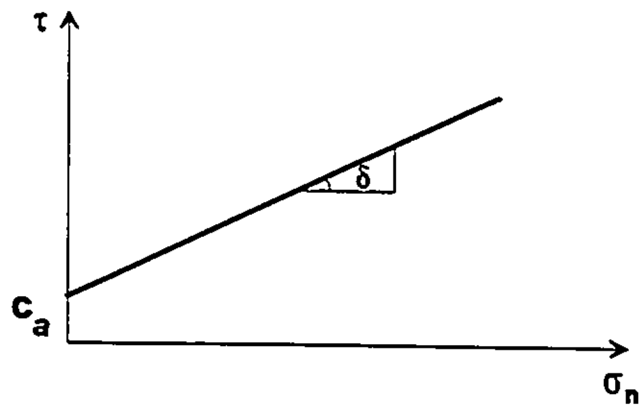

FIG. 2.6. Mohr-Coulomb failure criterion

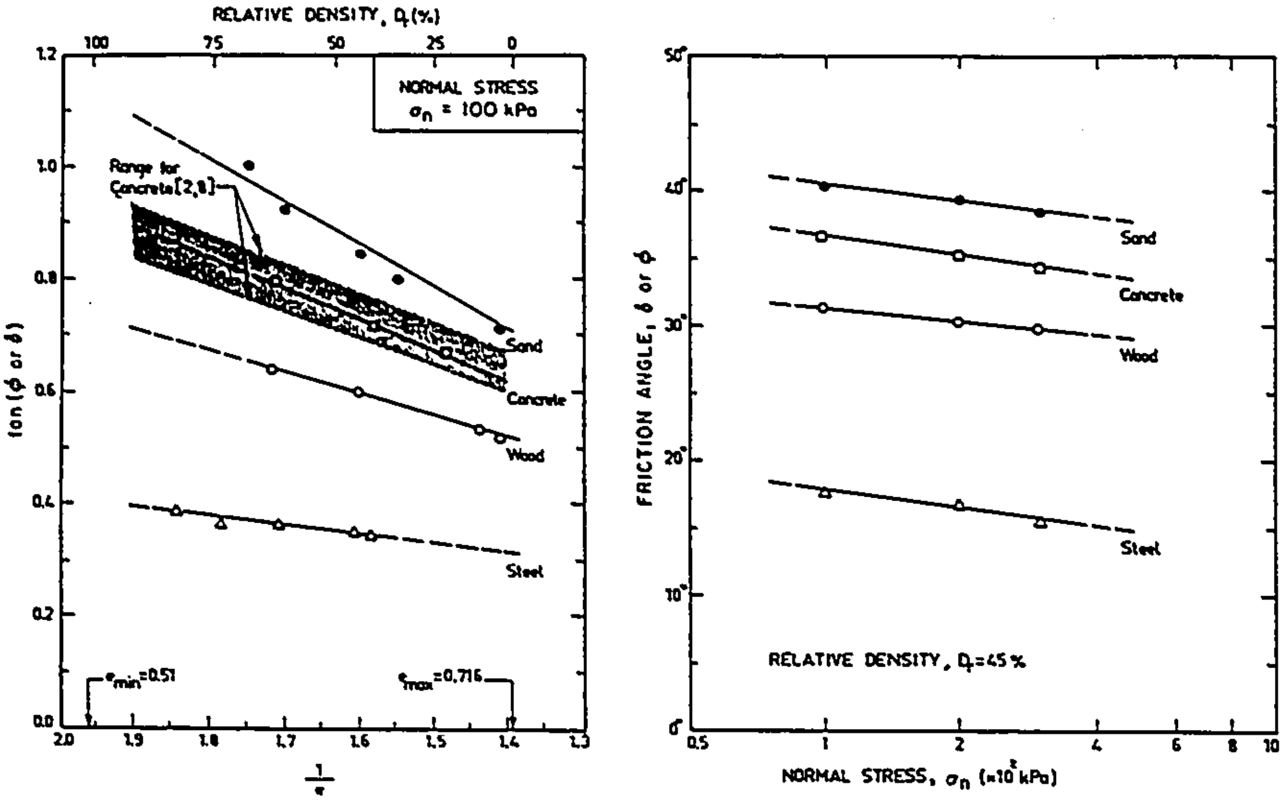

FIG. 2.7. Variation of skin friction (shear strength) with relative density and normal stress (After Acar *et al.* 1982)

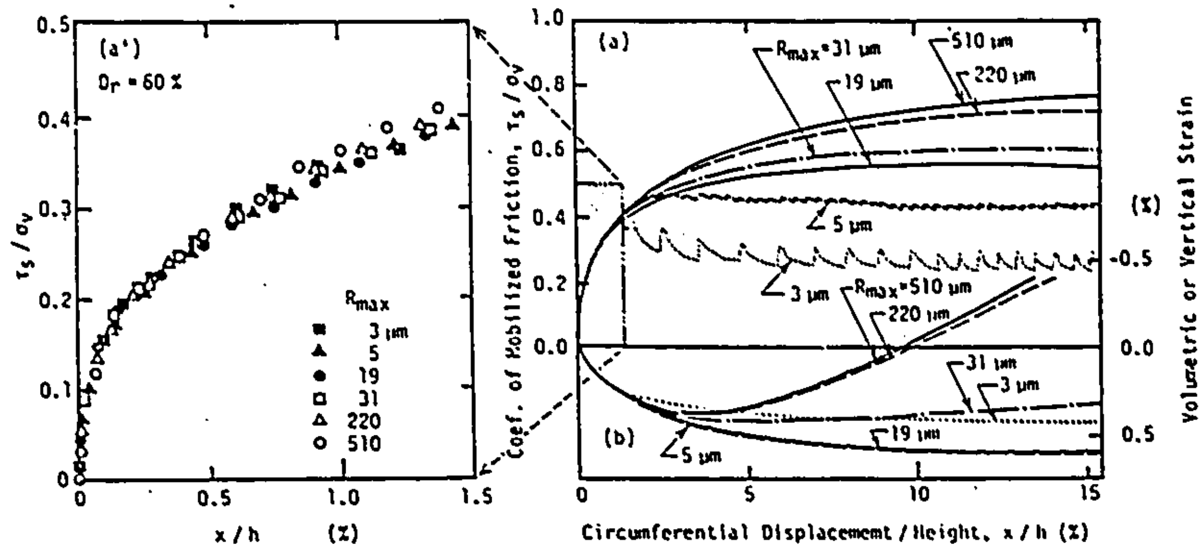

FIG. 2.8. Interface test results between steel and Tonegawa sand (After Yoshimi and Kishida 1981)

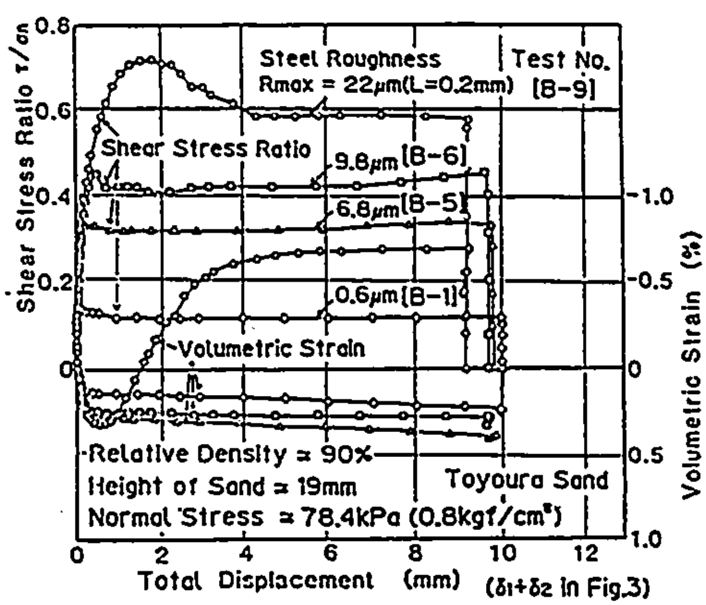

FIG. 2.9. Interface test results between steel and Toyoura sand (After Uesugi and Kishida 1986*a*)

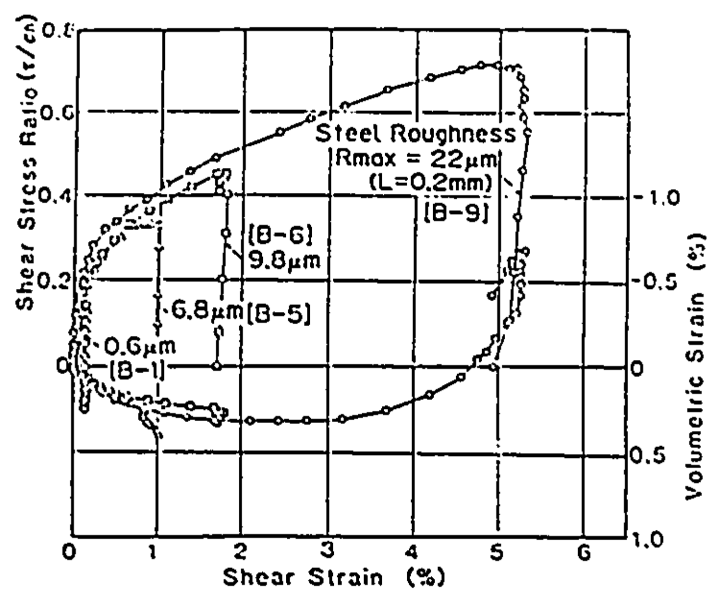

(a)

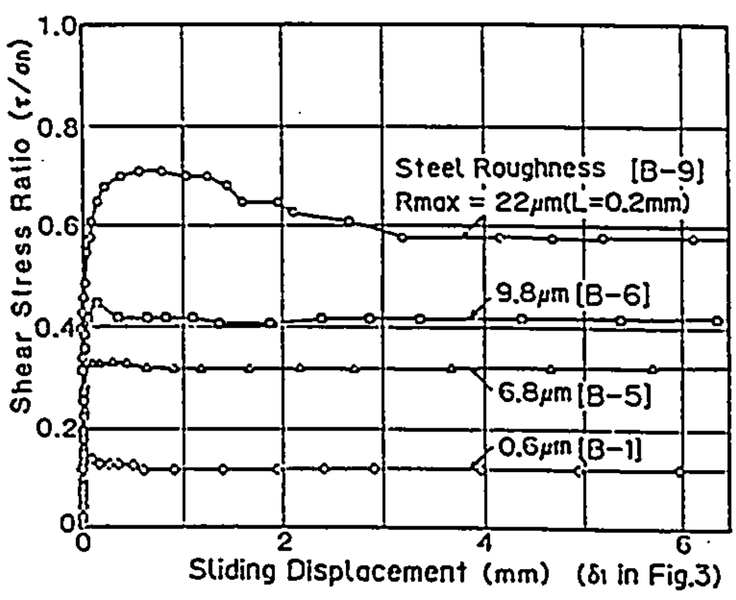

(b)

FIG. 2.10. Decomposition of results of Fig. 2.9: *(a)* Shearing deformation of sand sample; *(b)* Sliding displacement at the steel-sand contact surface

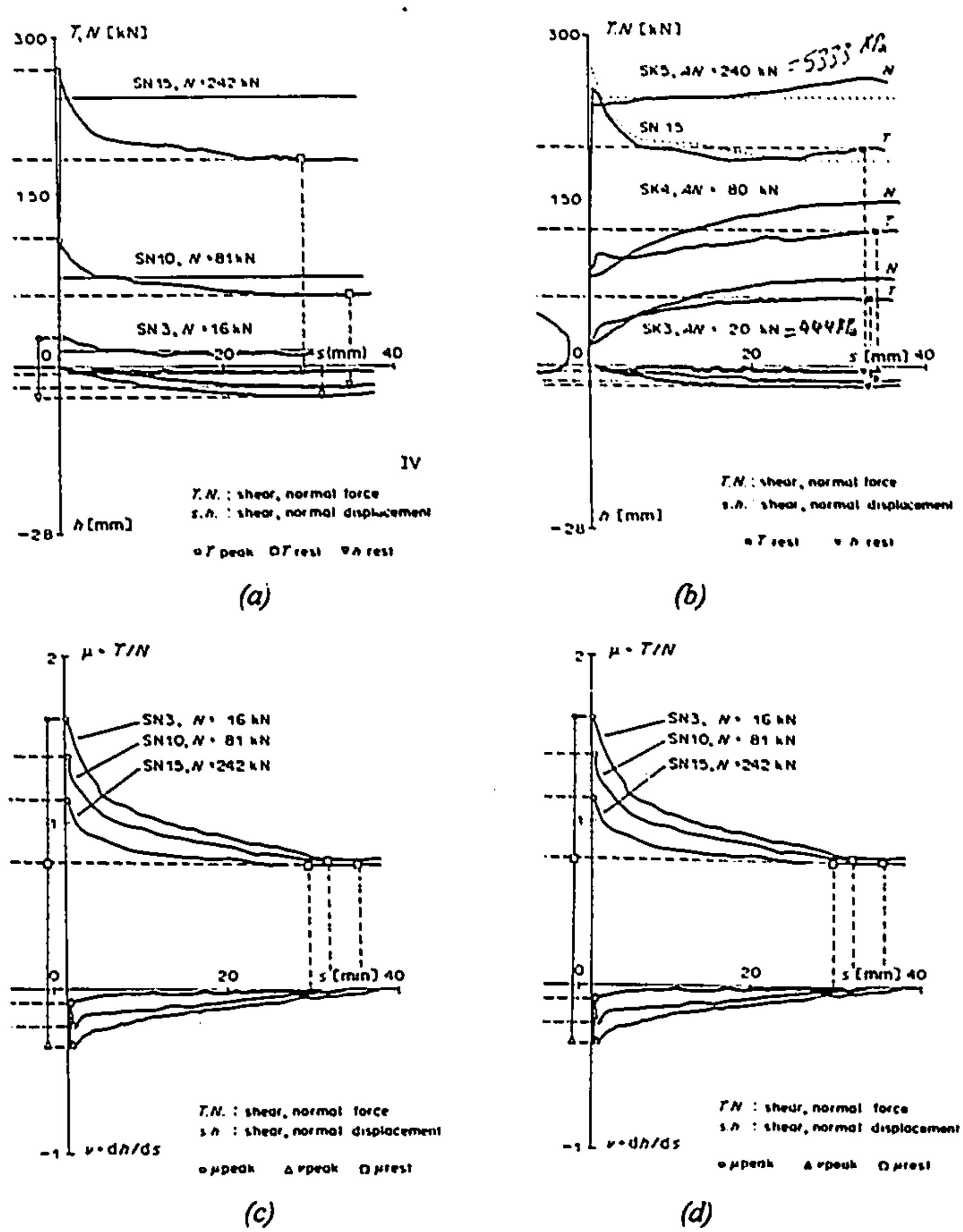

FIG. 2.11. Shear force, normal force, and volume change plots versus shear displacement for Sandstone joints: *(a)* Constant normal force; *(b)* Constant normal stiffness; *(c)* Normalized results of *a*; *(d)* Normalized results of *b*
(After Leichnitz 1985)

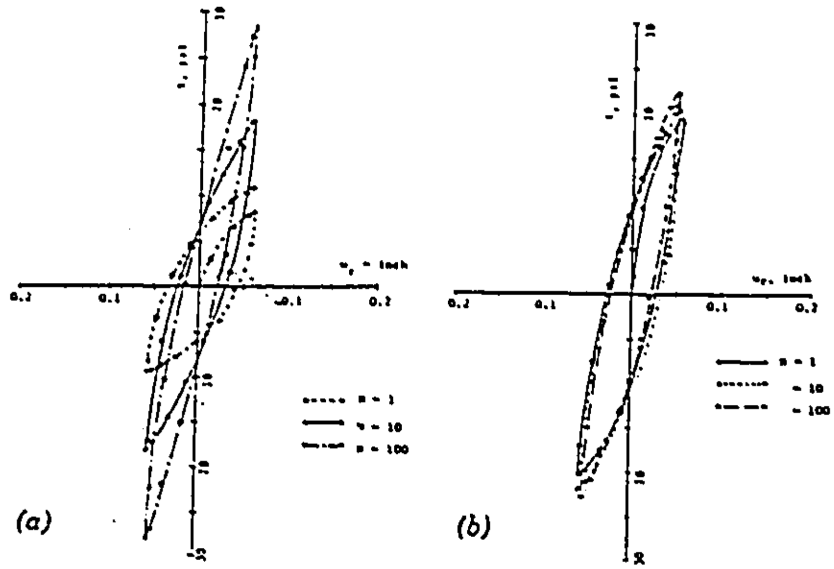

FIG. 2.12. Shear stress versus relative displacements for different N: σ_n = 193 kPa, u_r = 1.3 mm , Ω = 1 Hz.: *(a)* D_r = 15 %; *(b)* D_r = 80 % (After Desai *et al.* 1985)

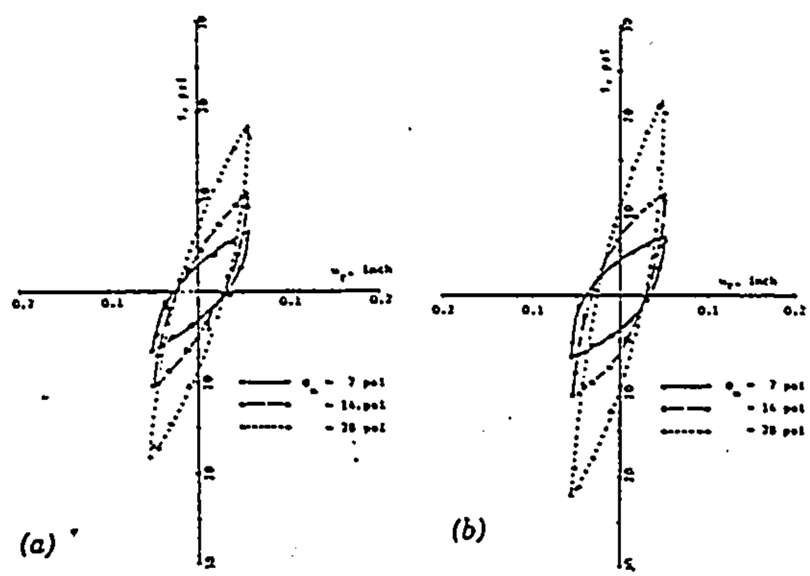

FIG. 2.13. Shear stress versus relative displacements for different σ_n : N=10, u_r = 1.3 mm , Ω = 1 Hz.: *(a)* D_r = 15 %; *(b)* D_r = 80 % (After Desai *et al.* 1985)

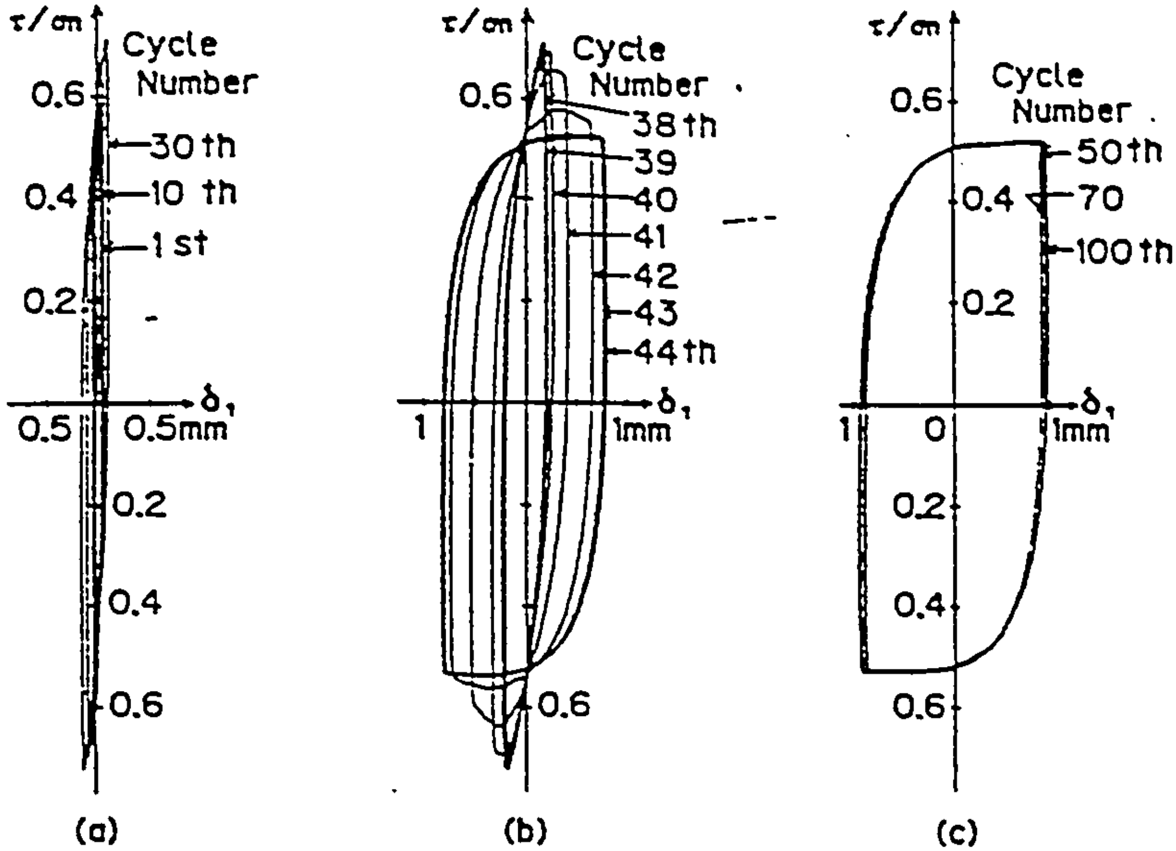

FIG. 2.14. Shear stress ratio, τ/σ_n vs. interface slip, δ_1: *(a)* Before interface failure; *(b)* Transient stage; and *(c)* After interface failure (After Uesugi and Kishida 1987*b*)

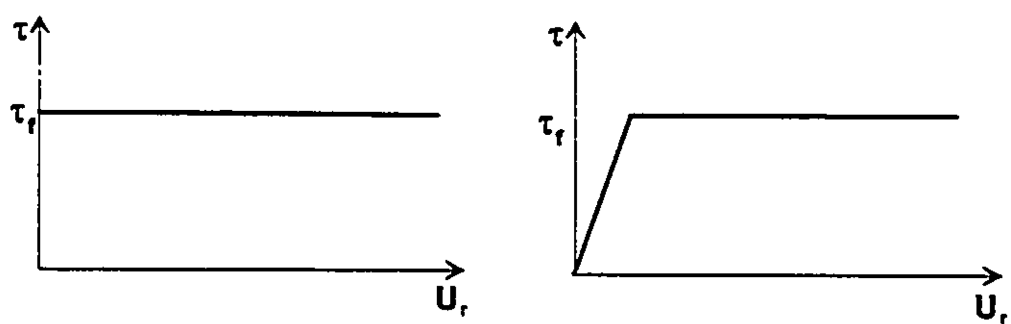

FIG. 2.15. Perfectly plastic models: *(a)*Rigid-perfect plastic; *(b)*Elastic-perfect plastic

CHAPTER 3

DESCRIPTION OF 3-D INTERFACE APPARATUS

A new apparatus for testing interface between two materials was developed since there was no experimental device available for achieving the objectives of this research. The interface apparatus will be referred to as:

- **C3DI**, i.e. Cyclic 3-Dimensional testing of Interfaces, if the test is performed using the direct shear type soil container;
- **C3DSSI**, i.e., Cyclic 3-Dimensional Simple Shear testing of Interfaces, if the test is performed using the simple shear type soil container.

During its description, however, the new interface apparatus is mostly referred to as C3DSSI. C3DSSI has several new features compared with other available devices for interface testing such as:

- capability of 3-D testing of interfaces
- monotonic loading at various loading rates
- simultaneous displacement or load controlled cyclic tests in all three directions
- circular or elliptical shearing on the interface plane
- various boundary conditions normal to the interface plane such as constant normal stiffness and constant volume
- separating the sliding displacement at the interface from the shear deformation of the soil mass.

The operation of the interface apparatus and the data acquisition are automated by a computer controlled system. The apparatus is schematically illustrated in Fig. 3.1. A photograph is shown in Fig. 3.2.

Three independent forces need to be applied to induce the three stress components at the interface plane, σ_n, τ_x, and τ_y, as shown in Fig. 1.2*a*. Three load cells and five LVDTs were employed to measure the loads and displacements in the three directions.

The description of C3DSSI is presented in the following sections:

3.1 Reaction Frame

A reaction frame is designed to withstand a vertical or horizontal load up to 25 kN as shown in Fig. 3.3. While the actuators used for applying the normal and tangential loads have each capacities of 10 kN, the tests are conducted at a load level less than 5 kN. Thus, the ratio between the applied load to the capacity of the frame is 1/5.

The frame consists of three horizontal 600 × 600 mm aluminium plates and four vertical steel bars. These reaction plates are 50 mm, 37.5 mm, and 37.5 mm thick, respectively located at the bottom, middle, and top of the frame. Four 25 mm diameter steel bars, covered by 50 mm outside diameter mechanical tubes, support the aluminium plates. The bottom and top plates provide vertical reaction, while the bottom and middle plates provide horizontal reaction.

3.2 Vertical Loading Unit

A pneumatic actuator is mounted on the top reaction plate of the frame for applying a load along the z axis normal to the contact surface as shown in Fig. 3.1. A load cell, with a maximum capacity of 6.6 kN, is attached to the vertical shaft, above the loading platen, for monitoring the normal load (Fig. 3.4). The accuracy of load measurement is 5 N. The loading platen (Fig. 3.1) is connected to a shaft which moves freely through a vertically mounted linear ball bushing bearing and is fixed against movement in the horizontal direction in the x-y plane. Therefore, the normal load along the z axis is applied to the specimen at the top and the reaction is provided from the bottom plate of the frame. An LVDT is attached to the mid plate of the frame for measuring the normal displacement of the specimen, either contraction or dilation. The accuracy of the displacement measurement is 0.002 mm.

3.3 Horizontal Loading Unit

The tangential shear stresses are applied to the interface plane through an X-Y loading table. The X-Y loading table consists of three plates attached to each other through a linear bearing system as illustrated in Figs. 3.5 and 3.6. A photograph of it during construction is shown in Fig. 3.7. As a result, the top plate is free to move both in the x- and y-directions without any rotation about vertical axis. The linear bearing systems were preloaded to minimize any backlash for eliminating the rocking of the specimen during application of shear loads. Two ball screw stepper motors are used for applying simultaneous shear loads to the contact surface. The programmable ball screw stepper motors used in C3DSSI have capacities of 9 kN. They are both controlled by computer and are capable of applying monotonic loads at rates ranging from 0.01 to 20 mm/min, as well as displacement or load controlled cyclic shears in the x- and y-directions simultaneously.

The stepper motor for applying load in the y-direction is fixed to the bottom reaction plate of the frame and its ram is attached to the centre of the edge of the mid plate of the X-Y loading table. The other stepper motor, for applying load in the x-direction, is front flange mounted on the mid plate of the X-Y table and its ram is attached to the middle of the edge of the top plate.

Two load cells, with maximum capacities of 4.5 kN each, are used between stepper motors and the loading table to monitor the x and y tangential forces applied to the contact surface. Tangential displacements in each direction (x or y) are measured by 4 LVDTs across the simple shear box, with an accuracy of 0.002 mm.

3.4 Direct shear and Simple Shear Soil Containers

Two types of soil containers can be used with the new interface apparatus, i.e., direct shear type and simple shear type.

• **Direct shear type container (C3DI):** A 25 mm thick, hollow aluminium box, with inside area of 100 × 100 mm, is placed on the steel plate which has an area of 300 × 300 mm as illustrated in Fig. 3.8. A thin layer of foam which is covered by a Teflon sheet is pasted to the bottom of the hollow aluminium box to prevent the leakage of the sand particles and to minimize the friction between the box and steel plate. Since the steel plate is longer than the soil surface, the area of contact surface remains constant during sliding.

Two LVDTs are used to measure the tangential displacements in the x- and y-directions as shown in Fig. 3.9. LVDT a_x measures the relative tangential displacement, u_x, between direct shear box and steel plate in the x-direction (Fig. 3.9a). LVDT a_y measures u_y, in the y-direction, which is perpendicular to the direction of u_x (Fig. 3.9b).

• **Simple shear type container (C3DSSI):** The simple shear soil container is similar to that of the friction testing apparatus by Uesugi and Kishida (1986), except that it can be sheared in two orthogonal directions, x and y, on the interface plane. A stack of 2 mm thick anodized, Teflon coated, square aluminium plates with an inside area of 100 × 100 mm (Fig. 3.10) is placed on the steel plate which has an area of 300 × 300 mm. Since the steel plate is longer than the soil surface, the area of contact surface remains constant during sliding.

Two sets of tangential displacements are measured to distinguish between the sliding displacement (slip) along the contact surface and the shear deformation of the soil mass in both x and y directions. All displacements are measured by LVDTs. Figures 3.11a and 3.11b illustrate the schematic diagrams of tangential displacements in the x and y directions, respectively. In the x-direction, the total tangential displacement, u_{xa}, is measured between the top aluminium plate and the steel specimen by the LVDT, a_x. The shear deformation of the soil mass, u_{xb}, is measured by the LVDT, b_x, which reads the relative tangential displacement between the top and bottom aluminium plates. The sliding displacement at the soil-steel interface, u_x, is obtained from $u_x = u_{xa} - u_{xb}$ (Fig. 3.11*a*). Figure 3.12 shows a photograph of the simple shear box assembly with the LVDTs a_x and b_x.

In the *y*-direction, the total tangential displacement, u_{ya}, between the top aluminium plate and the steel specimen is measured by LVDT, a_y. The shear deformation of the soil mass, u_{yb}, is measured by the LVDT, b_y, which reads the relative tangential displacement between the top and bottom aluminium plates. The sliding displacement at the soil-steel interface, u_y, is obtained from $u_y = u_{ya} - u_{yb}$ (Fig. 3.11*b*).

A photograph of the simple shear box with a steel plate during a 3-D test is shown in Fig. 3.13. The LVDTs a_x, b_x, and a_y are illustrated across the specimen.

3.5 Data Acquisition and Computer Control System

The control of C3DSSI and acquisition of data are fully computerized. Once the sample is prepared and placed in the apparatus, a computer program, BENCHMATE, is run on an IBM compatible PC which is connected to the testing apparatus thorough an interface unit. The test is controlled in a closed loop feedback manner. A computer controlled testing system usually consists of three major parts, the testing apparatus and transducers, interface unit (hardware), and software as illustrated in Fig. 3.14. A photograph of the complete system is shown in Fig. 3.15.

3.5.1 Interface Unit

The interface unit forms the communication link between the computer and the actuators/transducers as illustrated in Fig. 3.14. It consists of five modules which are connected to the computer thorough a bus-type interface card which is considered to be more versatile than serial interface systems as compared by Kuerbis and Vaid (1991). The modules are used for data acquisition and the conversion of control commands to analog outputs.

The 8-channel bridge conditioner module acts as a front-end conditioning card to be used between the A/D or analog multiplexer card and the transducers. Up to 8 transducers such as load cells, pressure transducers, and LVDTs can be connected to this module. The analog expansion and A/D converter modules provide multiplexers and connectors for all input channels. The converted signals from analog to digital by the A/D converter are transformed to the software via the interface card. The measured loads and displacements are then analyzed and compared to the target values so that new digital commands are issued which are transferred to stepper motor controller module via interface card. This module is used to provide pulses to a stepper motor translator module, which in turn provides power to energize the motor windings causing steps. Two identical stepper motors (1 and 2 in Fig. 3.14) are used to directly apply the tangential forces to the contact surface. A motorized air regulator, which is operated by a built-in stepper motor, adjusts the pressure for the E/P actuator to apply load in normal direction.

3.5.2 Software

A menu-form software, written in Q-BASIC, is prepared that can be customized and applied to almost any advanced testing sequence. The software is capable of performing a complete closed-loop control between one or more transducers and one or more controllers simultaneously. For example, once sinusoidal displacement controlled shear is applied in *x*-direction by stepper motor 1, stepper motor 2 can apply a constant shear load and E/P actuator apply a constant normal load or maintain the height constant.

The main menu of the software contains a number of options as listed below:

Configure Sensors
Configure Controls
Configure Graphics
Configure Sequence

Configure Sensors accesses a table menu which lists each sensor and its attributes. Some of the options included in configure sensors are creating a new sensor, labelling the sensor, calibrating the sensor, and running a sensor diagnostic. The calibration of the sensor can be done simply by adjusting the sensor to a known magnitude, such as a known displacement for LVDT transducer, and then offset and slope of the sensor will be automatically calculated and inserted in the table menu.

Configure Controls table menu is used to configure controllers and check their operation. Some of the options included in configure controls are creation of a new control, labelling the control, choosing the control type, and manually checking the performance of the control. Two control types are available in the software: open loop and closed loop. Three types of closed loop control are included, i.e., PID, dead band, and stepper motor control. The stepper motor closed loop control is used to control the three stepper motors in C3DSSI by maintaining the feedback sensor(s) at the set-point level.

Configure Graphics is used to set up or change graphics parameters. The graphs can be monitored on the screen in various combinations while a test is running. Two table menus are included in the graphics module: one enables the operator to preconfigure the graph templates and the other allows the preconfiguration of the curve templates.

A graph template contains the parameters that define a graph such as location, colour, limits etc.. A curve template contains the attributes of a curve. Sensors and results are tied to the curve templates according to the specific application. Curves are then plotted on the associated graph templates as the application dictates.

There are two types of graph templates available. They are X-Y and TIME-Y. An X-Y graph can be used to plot any value against another value such as LOAD-DISPLACEMENT, while the TIME-Y graph is used to plot any value against time such as LOAD-TIME or DISPLACEMENT-TIME. Versatile options available for displaying the outputs make it possible to view the progress and performance of the test.

Configure Sequence: The sequence used in the software is like a high level programming language that is used to set up scanning the sensors, saving the results, controlling, and displaying. A linear sequence of steps can be used to perform a test. These steps include scanning a sensor, resetting a graph, showing a sensor output on the screen, setting a controller, DO LOOPS for closing the control loops, saving sensor outputs, etc.. A controller can be set to a specified set point. The set point may be a sensor, combination of sensors, or an equation. The square, triangular, and sinusoidal waves are available for performing displacement/load controlled cyclic tests.

3.6 Constant (or variable) Normal Stiffness

The stiffness in the direction normal to the interface is usually denoted by K and it is defined as the ratio of the variation in the normal stress to the variation in the normal displacement at the upper boundary of the sample, i.e. $K = d\sigma_n \,/\, dv$. Three typical boundary conditions (Fig. 3.16) are generally used in laboratory experiments:

I. $K = 0$, i.e. $d\sigma_n = 0$; $dv \neq 0$ (constant normal stress)
II. $K = \infty$, i.e. $d\sigma_n \neq 0$; $dv = 0$ (constant volume)
III. K = Constant, i.e. $d\sigma_n \neq 0$; $dv \neq 0$ *and* $d\sigma_n \,/\, dv = K$ (constant normal stiffness)

Case I represents the condition in which the normal stress does not change during the process of shearing as shown in Fig. 3.16*a*. In this case, the interface may compress or dilate freely ($d\sigma_n = 0$; $dv \neq 0$). The constant normal stress condition is the simplest and the most frequently employed boundary condition in interface experiments.

Case II is the condition of constant volume. No displacement is allowed at the upper boundary of the sample in the direction normal to the interface plane as illustrated in Fig. 3.16*b*. During the test, the normal stress increases or decreases depending on the tendency of the soil to dilate or compress ($d\sigma_n \neq 0$; $dv = 0$).

Case III is the condition of constant normal stiffness (Fig. 3.16*c*) in which normal stress and normal displacement vary proportionally ($d\sigma_n \,/\, dv = K$). Case I and Case II are the lower and upper bounds of Case III, respectively.

In most of the available interface testing devices a simply supported reaction beam was used to impose the constant normal stiffness condition. The desired stiffness was achieved by varying the span or moment of inertia of the beam. Leichnitz (1985) described a computer-controlled direct shear device capable of applying constant normal stiffness for the investigation of the behaviour of rock discontinuities.

In C3DSSI, the boundary conditions in the direction normal to the interface are imposed by a computer controlled system which includes a pneumatic actuator, a motorized regulator, a load cell, an LVDT, and the closed-loop computer control unit. The stiffness, K, is specified as a set point. The computer control unit varies the pressure in the pneumatic actuator such that the ratio between the variation in the normal stress and the variation in the normal displacement is kept constant at the set point, K. A correction is made in the set point to account for the compliance of the testing device.

There are several advantages of employing a computer-controlled system over a mechanical system (a reaction beam) in constant normal stiffness tests. The reaction beam systems are difficult to assemble and require very precise adjustments. The correction for the normal compliance of the testing device is difficult. In order to achieve the desired stiffness, pre-calculations and calibrations are required. In a computer-controlled system, however, the corrections are performed automatically. Moreover, a variable stiffness condition during a test can only be simulated by a computer-controlled system where the set point is expressed as a function of the normal stress level. By specifying the value of K as zero or a very large number, the conditions of constant normal stress or constant volume can be simulated.

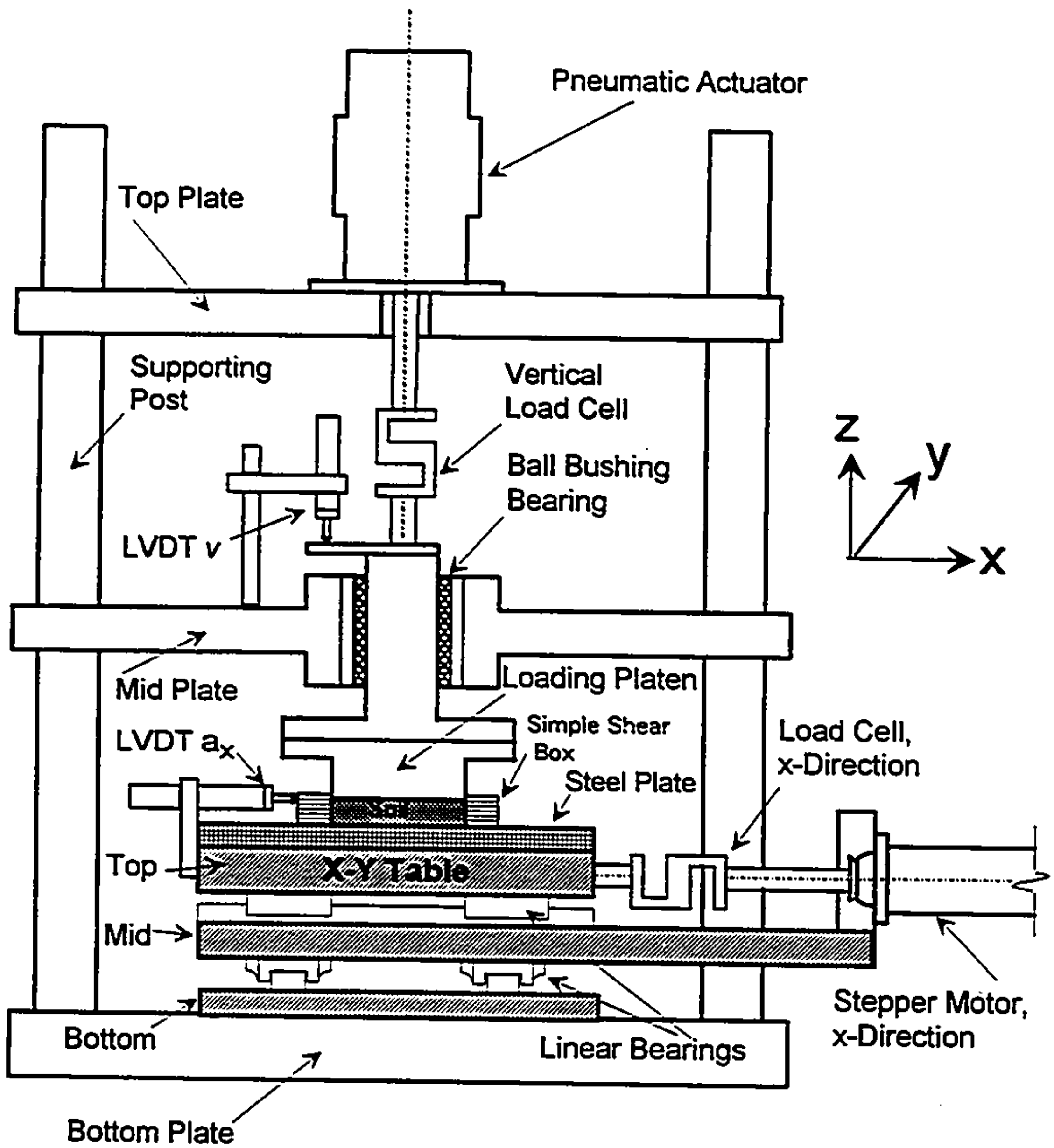

FIG. 3.1. Schematic view of C3DSSI.

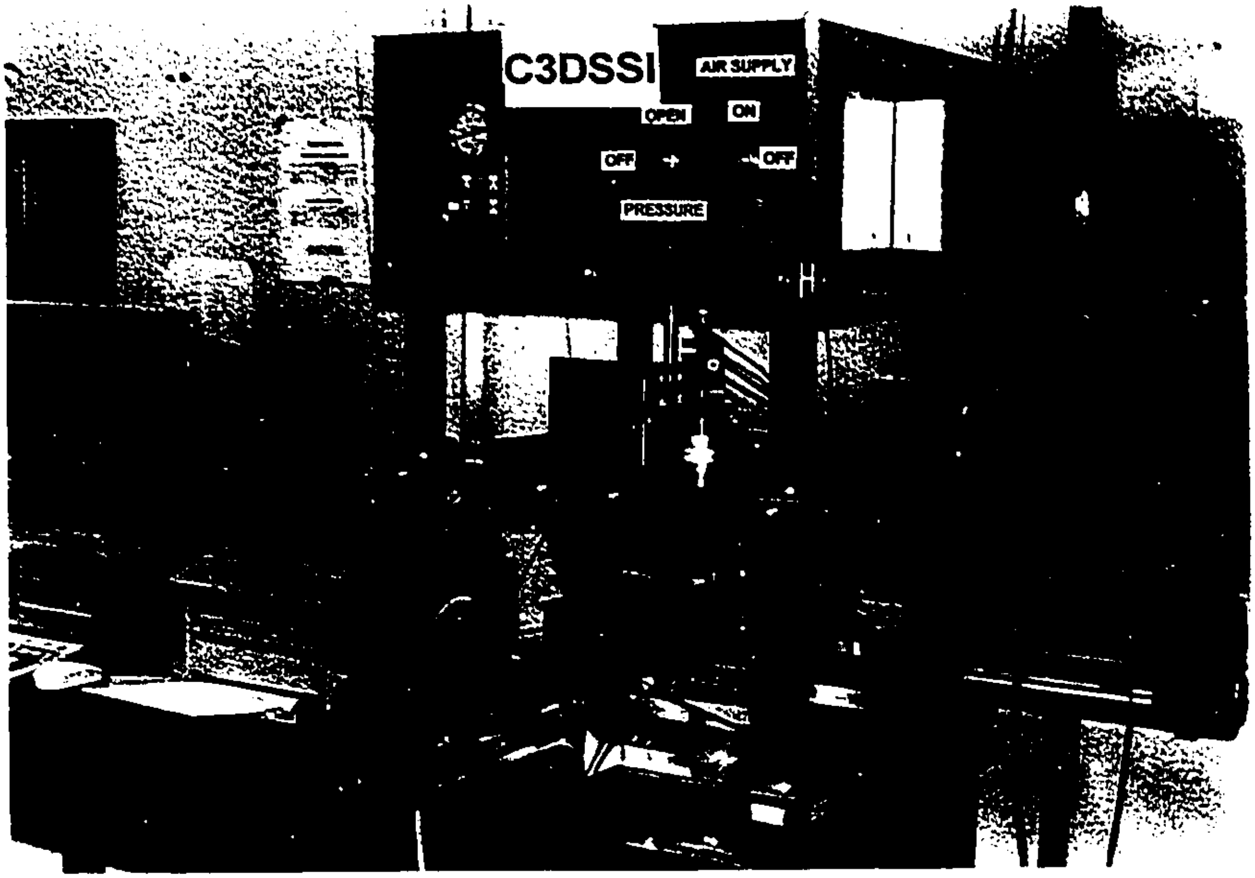

FIG. 3.2. Photograph of C3DSSI.

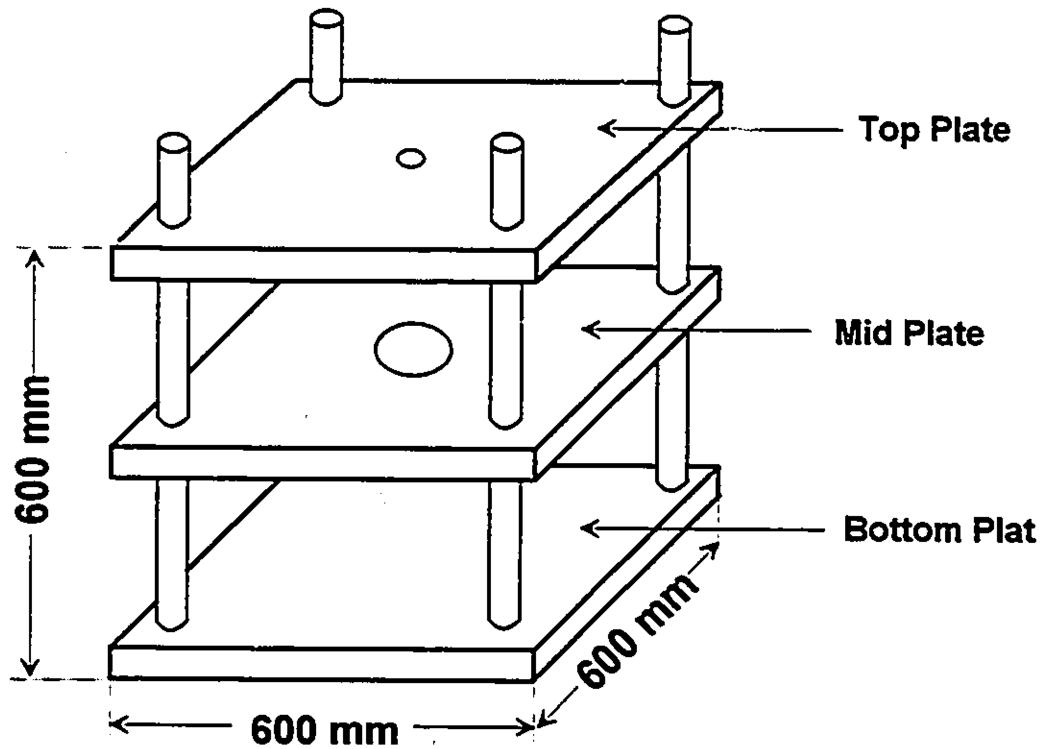

FIG. 3.3. Three-level reaction frame to withstand vertical and horizontal loads.

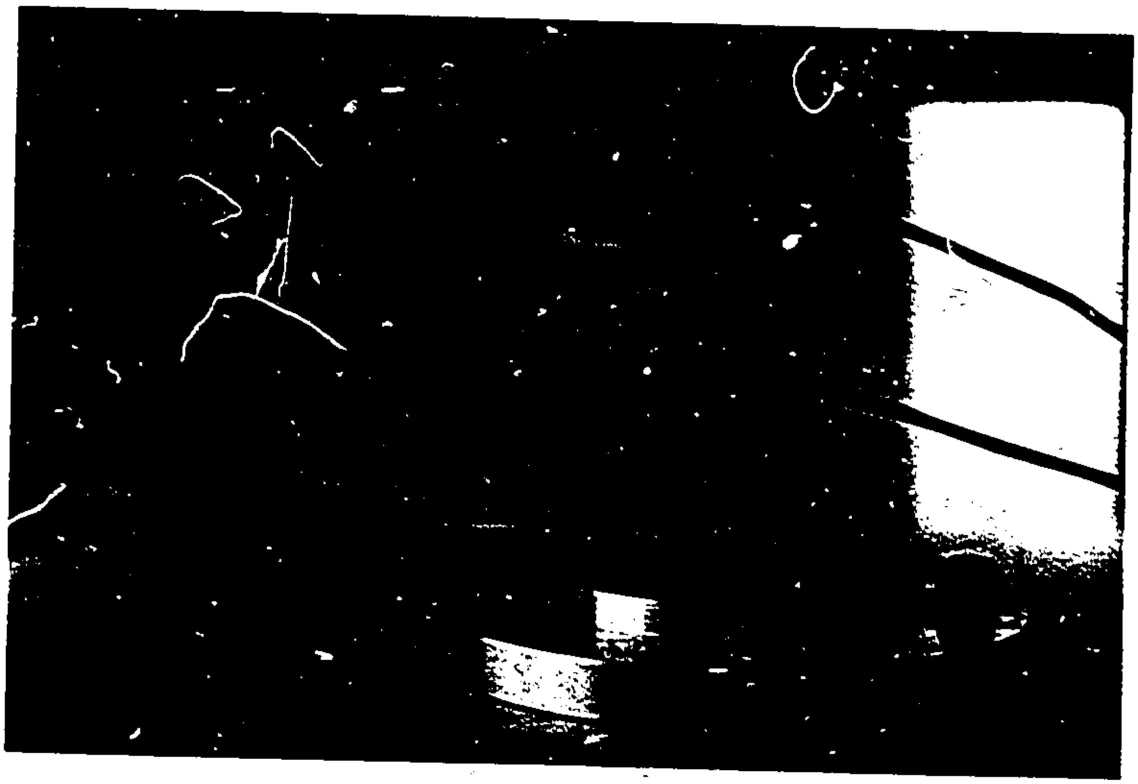

FIG. 3.4. Load cell and LVDT for measuring load and displacement in the normal direction.

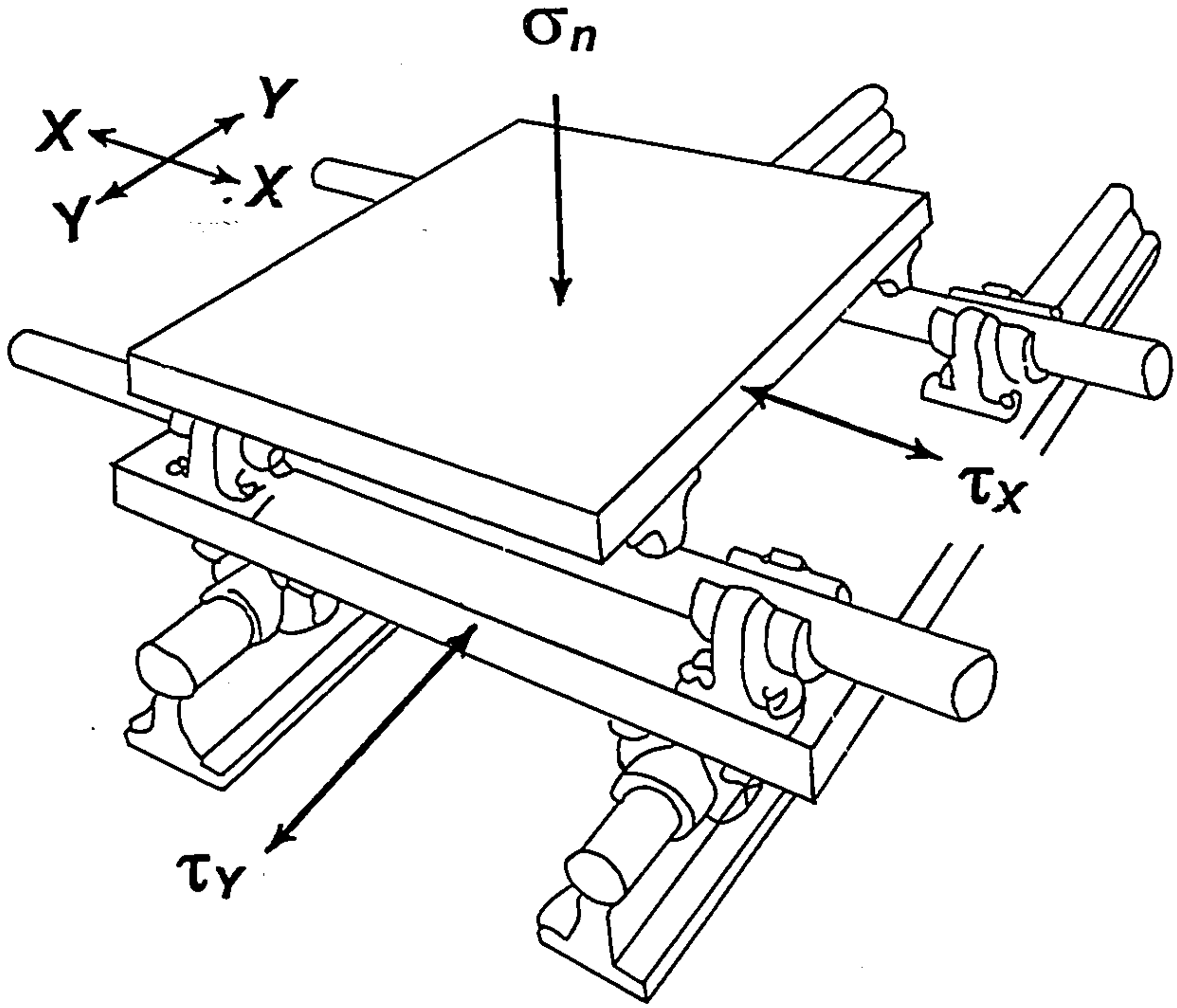

FIG. 3.5. Perspective of the *X-Y* loading table.

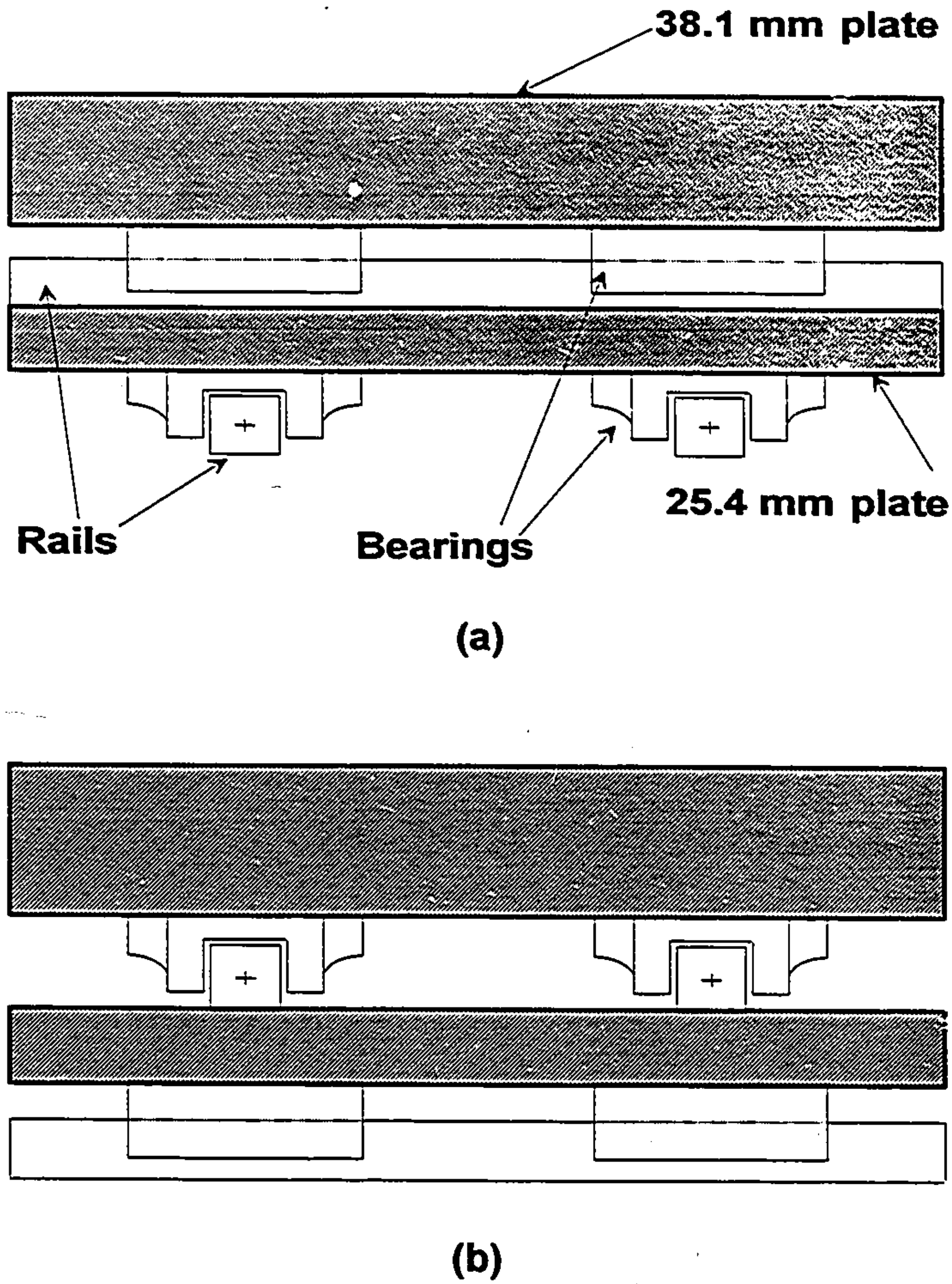

FIG. 3.6. *X-Y* loading table: (*a*) Front view; (*b*) Lateral view.

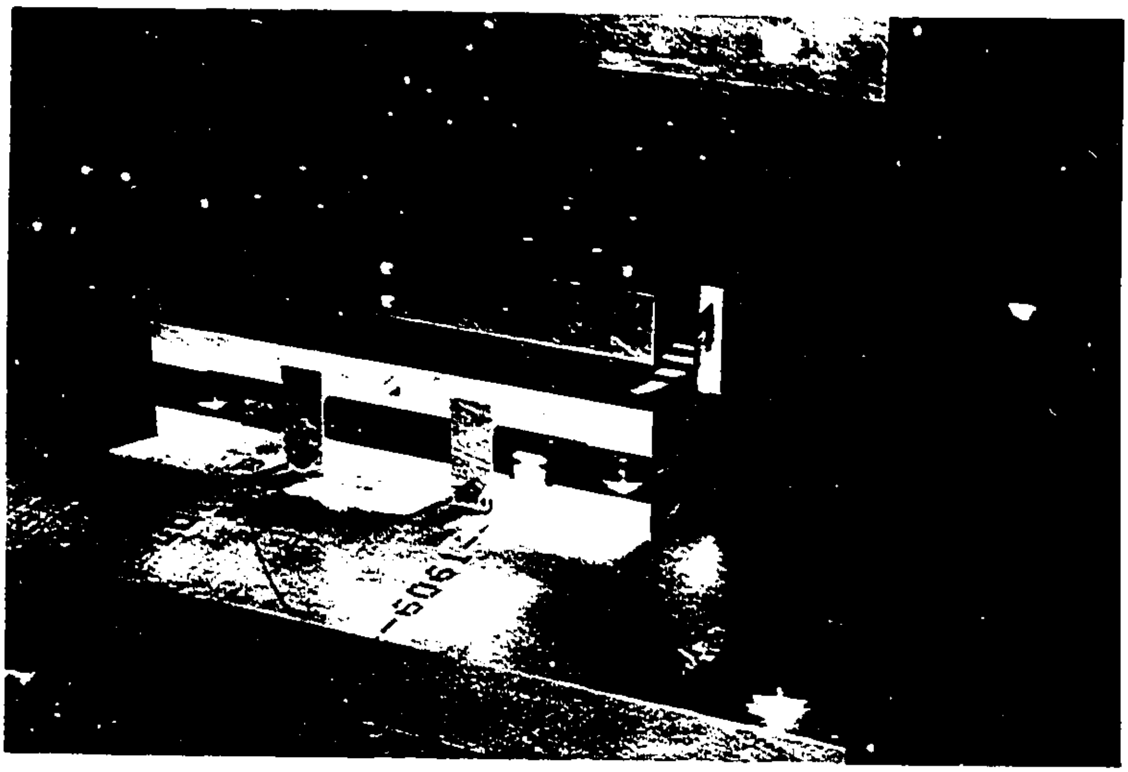

FIG. 3.7. *X-Y* loading table during construction of C3DSSI.

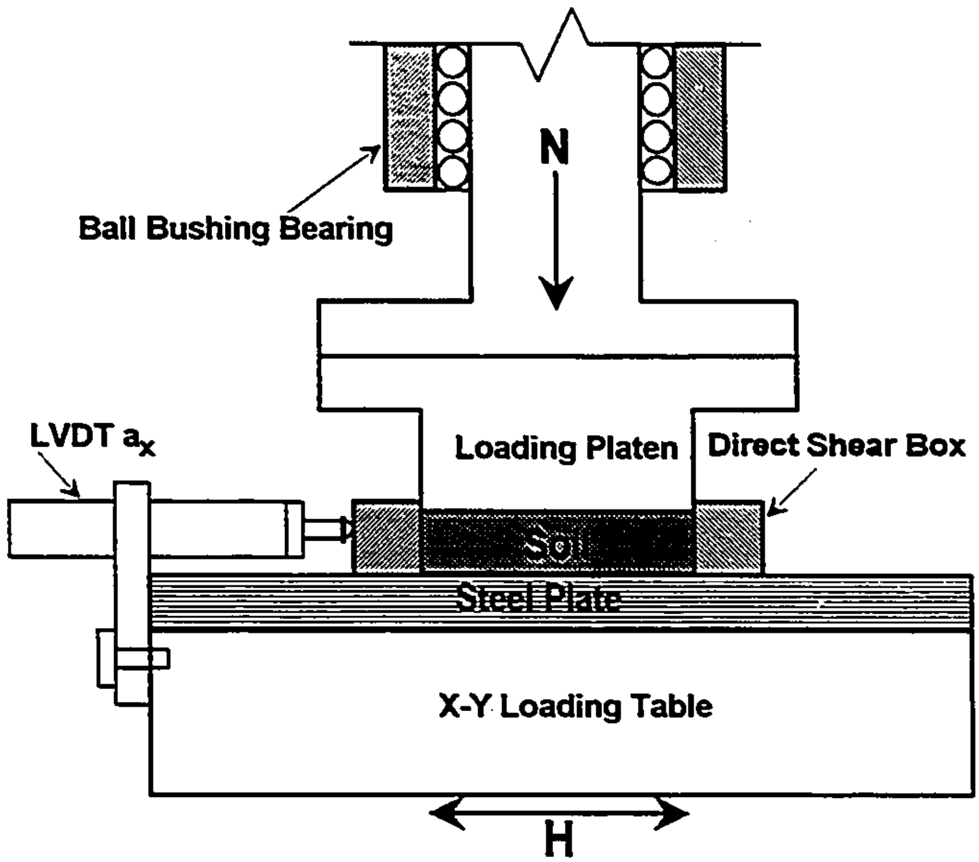

FIG. 3.8. Schematic of the direct shear box assembly (C3DI).

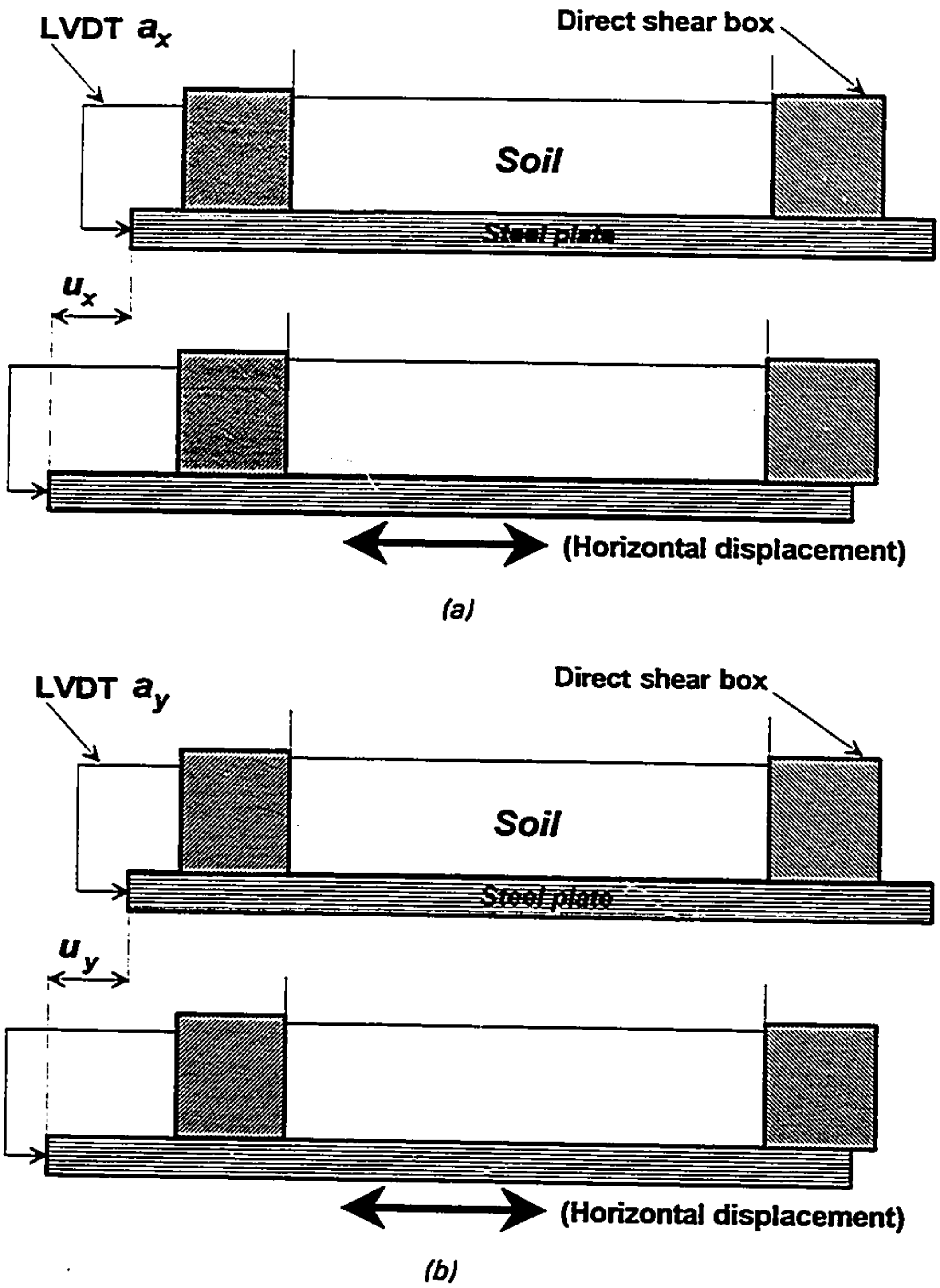

FIG. 3.9. Schematic diagrams of tangential displacements for direct shear box: *(a)* *x*-direction; *(b)* *y*-direction.

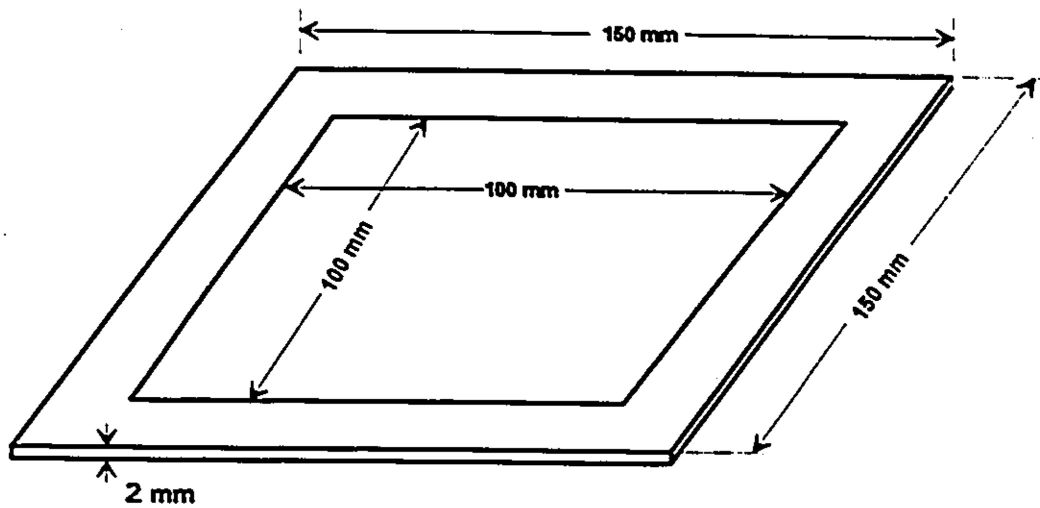

FIG. 3.10. Teflon coated aluminium plates used in the simple shear box.

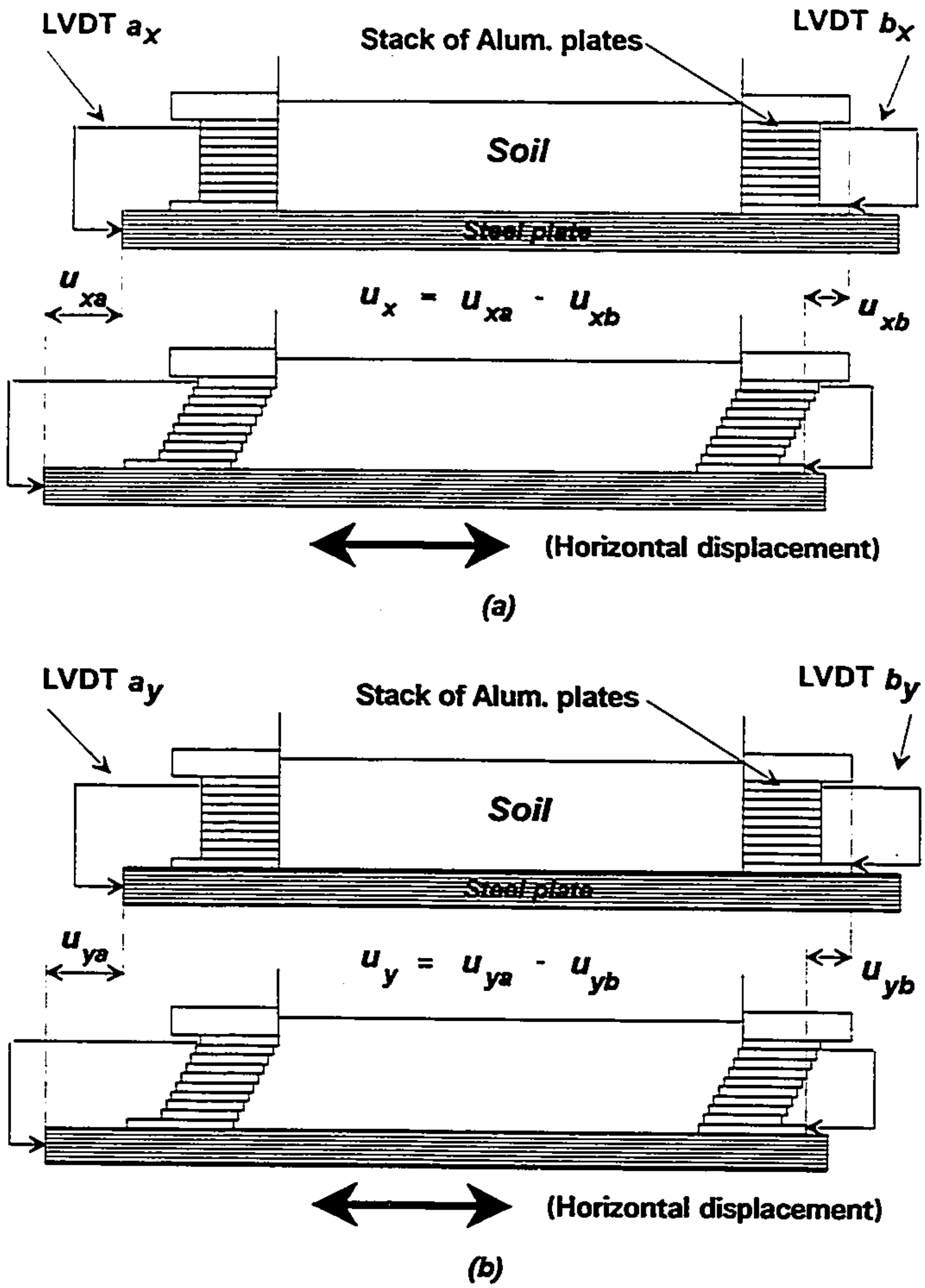

FIG. 3.11. Schematic diagrams of tangential displacements for simple shear box: *(a)* *x*-direction; *(b)* *y*-direction.

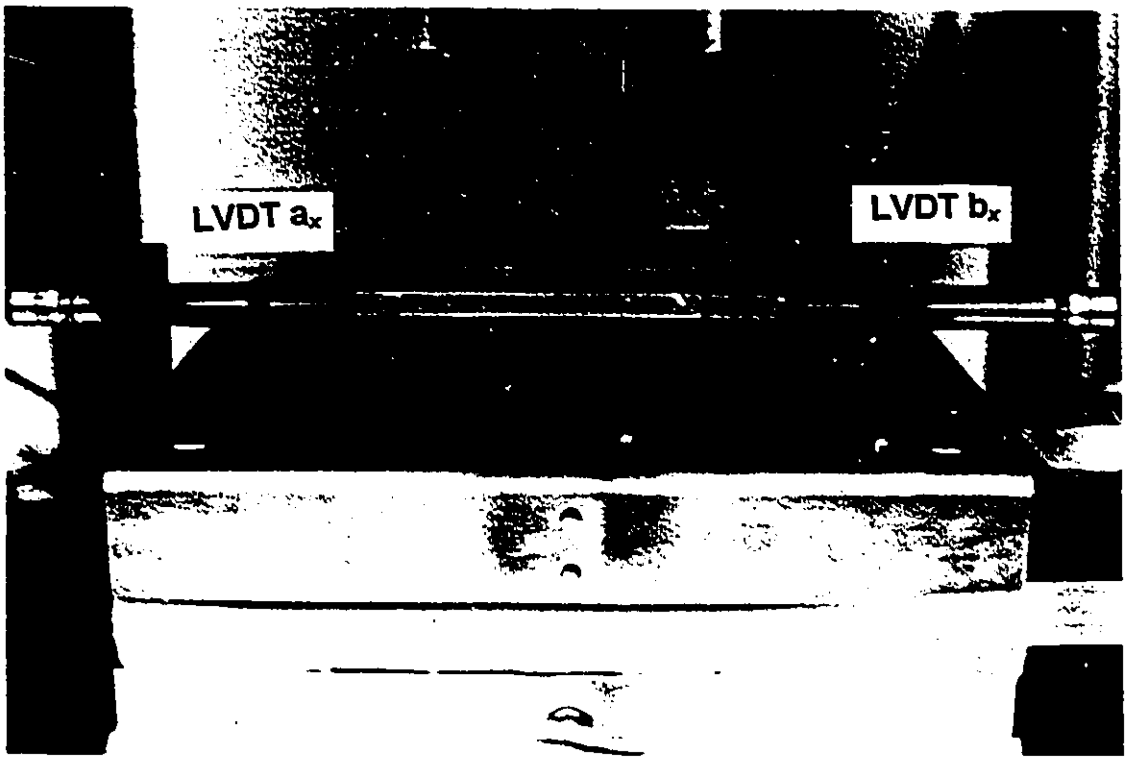

FIG. 3.12. Photograph of the simple shear box with LVDTs a_x and b_x.

LVDT a_x: to measure the total tangential displacement, u_{ax}

LVDT b_x: to measure the simple shear deformation of soil, u_{bx}
sliding displacement at the interface, $u_x = u_{ax} - u_{bx}$

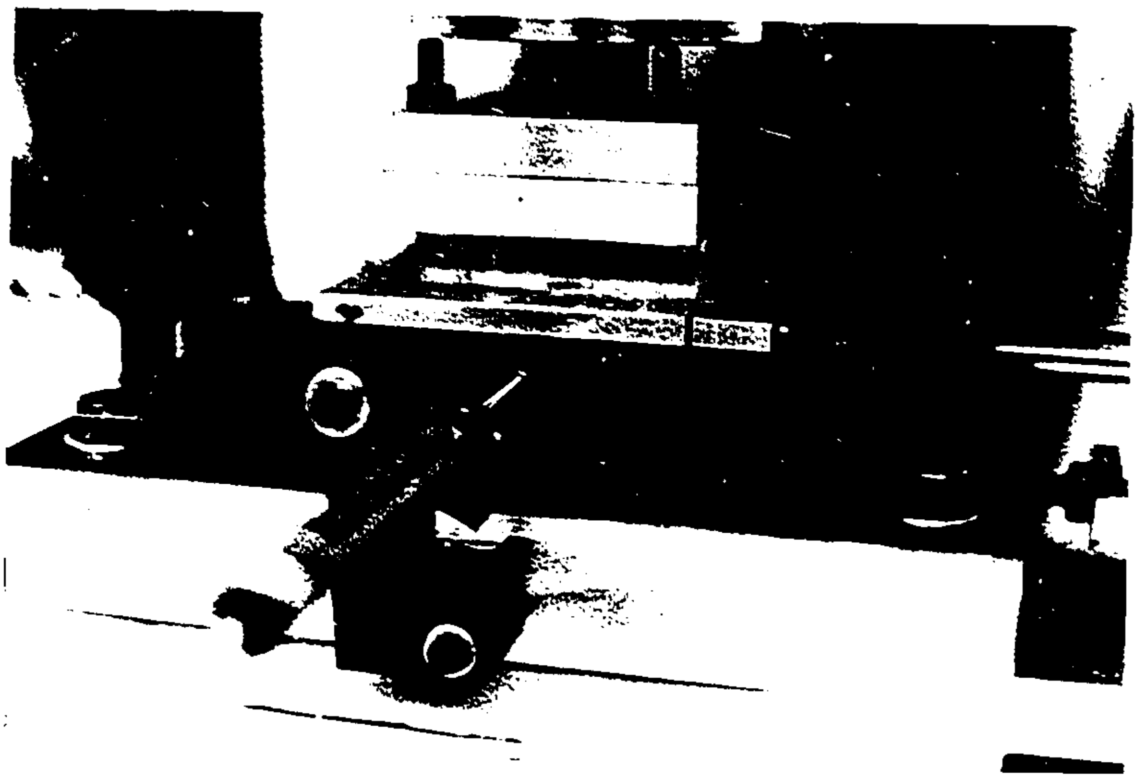

FIG. 3.13. Photograph of the simple shear box during a 3-D test.

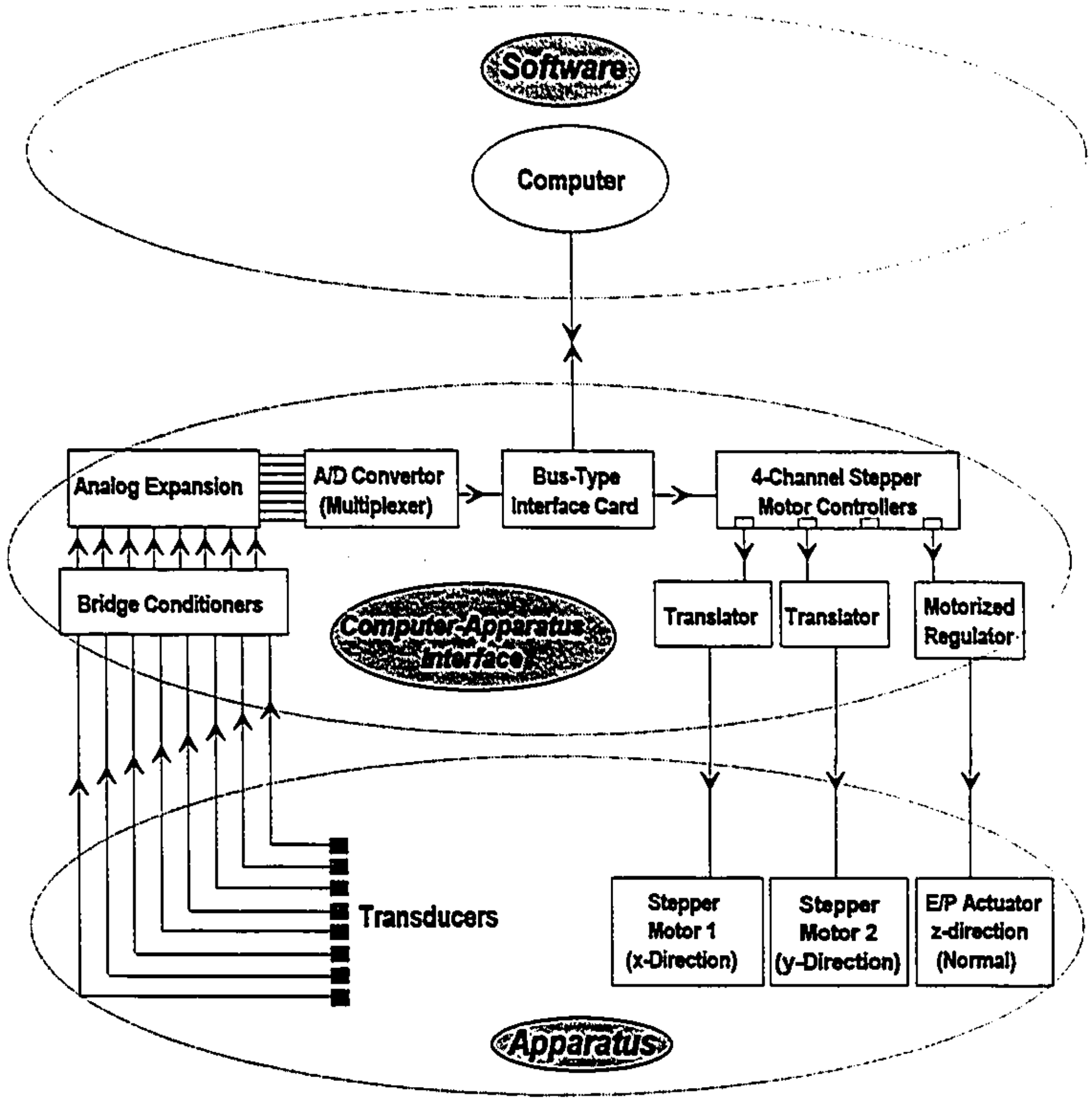

FIG. 3.14. Computer-controlled testing system.

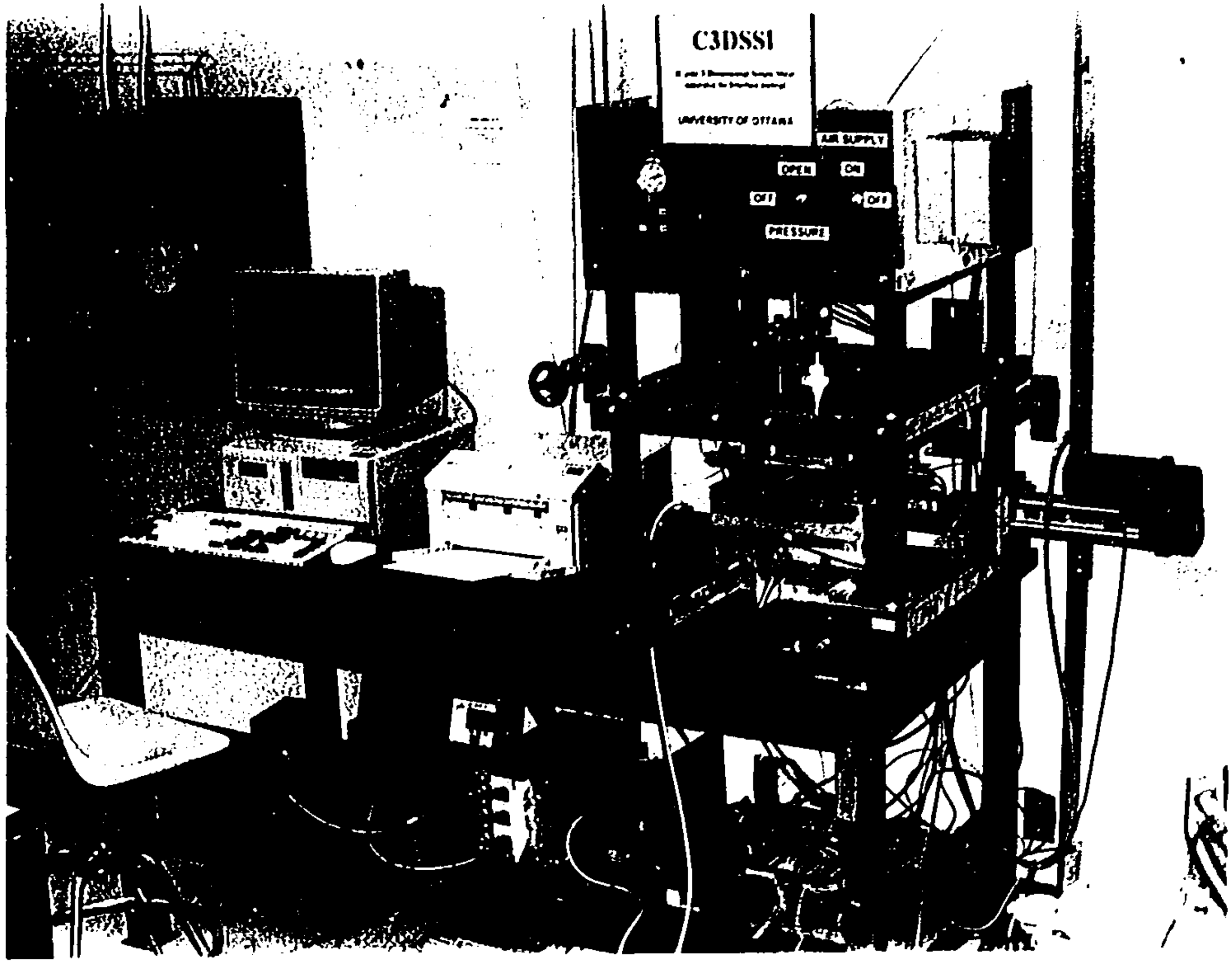

FIG. 3.15. Photograph of C3DSSI, stepper motor drivers, and computer-controlled interface unit system.

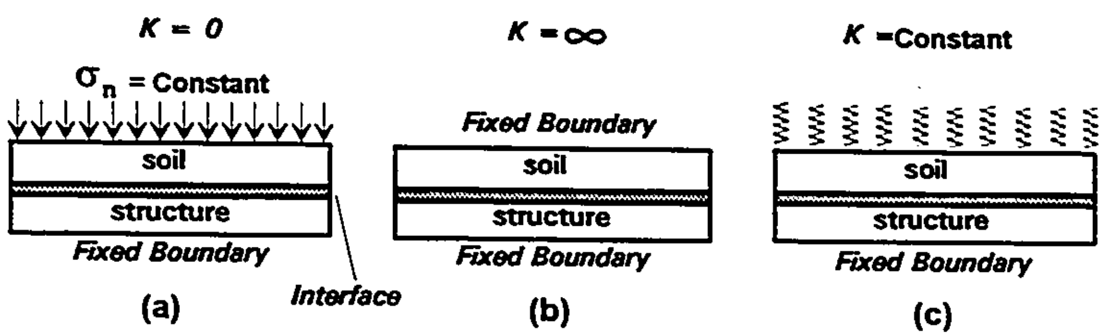

FIG. 3.16. Boundary conditions in the normal direction: (*a*) Constant normal stress; (*b*) Constant volume; (*c*) Constant normal stiffness.

CHAPTER 4

TESTING PROCEDURE

This chapter first describes the materials used throughout this study. Then the specimen preparation and placement procedures are described. Finally the correction of measured loads and displacements are discussed.

4.1 Interface Materials

• **Sand:** Three types of air-dried quartz (Silica) sands were used as the soil sample throughout this study. General properties of these sands are given in Table 4.1 and the grain size distributions are illustrated in Fig. 4.1. These sands were selected to study the effects of grain size and also grain shapes of the sand particles on the strength parameters and stress-displacement relations of interfaces. The results of such parametric studies are presented in Chapter 5. Sand No. 2 which is a medium crushed quartz sand with D_{50} of 0.6 mm was used in all other experiments, such as 3-D and constant normal stiffness tests, for studying the effect of various stress paths on the behaviour of sand-steel interface.

Table 4.1. Properties of Sands

Sand type	Mean grain size D_{50}(mm)	Max. unit weight γ_{max}(kN/m^3)	Min. unit weight γ_{min}(kN/m^3)	Min. void ratio e_{min}	Max. void ratio e_{max}
1. Coarse crushed Quartz	1.2	15.84	13.16	0.673	1.014
2. Medium crushed Quartz	0.6	16.05	13.09	0.651	1.024
3. Ottawa sand 20-30 (ASTM C-190)	0.7	17.71	15.37	0.496	0.724

• **Structural Material:** A 300 × 300 mm low carbon steel plate was selected as the structural material. It has been observed that the asperities of the surface have a significant effect on the behaviour of interface. The degree of roughness of a surface is usually defined based on the roughness profile which is a profile resulting from the intersection of a surface by a plane normal to the surface. The maximum peak-to-valley height, R_{max}, proposed by DIN standard, is used here to give a measure of surface roughness. When the single peak-to-valley Z_i is given for each of the five sampling lengths along the center line of the roughness profile (Fig. 4.1), R_{max} is represented by:

$$R_{max} = \frac{Z_1 + Z_2 + Z_3 + Z_4 + Z_5}{5}$$

The sampling length, L, could be adjusted as 0.25, 0.8, 2.5, or 8 mm, on the surface roughness tester used for this study. The best choice of L for sand-structural material interfaces would be the one closest to the mean grain size, D_{50}, of sand as suggested by Uesugi and Kishida (1987). In this study L has been set on 0.8 mm which is the closest to D_{50}s of 0.6, 0.7, and 1.2 mm as shown in Table 4.1.

Four types of surfaces are used in this study:

I. Smooth: which is a well-finished steel surface with R_{max} of 4 μm for $L = 0.8$ mm.

II. Sand blasted: The smooth surface was uniformly sand blasted to increase the roughness of the surface to 25 μm for $L = 0.8$ mm.

III. Artificially rusted surface: The surface of the steel plates can be artificially rusted in order to simulate a rough surface. The procedure was as follows:

- The surface was sand blasted to remove coats.
- The plate was submerged in Sodium Hydroxide solution, NaOH, with a normality of 0.3 for about 10 minutes to remove any grease existing on the surface.
- Then the plate was exposed to an HCl saturated environment. A period of four to eight weeks was sufficient to bring the surface to the desired surface roughness. The surface was cleaned to remove loose shallow layers of rust on the surface before it was employed as a rough steel specimen.

IV. ALO cloth: Aluminium Oxide (ALO) cloth (a type of sand paper) was also pasted on the plate to simulate a rough surface. They are commercially available at different numbers from fine to coarse surfaces. The use of ALO cloth provides a uniformly distributed roughness for investigating the effects of surface roughness on the interface behaviour. The ALO cloth was replaced at the beginning of each test to ensure that the initial surface roughness was the same.

4.2 Sample Preparation and Placement

4.2.1 Relative density of sand

Medium to dense sands were prepared by means of the Multiple-Sieving-Pluviation method, MSP, described by Miura and Toki (1982), with some modifications. The

Multiple-Sieving-Pluviation device used in this study has a funnel at the top for stocking the sand. The funnel is supported by a perspex cylinder as illustrated in Fig. 4.3. Six No. 4 sieves (opening 4.75 mm) are put under the funnel. Below these sieves at an adjustable distance is the soil container. The reason for stacking six sieves is to ensure uniform deposition of sand, and, therefore, produce a homogeneous sample. The rate of sand discharge is controlled by changing the diameter of the nozzle, d_n, attached at the bottom of the funnel.

A small bullet shape object was aligned with the centre line of the perspex cylinder between the funnel and sieves, to disperse the sand during flow before reaching the sieves, causing to increase the uniformity of relative density along the sand container. This was verified by using a number of graduated plastic tubes arranged as illustrated in Fig. 4.4. Line 1 shows the distribution of sand particles with 4 sieves and no bullet shape object. The influence of increasing the number of sieves from 4 to 6 is shown by line 2. Ultimately, line 3 is monitoring the effect of hanging the bullet shape object. A knife edge collar was placed on top of the soil container during sand pluviation to prevent sand particles from falling back into the soil container.

It seems that relative density can be produced under various combinations of the nozzle diameter, d_n, and the height of fall, h_f. However, it was observed in this study that the height of fall, that is defined as the distance between the lowest sieve and the base of the soil container, had little or no effect on the relative density. Change in relative density due to controlling the nozzle diameter was noticeable (Table 4.2). This agrees with results obtained by Miura and Toki (1982) except that no relative density less than 65% could be achieved.

Table 4.2. Multiple-Sieving-Pluviation method, MSP, for preparing medium to dense samples. h_f = 550 mm

	nozzle diameter, d_n (mm)					
	9	**13**	**18**	**24**	**35**	**scoop**
Sand 1	85 %	82 %	79 %	74 %	65 %	
Sand 2		88 %	84 %	75 %		60 %
Sand 3		93 %	88 %	84 %		62 %

For preparing loose sand samples, a funnel was moved uniformly by hand over the sand container at a certain height to achieve the desired relative density. Table 4.3 shows the obtained results. This method is referred to as Direct-Raining-Method.

Table 4.3. Direct-Raining-Method for preparing loose to medium samples.

	d_n=9 mm			d_n=13 mm		
h_f (mm)	200	150	100	200	150	100
Sand 1	59 %		48 %	40 %	33 %	24 %
Sand 2	30 %		24 %	17 %	12 %	8 %
Sand 3	38 %		26 %	17 %		6 %

4.2.2 Direct shear

To prepare the specimen for each test, the hollow aluminium box (soil container) was positioned at the center of the steel specimen. The sand was rained into the container at the desired density by one of the described methods. The top part of the sand specimen was levelled by a suction device. Then the plate which carried the soil container was fixed to the top of the *X-Y* loading table. Subsequently, the loading platen was moved downward to touch the sand surface. One LVDT for measuring the normal displacement in the *z*-direction and two LVDTs for measuring the shear displacements in the *x*- and *y*-directions were mounted before starting a test.

4.2.3 Simple shear

In order to align the stacks of Aluminium plates (simple shear box) in vertical direction, the 2 mm thick aluminium plates were piled up around a dummy sample as shown in Fig. 4.5. A hollow area is made on top of the dummy sample which is slightly larger than the cross-section area of loading platen. While the loading platen was lowered, the dummy sample and the stacks of aluminium plates around it were moved horizontally until the loading platen penetrated into the hollow part of the dummy sample. In this way the soil container plates were positioned correctly. Then the stack of plates were pressed down by four clamps at the corners to prevent the misalignment and misplacement of the plates.

The steel specimen together with the soil container plates were moved out of the apparatus, the dummy sample was removed, and then the sand was rained into the container. The top part of sand was levelled off by means of suction and then steel specimen and the soil container were placed back in the apparatus. After lowering the loading platen and placing it on the sand surface, the clamps for holding the stack of plates are removed. The steel specimen was fixed to the X-Y table by four bolts at the corners and the desired normal load was applied by the pneumatic actuator. Finally the LVDTs for measuring the tangential displacements were mounted across the specimen.

4.3 Correction of Measured Loads and Displacements

Whenever it was necessary, corrections were made on the measured values of load and displacements in order to take into account the following factors: 1) deformation of the testing apparatus under the applied loads; and 2) friction between the interior walls of the direct shear box and sand, friction at the bottom of the box, and also the friction in the linear bearing systems. Deformation of the testing device affects the measured displacements in the normal and tangential directions, while the friction affects the values of forces measured by the load cells.

The effect of the stiffness of C3DSSI on the measured values of displacements, in the vertical and horizontal directions, was taken into consideration. The vertical stiffness was measured at different load levels by using a rigid dummy sample instead of the soil. The load-displacement relation was linear and repeatable with a stiffness of 5000 kPa/mm. The maximum normal stress in the present study was only 500 kPa. For tests under the condition of constant normal stress, no corrections were required. Corrections were made for the tests under the condition of constant normal stiffness, however. For the horizontal stiffness no corrections were required since the tangential displacements were measured across the specimen.

The amount of normal force transferred to the interior walls of the direct shear and simple shear boxes was calculated on the basis of an estimated K_o for the sand and the angle of friction between the Aluminium surface and sand. It was found that about 10 % of the normal load is taken by the friction at the inside walls. Furthermore, since this load induces stresses at the bottom of the direct shear box, the tangential load required to overcome its shear resistance had to be subtracted from the tangential load measured by the load cell. An additional correction was also made to account for the friction in the bearing system which was found to be about 20 N (equivalent to 2 kPa stress at the interface). As a result, there were reductions in both normal and shear stresses. Calculations showed that the stress ratio, τ / σ_m, would be overestimated by up to 2 % if the corrections were not made.

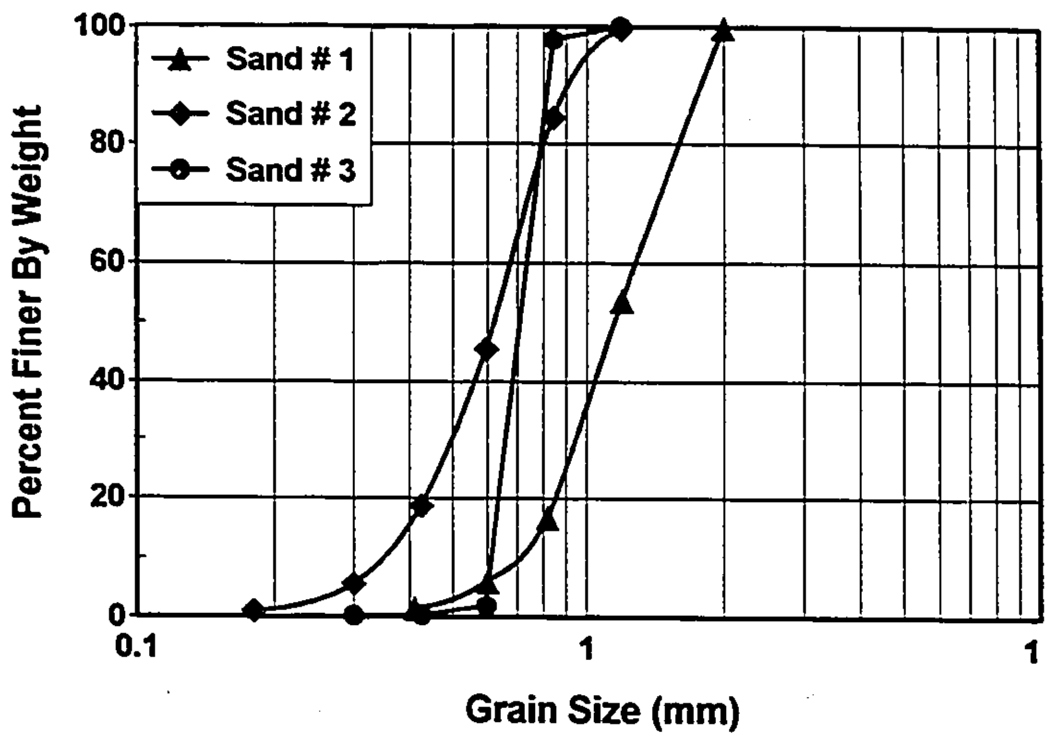

FIG. 4.1. Grain size distributions.

Sand # 1: Coarse Crushed Quartz (local # 16)

Sand # 2: Medium Crushed Quartz (local #24)

Sand # 3: Ottawa Sand, 20-30, ASTM C-190

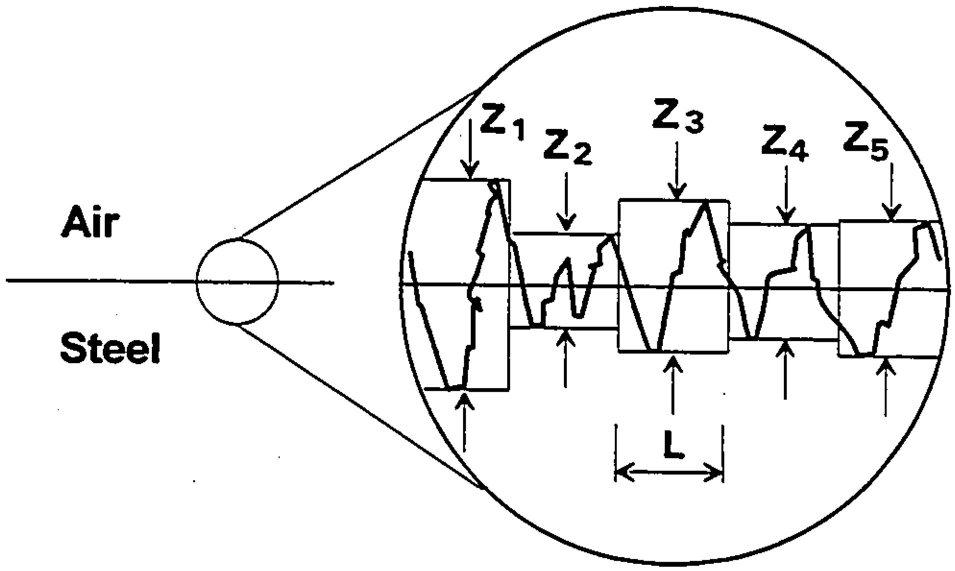

L : Gauge length

$$R_{max} = \frac{Z_1 + Z_2 + Z_3 + Z_4 + Z_5}{5}$$

FIG. 4.2. Illustration of surface roughness, R_{max}.

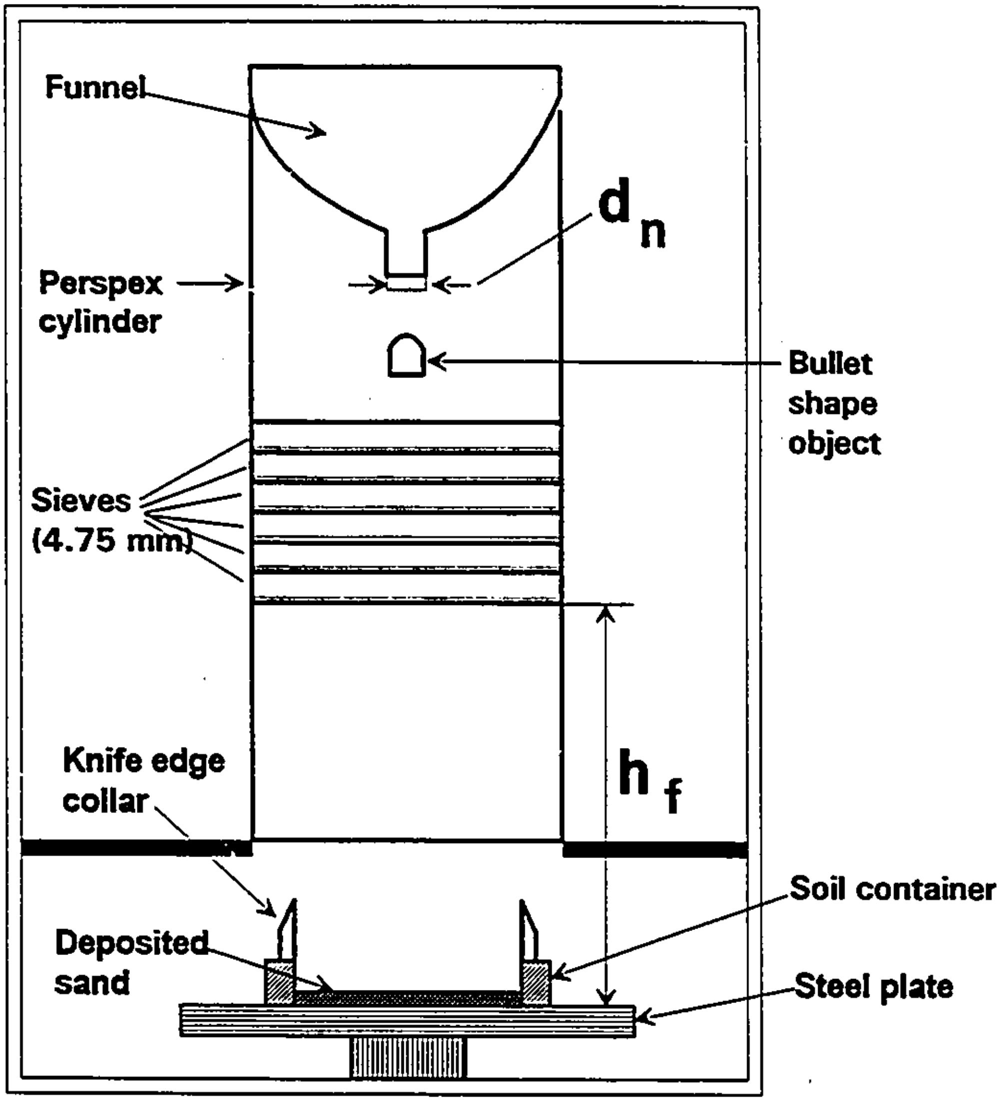

FIG. 4.3. Schematic view of Multiple-Sieving-Pluviation device.

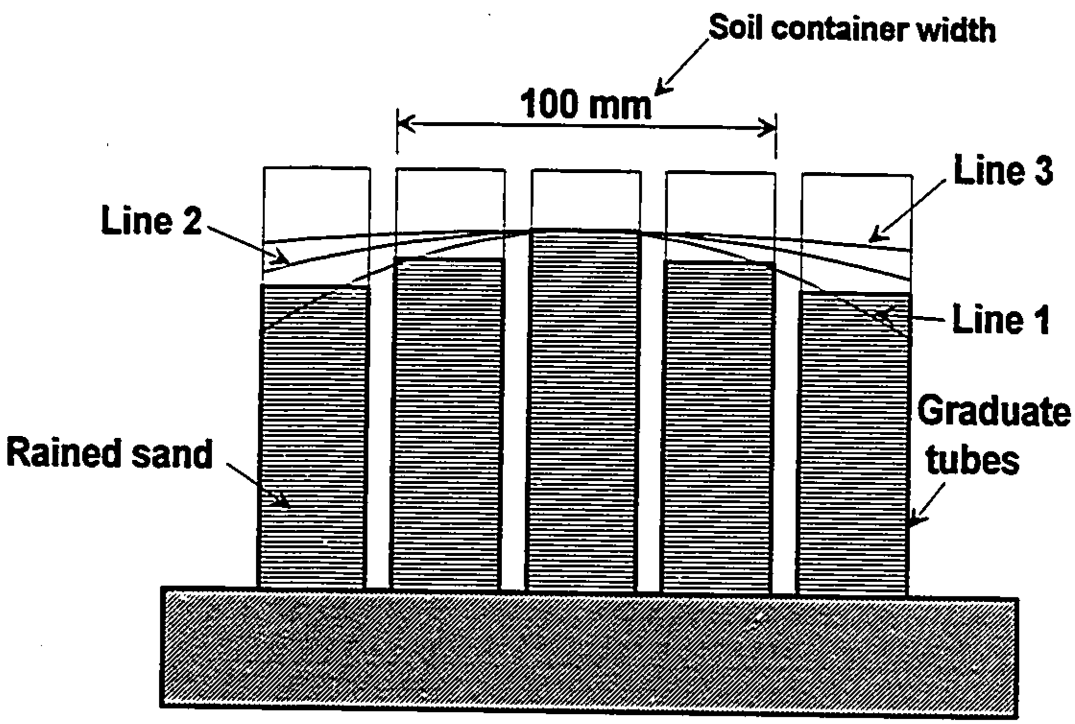

FIG. 4.4. Graduated plastic tubes for checking the uniformity of deposition of sand.

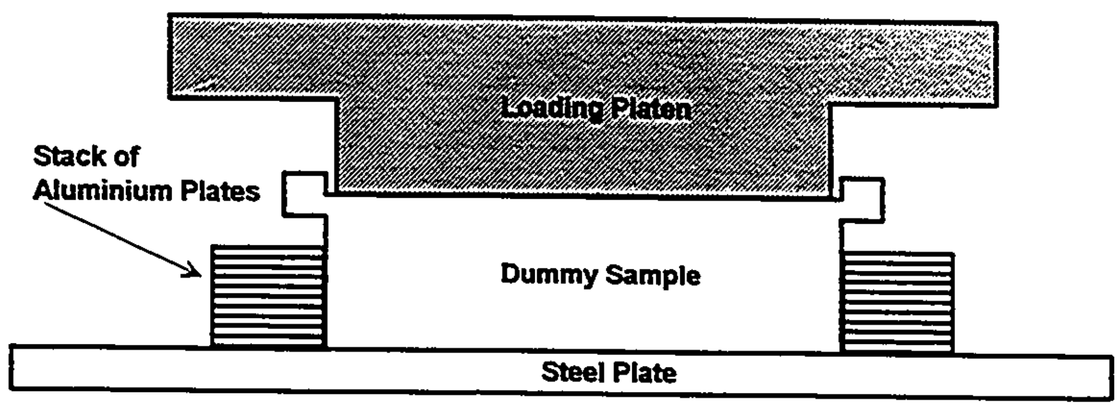

FIG. 4.5. Aligning and positioning of the stack of aluminium plates by the dummy sample.

CHAPTER 5

2-D CONSTANT NORMAL STRESS TESTS

(Verification of the New Apparatus)

5.1 Introduction

This chapter presents the results of some 2-D monotonic and cyclic tests under the condition of constant normal stress. The objective is to demonstrate the reliability of the operation of the automated control system and the performance of the mechanical components of the new interface testing apparatus. Effects of several parameters on the stress-displacement relations of interfaces are investigated. Comparisons are also made between the results obtained from the direct shear and the simple shear soil containers.

5.2 Monotonic Loading

The effects of magnitude of normal stress, initial relative density of sand, surface roughness, roundness of sand particles, and rate of shearing on the stress-displacement relations of interfaces are investigated in this section. The results of two monotonic tests are presented first to introduce the typical stress-displacement relations of interfaces. The first test result, illustrated in Figs. 5.1, is obtained by using the direct shear box. The second test result is obtained by using the simple shear box as shown in Fig. 5.2. These results are hereafter used as a benchmark for comparison purposes to study the effect of various parameters on the behaviour of sand-steel interfaces.

In both tests, the interface was subjected to an initial normal stress of 100 kPa and then monotonically sheared up to a total tangential displacement of 5 mm. Thesc experiments were displacement controlled using LVDT a_x (Figs. 3.9*a* and 3.11*a*), and the rate was 1 mm/min. The magnitude of normal stress was maintained constant during the process of shearing. The normal displacement, shear stress, and tangential displacement(s) were recorded at 5-second intervals.

Figures 5.1*a* and 5.1*b* show the plots of shear stress, τ, versus tangential displacement, u_x, and normal displacement, v, versus tangential displacement, u_x, respectively, for the interface between the sand blasted steel plate (R_{max} = 25 μm for L = 0.8 mm) and No. 2 sand with initial relative density of 88 %. The direct shear box was used as the soil container. A well-pronounced peak was observed at the shear stress of 80.0 kPa corresponding to tangential displacement of 1.14 mm. The shear stress then decreased and approached a residual shear stress of 62 kPa. The variation of normal displacement exhibited a small amount of compression at first, followed by dilation which is typical for an interface between a rough surface and dense sand.

Similar results were obtained from the experiments using the simple shear box as illustrated in Fig. 5.2. Two sets of tangential displacements. a_x and b_x, were measured as described in Section 3.4. Figure 5.2*a* illustrates the shear stress, τ, versus total tangential displacement, u_{xa}. The peak and residual shear strengths were 80.3 kPa and 62.0 kPa, respectively. The peak shear strength was reached at a total tangential displacement of 1.4 mm. Similar to the results obtained by direct shear box, the variation in normal displacement, shown in Fig. 5.2*b*, indicates a small amount of compression at first followed by a large amount of dilation. The test data also show that the peak strength was reached at the point of inflection of the normal displacement curve (Fig. 5.2b).

The total tangential displacement, u_{xa} consists of the sliding displacement, u_{xr} and the displacement due to the shear deformation of sand, u_{xb} as was illustrated in Fig. 3.11. It was observed that the major portion of shear deformation of sand took place before the peak shear strength was reached (Fig. 5.2*d*). Thereafter, the shear deformation of the sand mass was negligibly small while the sliding displacement at the contact surface continued (Fig. 5.2*c*). This observation indicated that the shear strength of the soil mass was higher than the shear strength at the interface. Otherwise, the shear failure would have occurred within the sand mass. The peak shear strength of this sand at 84% initial relative density measured 100 kPa under σ_n of 100 kPa which was 20% higher than the shear strength of the interface. The peak shear strength was reached at a sliding displacement of 0.6 mm. At this point, the shear deformation of the sand mass was 0.8 mm. The summation of these two values would result in the total tangential displacement of 1.4 mm as shown in Fig. 5.2*a*. These results are in good agreement with those reported by Uesugi and Kishida (1986) for an interface between Toyoura sand and a steel plate.

5.2.1 Effect of Normal Stress

Three tests were carried out in the direct shear box using the No. 1 sand and ALO cloth # 150 (very coarse) under constant normal stresses of 100, 250, and 500 kPa. The results are presented in Figs. 5.3 and 5.4.

Figures 5.3*a* and 5.3*b* show the plots of shear stress-tangential displacement and normal displacement-tangential displacement, respectively, for dense sand (D_r = 80 %) samples. Similar plots for loose sand (D_r = 25 %) are shown in Figs. 5.3*c* and 5.3*d*. A well-pronounced peak is observed for dense sand results, whereas loose sand samples exhibited a less pronounced peak. Both loose and dense samples compressed first followed by dilation during shearing. Loose samples, however, dilated much less than the dense samples. Moreover, the rate of dilation is lower at high normal stresses.

The normalized results of Figs. 5.3*a* and 5.3*c* are illustrated in Figs. 5.4*a* and 5.4*b*, for dense and loose sands, respectively. The maximum stress ratio, i.e. the coefficient of friction, $(\tau / \sigma_n)_{max}$, was higher at low normal stresses. The same trend was observed for loose samples except that the peak was less pronounced than that of dense samples. However, the post-peak behaviour showed softening as such that the response curves approached a residual stress ratio of 0.65 for both dense and loose samples irrespective of the magnitude of normal stress.

Similar results are presented in Fig. 5.5 between the No. 2 sand and the sand blasted steel plate (R_{max} = 25 μm for L = 0.8 mm) under normal stresses of 100, 300, and 500 kPa, by using the simple shear soil container. The initial relative density of sand was 88 %. Here also the peak stress ratio, $(\tau / \sigma_n)_{max}$, was higher for low normal stress as illustrated in Fig. 5.5*d*. The peak stress ratio varied between 0.76 and 0.80 for normal stresses ranging from 500 to 100 kPa. Figure 5.5*a* indicates that a greater sliding displacement was required to mobilize the peak shear stress for a higher normal stress (e.g. 0.6 mm for 100 kPa and 1.0 mm for 500 kPa). A similar trend is observed in plots of shear stress versus shear deformation of sand in Fig. 5.5*c*.

5.2.2 Effect of Initial Relative Density of Sand

Based on the results obtained by using the direct shear box, it was shown in the previous section that a well-pronounced peak was observed for the dense sand. Similar results for an interface between the sand blasted steel plate and the No. 2 sand are presented in Figs. 5.6 and 5.7. The constant normal stress was 100, 300, and 500 kPa in these tests. The simple shear soil container was used in the experiments. The results obtained for initial relative densities of 88 % and 22 % are presented to demonstrate the effect of dense and loose sand specimens on the behaviour of the interface. Figures 5.6*c* and *d* indicate that in the case of loose sand (D_r = 22 %), shear deformation of sand mass exceeded the sliding displacement at the interface, showing that the failure had occurred within the sand mass. In other words, the angle of internal friction for the loose sand was smaller than the angle of friction between the loose sand and the steel plate. The higher dilatancy potential of the dense sand is demonstrated in Fig. 5.6*b*.

The results shown in Fig. 5.6 were normalized by the normal stress and they are presented in Fig. 5.7. Higher peak strengths were observed for the dense sand and for low normal stresses. It seems, however, that the residual stress ratios were approximately the same, irrespective of the magnitude of the normal stress, and the relative density of sand. This is due to the fact that the dense sand work softened and loose sand work hardened during shearing and eventually approached a stable stress ratio which was about 0.6 for the materials tested.

Another set of test results are presented in Fig. 5.8. The interface was between the No. 2 sand and the sand blasted steel plate. These tests were conducted under the normal stress of 100 kPa for initial relative densities of 15, 30, 45, 60, and 88 %. The shear stress-displacement plots clearly indicate that the peak strengths were high at higher densities. The residual strengths were the same, however. Figures 5.8*c* and *d* indicate that the shear deformation of the sand mass increased with decrease in relative density. For initial relative densities of 30 % and higher, a pronounced failure occurred at the interface as shown in Fig. 5.8*c*, whereas for the 15 % case, shear deformation continued within the sand mass.

5.2.3 Effect of Surface Roughness

The effect of three different surface roughnesses on the stress-displacement relations of the interfaces are demonstrated in Fig. 5.9. The surfaces include the smooth steel surface (R_{max} = 4 μm for L = 0.8 mm), sand blasted steel plate (R_{max} = 25 μm for L = 0.8 mm), and the artificially rusted steel plate. The surface roughness of the rusted plate was not monitored because of the risk of damaging the needle of the surface roughness profiler device. The presented results indicate that surface roughness significantly affected the peak and residual strengths as well as the stiffness of both sliding displacement response as well as shear deformation of the sand mass. The interface response to volume change became more dilative as the roughness of the interface increased.

Several tests were performed between the No. 2 sand and the smooth steel plate (R_{max} = 4 μm for L = 0.8 mm) under normal stresses of 100, 300, and 500 kPa. Results are presented in Figs. 5.10 and 5.11.

Figure 5.10 indicates that:

- A pronounced peak is observed at the interface for both dense (D_r = 88 %) and loose (D_r = 22 %) sands.
- No difference exist at peak and residual strengths between dense and loose sands.
- The initial stiffness of loose sand, i.e. the ratio between shear stress and tangential displacement, is low for loose sands.
- As normal stress increased, a clear stick-slip behaviour was observed after peak strength.
- The volume change results of Fig. 5.10*b* show compression for all cases, however, loose sand compressed more than the dense sand.

The normalized results of Fig. 5.10, presented in Fig. 5.11, illustrate that normal stress had no effect on the stress ratio as opposed to the rough surface that the peak strength was high at low normal stresses. This fact is more clearly demonstrated in Fig. 5.12, which compares the results of tests on interfaces with rough and smooth surface. These tests were performed using dense sand samples under various normal stress conditions.

5.2.4 Effect of Roundness of Sand Particles

A comparison is made between the stress-displacement relations of the No. 2 sand (crushed quartz with D_{50} = 0.6 mm) and the No. 3 sand (Ottawa sand with D_{50} = 0.7 mm). The results of four tests on interfaces between these sands in dense state (initial relative densities of 88 % and 92 % for the No. 2 and No. 3 sands, respectively) and rough and smooth surfaces are presented in Fig. 5.13. The normal stress was 500 kPa. It is observed that:

- Sand No. 2 experienced higher peak and residual strengths for both rough and smooth surfaces compared to sand No. 3. This is attributed to the angularity of the particles in the crushed sand. Increasing angularity increases the interlocking of the sand grains with the asperities of the steel plate.

- The stick-slip mode in the case of smooth surface was observed in both sands. This observation complies with the results reported by others (e.g. the presented results in Fig. 2.8 by Yoshimi and Kishida, 1981).

- Higher dilation was experienced by the interface between Ottawa sand and the rough surface.

5.2.5 Rate Effects

The behaviour of the interface was examined for rate of shearing effects under various normal stresses and surface roughness. The results are presented in Figs. 5.14 through 5.16. The results indicate that rate of shearing had no effect on the stress-displacement relations of sand-steel interfaces for the examined rates between 0.1 to 10 mm/min. This behaviour is shown in Figs. 5.14 and 5.15 which illustrate the stress-displacement relations of interfaces between loose (D_r = 22 %) as well as dense (D_r = 88 %) No. 2 sand and the smooth steel plate (R_{max} = 4 μm for L = 0.8 mm), under normal stresses of 100, 300, and 500 kPa.

Three other tests were conducted under tangential displacement rates of 0.1, 1, and 10 mm/min. The interface was between the No. 2 sand at D_r = 88 % and the sand blasted steel plate (R_{max} = 25 μm for L = 0.8 mm), and was subjected to a normal stress of 100 kPa. As illustrated in Fig. 5.16, no difference was observed in the stress-displacement plots of those interfaces due to the variations in the tangential displacement rates.

5.3 Cyclic Loading

Two displacement controlled cyclic tests were performed under a constant normal stress of 500 kPa at a tangential displacement amplitude of 1 mm. The direct shear box was used in these tests. The load was applied sinusoidally with a period of 200 seconds. The surface in both tests was ALO cloth #150 (very rough). The No. 1 sand was used with relative densities of 80 % and 25 %. The test results are shown in Fig. 5.17. The total number of cycles, N, was 50. The tangential displacement amplitude of 1 mm chosen for the cyclic tests was less than the tangential displacement required for the interface to fail under monotonic loading conditions. The tangential displacement corresponding to the peak strength was 1.5 mm in the monotonic loading test for the normal stress of 500 kPa acting on the interface (Fig. 5.3*a*) between ALO cloth #150 and dense sand.

At the tangential displacement amplitude of 1 mm, the mobilized shear stress increased with increasing number of displacement cycles for both dense and loose sands, but the increase was higher for loose sand than that for dense sand. This behaviour is due to the densification of the sand. Both samples stabilized at a shear stress of about 400 kPa which is higher than the peak shear stress value of 360 kPa in the monotonic test. The general trend of these results is in good agreement with those obtained by Desai et al. (1985), which are presented in Fig. 2.12.

Similar tests were performed under a constant normal stress of 100 kPa between the medium crushed quartz sand (No. 2) and the sand blasted steel plate (R_{max} = 25 μm for L = 0.8 mm) by using the *direct* shear box. The tangential displacement amplitudes were 0.75 mm and 0.5 mm. For the same interface under monotonic loading conditions, the tangential displacement corresponding to the peak strength (80.0 kPa) was 1.14 mm as shown in Fig. 5.1. Under cyclic loading conditions, the shear stress increased with increasing number of cycles up to 80.3 kPa and 83.6 kPa at cycles 1 and 4, for the tangential displacement amplitudes of 0.75 mm and 0.5 mm, respectively (Fig. 5.18). After which the shear stress decreased and eventually stabilized at 62 kPa. The peak and residual shear strengths had about the same values as those in a monotonic test for the same conditions. Therefore, with amplitudes less than that required to fail the interface in monotonic shearing, the peak and post-peak conditions may or may not be reached in cyclic tests depending on the surface roughness and the magnitude of the tangential displacement amplitude.

A Similar cyclic test was conducted on an interface between the No. 2 sand and the sand blasted steel plate by using the *simple* shear box. The results are presented in Figs. 5.19 through 5.22. Total number of cycles was 55. The amplitude of total tangential displacement was set at 0.75 mm which is smaller than the total tangential displacement of 1.4 mm at peak for monotonic test (Fig. 5.2*a*). The amplitude of the sliding displacement at the interface and the shear deformation of sand mass varied with cycles as illustrated in Figs. 5.19*c* and *d*, respectively. The normal displacement experienced a gradual decrease, which is due to the compression of sand with cycles (Fig. 5.19*b*).

Figure 5.20 illustrates the same plots only at cycles 1, 12, and 55. The peak shear strength was reached at cycle 12. It is observed that the shear stress, which was 72.0 kPa at the maximum displacement amplitude during the first cycle, reached a peak of 83.0 kPa at cycle 12 after which the shear stress decreased and stabilized at 60.0 kPa.

The plots of shear stress versus time shown in Fig. 5.21 clearly illustrate the variation of shear stress with number of cycles. Shear stress amplitude stabilized after about 30 cycles equivalent to 6000 seconds.

Figures 5.22*a*, *b*, and *c* illustrate the total tangential displacement, shear deformation of sand mass, and sliding displacement with time, respectively. During the first cycle, the maximum shear deformation of sand was 0.5 mm, i.e. 2/3 of the total displacement amplitude of 0.75 mm. As number of cycles increased, the shear deformation amplitude reduced and the sliding displacement amplitude increased. The shear deformation amplitude reduced to a value of 0.15 mm, and sliding displacement amplitude increased to 0.6 mm, thereafter they remained at this value. The stabilization took place after about 30 cycles equivalent to 6000 seconds, which is equivalent to the same time that the shear stress variations had slowed down as shown in Fig. 5.21. These observations agree qualitatively well with the results reported by Uesugi *et al.* (1989) which are presented in Fig. 2.14.

5.4 Simple Shear versus Direct Shear Type Soil Containers

It is of interest to investigate the effects of type of the soil boxes, i.e. direct shear type or simple shear type, on the monotonic as well as cyclic behaviour of sand-steel interfaces as discussed by Fakharian and Evgin (1995). The results of Figs. 5.1 and 5.2 are presented together in Fig. 5.23 in order to make comparisons between using the direct shear and simple shear soil containers. It is observed that the peak and residual shear strengths obtained in both types of tests are the same. However, when the initial stiffness (i.e. the slope of the shear stress-tangential displacement curve) is considered, the stiffness related to the total tangential displacement (i.e. the shear deformation of the sand mass plus the sliding displacement at the interface) has a lower value in the simple shear tests. The peak is reached at a total tangential displacement of 1.14 mm for direct shear and 1.4 mm for simple shear boxes. On the other hand, the stiffness related to the sliding displacement, is much larger in the simple shear tests than the stiffness related to the direct shear tests. These results are in good agreement with those reported by Uesugi and Kishida (1986). The sliding displacement at peak stress was about 0.6 mm which is less than one half of that observed in the tests using the direct shear box.

In simple shear testing of soils, failure was defined by Budhu (1988) as the maximum stress ratio mobilized on a plane which is not necessarily a horizontal plane. In testing of interfaces, however, the failure occurs along the interface plane which is a horizontal plane, provided that the angle of friction between the steel surface and sand is lower than the friction angle of the sand mass. As demonstrated in Fig. 5.23*d*, the shear deformation of sand mass in simple shear device, which was dominant before the peak, was negligibly small after peak point, during which the sliding displacement or slip at the interface increased as shown in Fig. 5.23*c*. This shows that the failure took place at the interface and not within the sand mass. Since the stress state and the failure plane were the same in both testing, they provided the same strengths.

A similar comparison is made between the results obtained from the direct shear and simple shear boxes by a loose sand specimen as shown in Fig. 5.24. The No.2 sand with an initial relative density of 22% was used with the sand blasted steel surface. In both tests the interface was monotonically sheared up to a total tangential displacement of 5 mm. The plots of shear stress versus sliding displacement, Fig. 5.24*c*, shows that the sliding displacement obtained from the simple shear box was only 1.3 mm at the end of the test, whereas the shear deformation of sand was 3.7 mm, as demonstrated in Fig. 5.24*d*. This indicates that the failure occurred within the sand mass and not at the interface. The shear strength of the loose sand has been lower than that of the interface, therefore, sliding displacement almost stopped after failure occurred within the sand mass.

With the direct shear box, however, it would not be possible to distinguish between the two displacements. The test results show that the shear stress merged at a total tangential displacement of 3.7 mm, after which the shear stress remained at a constant level of 62 kPa. The 62 kPa is close to the residual strength of the interface between the sand blasted steel surface and the No. 2 sand. The fact that both direct shear and simple shear boxes have given the same residual strength might be an indication that the residual strengths of both the loose sand and the sand-steel interface are about the same.

As was shown in Figs. 5.17 and 5.18, in cyclic testing of the interfaces using the direct shear box, failure may or may not occur at the interface. The mechanism of failure and post-peak behaviour is best understood when the results of simple shear box are evaluated. As demonstrated in Figs. 5.19 through 5.22, it was the reduction of shear deformation amplitude of sand mass and increase in sliding displacement of the interface that eventually caused the interface to fail and experience the post-peak softening behaviour.

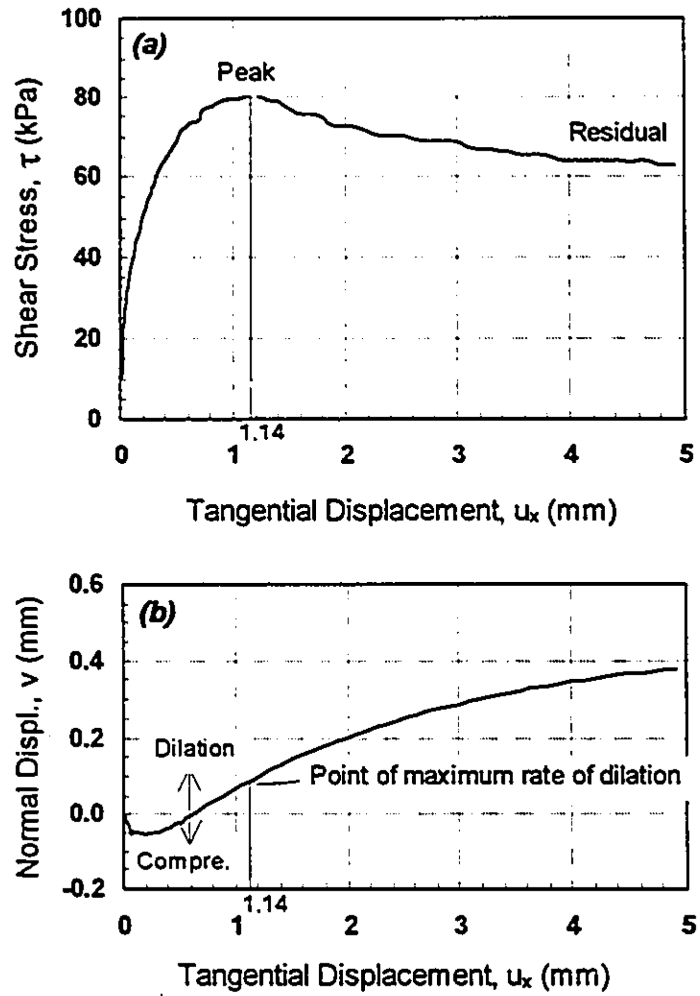

FIG. 5.1. Monotonic test results by using *direct* shear box: 2-D constant normal stress.

Surface: Sand blasted steel plate (R_{max} = 25 μm for L = 0.8 mm)
Sand: No. 2, D_r = 88 %
σ_n = 100 kPa

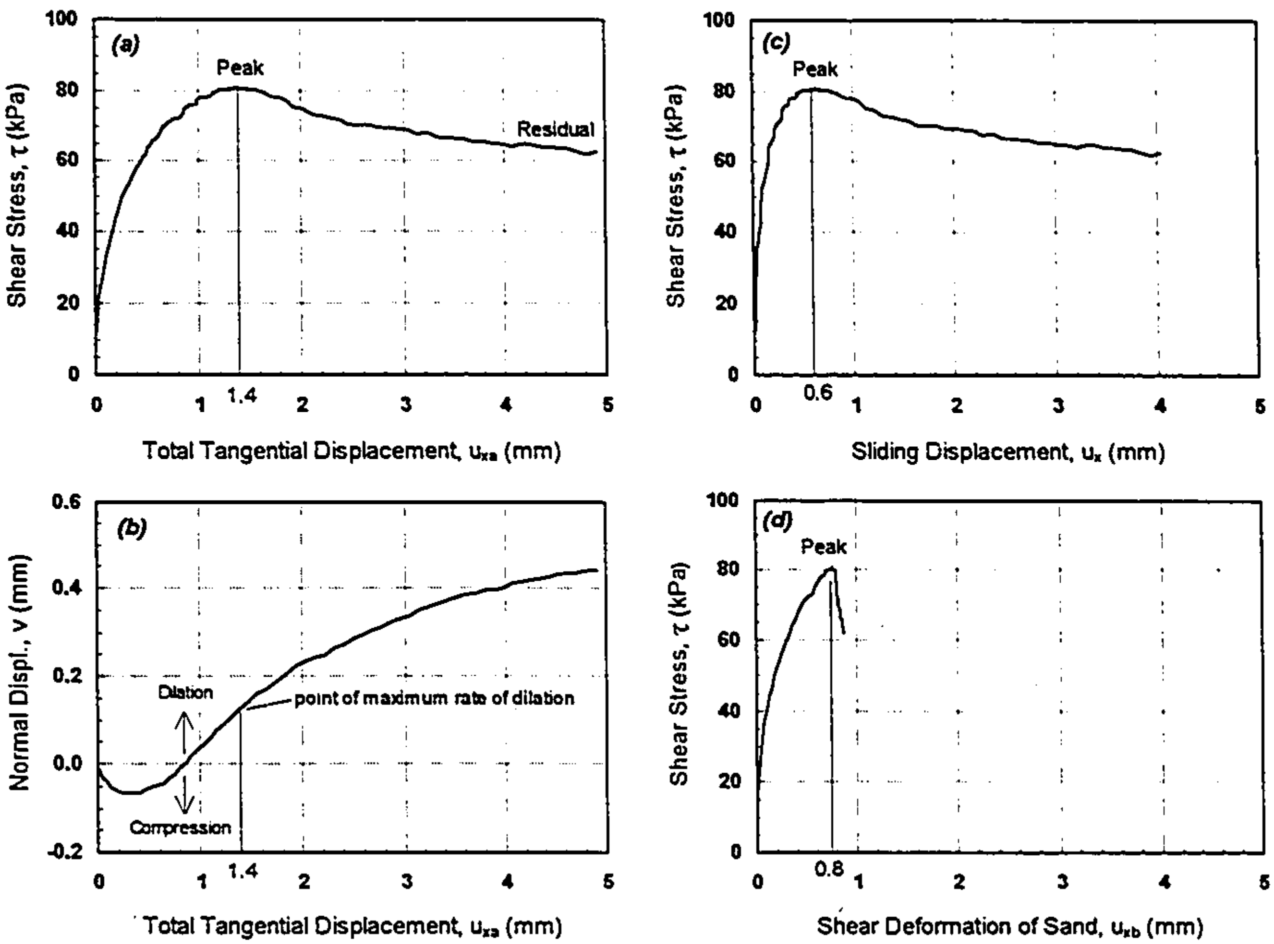

FIG. 5.2. Monotonic test result by using *simple* shear box: 2-D constant normal stress.

Surface: Sand blasted steel plate (R_{max} = 25 μm for L = 0.8 mm)
Sand: No. 2, D_r = 88 %
σ_n = 100 kPa

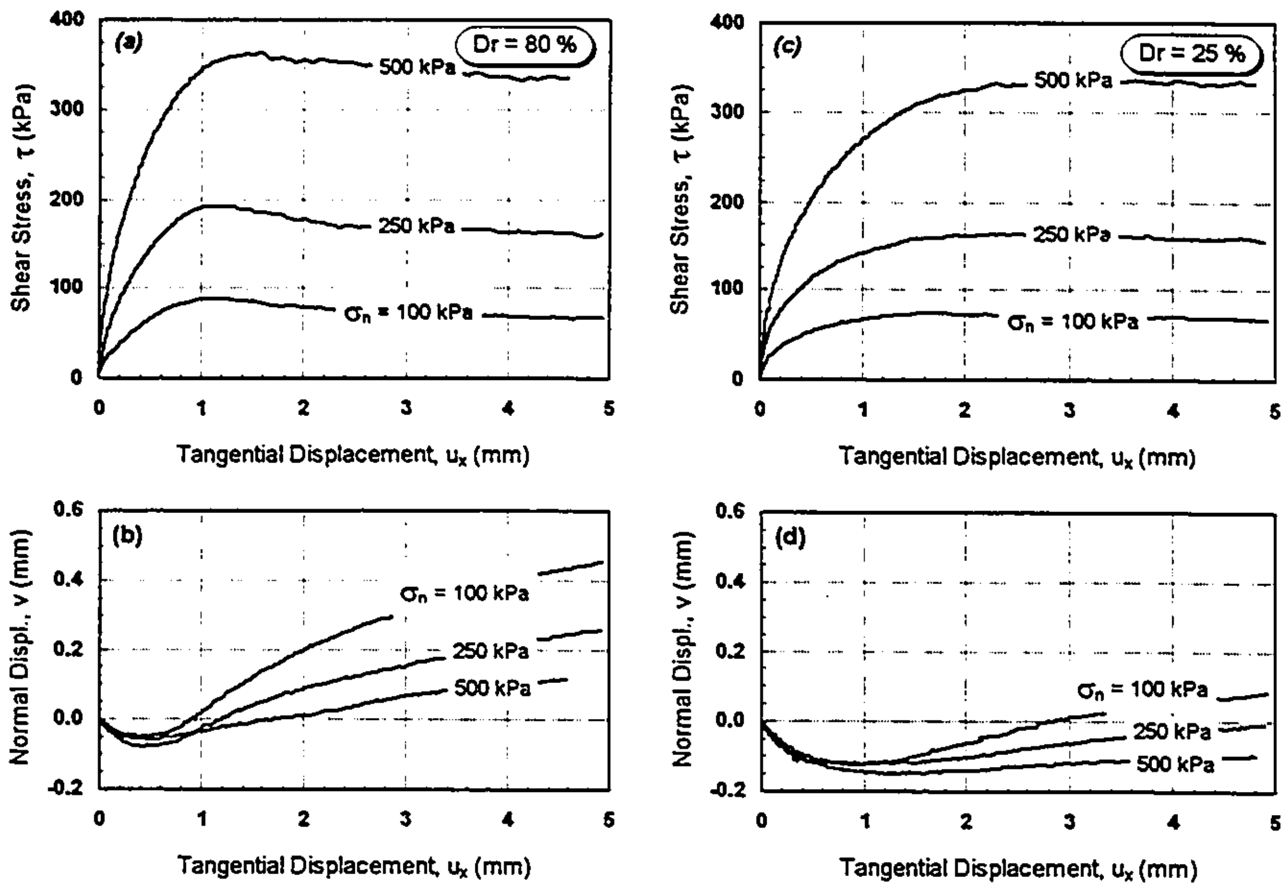

FIG. 5.3. 2-D tests under constant normal stresses of 100, 250, and 500 kPa, using *direct* shear box.

Surface: ALO cloth # 150

Sand: No. 1, D_r = 80 % & 25 %

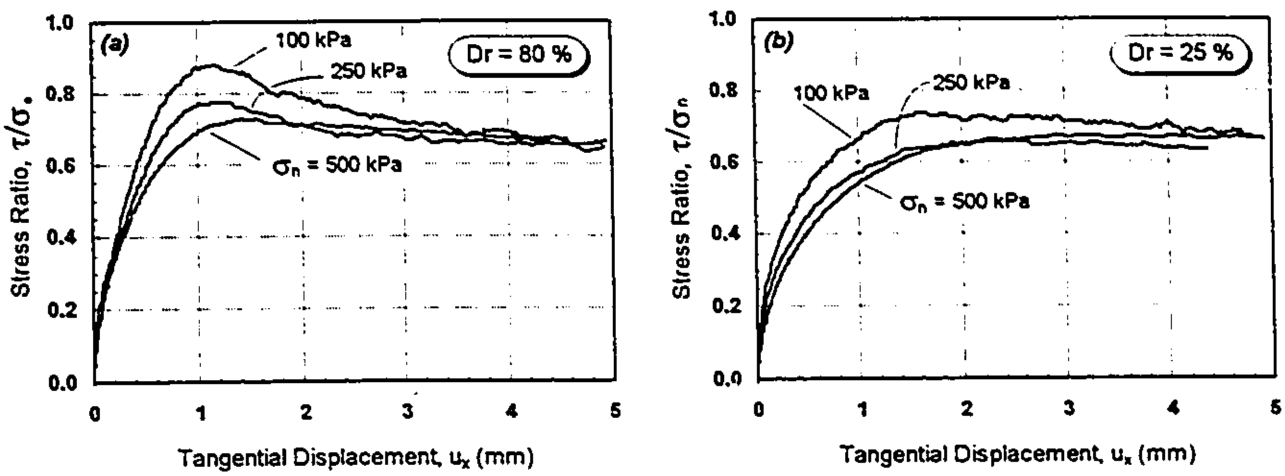

FIG. 5.4. Normalized results of Fig. 5.3: *(a)* dense; *(b)* loose.

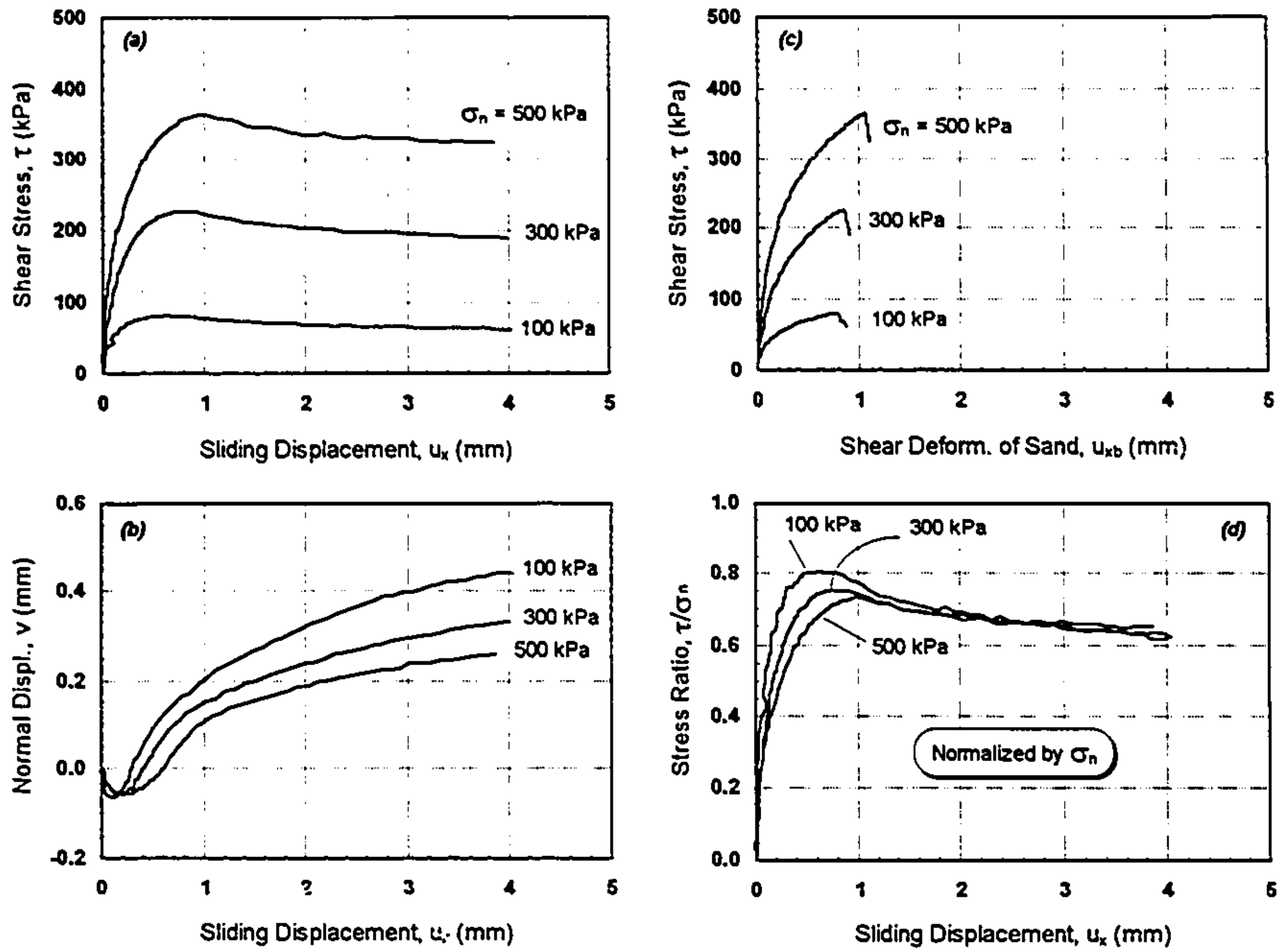

FIG. 5.5. 2-D tests under constant normal stresses of 100, 300, and 500 kPa, using *simple* shear box.

Surface: Sand blasted steel plate (R_{max} = 25 μm for L = 0.8 mm)

Sand: No. 2, D_r = 88 %

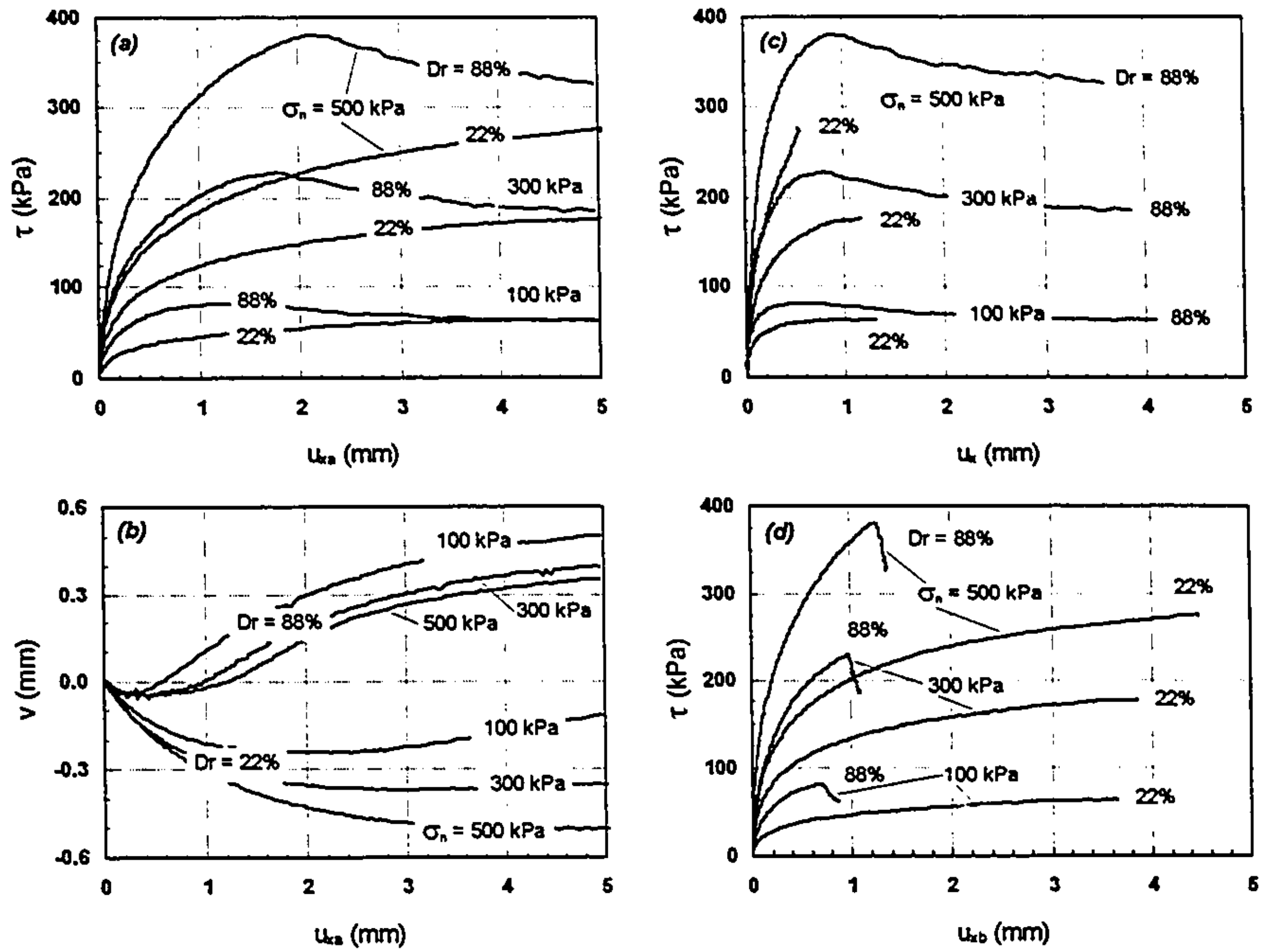

FIG. 5.6. Comparisons between the results of tests with dense and loose sands on a rough surface; using *simple* shear box.

Surface: Sand blasted steel plate (R_{max} = 25 μm for L = 0.8 mm)
Sand: No. 2, D_r = 88 % and 22 %
σ_n = 100, 300, and 500 kPa

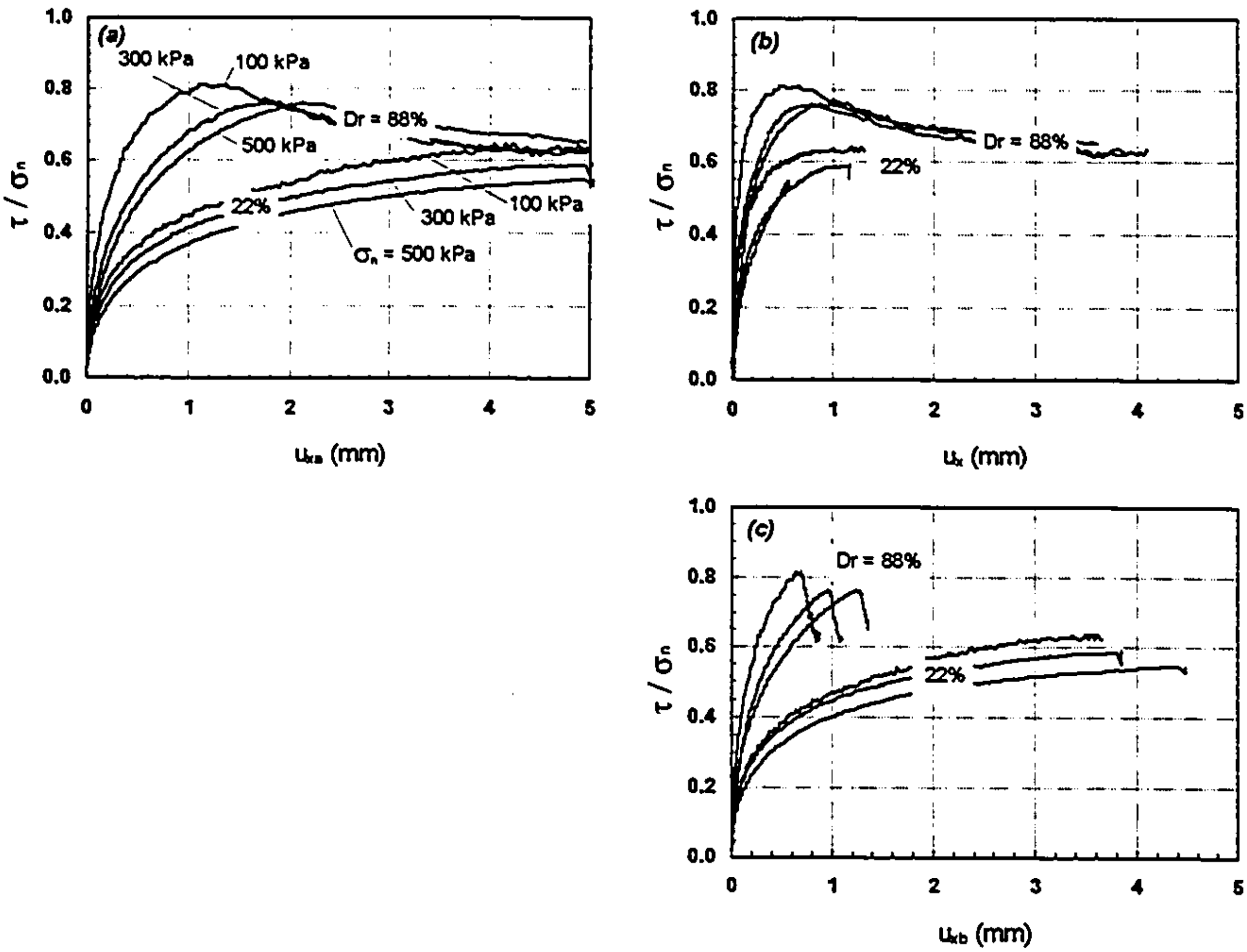

FIG. 5.7. Normalized results of Fig. 5.6.

Surface: Sand blasted steel plate (R_{max} = 25 μm for L = 0.8 mm)
Sand: No. 2, D_r = 88 % and 22 %
σ_n = 100, 300, and 500 kPa

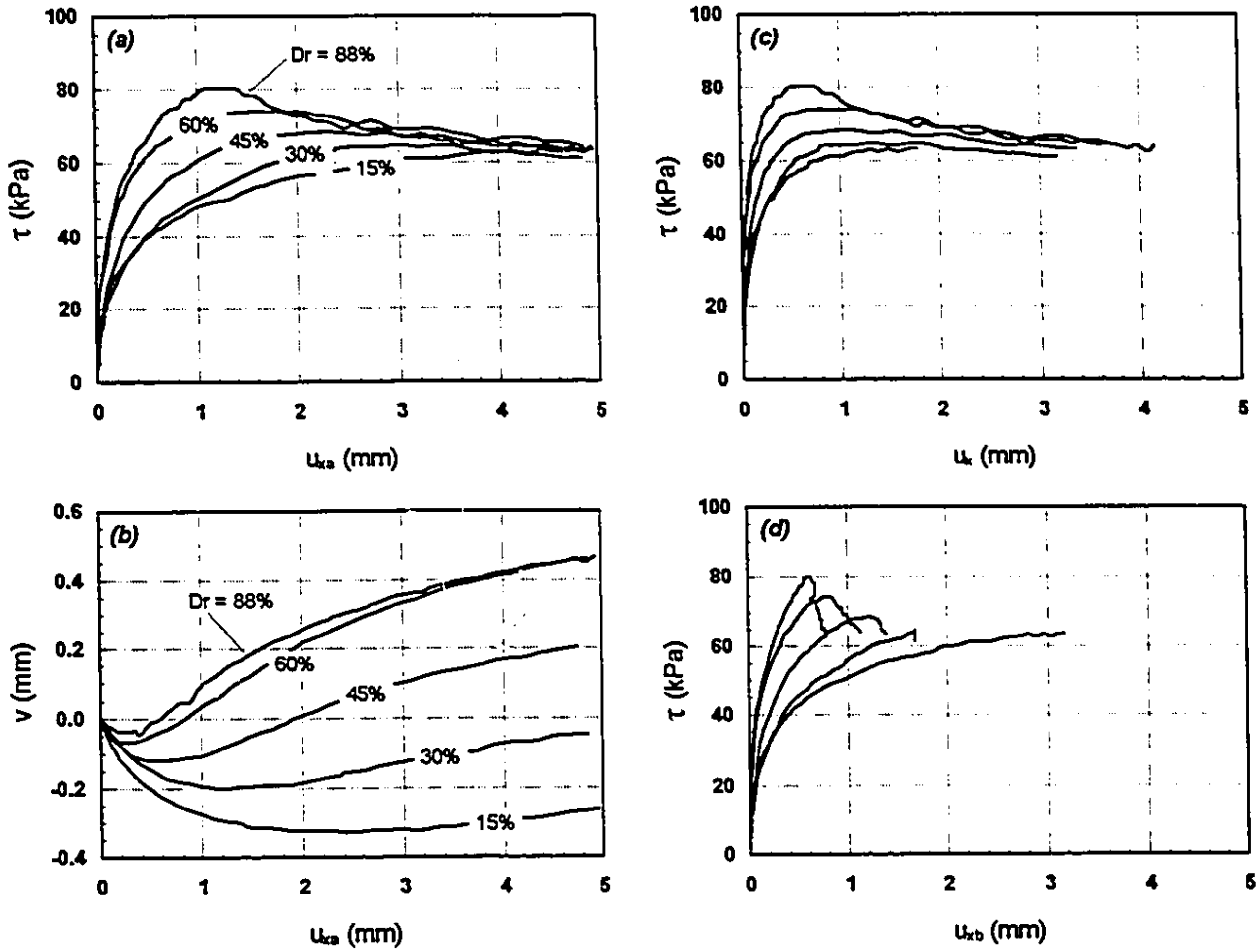

FIG. 5.8. Comparisons between the results of tests with initial relative densities of 15, 30, 45, 60, and 88 %.

Surface: Sand blasted steel plate (R_{max} = 25 μm for L = 0.8 mm)
Sand: No. 2
σ_n = 100 kPa

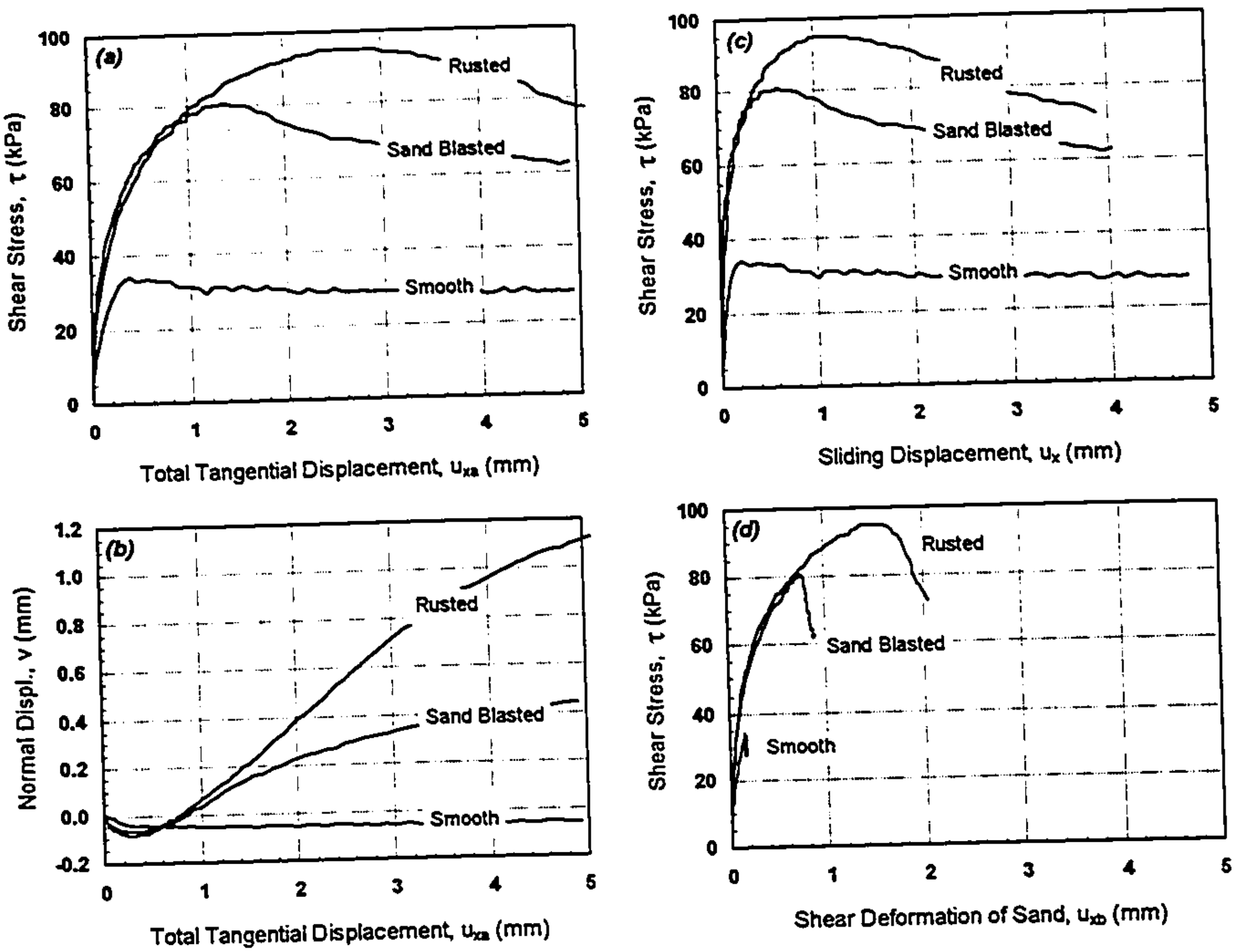

FIG. 5.9. Effect of various surface roughnesses on stress-displacement relations and volume change.

Surfaces: Smooth: $R_{max} = 4$ μm; Sand blasted: $R_{max} = 25$ μm; and Rusted steel plate
Sand: No. 2, $D_r = 88$ % and 22 %
$\sigma_n = 100$, 300, and 500 kPa

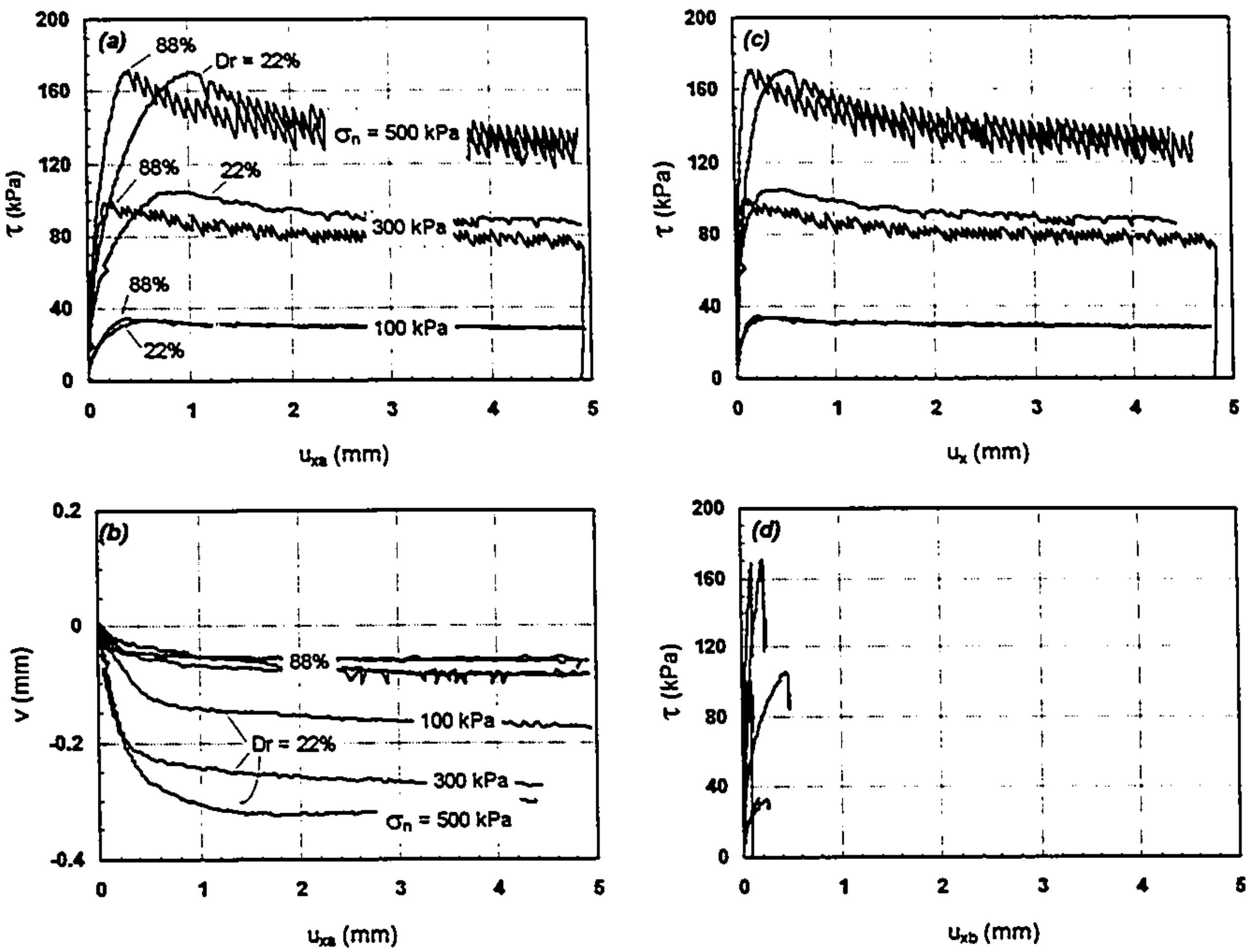

FIG. 5.10. Comparisons between the results of tests with dense and loose sands on the smooth surface, using *simple* shear box.

Surface: Smooth steel plate (R_{max} = 4 μm for L = 0.8 mm)

Sand: No. 2, D_r = 88 % and 22 %

σ_n = 100, 300, and 500 kPa

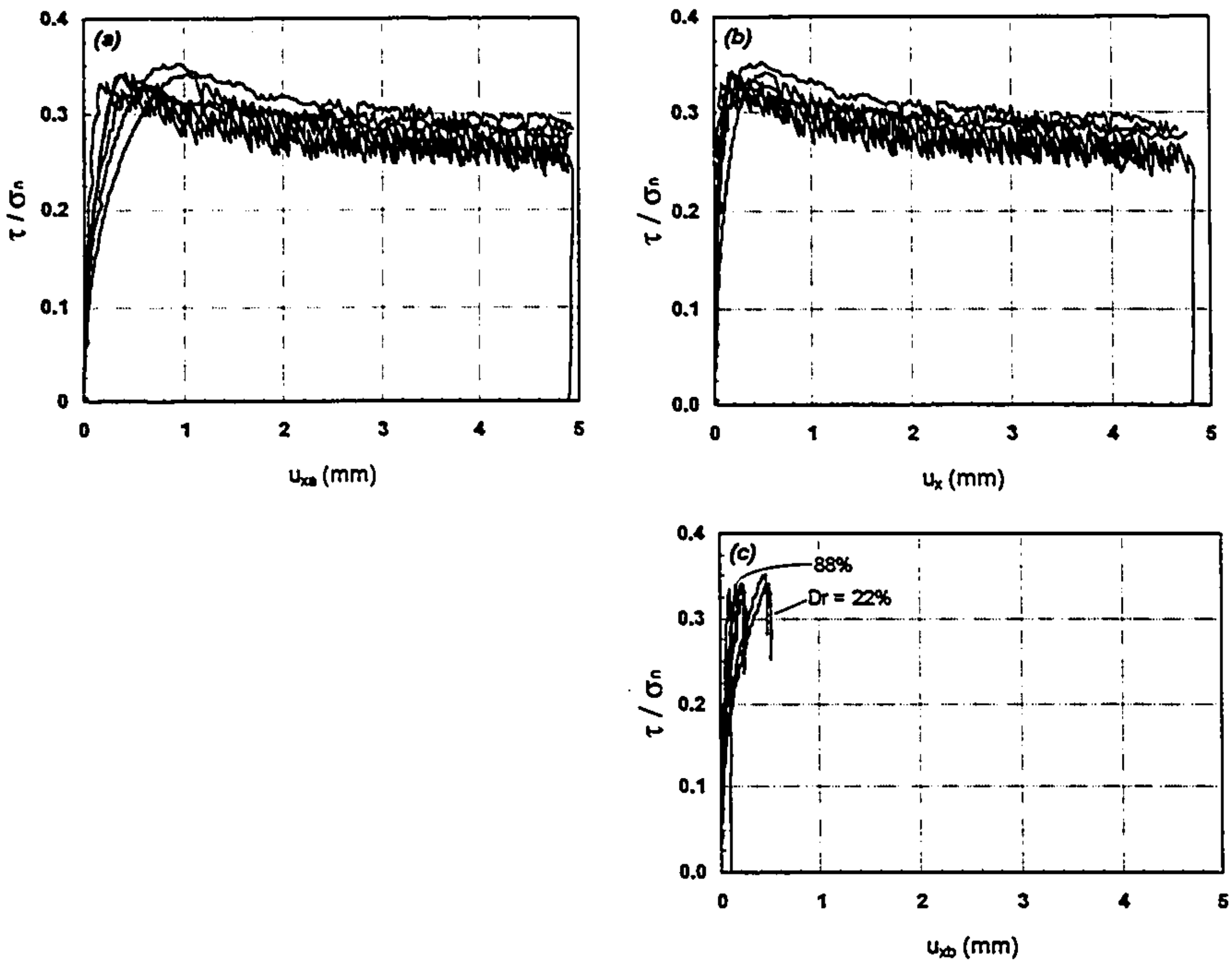

FIG. 5.11. Normalized results of Fig. 5.9.

Surface: Smooth steel plate (R_{max} = 4 μm for L = 0.8 mm)
Sand: No. 2, D_r = 88 % and 22 %
σ_n = 100, 300, and 500 kPa

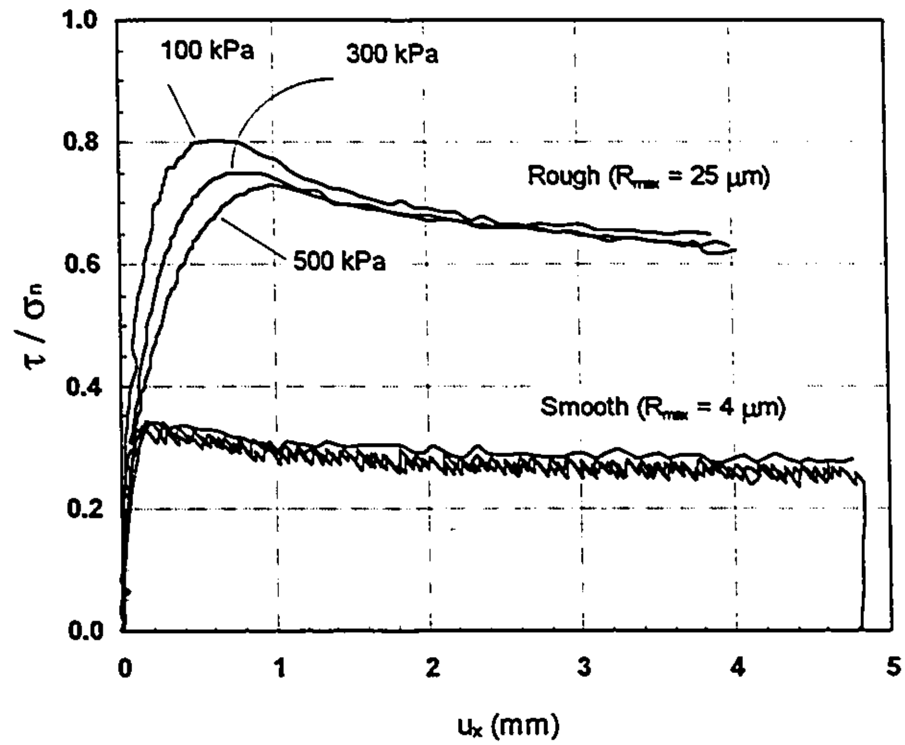

FIG. 5.12. Effects of surface roughness and normal stress.

Surface: Sand blasted and smooth steel plates (R_{max} = 25 & 4 μm for L = 0.8 mm)
Sand: No. 2, D_r = 88 %
σ_n = 100, 300, and 500 kPa

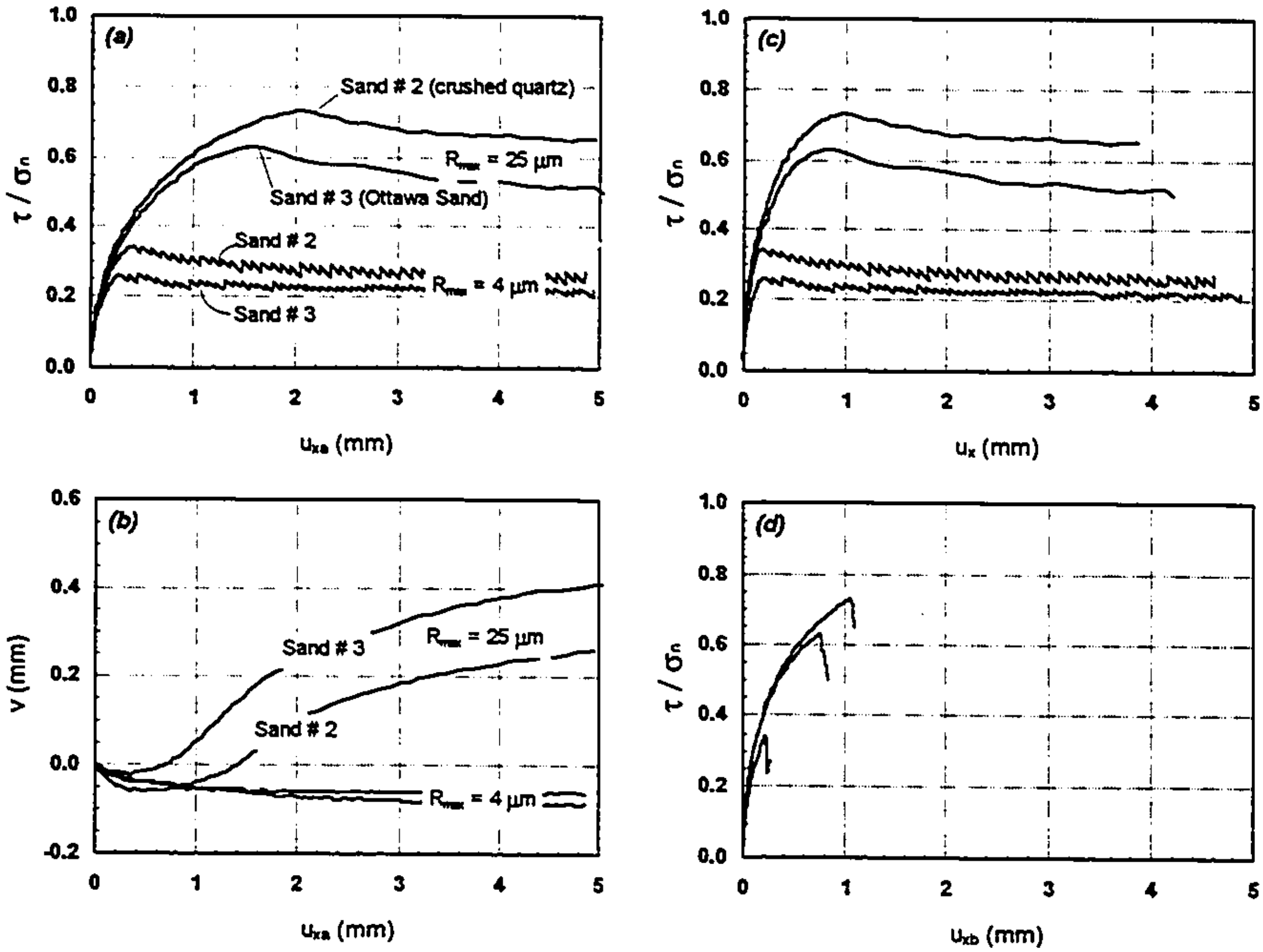

FIG. 5.13. Effect of sand type.

Surface: Sand blasted and smooth steel plates (R_{max} = 25 & 4 µm for L = 0.8 mm)
Sand: No. 2 (D_r = 88 %) and No. 3 (D_r = 92 %)
σ_n = 100 kPa

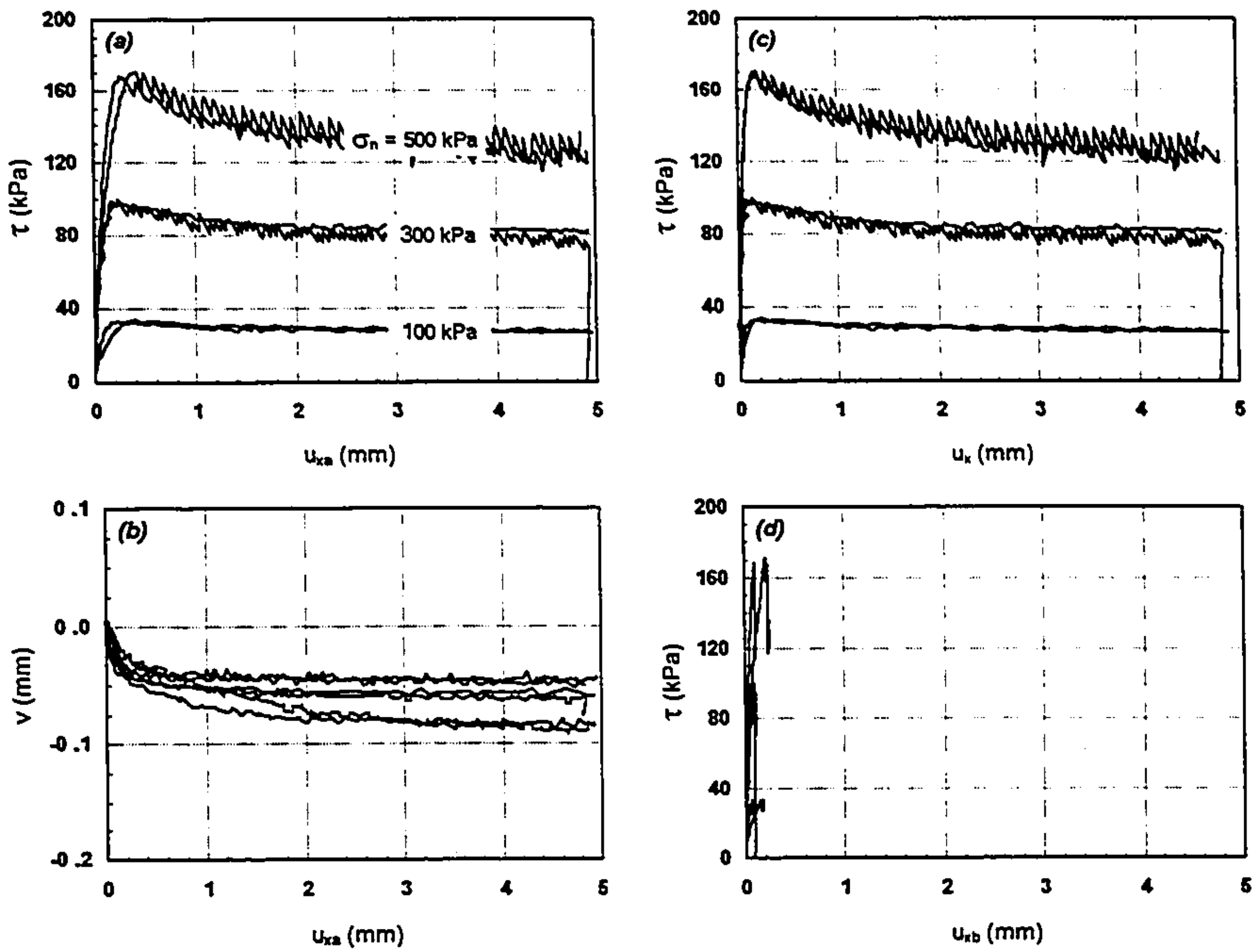

FIG. 5.14. Rate of shearing effects; smooth surface and dense sand.

Rates: 1 and 10 mm/min.

Surface: Smooth steel plate (R_{max} = 4 μm for L = 0.8 mm)

Sand: No. 2 (D_r = 88 %)

σ_n = 100, 300, and 500 kPa

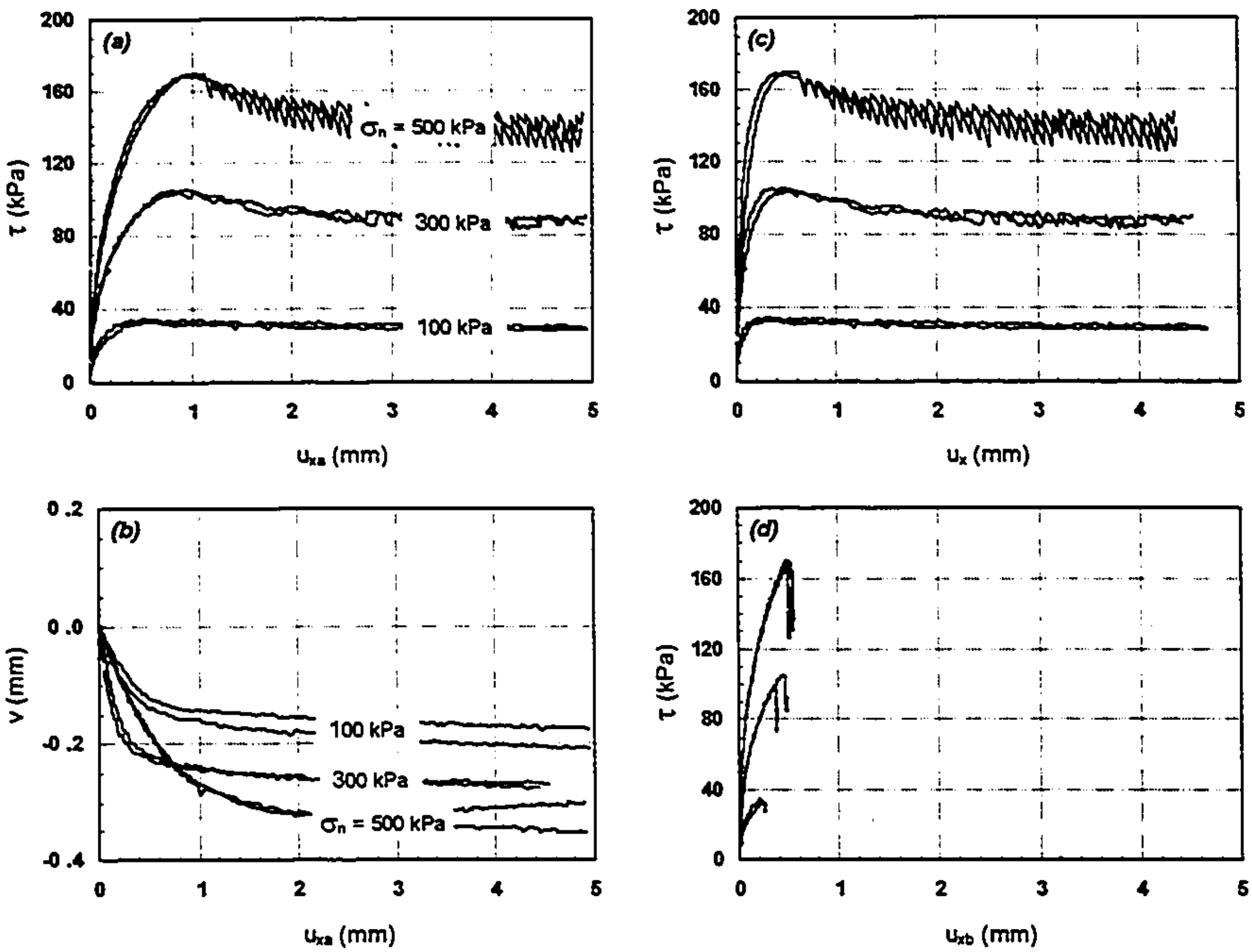

FIG. 5.15. Rate of shearing effects; smooth surface and loose sand.

Rates: 1 and 10 mm/min.

Surface: Smooth steel plate (R_{max} = 4 μm for L = 0.8 mm)

Sand: No. 2 (D_r = 22 %)

σ_n = 100, 300, and 500 kPa

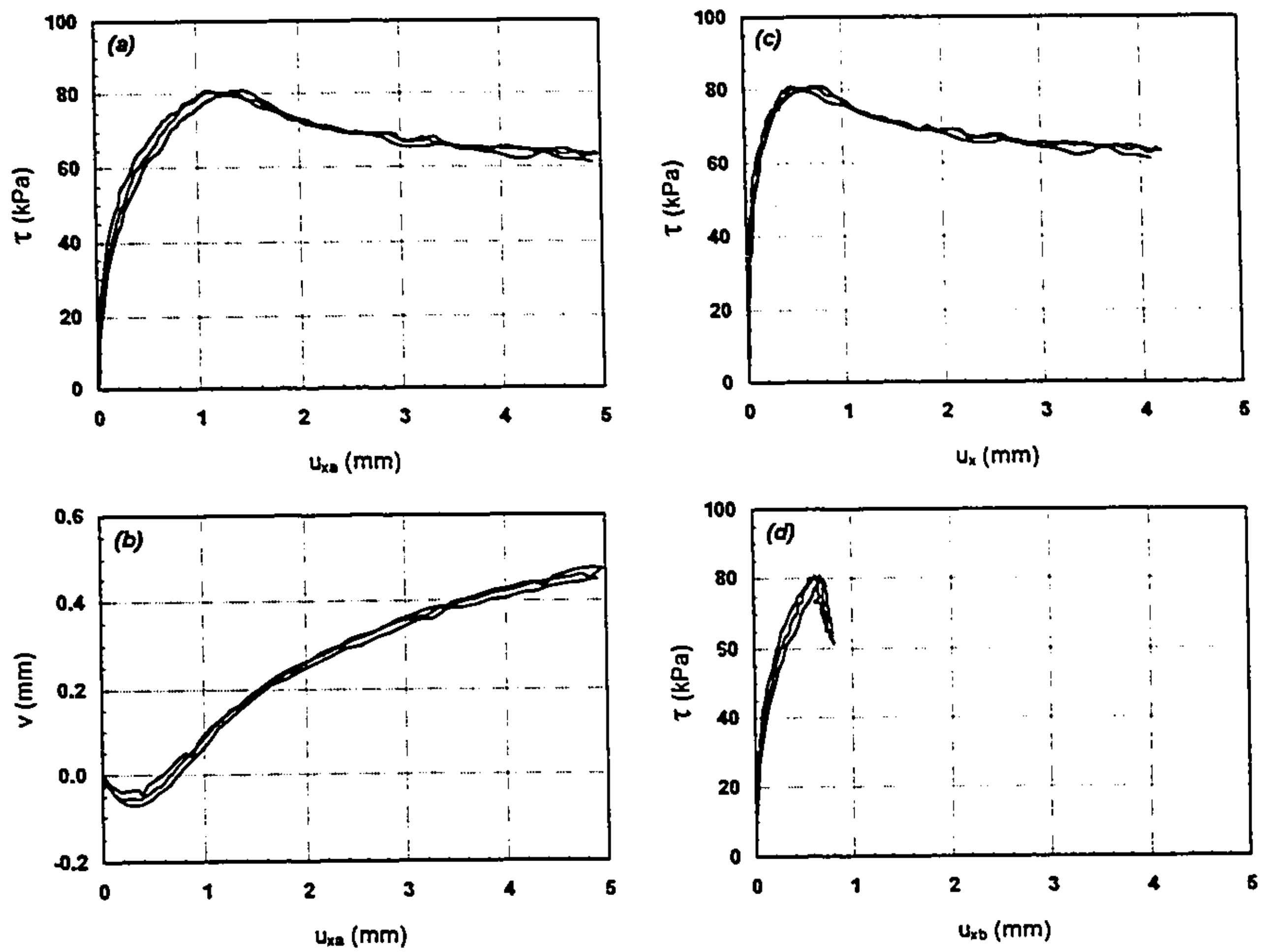

FIG. 5.16. Rate of shearing effects; rough surface and dense sand.

Rates: 0.1, 1, and 10 mm/min.

Surface: Sand blasted steel plate (R_{max} = 25 μm for L = 0.8 mm)

Sand: No. 2 (D_r = 88 %)

σ_n = 100 kPa

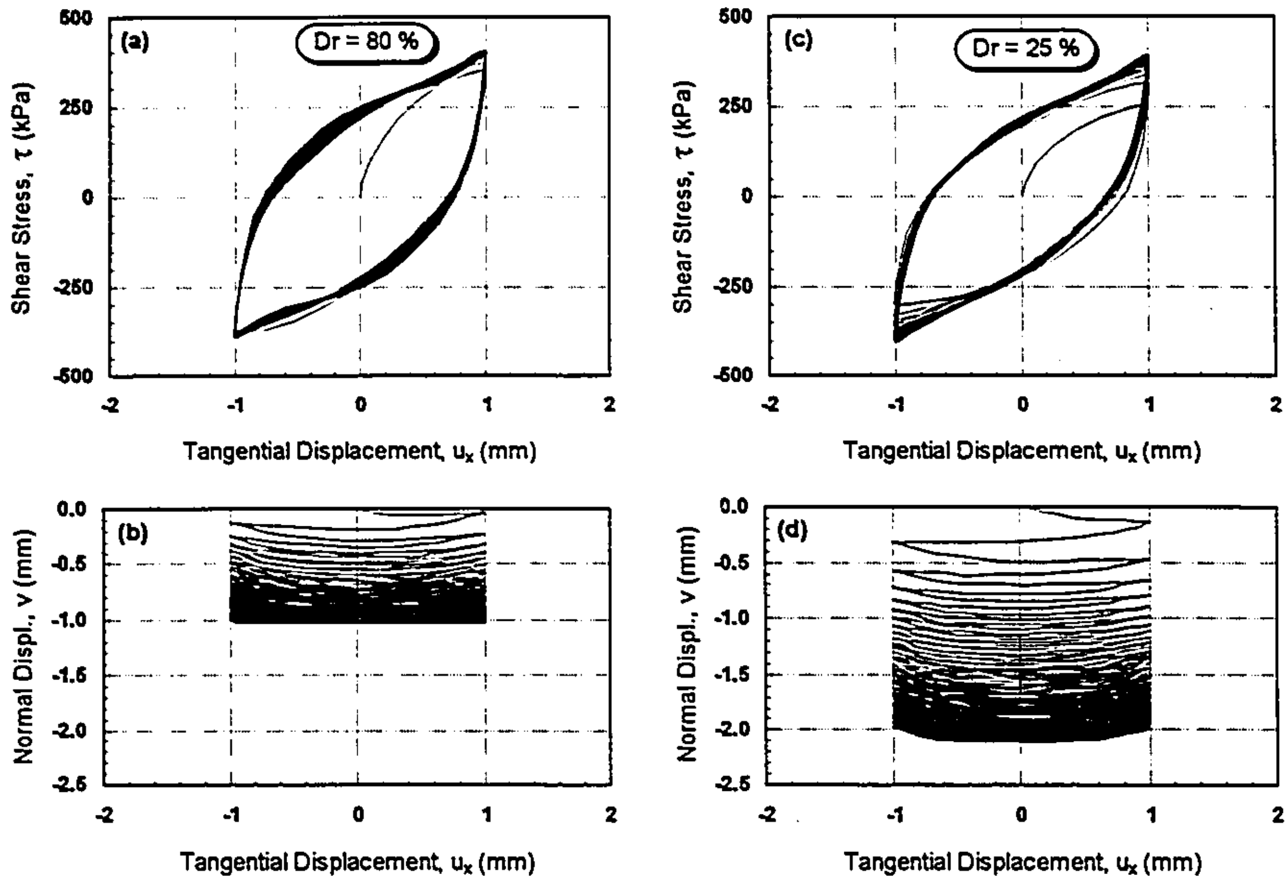

FIG. 5.17. Cyclic tests with *direct* shear box: *(a)* and *(b)* dense sand (D_r = 80 %); *(c)* and *(d)* loose sand (D_r = 25 %); <u>no failure occurred</u>.

Surface: ALO cloth # 150
Sand: No. 1
σ_n = 500 kPa

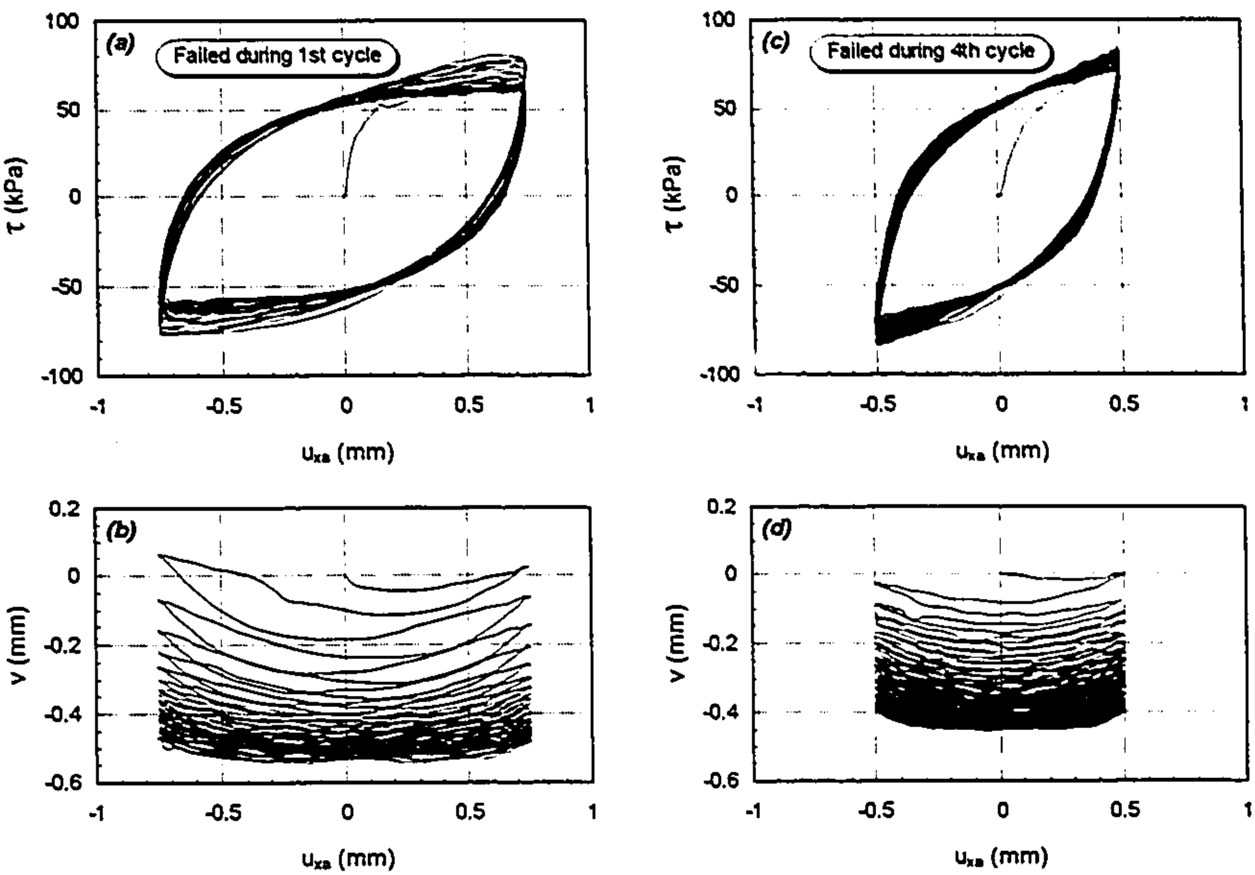

FIG. 5.18. Cyclic tests with *direct* shear box: *(a)* and *(b)* displacement amplitude = 0.75 mm; *(c)* and *(d)* displacement amplitude = 0.50 mm; failure occurred.

Surface: Sand blasted steel plate (R_{max} = 25 μm for L = 0.8 mm)
Sand: No. 2, D_r = 88 %
σ_n = 100 kPa

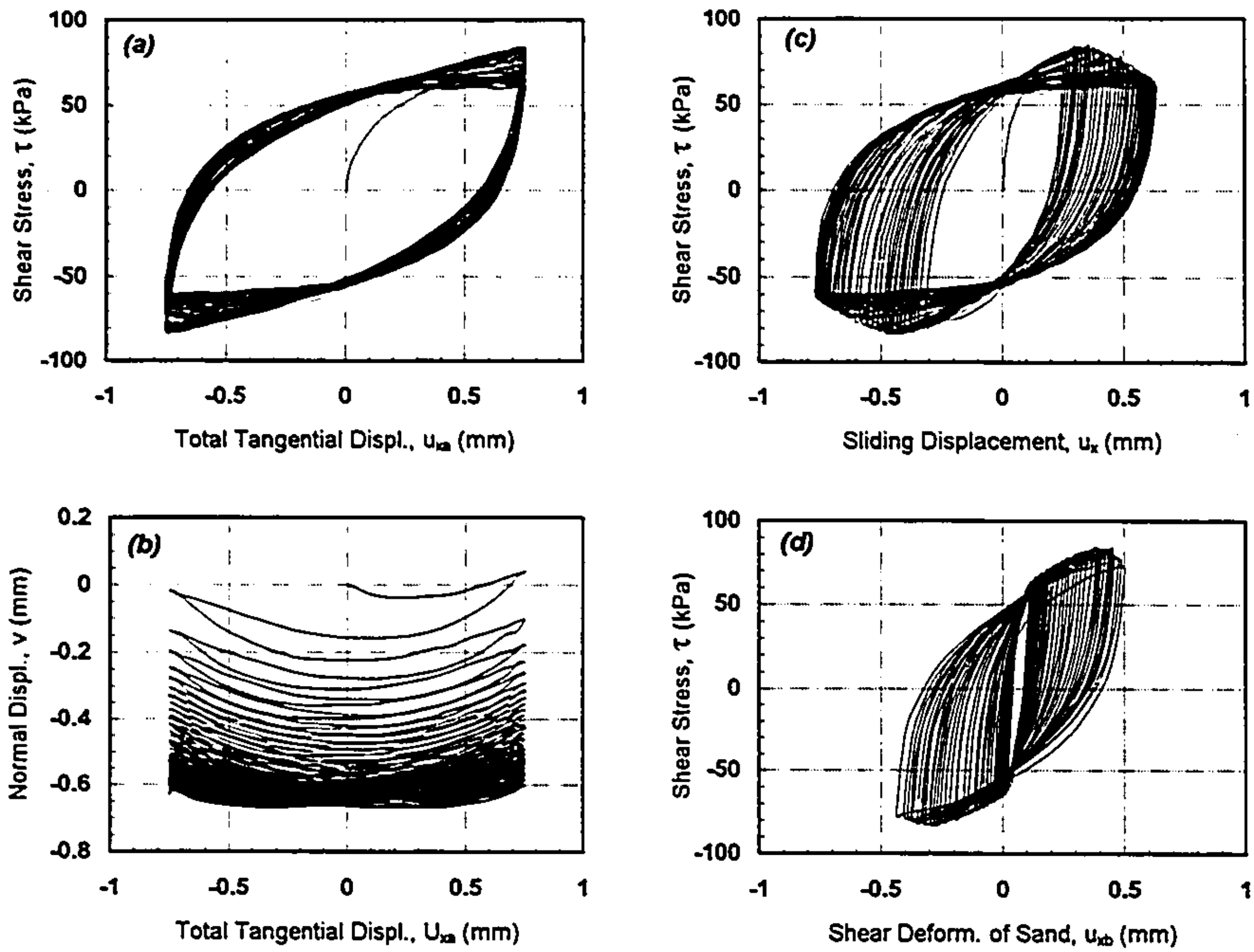

FIG. 5.19. Cyclic tests with *simple* shear box: Total tangential displacement amplitude = 0.75 mm.
(Failure occurred)

Surface: Sand blasted steel plate (R_{max} = 25 μm for L = 0.8 mm)

Sand: No. 2, Dr = 88 %

σ_n = 100 kPa

N (No. of cycles) = 55

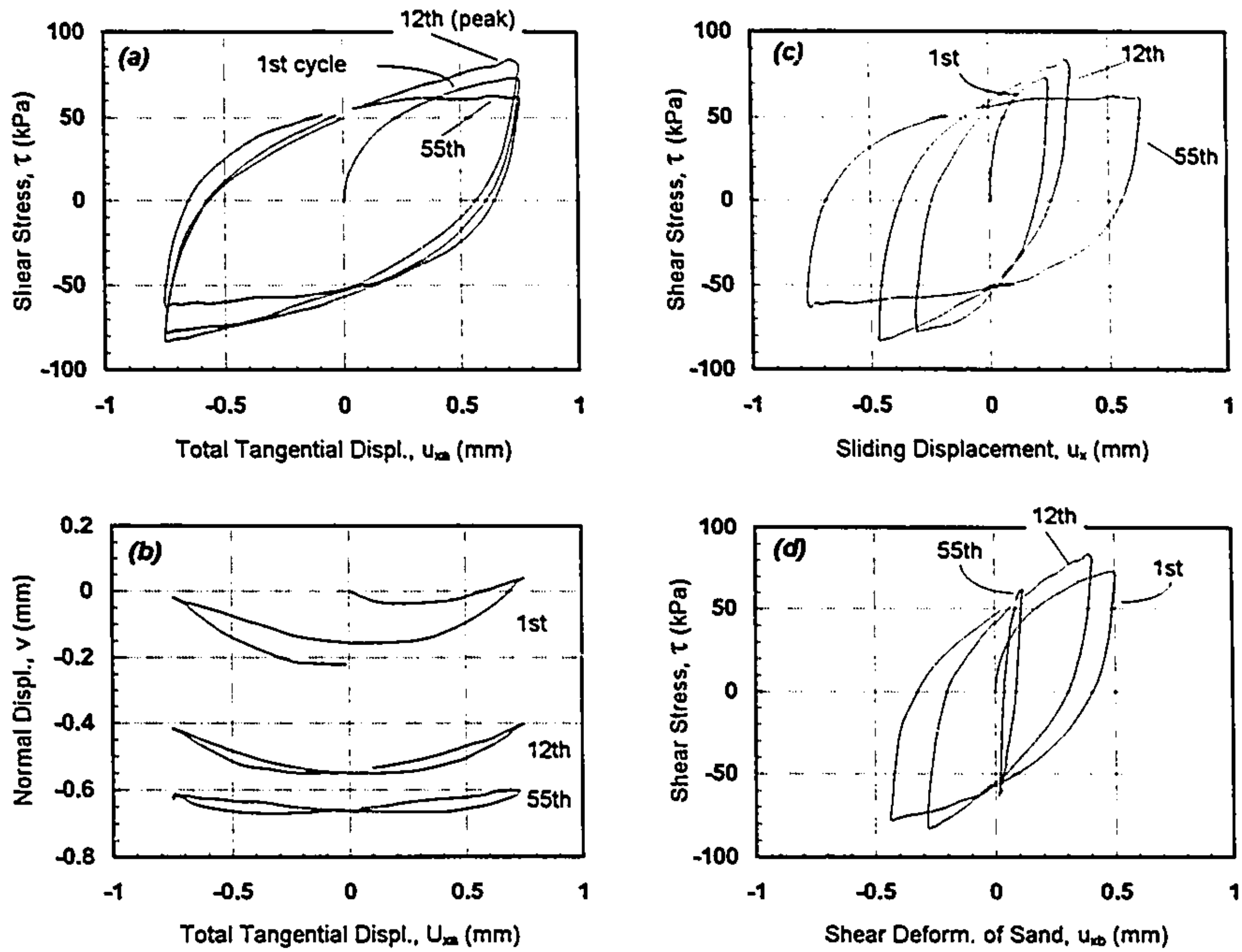

FIG. 5.20. Complete loop at cycles 1, 12, and 55 for results of Fig. 5.19

$\tau = 72.0$ kPa at maximum amplitude for cycle 1

$\tau = 83.0$ kPa at maximum amplitude for cycle 12 (peak strength)

$\tau = 60$ kPa at maximum amplitude for cycle 55 (residual strength)

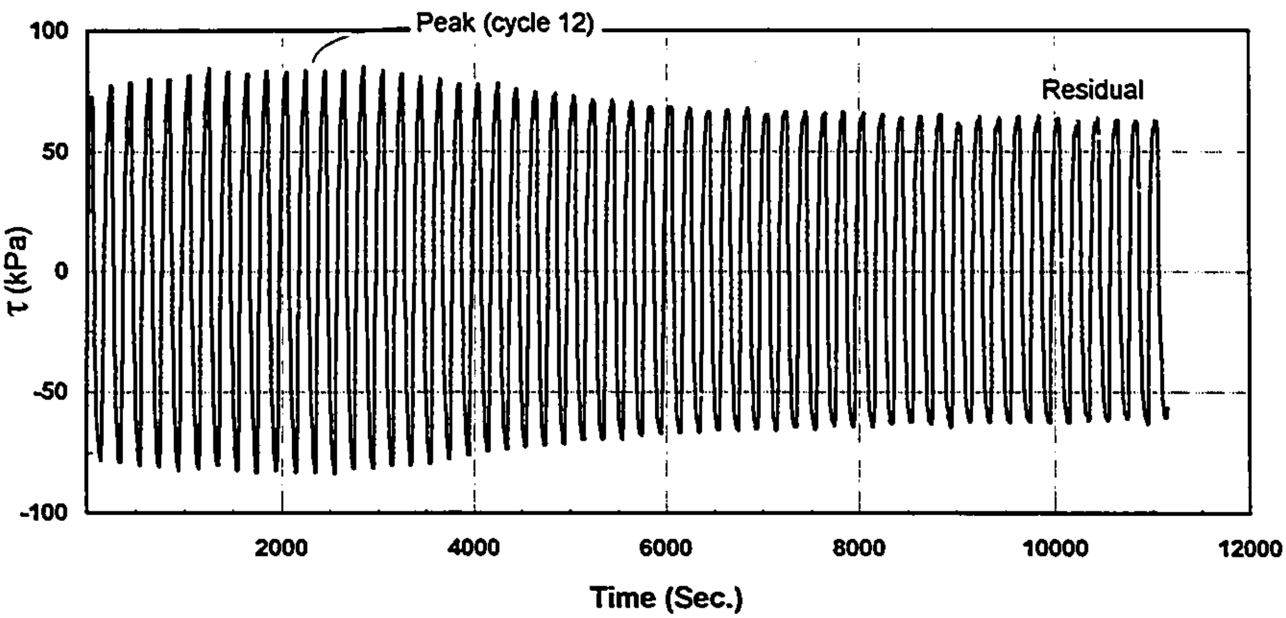

FIG. 5.21. Variations of shear stress with time for results of Fig. 5.19.

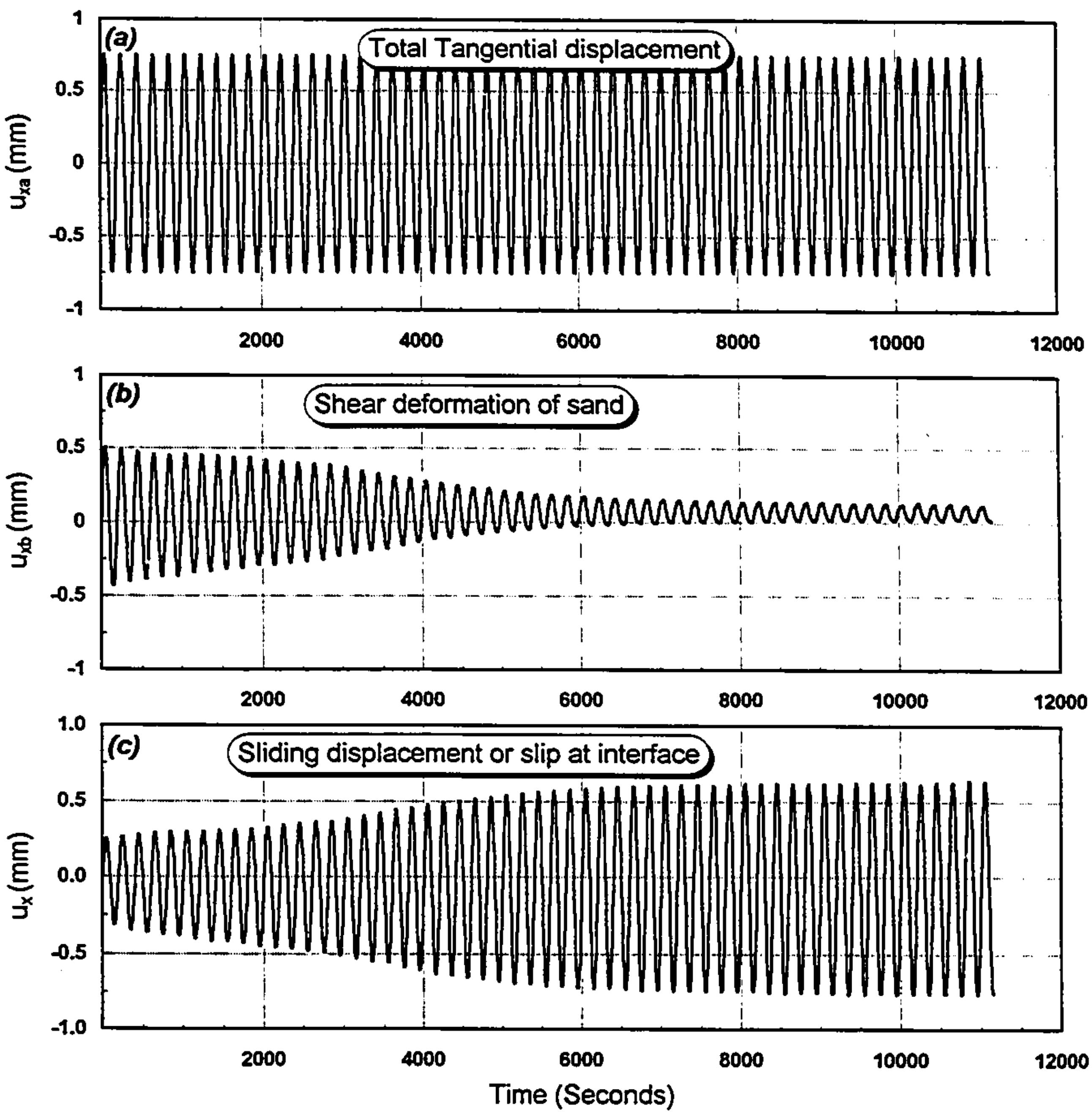

FIG. 5.22. Variations of tangential displacements with time for results of Fig. 5.19.

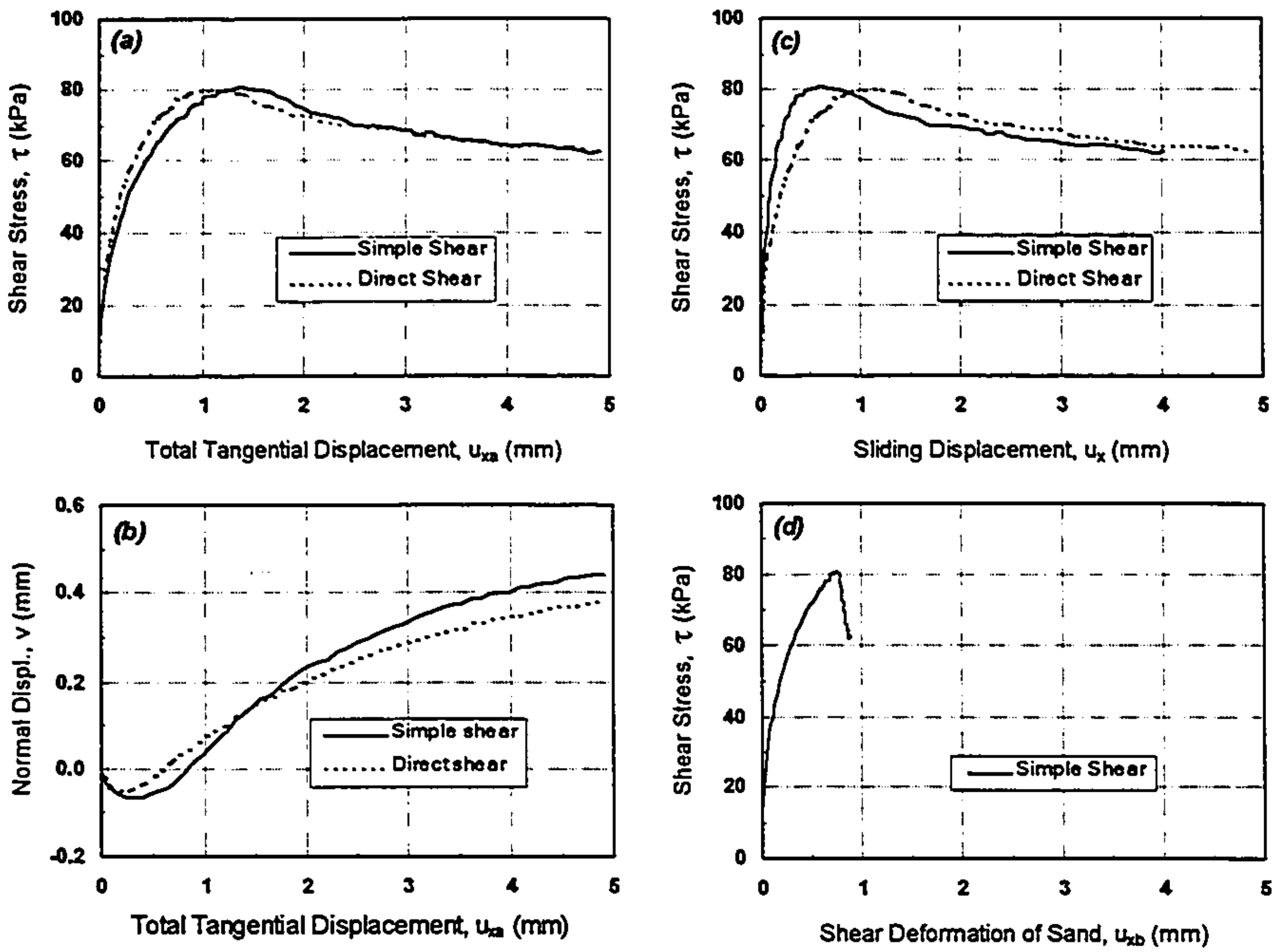

FIG. 5.23. Comparison between <u>direct</u> and <u>simple</u> shear monotonic test results for *dense* sand.

σ_n = 100 kPa; D_r = 84%; sand blasted steel surface.

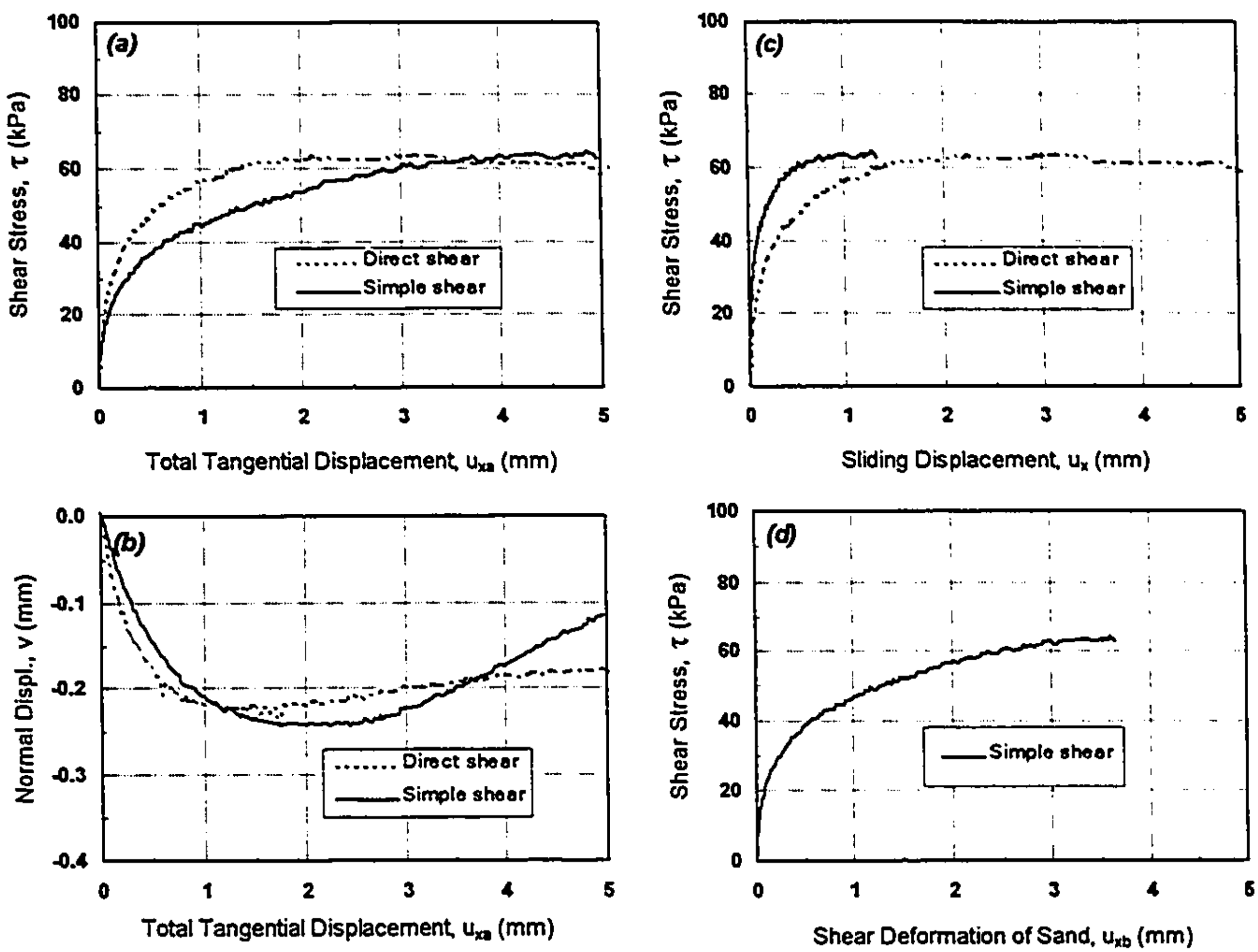

FIG. 5.24. Comparison between direct and simple shear monotonic test results for *loose* sand.

σ_n = 100 kPa; D_r = 22%; sand blasted steel surface.

CHAPTER 6

3-D CONSTANT NORMAL STRESS TESTS

A series of monotonic and cyclic 3-D tests were conducted under the condition of constant normal stress to study the influence of stress paths on the behaviour of a sand-steel interface. The monotonic tests include: (1) stepwise loading, i.e. the shear stresses in the *x*- and *y*-directions were applied stepwise; (2) simultaneous loading, i.e. the interface was sheared in the *x*- and *y*-directions simultaneously. Two types of 3-D cyclic tests were performed: (1) Displacement-controlled cyclic test in one direction while a constant shear stress was applied in the orthogonal direction; (2) Rotational loading, i.e. the interface was sheared in a displacement-controlled manner on an elliptical (or circular) path on the *x*-*y* plane.

6.1 Monotonic Loading Tests

6.1.1 Stepwise loading

Fakharian and Evgin (1993) presented the results of two tests on the interface between the No. 1 sand and ALO Cloth # 150 as shown in Fig. 6.1. The direct shear box was used in those experiments. The first test (Fig. 6.1*a*, *b*) was conducted by using a dense sand (D_r = 80 %), whereas the second test (Fig. 6.1*c*, *d*) was carried out by using a loose sand (D_r = 25%). The procedure for each test was as follows:

The interface was sheared to a tangential displacement of 5 mm first in the *x*-direction under a constant normal stress of 250 kPa (Figure 6.1*a*). Then, the shear stress was lowered to zero and all three LVDTs in the *x*, *y*, and *z*-directions were set to zero, while the normal stress was maintained at 250 kPa. Thereafter, the interface was sheared in the *y*-direction while the shear stress in the *x*-direction was maintained at zero.

Figure 6.1*a* shows that for the dense sand specimen, there was a well pronounced peak in the shear stress-tangential displacement curves during first time shearing, i.e., in the *x*-direction. However, in the second time shearing which was in the *y*-direction, there was no pronounced peak and the shear stress approached the residual shear stress. When the specimen was sheared first time in the *x*-direction, it compressed first and then dilated. During the second time shearing, i.e., the loading in the *y*-direction, the specimen started dilating. The dilation rate at the beginning of loading in the *y*-direction appears to be the same as the dilation rate at the end of the loading in the *x*-direction.

The test results for the loose sand specimen are given in Fig. 6.1*c*, *d*. Figure 6.1*c* shows the same trend as that for the dense specimen except that the peak is less pronounced as compared to the dense specimen. The specimen compressed more during shearing in the *y*-direction as observed in Fig. 6.1*d*.

These test results suggest that the peak failure at the interface appeared once during the first time shearing. Subsequent shearing of the interface in an orthogonal direction, did not produce a peak and the shear stress-tangential displacement curves approached the residual shear stress, which was reached in the first time shearing in the *x*-direction.

6.1.2 Simultaneous loading

Fakharian and Evgin (1996) presented some 3-D monotonic test results for an interface between the No. 1 sand and the ALO Cloth # 150. The direct shear box (C3DI) was used in that study to simulate the behaviour of a typical interface element on the shaft of an axially-laterally loaded pile. Similar tests were conducted by using C3DSSI between the No. 2 sand, with an initial relative density of 88%, and the sand blasted steel plate (R_{max} = 25 μm for L = 0.8 mm). The tests were performed under a constant normal stress of 100 kPa. The interface was subjected to a shear stress, first in the y-direction, less than the peak shear strength in a 2-D test. Thereafter, the interface was sheared in the x-direction, while the shear stress in the y-direction and the normal stress in the z-direction were maintained at constant values.

When the interface was sheared in the x-direction at $\tau_y = 0$, the peak and residual shear stresses were 80.3 kPa and 62.0 kPa, respectively (same as 2-D test data shown in Fig. 5.2). Three other tests were conducted with τ_y maintained at 20, 40, and 60 kPa. These stresses were about 25%, 50% and 75% of the peak shear stress for the 2-D case, respectively. The results are presented in Figs. 6.2 through 6.4.

Figure 6.2*a* illustrates the shear stress τ_x versus sliding displacement, u_x. The plots of shear stress, τ_x, versus shear deformation of sand mass, u_{xb}, are given in Fig. 6.2*b*. These figures show that the peak and residual stresses in the x-direction were small when the constant shear stress in the y-direction was large. For example, while the peak shear strength in the x-direction was 80.3 kPa for $\tau_y = 0$, its value decreased to 78, 67, and 55 kPa when the tests were conducted with τ_y maintained at 20, 40, and 60 kPa, respectively. Figures 6.2*c* and 6.2*d* show that during shearing in the x-direction, the sliding displacement continued also in the y-direction although there was no change in the shear stress value, i.e. $\Delta\tau_y$=0.0. The trend was such that for higher constant shear stress in the y-direction, larger sliding displacement took place in that direction. During the experiments, it was possible to maintain the shear stress, τ_y, constant at values of 20 and 40 kPa until the end of shearing in the x-direction. In the case of constant shear stress of 60 kPa, however, it was not possible to maintain τ_y at this stress level and it started to decrease after the peak shear stress in the x-direction was reached and eventually both τ_x and τ_y reached their residual values.

The paths followed by the shear stress, sliding displacement, and shear deformation of sand on the x-y plane are illustrated in Figs. 6.3*a*, 6.3*b*, and 6.3*c*, respectively. The horizontal axes exhibit the shear stress or tangential displacement components in the x-direction. The shear stress or tangential displacements in the y-direction are shown on the vertical axes of those graphs. During the test along the x-axis direction when $\tau_y = 0$, the shear stress, τ_x, moved from the origin *o* to point *a* at which the peak shear strength was experienced at 80.3 kPa. After the peak value, the stress path reversed its direction and moved on the same line until the residual strength of 62.0 kPa was reached at point *b*. Obviously, both the sliding displacement and shear deformation of sand occurred along the x-axis for that case as illustrated by the paths *oi* and *olm* in Figs. 6.3*b* and 6.3*c*, respectively. Thus, the directions of the shear stress and displacement paths coincided for the case of $\tau_y = 0$ throughout shearing.

During the τ_y = 20 kPa test, interface was sheared first from 0 to 20 kPa in the y-direction, as shown by the path *oc* in Fig. 6.3*a*. The magnitudes of the sliding displacement and shear deformation in the y-direction were both 0.03 mm at τ_y =20 kPa. Subsequently, the interface was sheared in the x-direction along the path *cd*. The shear strength in the x-direction attained its peak value at point *d* after which reduced to a residual value at point *e*. The orientations of the sliding displacement path *oj* (Fig. 6.3*b*) and the shear deformation path of the sand mass *npq* (Fig. 6.3*c*) were different than the orientation of the corresponding shear stress path, *cde*.

Although only the shear stress, τ_x, was changing during the loading along the path *cde*, both the sliding displacement and shear deformation of sand had components in the y-direction as well as in the x-direction. This type of response is different than the response of an elastic material which would deform in the x-direction alone. Similar results were obtained by Degroot *et al.* (1993) for the Boston Blue Clay tested in a 3-D simple shear testing apparatus. Their specimens were consolidated first under a combination of a normal stress and a shear stress in a direction other than the x-axis direction. Subsequently, the specimens were sheared in the x-direction under undrained conditions. In all these experiments, specimens had a component of shear strain in the y-direction during the undrained shearing in the x-direction. These results clearly demonstrate that the behaviour of both the interface and the sand mass are plastic in nature almost right from the beginning of shearing.

The stress path for $\tau_y = 60$ kPa case is indicated by *ofgh* in Fig. 6.3a. In this case, unlike the two other cases with lower values of τ_y, the shear stress components in both x and y directions sharply reduced after the peak shear strength indicated by point g. The residual strength was reached at point h. The corresponding displacement and deformation paths are indicated as *ok* and *orst* in Figs. 6.3*b* and 6.3*c*, respectively.

The peak and residual shear strength envelopes are illustrated in Fig. 6.3*a*. Both envelopes are circular with radii of 80 and 62 kPa, respectively. The points labelled as "failure points" in Fig. 6.3*c* indicate that the major portion of the shear deformation in the sand mass took place before the peak strength of the interface was reached. Thereafter, the shear deformation rate decreased rapidly as the sliding displacement at the interface continued to increase.

The circular shapes of the peak and residual shear strength envelopes confirm that the magnitudes of the resultant peak and residual shear strengths are not affected by the stress paths. This fact was illustrated further by plotting the resultant of shear stress components, $(\tau_x^2 + \tau_y^2)^{1/2}$, versus the resultant of sliding displacements, $(u_x^2 + u_y^2)^{1/2}$ in Fig. 6.4. The data show that the resultant shear stress versus sliding displacement curves for various τ_y values are almost identical irrespective of the magnitude of τ_y.

The cause of reduction in τ_y, after the peak strength was reached in the $\tau_y = 60$ kPa test, is as follows: In this experimental work, either a constant load or a displacement rate was specified to operate the stepper motors. The stepper motor ram in the x-direction was displaced at a constant rate of 1 mm/min to apply the shear stress τ_x which increased steadily up to the peak shear strength and then decreased toward the residual value. Meanwhile, a constant load was specified for the stepper motor in the y-direction to maintain τ_y constant at 60 kPa. When τ_x was increasing or decreasing, the stiffness of the soil was also changing. For this reason, the amount of reaction provided by the soil against the ram of the stepper motor in the y-direction was not constant. In order to compensate for the changes taking place in the stiffness of the soil, the stepper motor in the y-direction had to displace its ram at a rate of displacement specified by the operator at the beginning of the experiment. The ram of the stepper motor in the y-direction was displaced at the specified rate only when the shear stress in the y-direction was not at its constant value. In the experiment with constant shear stress, τ_y = 60 kPa, the rate of displacement in the y-direction was 1 mm/min, same as the rate of displacement in the x-direction. This specified rate of displacement was not high enough to compensate for the rapid changes taking place in the soil stiffness and to maintain the τ_y at its specified constant value of 60 kPa. Subsequent tests with a larger rate of displacement in the y-direction showed that the point h moved along the residual shear strength circle toward the point z.

6.2 Cyclic Tests

6.2.1 Displacement controlled cyclic tests with a constant shear stress in orthogonal direction to cycles

The test procedure for the results presented here is similar to those explained in subsection 6.1.2, for 3-D simultaneous monotonic tests, except that the interface was subjected to a two-way tangential displacement controlled cyclic shearing in the x-direction. The No. 2 sand at an initial relative density of 88% and the sand blasted steel plate (R_{max} = 25 μm for L = 0.8 mm) were used as interface materials. The interface was first subjected to a constant shear stress in the y-direction. The specified magnitudes of τ_y were less than the peak strength in a monotonic test which was 80.3 kPa under a constant normal stress of 100 kPa. Thereafter, the interface was subjected to a tangential displacement controlled sinusoidal shearing with an amplitude of 0.75 mm and a period of 200 seconds, while the shear stress in the y-direction, τ_y, was maintained constant. The tangential displacement amplitude of 0.75 mm corresponds to the total tangential displacement, u_{xa}, and is less than the total tangential displacement, 1.4 mm, at peak strength in monotonic loading.

Four test results are presented with τ_y maintained at 20, 30, 40, and 60 kPa, i.e. at 1/4, 3/8, 1/2, and 3/4 of the peak stress of 80.3 kPa in a 2-D monotonic test. For $\tau_y = 0$, that is a 2-D cyclic displacement controlled test, the results were presented in Figs. 5.19 to 5.22. It was shown that the shear stress, which was 72.9 kPa at the end of first cycle, reached a peak of 83.0 kPa at cycle 12 after which the shear stress decreased and stabilized at 60 kPa.

The cyclic test results for the interface subjected to a constant normal stress of 100 kPa, and a constant shear stress of 20 kPa in the y-direction, τ_y, are illustrated in Figs. 6.5 to 6.10. The shear stress-tangential displacements in the x-direction and volume change behaviour of the specimen are shown in Figs. 6.5 and 6.6. As the number of cycles increased, the mobilized shear stress increased to a peak, τ_{xp}, of 81.7 kPa at cycle 5 in the x-direction. Thus the resultant peak strength, $(\tau_p)_{result}$ is :

$$(\tau_p)_{result} = (\tau_{xp}^2 + \tau_y^2)^{1/2} = (81.7^2 + 20.0^2) = 84.1\ kPa$$

Thereafter, the shear stress reduced and stabilized at a residual strength, τ_{xres}, of 59 kPa in the x-direction. Thus the resultant residual strength, $(\tau_{res})_{result}$ is:

$$(\tau_{res})_{result} = (\tau_{xres}^2 + \tau_y^2)^{1/2} = (59.0^2 + 20.0^2) = 62.3\ kPa$$

The plots of total tangential displacement, shear deformation of sand, and sliding displacement versus time, in the x- and y-directions, are illustrated in Figs. 6.7 and 6.8, respectively. Figure 6.7 indicates that as the number of cycles increased, the amplitude of sliding displacement, u_x, increased and the amplitude of shear deformation of sand, u_{xb}, decreased. Figure 6.8 shows that while the sliding displacement in the y-direction increased during cycles in the x-direction, the shear deformation of sand increased a small amount and then stabilized after about 5 cycles when failure occurred.

The resultant shear stress, $(\tau_x^2 + \tau_y^2)^{1/2}$, is plotted versus the resultant sliding displacement, $(u_x^2 + u_y^2)^{1/2}$, as shown in Fig. 6.9. It seems that the envelope of the maximum shear stress at each cycle follows a path similar to the monotonic test results.

Figure 6.10 illustrates the shear stress and sliding displacement paths on the interface plane for $\tau_y = 20$ case. First the shear stress, τ_y, was monotonically increased from zero to 20 kPa. This path is illustrated between points o and i in Fig. 6.10a. Subsequently, the interface was subjected to a two-way tangential displacement controlled cyclic shearing in the x-direction, while τ_y was maintained at 20 kPa. Therefore, the stress path remained parallel to the x-axis at $\tau_y = 20$ kPa. The displacement controlled cyclic tests in the x-direction under a constant σ_n of 100 kPa, and a constant τ_y of 20 kPa produced a peak of 81.7 kPa (Fig. 6.10*a*). Figure 6.10*b* illustrates that during the displacement controlled cyclic shearing in the x-direction, the sliding displacement in the y-direction continued although shear stress, τ_y, was kept constant at 20 kPa in that direction. The rate of sliding displacement, u_y, increased with increasing number of cycles. Figure 6.10*b* also indicates that the amplitude of sliding displacement in the x-direction, u_x, increased when the number of cycles was increased. Eventually, u_x approached a constant value of 0.67 mm whereas the amplitude of total tangential displacement was 0.75 mm. The comparison between Figures 6.10*a* and 6.10*b* indicates that the shear stress and sliding displacement increments followed different paths on the interface plane. After 30 cycles, the interface had already slided about 6 mm in the y-direction while the shear stress in the y-direction was constant, and interface was only subjected to cyclic shearing in the x-direction. In fact Fig. 6.10 demonstrates the coupling effects between shear stresses and sliding displacements in the x- and y-directions.

Other tests with τ_y at 30, 40, and 60 kPa exhibited the same trend as illustrated in Figs. 6.11 through 6.13. However, the higher τ_y resulted in higher rate of sliding in the y-direction. For example, 23 cycles required to create a sliding displacement of 4 mm in the y-direction, u_y, for $\tau_y = 20$ kPa. To generate the same amount of sliding displacement in the y-direction, the number of cycles reduced to 12, 8, and 2 cycles for τ_ys of 30, 40, and 60 kPa, respectively. This observation is in accordance with those presented in Fig. 6.3, for 3-D monotonic test results that also exhibited higher rate of sliding displacement in the y-direction at higher values of τ_y.

Some other comparisons for different values of constant τ_y are presented in Table 6.1. It is observed that at higher values of τ_y, the number of cycles required to bring the interface to a state of failure decreased. For example, at $\tau_y = 40$ kPa, only 3 cycles were needed to fail the interface as compared to 12 cycles for $\tau_y = 0$. It is also observed that the peak strength in the x-direction, τ_{xp}, and the residual strength in that direction, τ_{xres}, decreased by increasing the magnitude of τ_y. However, resultant peak and residual strengths, $(\tau_p)_{result}$ and $(\tau_{res})_{result}$, were about the same in all four cases, with an average of 82.8 kPa and 62.3 kPa, respectively. Therefore, similar to the 3-D monotonic results presented in Fig. 6.4, the resultant peak and residual strengths are not affected by stress paths. Thus, there exist a circular peak strength envelope and a circular residual strength envelope for an isotropic interface, as demonstrated in Fig. 6.14, for different values of τ_y.

TABLE 6.1. Summary of results for tests with different constant τ_y.

Constant τ_y (*kPa*)	No of cycles to failure, N_f	τ_{xp} (*kPa*)	$(\tau_p)_{result}$ (*kPa*)	τ_{xres} (*kPa*)	$(\tau_{res})_{result}$ (*kPa*)
0	12	83.0	83.0	60.0	60.0
20	5	81.7	84.1	59.0	62.3
30	4	76.3	82.0	57.4	64.7
40	3	71.5	82.0	47.5	62.1

The influence of the magnitude of τ_y on the normal displacement, v, in the z-direction, is illustrated by plotting the normal displacement against the sliding displacement in the y-direction, u_y (Fig. 6.15). More compression occurred under lower values of τ_y. For example a total compression of 0.4 mm took place for $\tau_y = 20$ kPa. The total compression for 2-D cyclic tests ($\tau_y = 0$) was 0.65 mm (Fig. 5.18*b*). $\tau_y = 30$ kPa caused the interface to compress first and then dilated by increasing the cycles. τ_ys of 40 and 60 kPa exhibited dilation from beginning. Thus the interface showed a dilatant behaviour under high values of τ_y. In this type of testing, the variation in normal displacement of the interface is controlled by two factors: (1) Cyclic displacement controlled shearing in the x-direction under which the normal displacement is compressive; (2) Tangential displacement in the y-direction, due to the constant shear stress τ_y, under which the normal displacement is dilatant. Under lower values of τ_y, the behaviour of the interface is mostly dominated by the cycles in the x-direction, therefore normal displacement is compressive. Under higher values of τ_y, however, the volume change is mostly dominated by the increasing tangential displacement in the y-direction, therefore, exhibits dilatant behaviour.

Large movements causing catastrophic failures may occur when a layer is subjected to cyclic loads at the presence of a shear load perpendicular to the direction of cycles. Such a failure may occur, for example, in slopes subjected to cyclic loads resulting from an earthquake motion in the direction perpendicular to the slope while the gravity based shear forces exist in the direction parallel to the slope.

6.2.2 Rotational loading

The objective of these experiments was to rotate the sand sample over the steel plate along a circular or elliptical path. To produce elliptical total tangential displacement path, the interface was subjected to sinusoidal displacement controlled cycles in the x- and y-directions, simultaneously, at equal frequencies. However, cycles in one of the directions started one quarter of a cycle later than the other so that the two motions were 90° out of phase with each other as illustrated in Fig. 6.16a. Assume that the interface is subjected to a sinusoidal total tangential displacement controlled cycles in the x-direction with an amplitude of u_{xao} and a period of T in the x-direction. Thus the equation of such a path is:

$$u_{xa} = u_{xao}.\sin[(\frac{2\pi}{T})t] \qquad \text{Eq. 6.1}$$

If after one quarter of the first cycle, i.e. at the time $T/4$, the interface be subjected to another sinusoidal total tangential displacement controlled cycles with an amplitude of u_{yao} and the same period of T, in the y-direction, then the equation of such a path becomes:

$$u_{ya} = u_{yao}.\sin[(\frac{2\pi}{T})t - \frac{\pi}{2}] \qquad \text{Eq. 6.2}$$

Combination of Eqs. 6.1 and 6.2 results:

$$(\frac{u_{xa}}{u_{xao}})^2 + (\frac{u_{ya}}{u_{yao}})^2 = 1 \qquad \text{Eq. 6.3}$$

which is an equation for an ellipse. This path is illustrated in Fig. 6.16b. Specifying $u_{xao} = u_{yao}$, i.e. equal total tangential displacement amplitudes in the x- and y-directions results:

$$u_{xa}^2 + u_{ya}^2 = u_{xao}^2 \qquad \text{Eq. 6.4}$$

which is an equation of a circle as illustrated in Fig. 6.16*c*.

Such displacement paths were simulated by the computer-controlled system. LVDTs a_x and a_y were used to generate the elliptic and circular paths, therefore, the total tangential displacements were rotating along those paths.

A ***cyclic tangential displacement amplitude ratio*** is defined as the ratio between the amplitude of total tangential displacement in the *y*-direction, u_{yao}, and the amplitude of total tangential displacement in the *x*-direction, u_{xao}. u_{yao} and u_{xao} are the minor and the major axis of the ellipse in the *y*- and *x*-directions, respectively. Thus, the magnitude of cyclic tangential displacement amplitude ratio, u_{yao} / u_{xao}, determines the shape of the ellipse such that a ratio of 0.0 is a straight line, and a ratio of 1.0 is a full circle.

Four tests were conducted with the cyclic tangential displacement amplitude ratios of 0, 0.33, 0.66, and 1.0. The ratio 0.0 indicates a 2-D test similar to those presented in Figs. 5.19 through 5.22. The No. 2 sand with an initial relative density of 88% and the sand blasted steel plate (R_{max} = 25 μm for L = 0.8 mm) were used in all tests performed in this group of experiments.

Test results for cyclic tangential displacement amplitude ratio of 0.33 are presented in Figs. 6.17 through 6.22. The shear stress-tangential displacements in the *x*-direction and volume change results are shown in Fig. 6.17. The results at 1st cycle, 10th cycle (failure), and 53th cycle are presented individually in Fig. 6.18. Cycles are defined based on a complete loop in the *x*-direction. The general trend in these results are similar to that of 2-D cyclic tests in which u_{yao} / u_{xao} is zero. However, due to the rotational format of the cycles, a more rounded corners are observed at the amplitude points as compared with the 2-D results that exhibited sharp corners. A failure occurred at cycle 10 with peak and residual strength components in the *x*-direction measured as 73.0 and 53.0 kPa. The resultant peak and residual strengths were 75.0 and 55.0 kPa, respectively. Therefore, the shear strengths were lower than the peak and residual strengths of 84.0 and 62.0 kPa, respectively, for a 2-D test (u_{yao} / u_{xao} = 0).

The variation of tangential displacements in the x- and y-directions are presented in Figs. 6.19 and 6.20, respectively. The same trend is observed in both directions, i.e. the amplitude of shear deformation of sand decreased as the amplitude of sliding displacement at the interface increased in the x- and y-directions. Shear stress and tangential displacement paths on the x-y plane are illustrated in Figs. 6.21 and 6.22. Shear stress loops expanded with increase in the number of cycles, and started to shrink after the peak strength was reached at cycle 10. The total tangential displacement path is an ellipse with its major axis in the x-direction, and the minor axis in the y-direction. The major axis has a magnitude of 1.50 mm which is twice that the total tangential displacement amplitude of the cycles in the x-direction as illustrated in Fig. 6.19*a*. On the other hand, the minor axis has a magnitude of 1.0 mm which is twice that the total tangential displacement in the y-direction as illustrated in Fig. 6.20*a*. In fact the ellipse is a combination of Figs. 6.19*a* and 6.20*a*.

The shear deformation of sand mass and sliding displacement also exhibited elliptic paths as illustrated in Figs. 6.21*c* and 6.21*d*, respectively. The shear deformation moved along the x-axis up to 0.5 mm and then started to follow an elliptic path and intersected the y-axis at a shear deformation of 0.3 mm in that direction. 0.5 and 0.3 mm are the maximum shear deformations during the 1st cycle in the x- and y-directions, respectively, as illustrated in Figs. 6.19*b*, and 6.20*b*. The ellipse kept shrinking as the shear deformation in the sand mass tapered off. On the other hand, the elliptic path of sliding displacement expanded with increase in the number of cycles as illustrated in Figs. 6.21*d* and 6.22*d*. This expanding path is also due to the increase in sliding displacement amplitudes in the x- and y- directions with increase in the number of cycles as illustrated in Figs. 6.19*c* and 6.20*c*.

In order to study the influence of variation in u_{yao} / u_{xao} on shear stress, tangential displacements, and volume change results of the interface, several comparative figures are presented in Figs. 6.23 through 6.28. Shear stress paths for different u_{yao} / u_{xao} on the x-y plane, illustrated in Fig. 6.23, show that the variations of the shear stress within each cycle diminished as the u_{yao} / u_{xao} approached unity. For example, the shear stress paths for u_{yao}/ u_{xao} of 0.33 has an elliptic shape (Fig. 6.23*b*) whereas the u_{yao} / u_{xao} of 1.0 illustrates a circular shape (Fig. 6.23*d*). This was further examined by plotting the absolute value of the resultant shear stress against time as shown in Fig. 6.24 for different values of u_{yao} / u_{xao}. For example, for u_{yao} / u_{xao} of 0.0 (2-D test) the magnitude of resultant shear stress varied between 0.0 and 84.0 kPa at peak, and 0.0 and 62.0 kPa at residual state, as shown in Fig. 6.24*a*. These variations dramatically decreased for u_{yao} / u_{xao} of 1.0, as shown in Fig. 6.24*d*. Especially at residual state, the variations are negligibly small indicating that the magnitude of the resultant shear stress during cycling did not change. In other words, the shear stress path was a full circle.

The influence of u_{yao} / u_{xao} on the variations of shear deformation of sand and sliding displacement are illustrated in Figs. 6.25 and 6.26, respectively. They all resemble in pattern except that the shape of the paths varied from a straight line for $u_{yao} / u_{xao} = 0.0$, to a full circle for $u_{yao} / u_{xao} = 1.0$. The shear deformation paths were contractive because of the stiffening of the sand mass with cycles. On the other hand, the sliding displacement paths exhibited expansive patterns, which was due to increase in the sliding displacement amplitudes in the *x*- and *y*-directions with increase in cycles.

The volume change responses of the sample with increasing cycles exhibited higher average compression at the end of 51 cycles for higher values of u_{yao} / u_{xao} (Fig. 6.27). The rate of increase, however, reduced with increase in the magnitude of the cyclic tangential displacement amplitude ratio, u_{yao} / u_{xao}, as illustrated in Fig. 6.28. The higher compression of the sand with increasing u_{yao} / u_{xao} is associated with the fact that the sand mass was cycled in two perpendicular directions simultaneously, giving the sand particles more opportunity to rearrange and fill the gaps to lower the void ratio. The higher tendency of sand mass to compression during rotational paths, as compared to 2-D cyclic loading, would probably cause the sand mass to liquefy with less number of cycles, had the tests were conducted under undrained conditions. This is due to the fact that higher tendency to compression of the undrained sand mass, under two-way cyclic loading, causes larger pore water pressure development, and as a result the liquefaction or undrained failure of sand. This observation complies with the results presented by Ishihara and Yamazaki (1980) who studied the effects of rotational loading on the liquefaction behaviour of the Fuji River Sand. Those researchers had realized that lower stress levels and fewer number of cycles were required to liquefy the undrained sand as the path of the shear stress on the *x*-*y* plane approached a full circle.

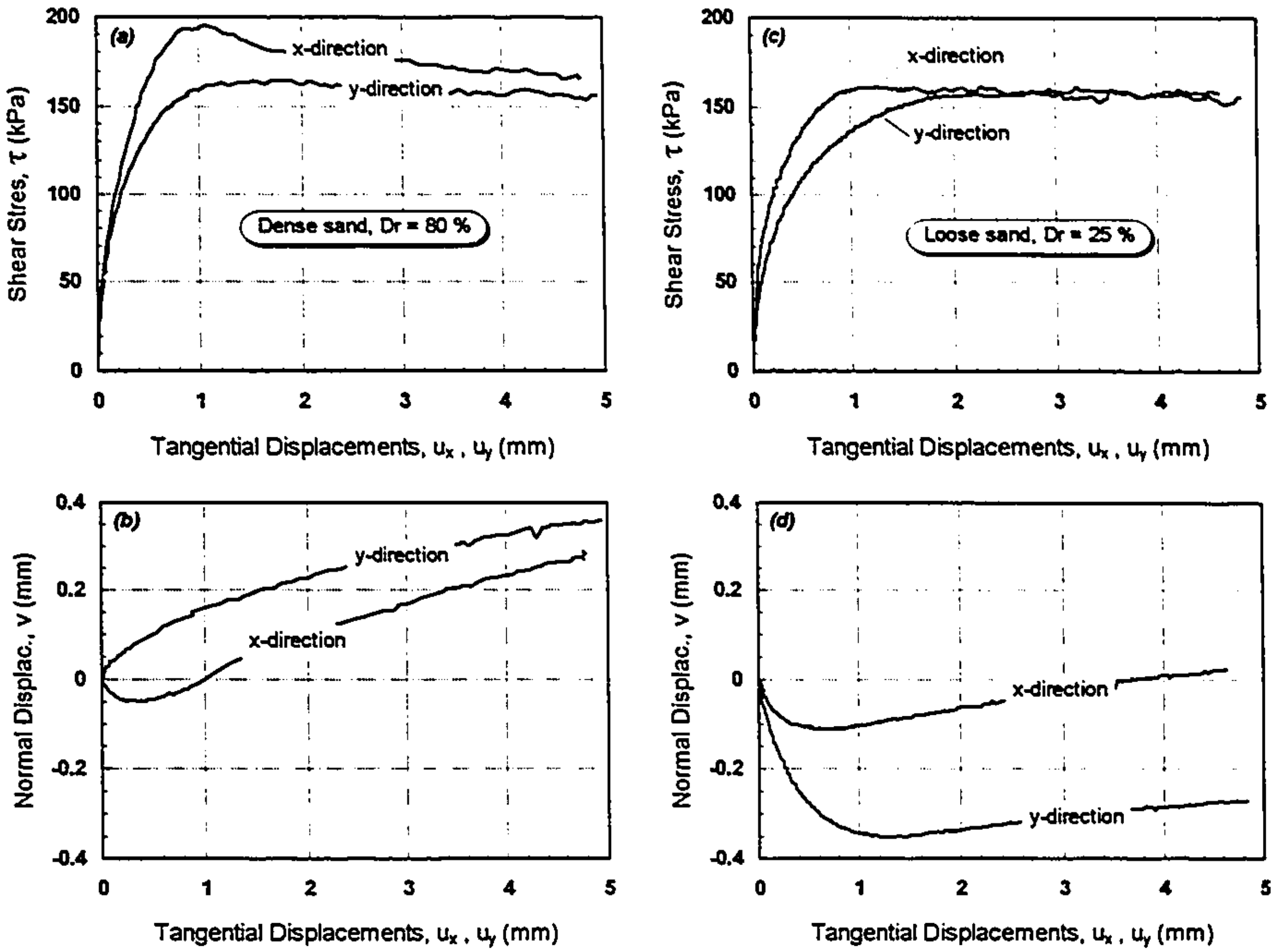

FIG. 6.1. 3-D stepwise monotonic shearing under a constant normal stress; *Direct* shear box; *(a)* and *(b)*: Dense sand; *(c)* and *(d)*: Loose sand

Surface: ALO cloth # 150

Sand: No. 1; Dense ($D_r = 80\%$) and loose ($D_r = 25\%$)

$\sigma_n = 250$ kPa

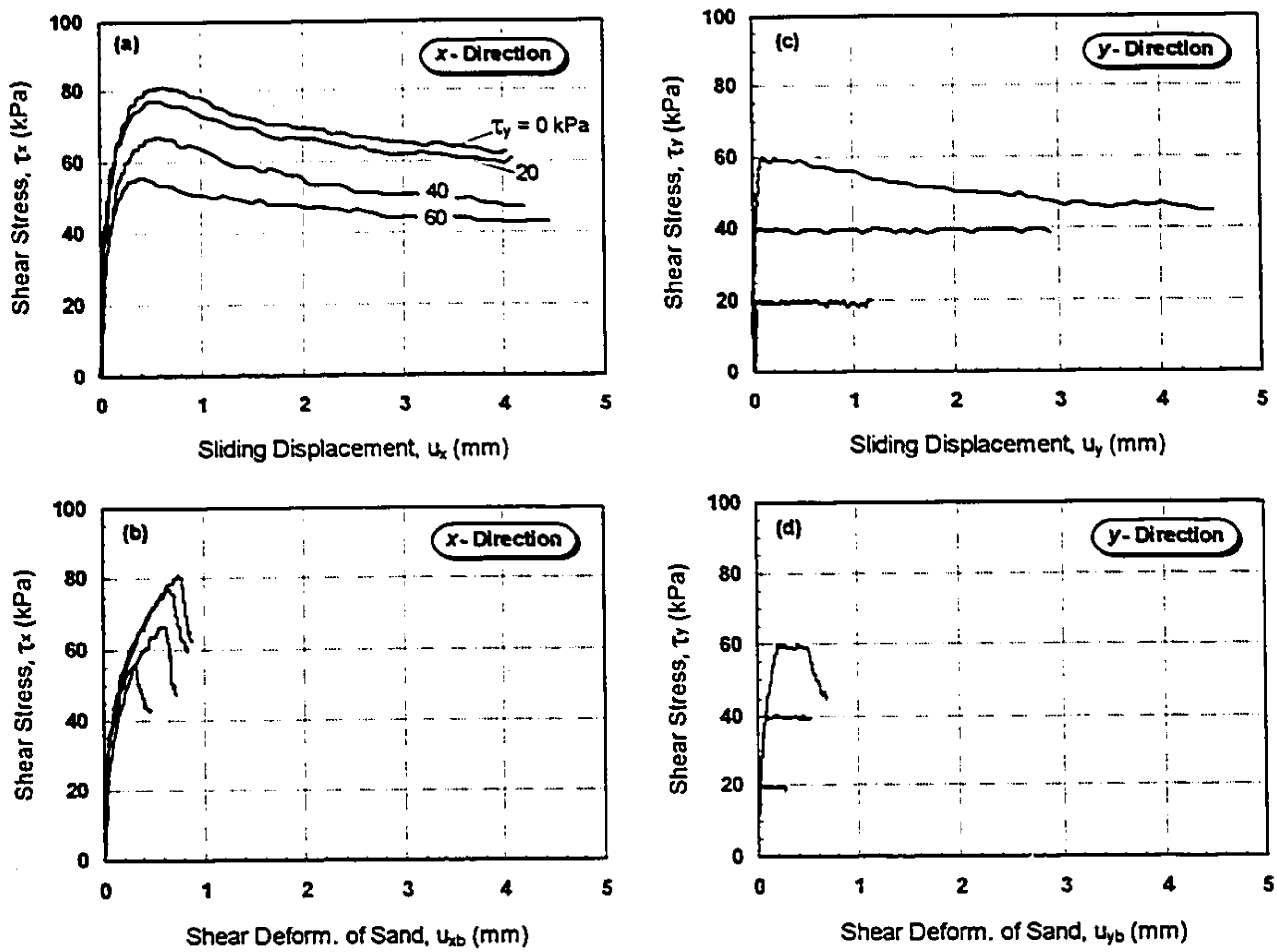

FIG. 6.2. 3-D simultaneous monotonic shearing under a constant normal stress; *Simple* shear box; *(a)* and *(b)*: x-direction ; *(c)* and *(d)*: y-direction

Surface: Sand blasted steel plate (R_{max} = 25 μm for L = 0.8 mm)

Sand: No. 2; Dense (D_r = 88%)

σ_n = 100 kPa

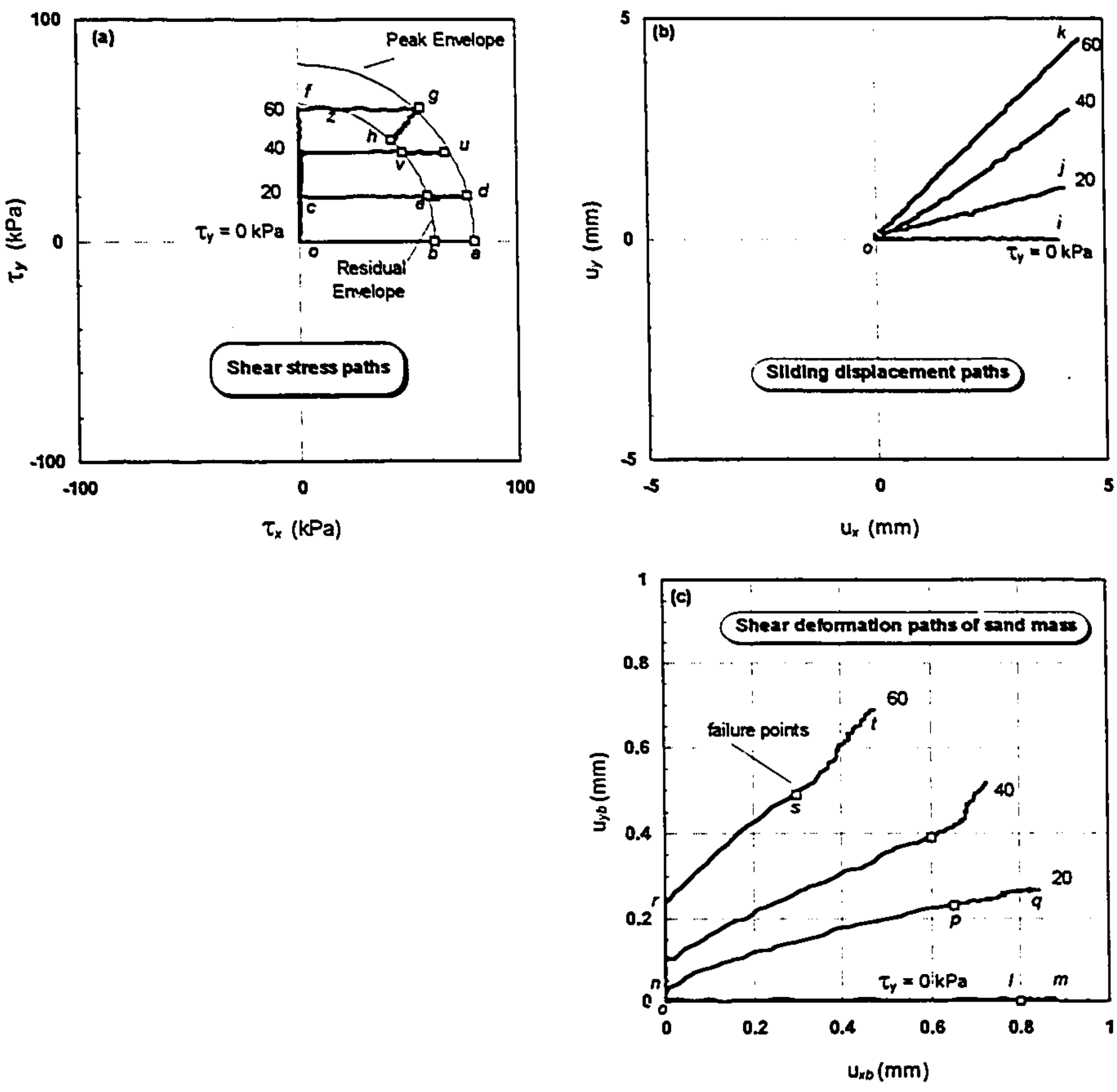

FIG. 6.3. 3-D simultaneous monotonic shearing under a constant normal stress; *Simple* shear box; *(a)* shear stress; *(b)* sliding displacement; *(c)* and shear deformation of and paths on the *x-y* plane.

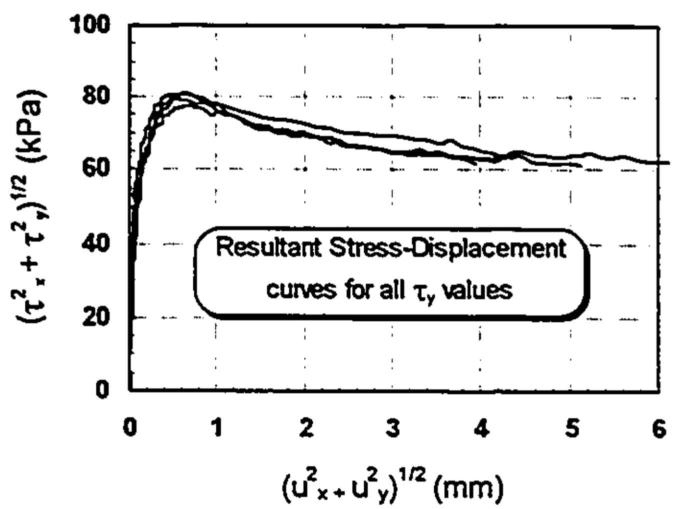

FIG. 6.4. Resultant shear stresses *vs.* resultant sliding displacements in the 3-D simultaneous monotonic shearing under a constant normal stress; *Simple* shear box.

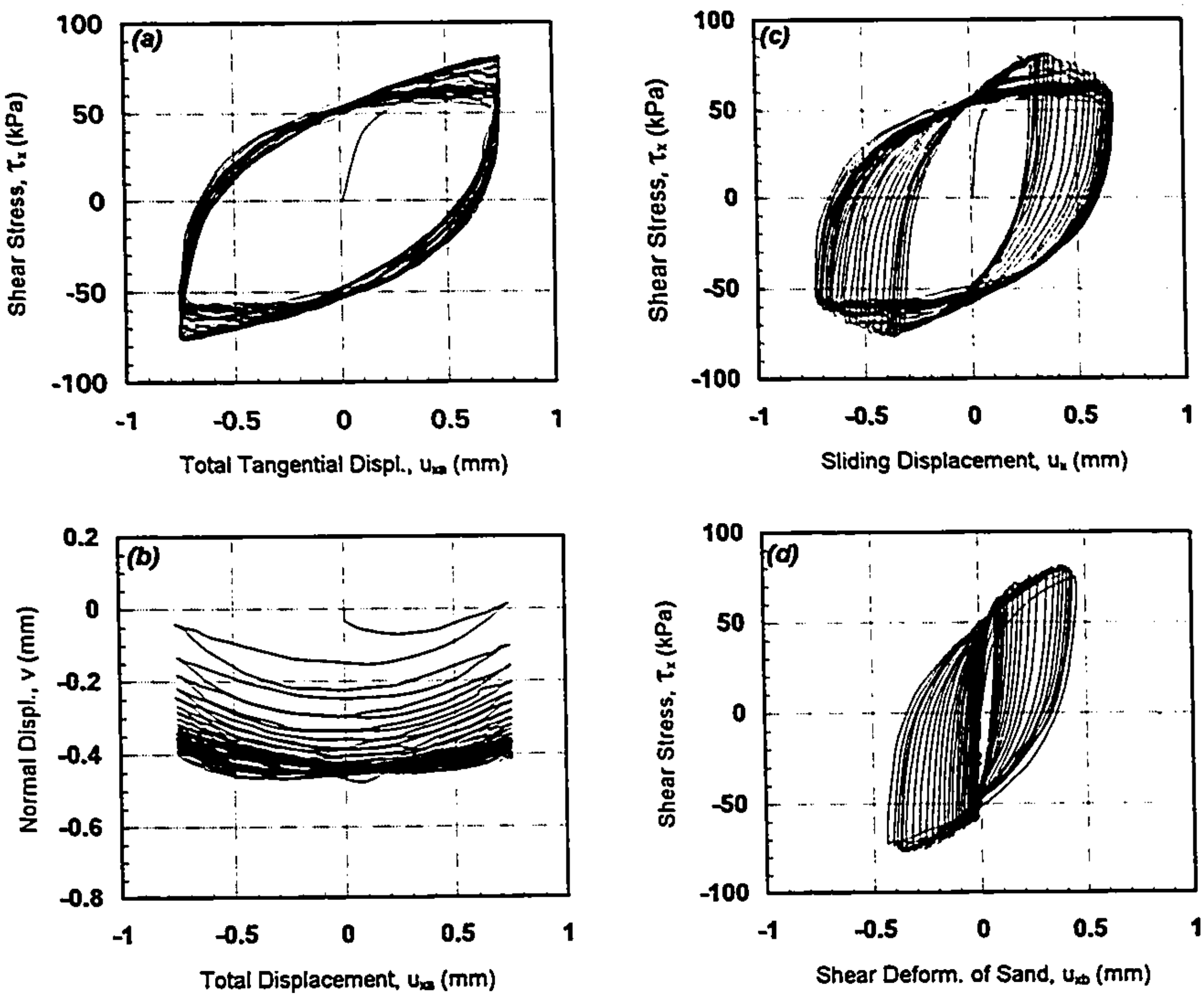

FIG. 6.5. Results of a 3-D cyclic test in the x-direction for $\tau_y = 20$ kPa under Constant normal stress.

Surface: Sand blasted steel plate ($R_{max} = 25$ μm for $L = 0.8$ mm)
Sand: No. 2; Dense ($D_r = 88\%$)
$\sigma_n = 100$ kPa

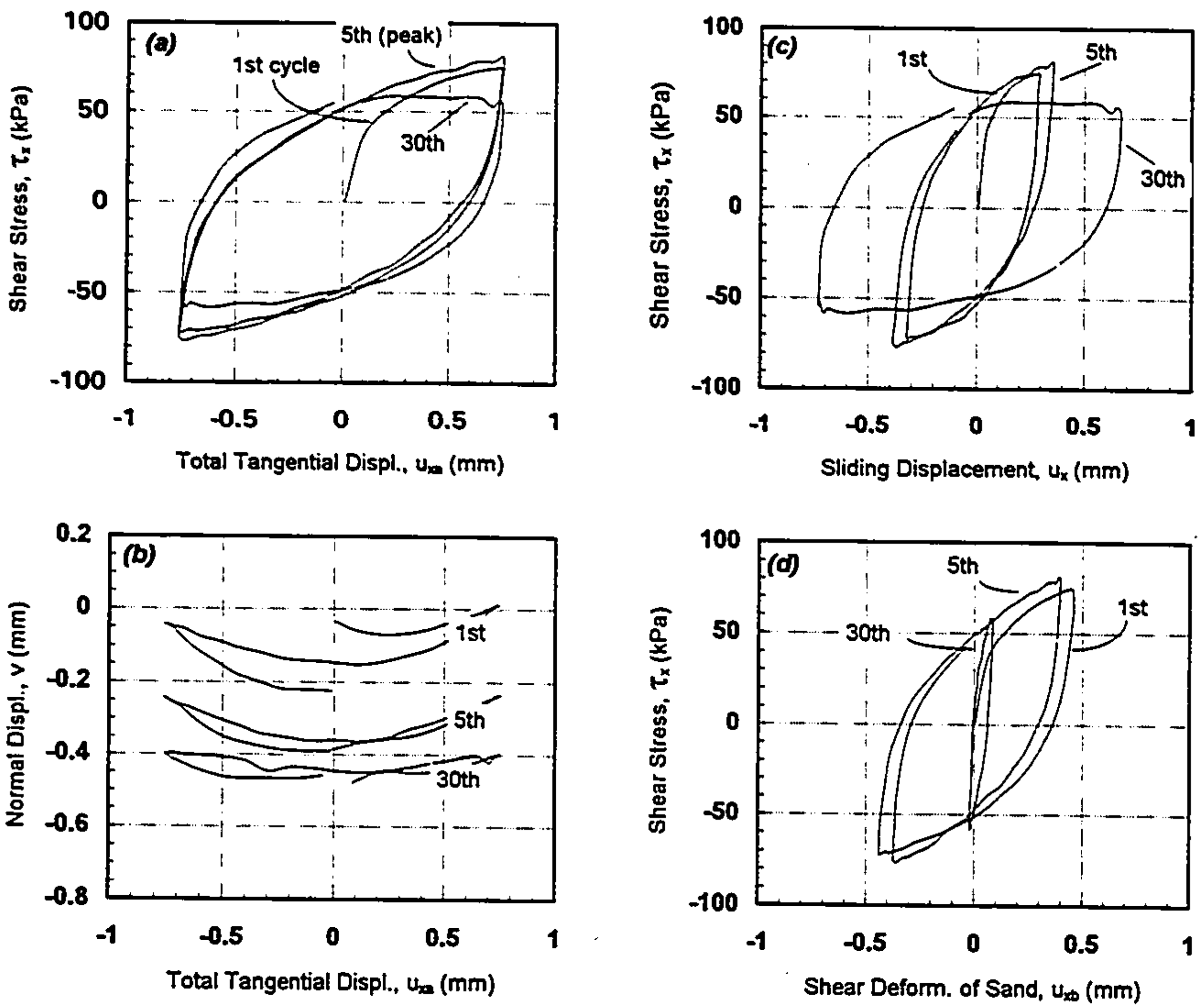

FIG. 6.6. Complete loops at cycles 1, 5, and 30 from the results shown in Fig. 6.5.

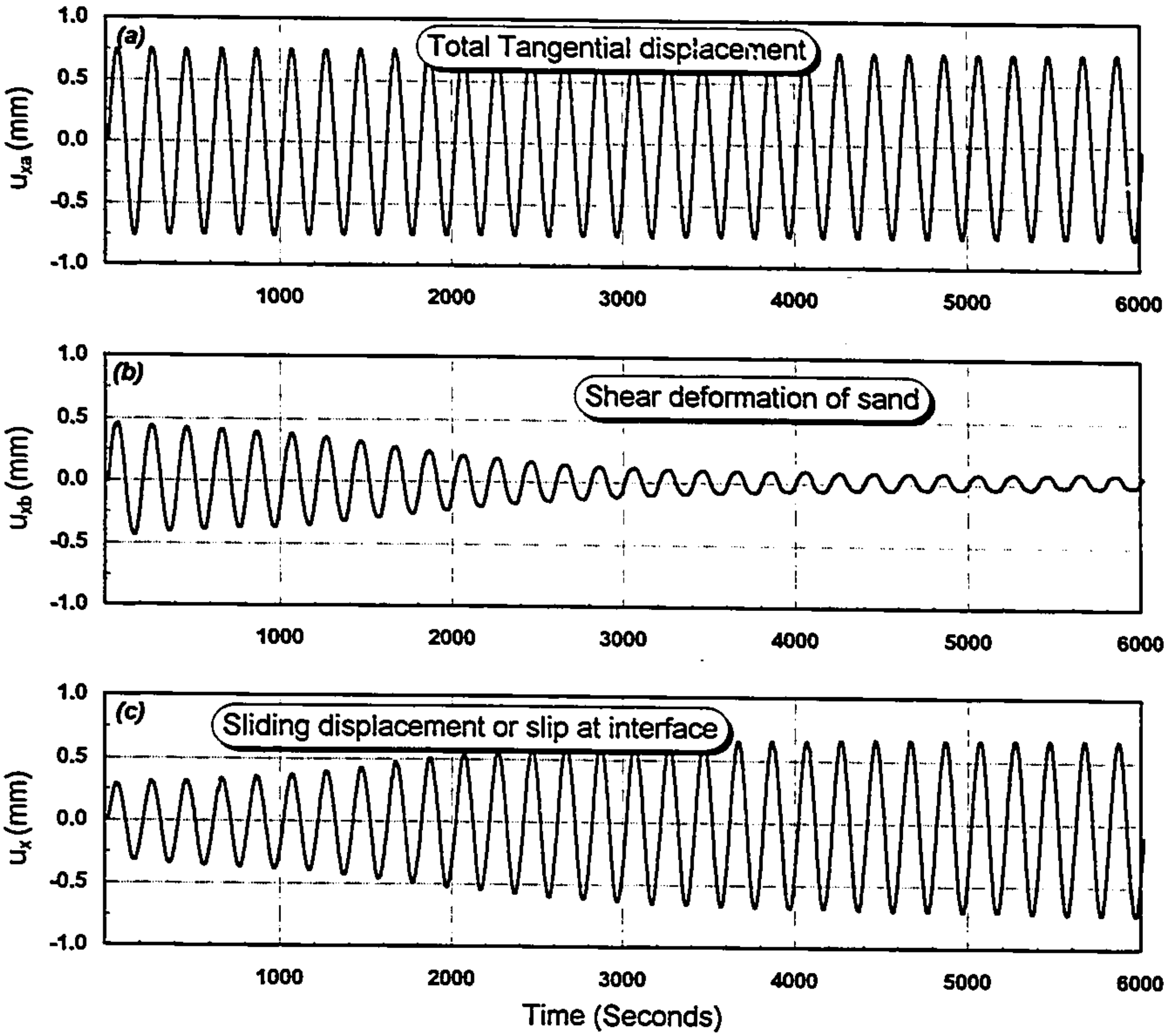

FIG. 6.7. Variation of tangential displacements in the *x-direction* with time for results shown in Fig. 6.5.

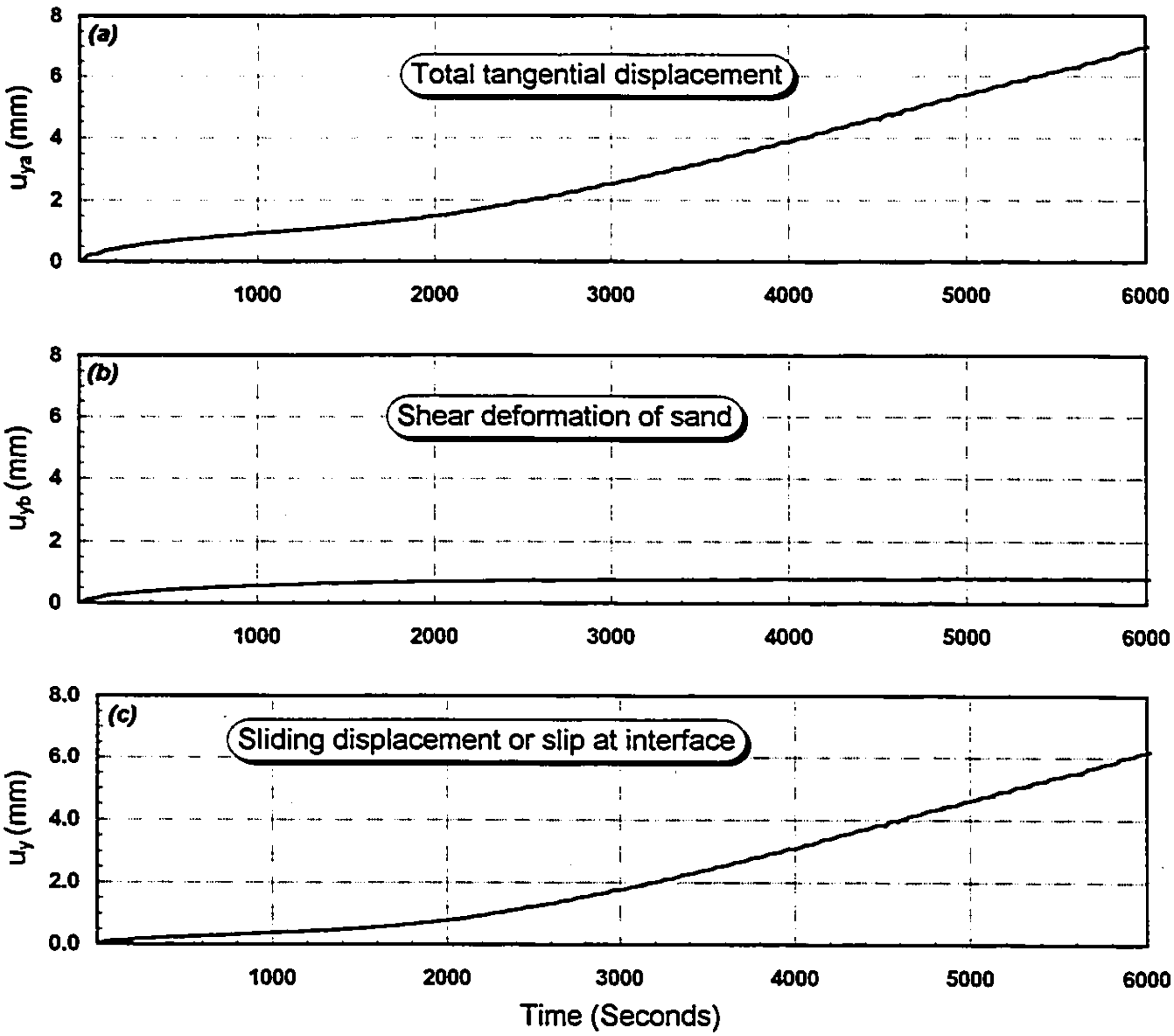

FIG. 6.8. Variation of tangential displacements in the *y-direction* with time for results shown in Fig. 6.5.

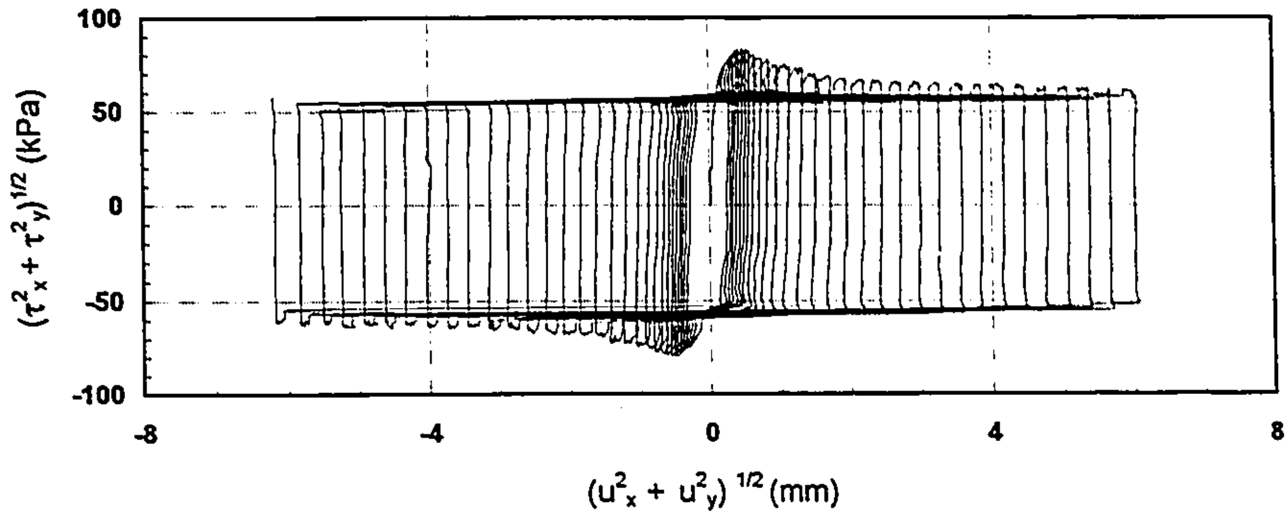

FIG. 6.9. Resultant shear stress vs. resultant sliding displacement.

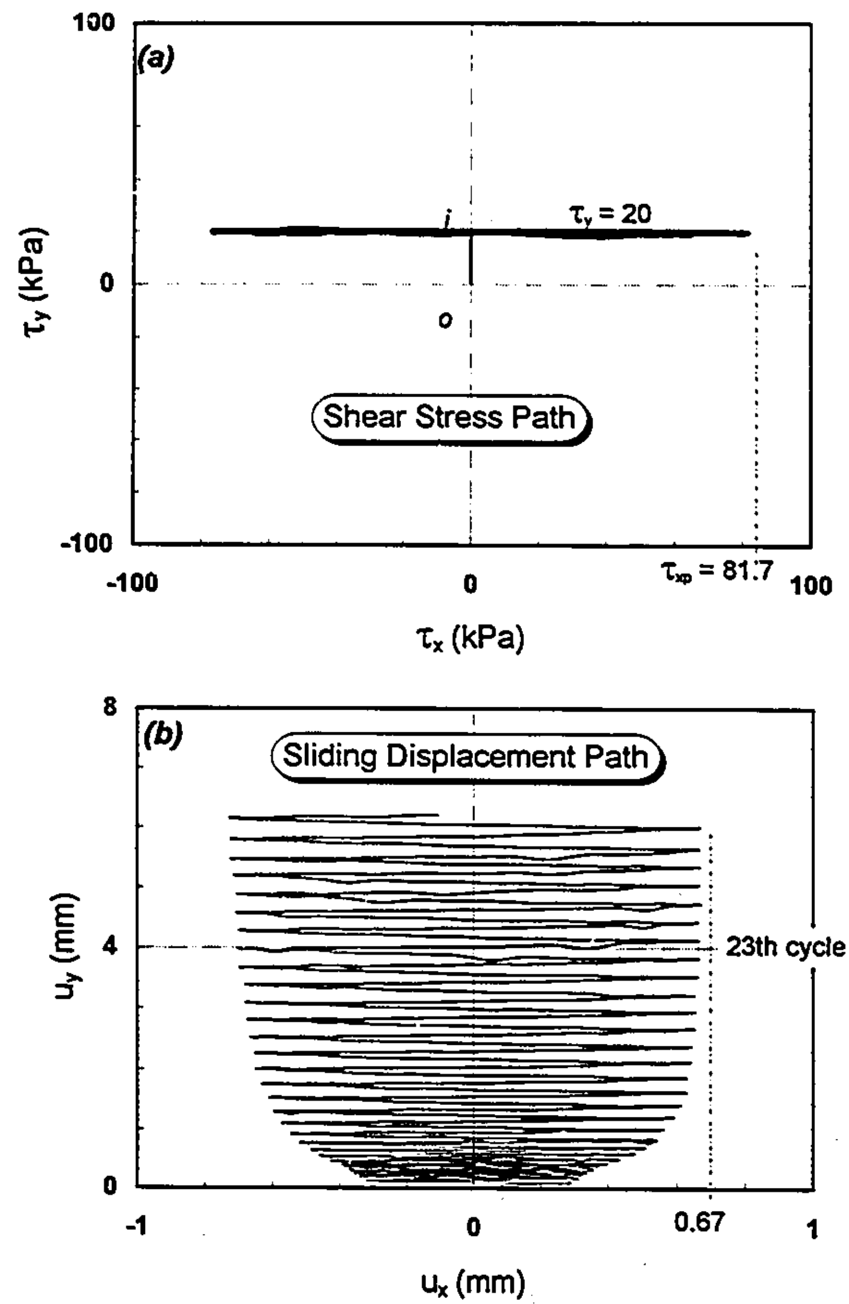

FIG. 6.10. Shear stress and sliding displacement paths on the *x-y* plane.

$\tau_y = 20$ kPa

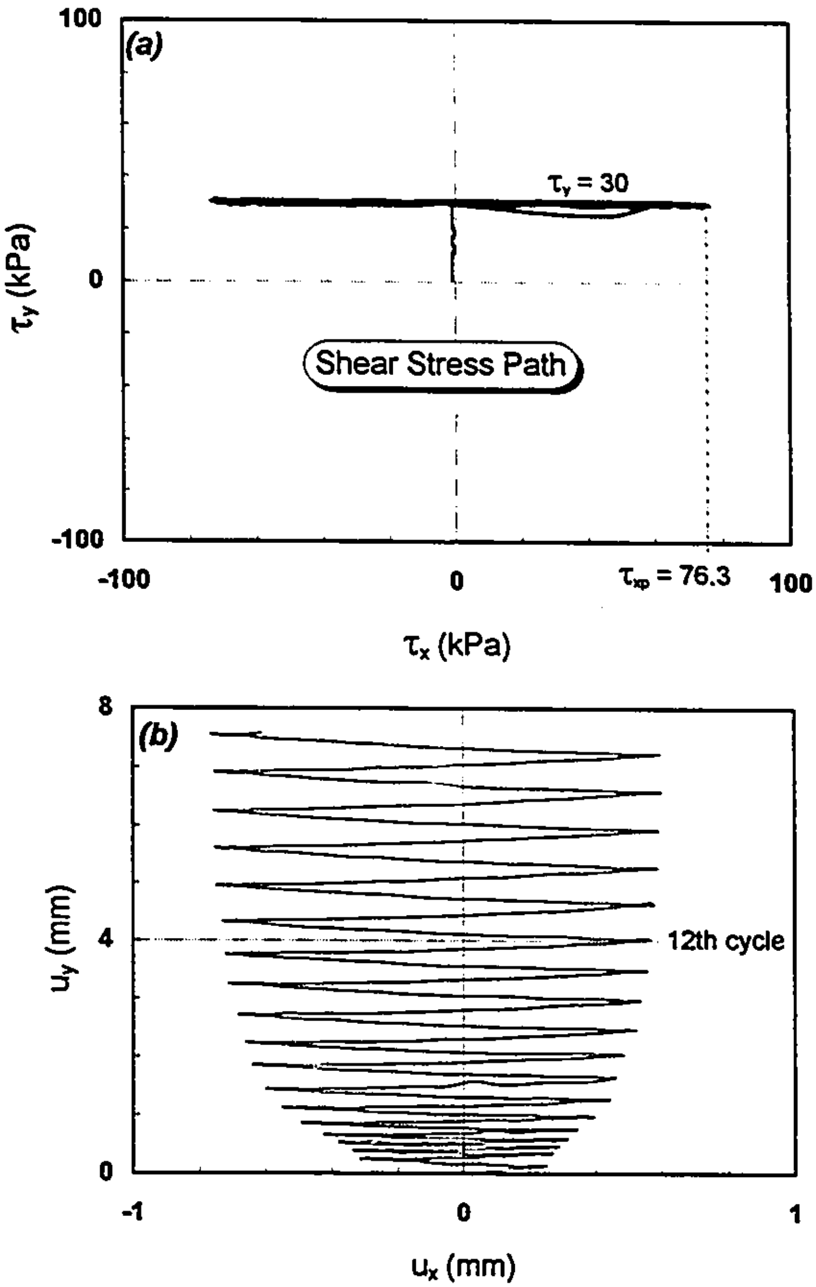

FIG. 6.11. Shear stress and sliding displacement paths on the *x-y* plane.

$\tau_y = 30$ kPa

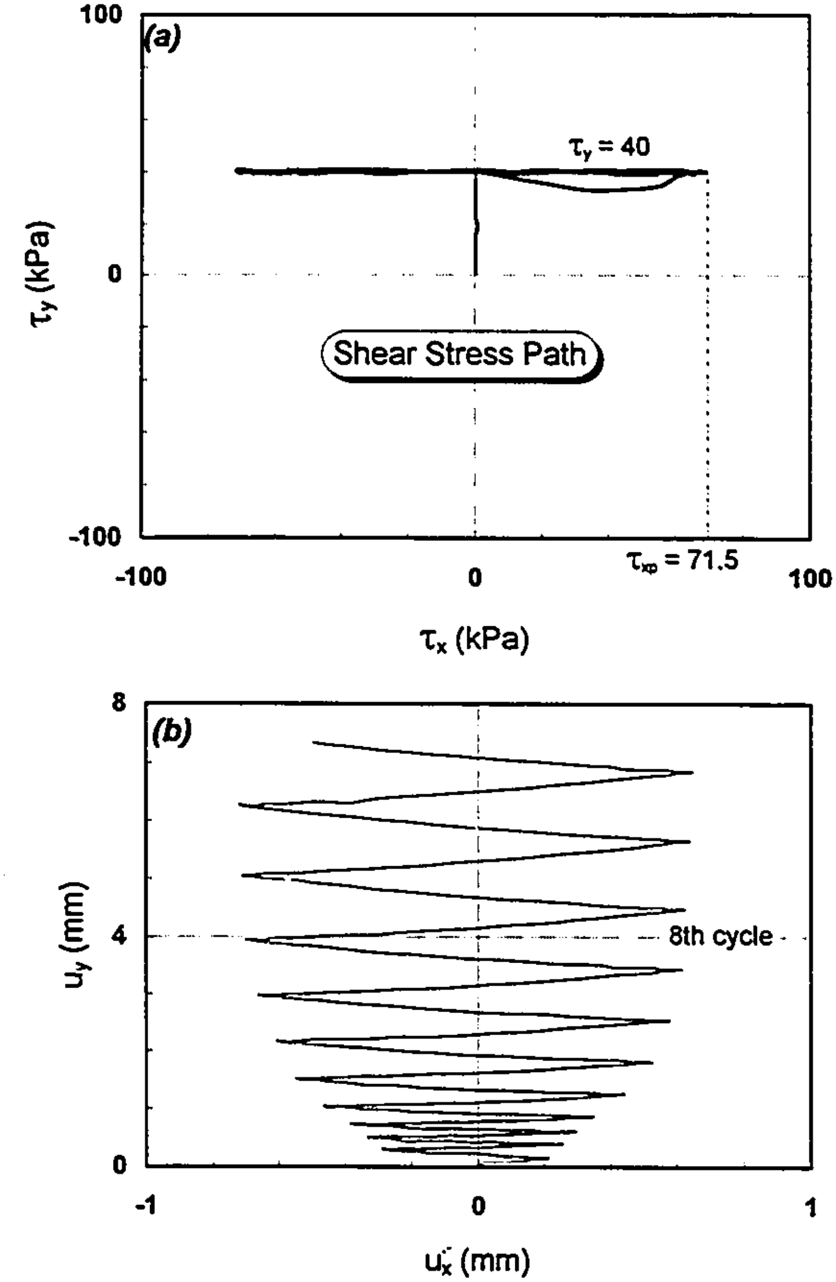

FIG. 6.12. Shear stress and sliding displacement paths on the *x-y* plane.

$\tau_y = 40$ kPa

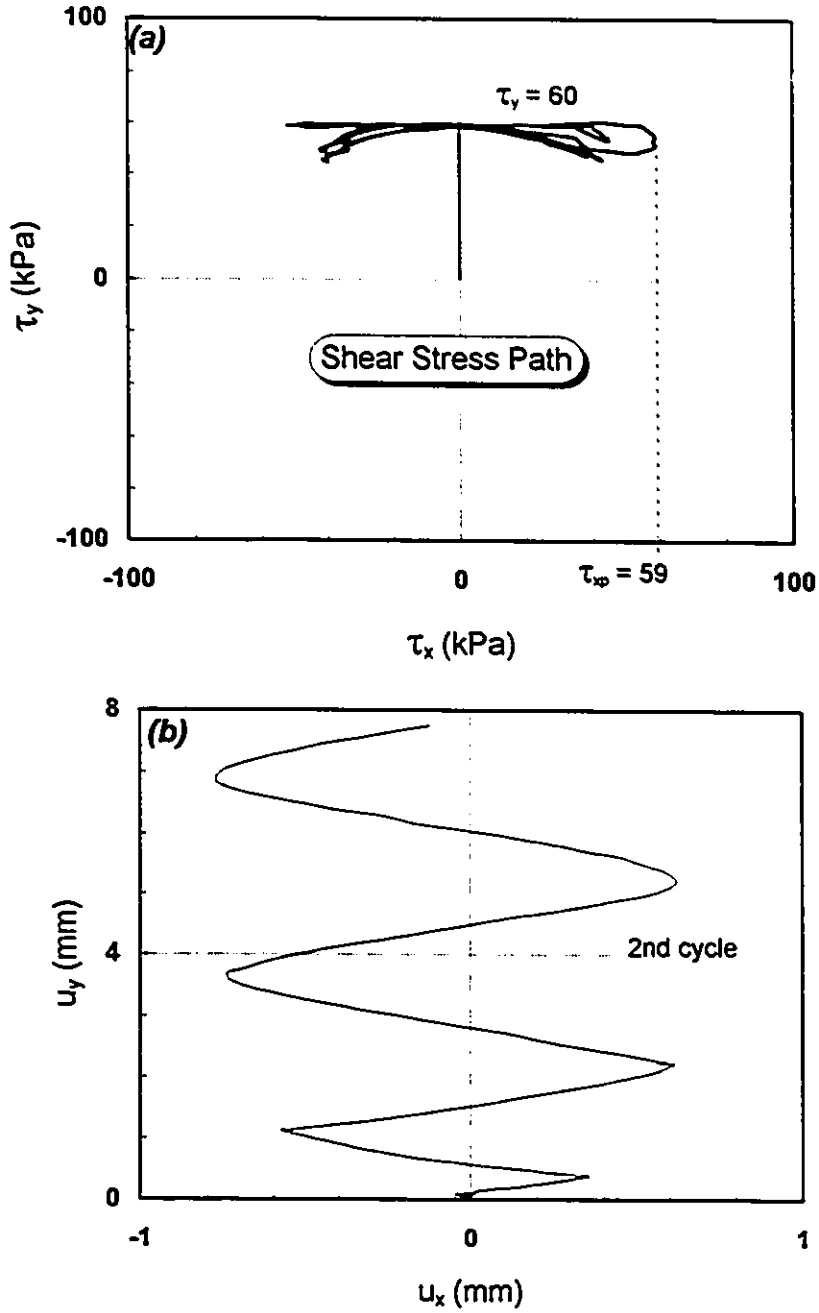

FIG. 6.13. Shear stress and sliding displacement paths on the *x-y* plane.

$\tau_y = 60$ kPa

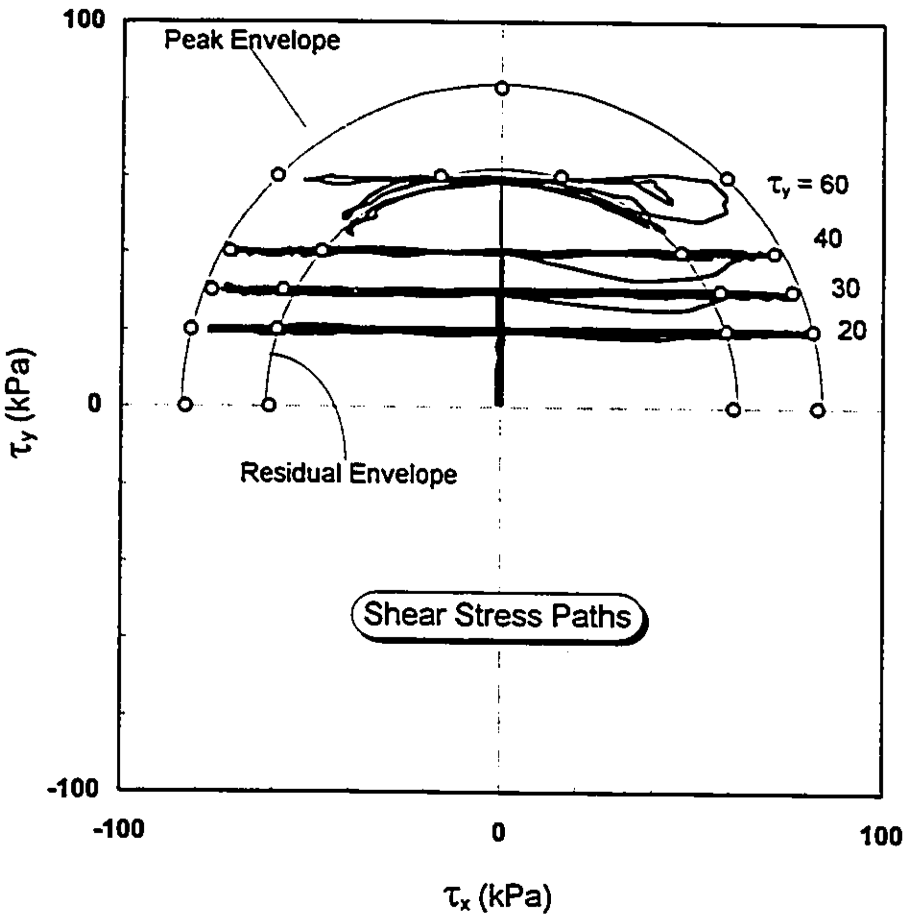

FIG. 6.14. Shear stress paths for various values of τ_y.

τ_y = 20, 30, 40, and 60 kPa

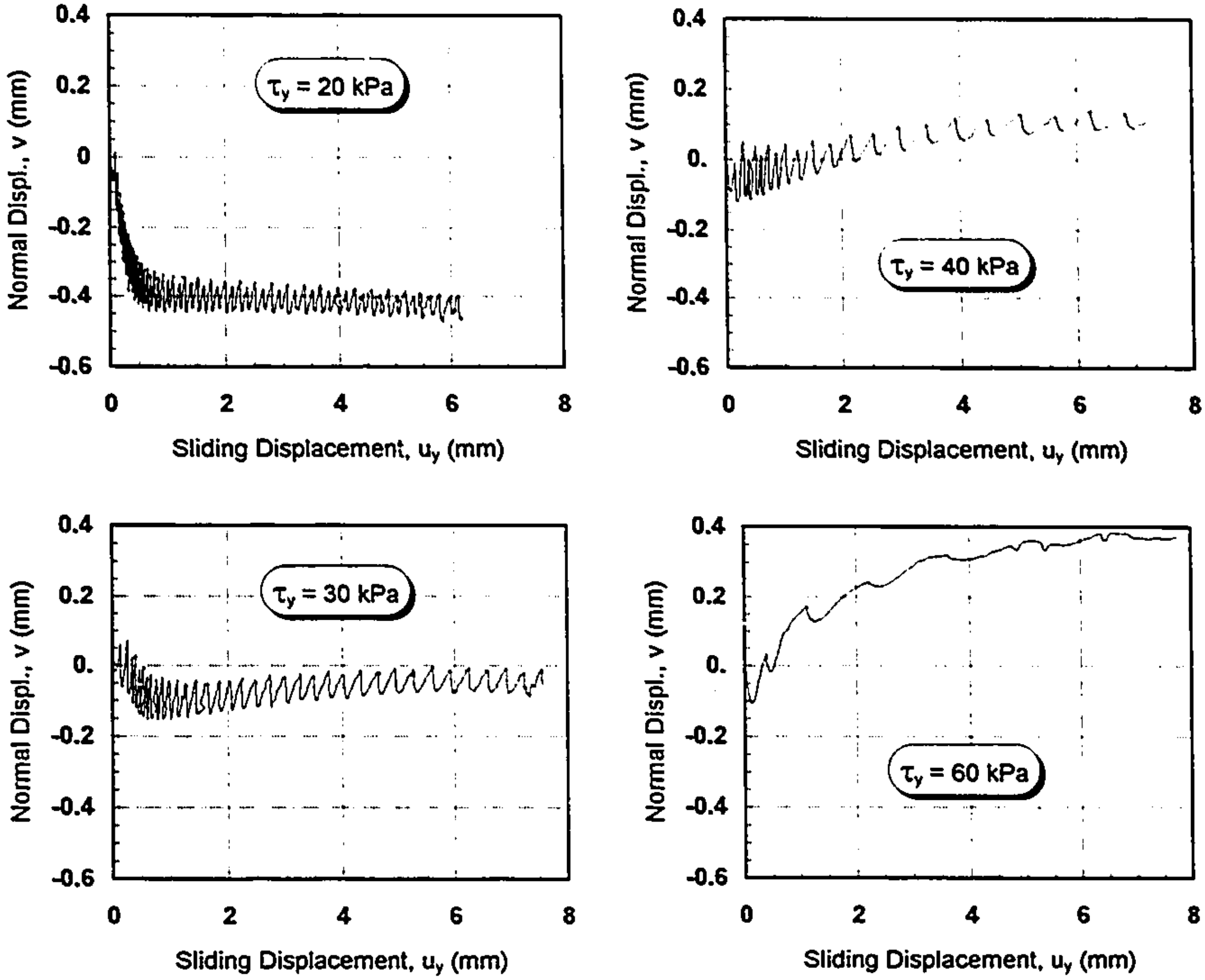

FIG. 6.15. Variations of volume change with sliding displacement in the y-direction for various τ_y values.

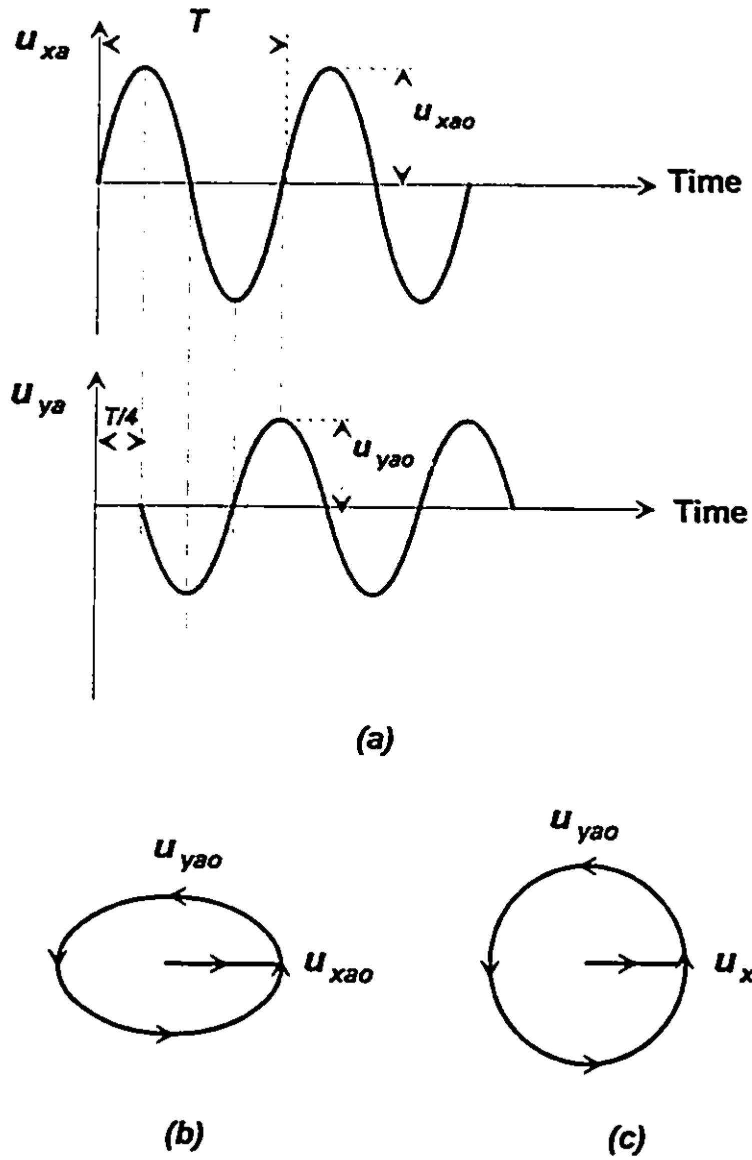

FIG. 6.16. Generating the rotational tangential displacement paths; *(a)* Sinusoidal waves in the x- and y-directions; *(b)* Elliptic path; *(c)* Circular path

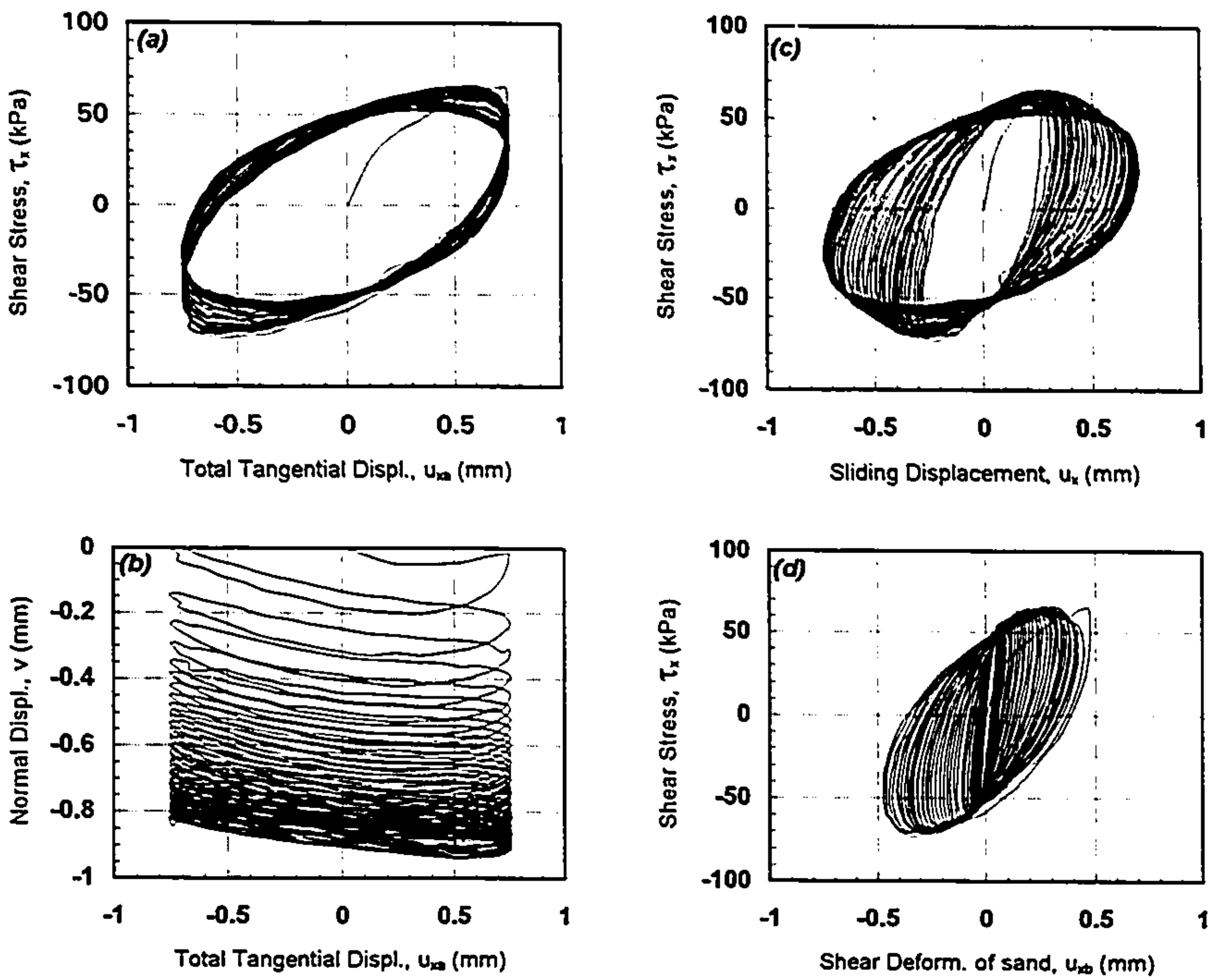

FIG. 6.17. Components of results in the x-direction for a 3-D cyclic rotational shearing test.

$u_{yao} / u_{xao} = 2/3$

Surface: Sand blasted steel plate ($R_{max} = 25$ μm for $L = 0.8$ mm)

Sand: No. 2; Dense ($D_r = 88\%$)

$\sigma_n = 100$ kPa

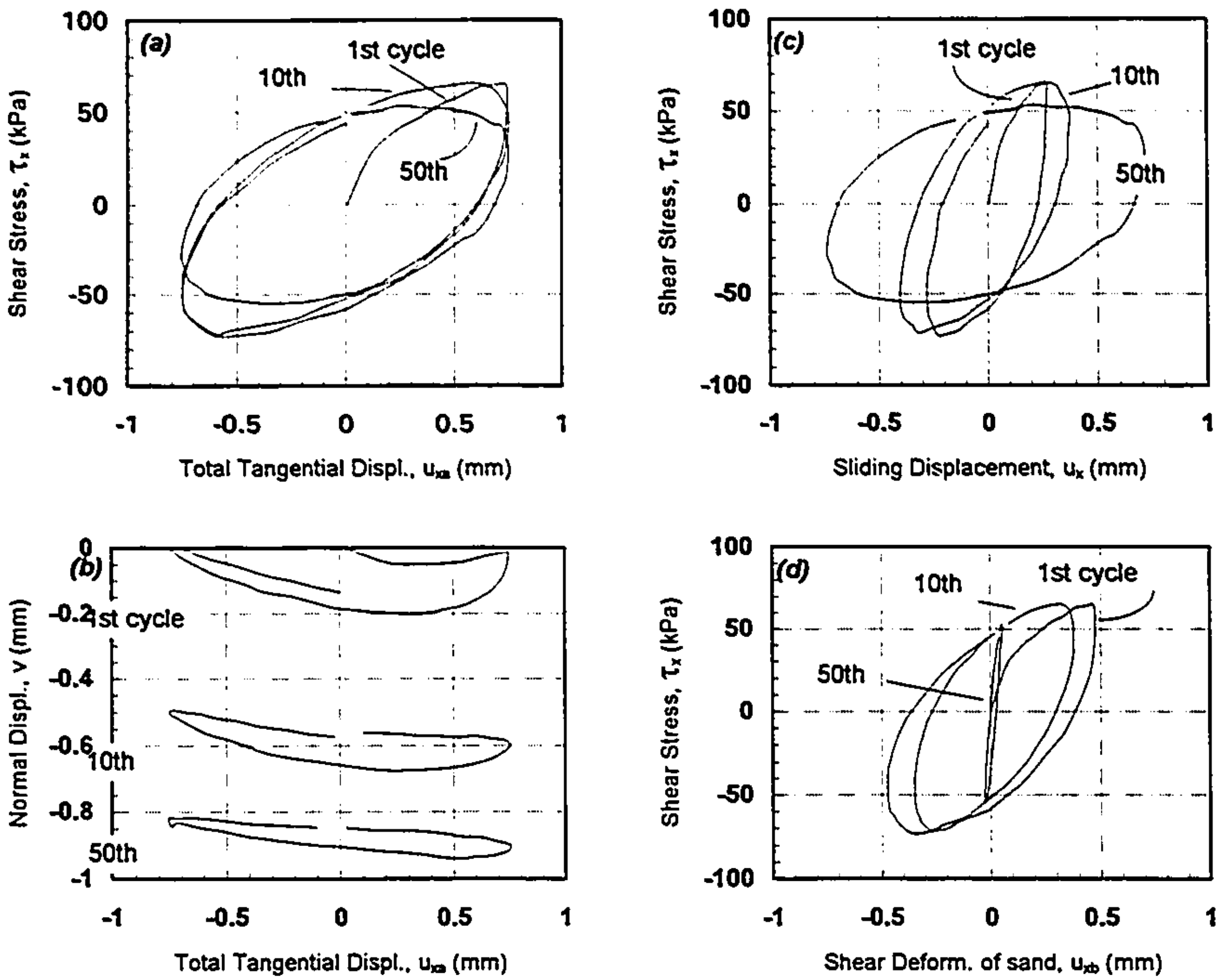

FIG. 6.18. Components of results in the x-direction for a 3-D cyclic rotational shearing test at cycles 1, 10, and 50.

$u_{yao} / u_{xao} = 2/3$

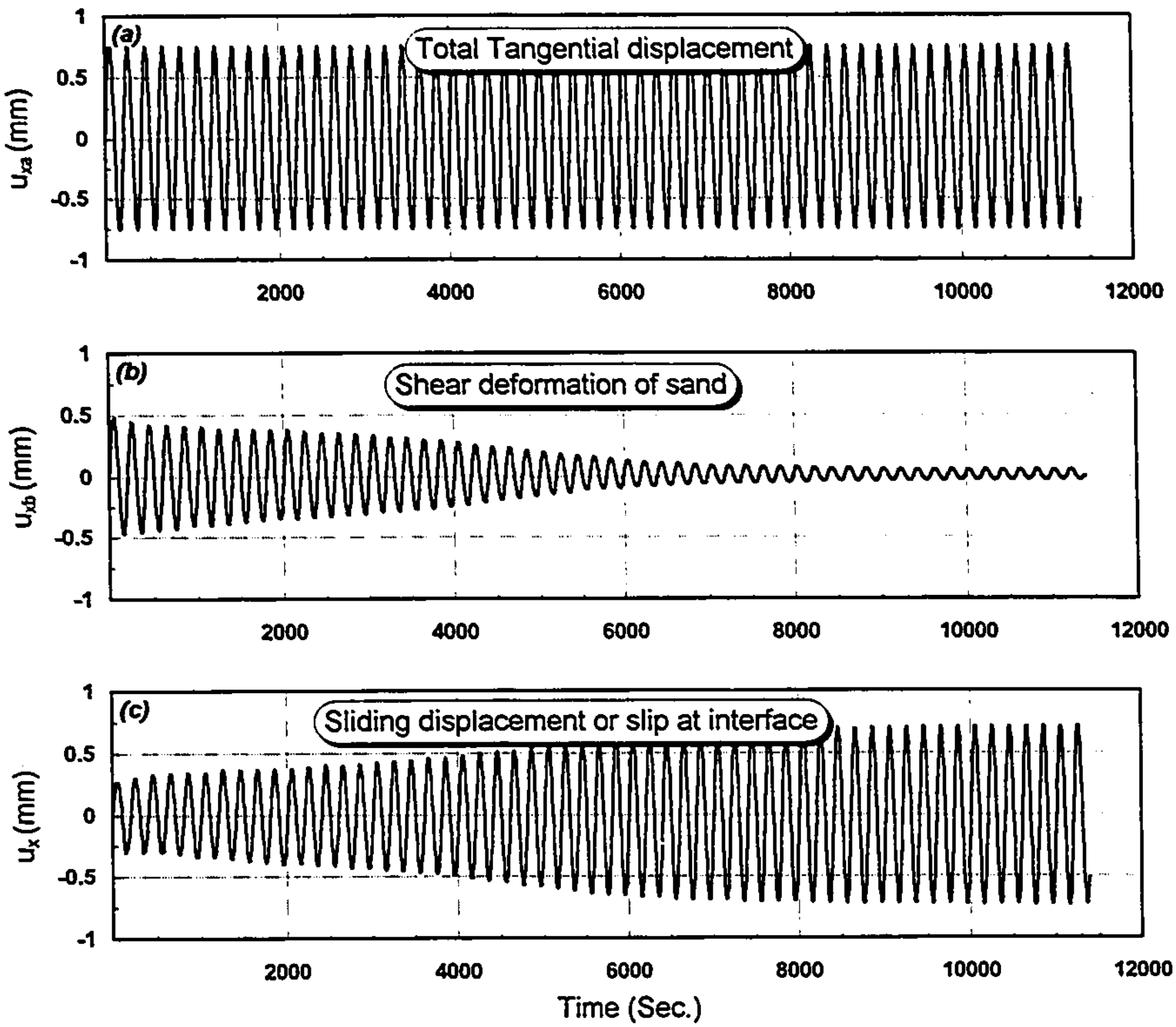

FIG. 6.19. Variation of tangential displacements in the *x-direction* with time for the results shown in Fig. 6.17.

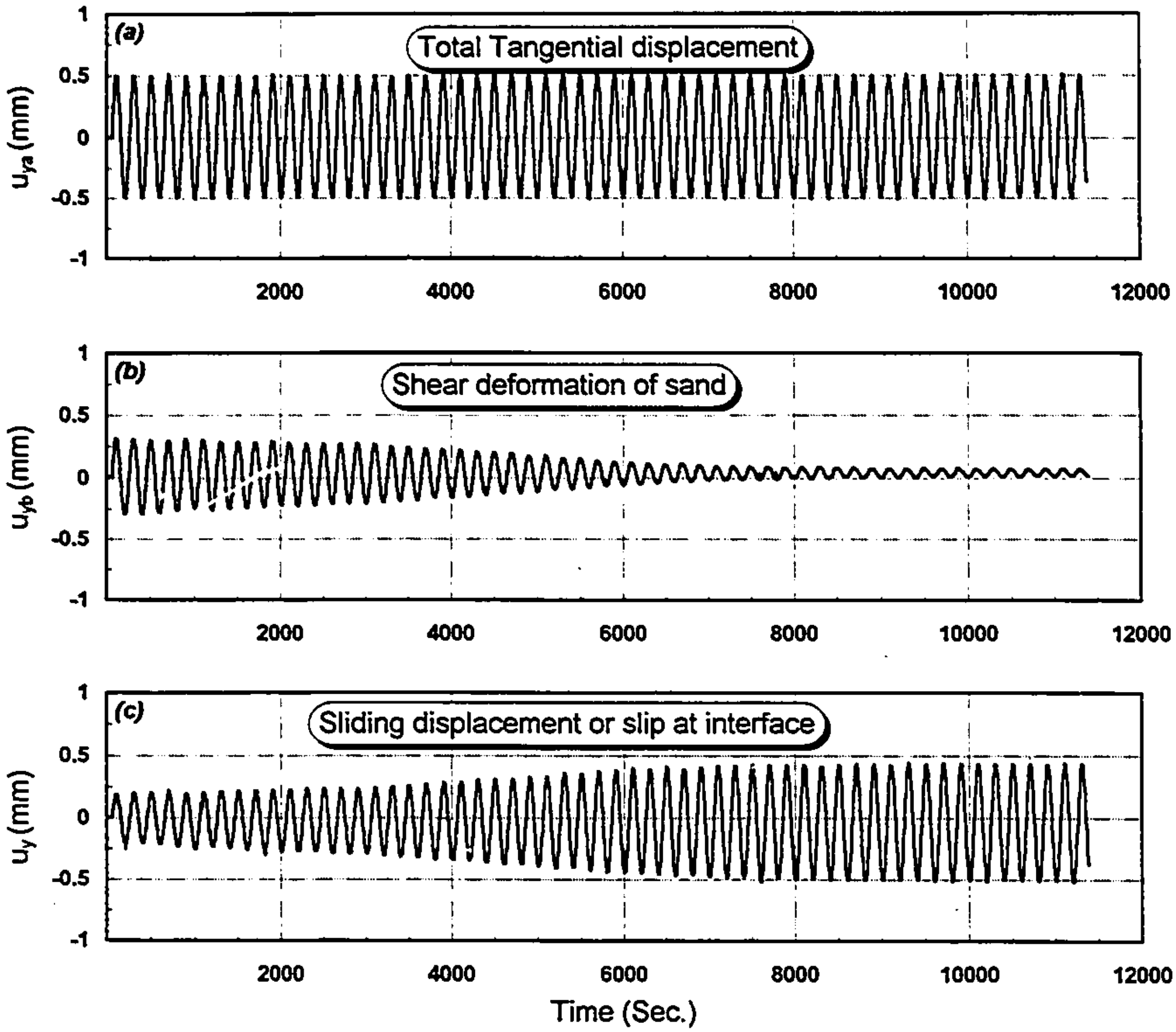

FIG. 6.20. Variation of tangential displacements in the *y-direction* with time for the results shown in Fig. 6.17.

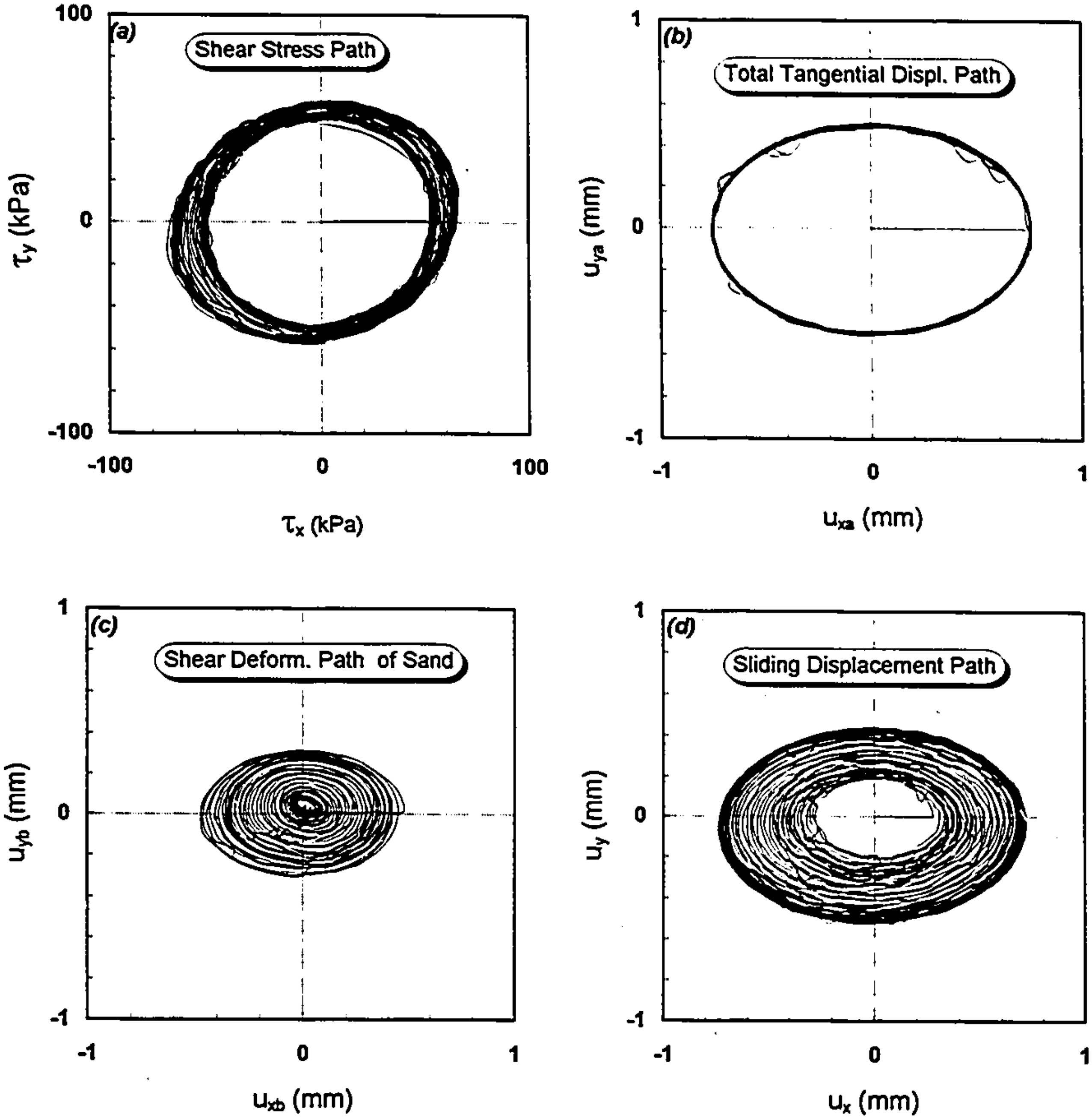

FIG. 6.21. Shear stress and tangential displacement paths on the *x-y* plane for the results shown in Fig. 6.17.

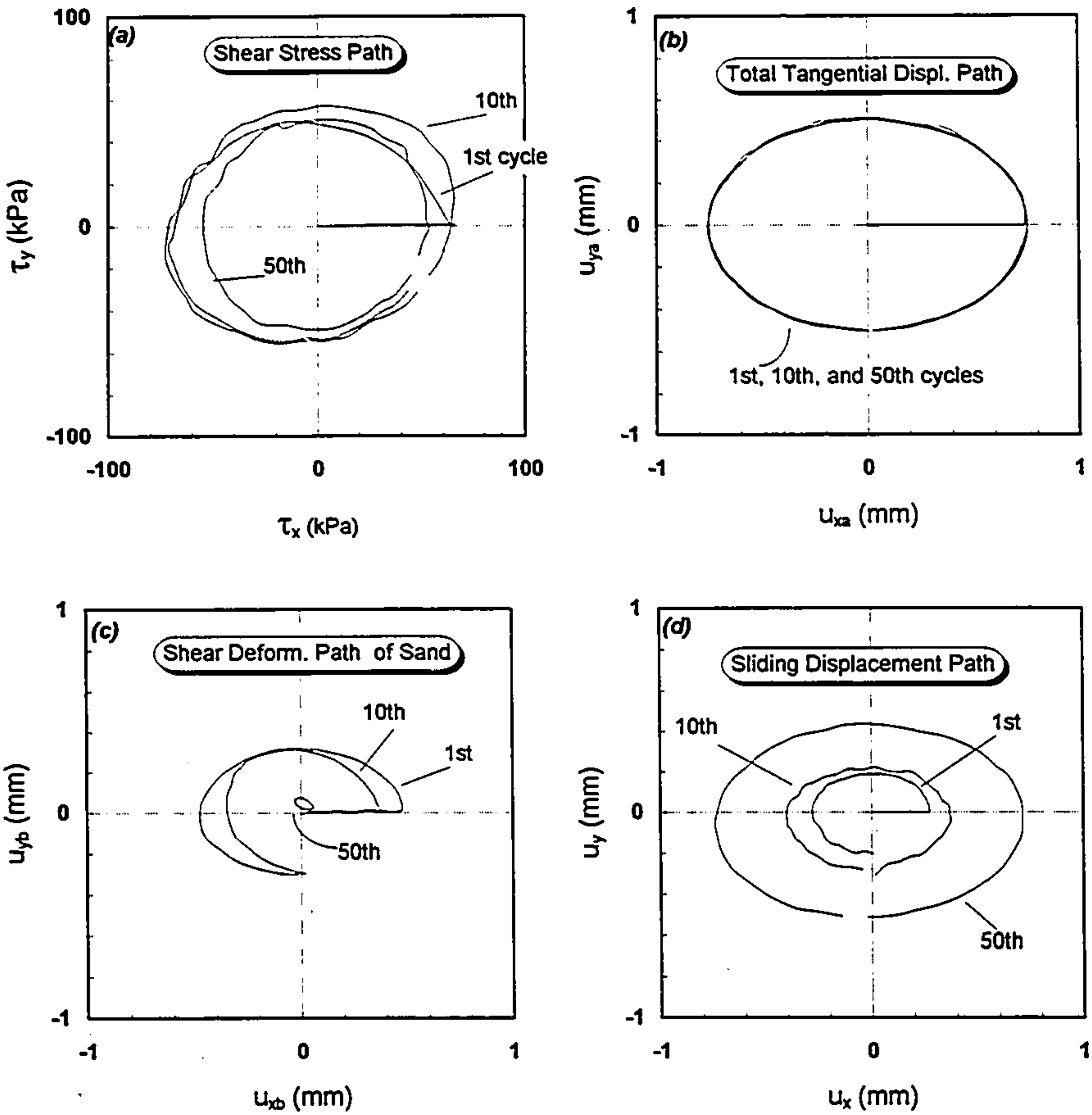

FIG. 6.22. Shear stress and tangential displacement paths on the *x-y* plane at cycles 1, 10, and 50.

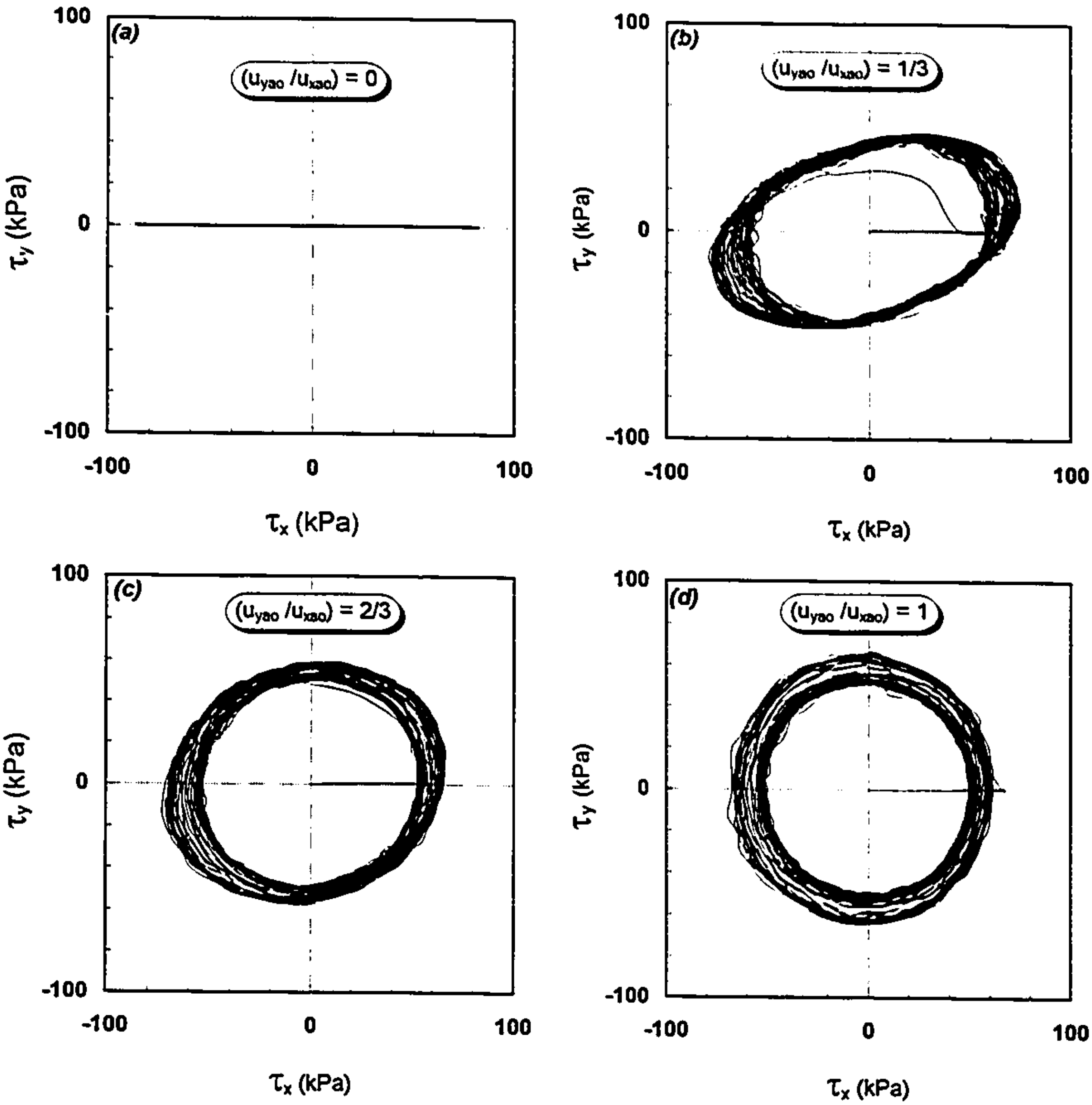

FIG. 6.23. Shear stress paths for different u_{yao} / u_{xao}

Surface: Sand blasted steel plate (R_{max} = 25 μm for L = 0.8 mm)
Sand: No. 2; Dense (D_r = 88%)
σ_n = 100 kPa

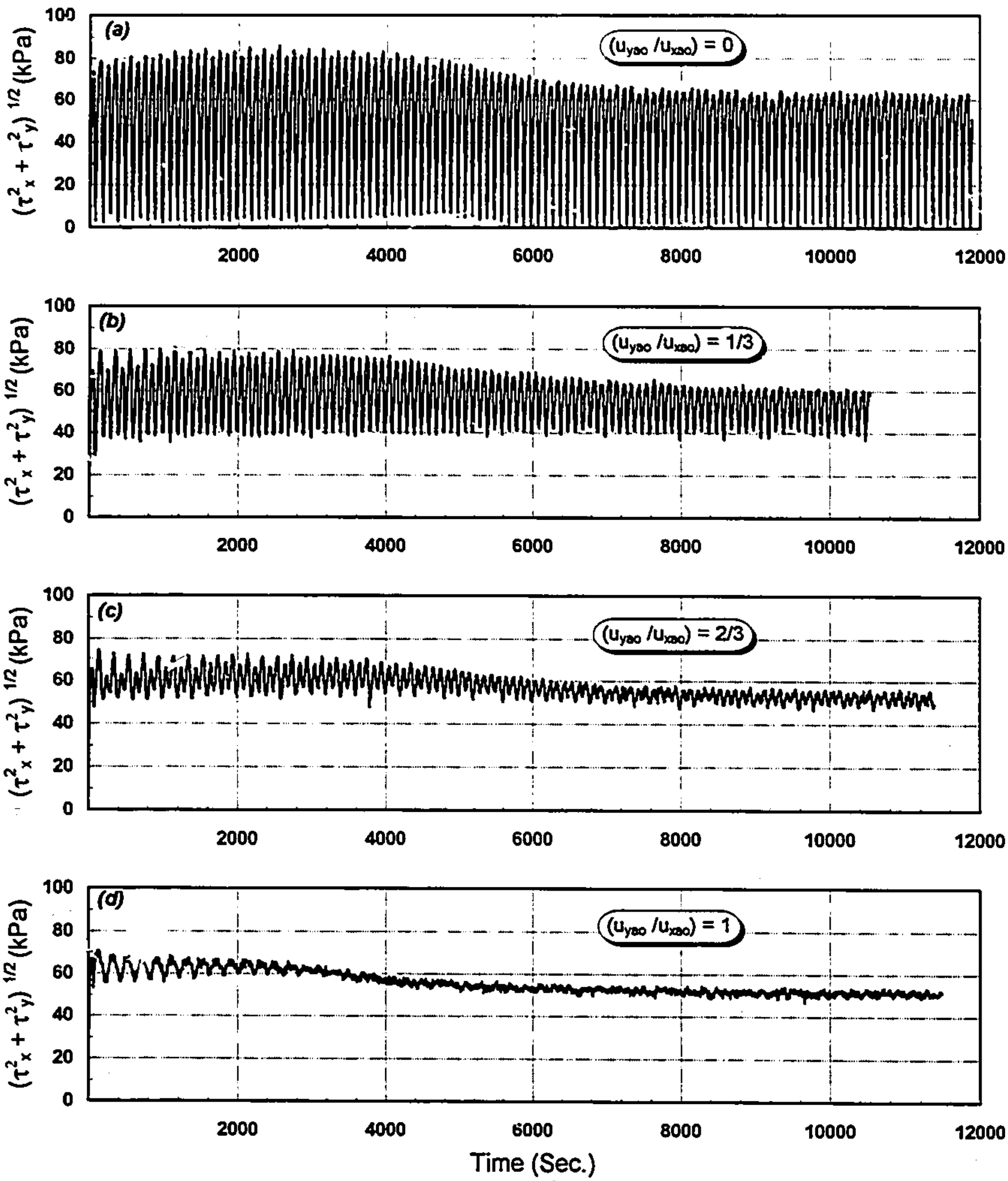

FIG. 6.24. Variations of resultant shear stress with time for different u_{yao}/u_{xao}

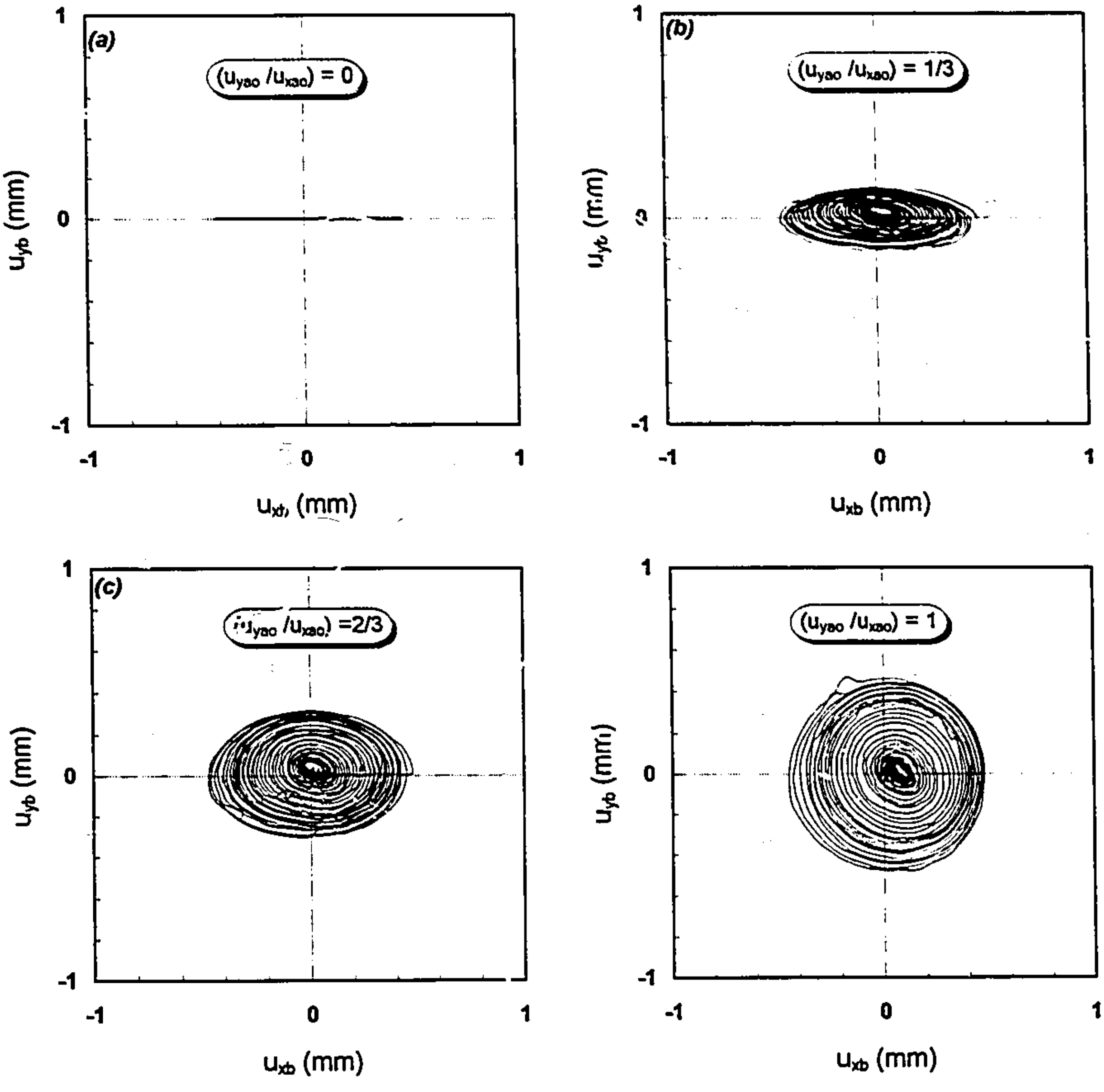

FIG. 6.25. Shear deformation paths of sand for different u_{yao} / u_{xao}

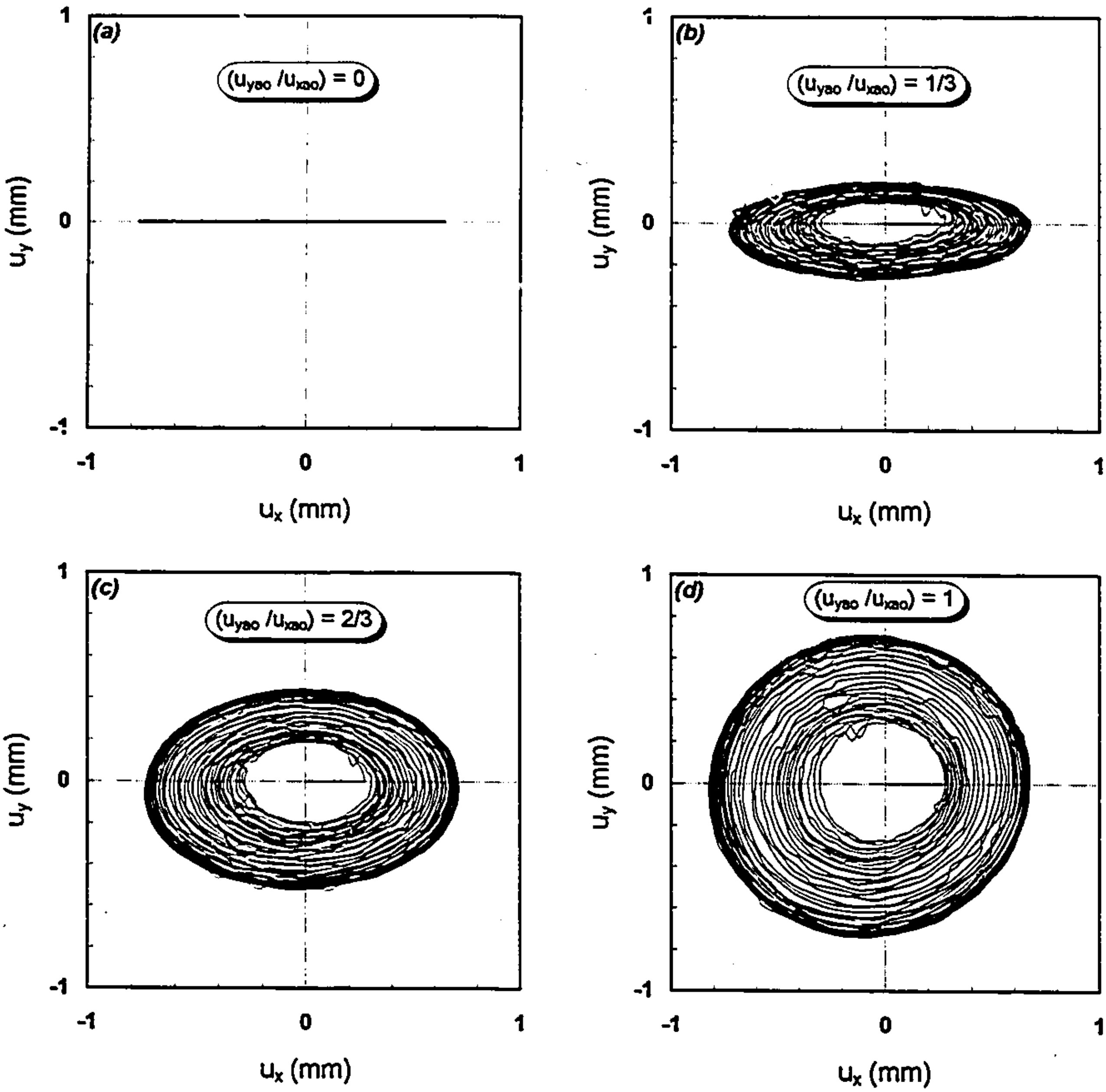

FIG. 6.26. Sliding displacement paths for different u_{yao} / u_{xao}

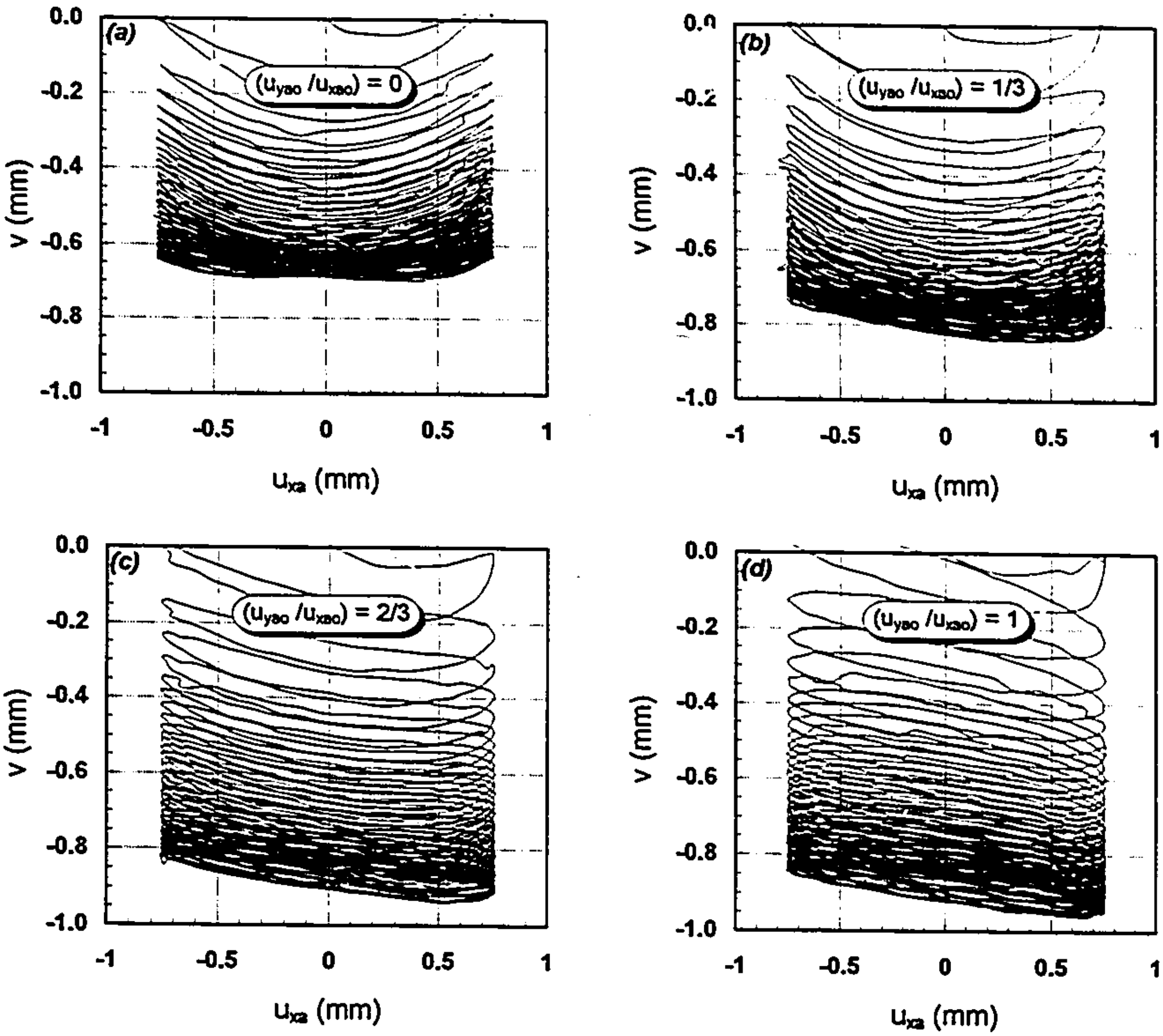

FIG. 6.27. Volume change results for different u_{yao} / u_{xao}

No. of cycles = 50

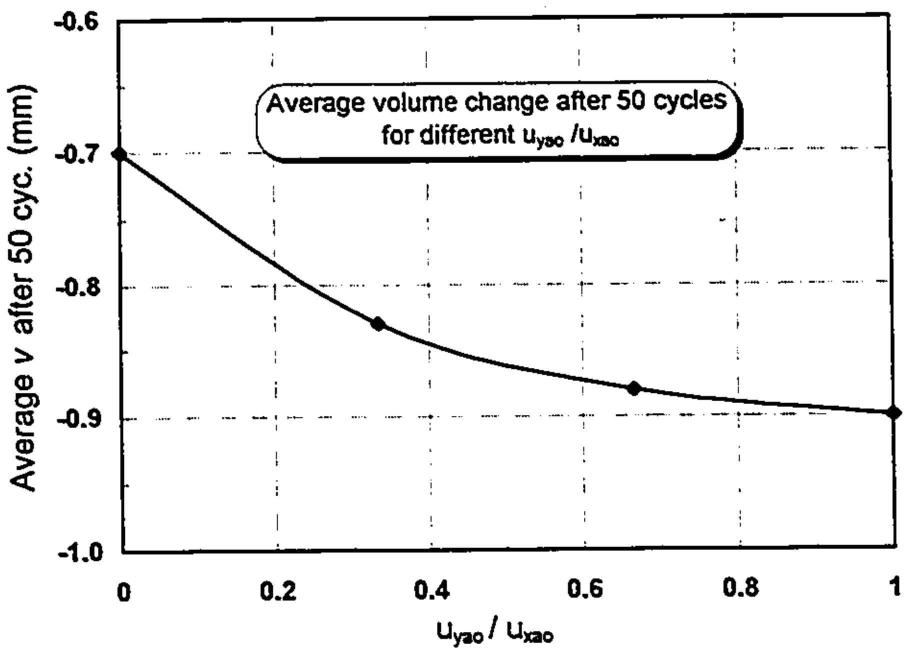

FIG. 6.28. Variation of average volume change with u_{yao} / u_{xao} after 50 cycles

CHAPTER 7

CONSTANT NORMAL STIFFNESS TESTS

As pointed out in the introduction and literature review chapters, the boundary conditions in the direction normal to the interface plane influence the stress-displacement relations of interfaces. Three boundary conditions, i.e. constant normal stress, constant volume, and constant normal stiffness, were identified and explained in detail in Chapter 3. The procedure for performing the constant normal stiffness tests by the computer-controlled testing apparatus system was also described in that chapter.

All test results presented in Chapters 5 and 6 were related to those under the condition of constant normal stress. The results presented in this chapter were obtained under the constant normal stiffness test condition. One of the most important applications of these results is in the analysis of the shaft resistance of axially loaded piles.

Four groups of test results are presented. The first group is related to 2-D monotonic tests. The effects of the magnitude of initial normal stress and normal stiffness on the behaviour of sand-steel interface are studied. The second group contains the 3-D monotonic tests under the constant normal stiffness condition. Group 3 describes the two-way cyclic tangential displacement controlled test results. Group 4 describes the one-way cyclic shear stress controlled test results. The effect of parameters such as the magnitude of the constant normal stiffness and the tangential displacement amplitude on the shear stress degradation of sand-steel interfaces are described.

The No. 2 sand at an initial relative density of 88% and the sand blasted steel plate (R_{max} = 25 μm for L = 0.8 mm) were used as the interface materials in all tests discussed in this chapter. The simple shear type soil container was employed to distinguish the sliding displacement at the interface from the shear deformation of sand mass.

7.1 Monotonic 2-D Tests

7.1.1 Effect of the magnitude of initial normal stress

Three tests were conducted under constant normal stiffness, K, of 800 kPa/mm starting with initial normal stresses of 100, 200, and 300 kPa. The rate of total tangential displacement was set at 1 mm/min. The results of these three constant normal stiffness tests are presented in Fig. 7.1. A comparison between the results given in Figs. 5.5 (for constant normal stress tests, K = 0) and 7.1 shows how a different boundary condition influences the stress-displacement relations.

Figure 7.1*a* shows that shear stress increased steadily and then approached gradually a horizontal asymptote. No apparent peak was observed in any of the tests with three different initial stresses as opposed to the results of the constant normal stress tests presented in Fig. 5.5. The normal stress and normal displacement variations with sliding displacements are plotted in Figs. 7.1*b* and 7.1*c*, respectively. The normal stress reduced first and then increased. The normal displacement was compressive at the beginning and then a large amount of dilation took place. As the tangential displacement continued, the dilation rate reduced and the normal displacement curve eventually levelled off and stabilized. No significant difference was observed in the trends of the normal displacement plots for various initial normal stresses.

In Fig. 7.1*d*, the shear stresses were normalized by the corresponding normal stress at each load level, and plotted against sliding displacements. The results are similar to the normalized results related to the constant normal stress tests as were presented in Fig.

5.5*d*. This observation implies that although the constant normal stiffness boundary condition influences the stress-displacement relations significantly, the stress ratio versus sliding displacement relations remain almost the same in all stress path tests. These results are in good agreement with those presented by Leichnitz (1985) for a sandstone interface as shown in Fig. 2.11. In the constant normal stiffness tests, the magnitude of the initial normal stress is affecting the peak stress ratio (Fig. 7.1*d*) in the same way as in the constant normal stress tests, i.e., the higher the initial normal stress, the lower the peak stress ratio. The peak stress ratios in the constant normal stiffness tests, however, seem to be slightly lower than those of the constant normal stress tests at the corresponding initial normal stress values. This is due to the changes taking place in the normal stress during the constant normal stiffness tests. For example, for the initial normal stress of 100 kPa, the normal stress increased to 200 kPa at the time when the peak shear strength was reached. Since the peak stress ratios reduced as the normal stress increased, the constant normal stiffness tests for dilatant interfaces gave slightly lower values of peak stress ratios than the constant normal stress tests. For practical purposes, however, the effect of the intensity of normal stress on the peak stress ratio may be assumed negligible, at least within the range of stresses used in this study.

The stress paths in a τ-σ plot for all three constant normal stiffness tests, with the initial values of σ_n at 100, 200, and 300 kPa, are illustrated in Fig. 7.2. The peak and residual envelopes have slopes of 0.74 and 0.62, respectively. In all the three tests, the initial normal stress reduction, corresponding to the compression of sand, is clearly demonstrated. After this stage, the interface started dilating which resulted in an increase in normal stress, and therefore, an increase in shear stress. Although both the normal stress and shear stress continued to increase until the end of the test, the stress paths touched the peak envelope (denoted by diamond markers), and bounced back inward, moved towards the residual envelope and stopped changing afterwards (denoted by circle markers). There is a similarity between these stress paths and the effective stress paths, in *p-q* space, for overconsolidated clays in consolidated undrained triaxial tests.

7.1.2 Effect of the magnitude of normal stiffness

The influence of the magnitude of constant normal stiffness, K, on the stress-displacement relations of the sand-steel interface are presented in Fig. 7.3. K was assigned values from 0 to 1200 kPa/mm in different tests. Figures 7.3*a* and 7.3*b* show that under higher K values, higher normal stresses, and therefore, higher shear stresses were mobilized. No reduction was observed in the shear stress variations until the end of the test at a sliding displacement of 6 mm. The volume change results, plotted in Fig. 7.3*c*, represent lower dilation for higher K values. The stress ratio versus sliding displacement curves, illustrated in Fig. 7.3*d*, indicate that the stress ratio variations are practically independent of the magnitude of K.

A practical implication of these monotonic test results under the condition of constant normal stiffness, is related to axially loaded piles embedded in dense Silica sand. During the monotonic axial loading (either tensile or compressive) of the pile, the normal pressure from the surrounding sand mass would increase. The increase in the lateral stress, which is in fact the normal stress at the pile-sand interface, would result in an increase in the mobilized shear stress, thus increasing the shaft resistance of the pile. Boulon and Foray (1986) demonstrated this by a finite element analysis and t-z method of analysis of model piles in loose and dense Hostun No. 2 sand. The parameters for the interface model were obtained on the basis of several monotonic shearing tests under the condition of constant normal stiffness by using a direct shear box.

7.2 Monotonic 3-D Tests

Two 3-D constant normal stiffness tests were conducted for K values of 400 and 800 kPa/mm. The initial normal stress, σ_{no}, in both tests was 100 kPa. Each test started by increasing the shear stress in the y-direction, τ_y, from zero to 30 kPa. Subsequently, the samples were sheared in the x-direction while τ_y was kept constant at 30 kPa. In order to maintain the normal stiffness constant during shearing in the x-direction, adjustments were made in the magnitude of the normal stress. The plots of the resultant shear stress, $(\tau_x^2 + \tau_y^2)^{1/2}$, versus resultant sliding displacement, $(u_x^2 + u_y^2)^{1/2}$, are shown in Fig. 7.4*a*. These plots illustrate that a higher shear stress was mobilized for a higher K

value. The 3-D results for shear stress, τ, versus sliding displacement, u_x, are consistent with the results presented in Fig. 7.3*a* for 2-D experiments at the same K values of 400 and 800 kPa/mm.

The resultant stress ratio, $(\tau_x^2 + \tau_y^2)^{1/2} / \sigma_n$, is plotted against the resultant of sliding displacements in Fig. 7.4*b*. Similar to the 3-D test results under the condition of constant normal stress, the plots for both values of K are almost identical and they resemble the stress ratio plots of all other tests presented in Chapters 5, 6, and 7, for the interface between the No. 2 sand at an initial relative density of 88%, and the sand blasted steel plate (R_{max} = 25 μm for L = 0.8 mm).

7.3 Two-Way Tangential Displacement Controlled Cyclic Tests

As pointed out in the introduction chapter, failure of piles arising from cyclic degradation of shaft resistance has been recognized to be predominant under two-way cyclic axial displacement controlled loading. In such loading conditions, failure can occur at very low load levels in some sand soils due to a reduction in shaft resistance (Chan and Hanna 1980). This degradation of shaft resistance is particularly important in long piles such as those used in offshore environments and for drilled shafts (Turner and Kulhawy 1990). Two main contributing factors have been identified as the cause of the degradation of shaft resistance of the piles under such loading conditions:

(1) Sliding displacement or slip at the interface: Based on a series of two-way displacement controlled cyclic test results, Uesugi *et al.* (1989) and Uesugi and Kishida (1991) concluded that the dominant factor in the degradation of the frictional resistance at a sand-steel interface was the sliding displacement at the interface. These tests were conducted under *constant normal stress* conditions using a simple shear box. Their results were especially important for the case of small displacement amplitudes. A typical result from their study was presented in Fig. 2.14 for two-way displacement controlled tests at small amplitudes. The results presented in Chapter 5 obtained in this study (Figs. 5.19 through 5.22) were in very good agreement with their results under constant normal stress conditions. It was shown that at small displacement amplitudes, the mobilized maximum shear stress increased with the increase in the number of cycles. Eventually, however,

after the peak strength was reached, the shear stress started decreasing with the number of cycles and after a certain number of cycles, the hysterisis curves converged to a loop, equivalent to the residual shear strength of the interface in monotonic shearing. The stiffening of the sand with cycles, adjacent to the interface, and thus gradual decrease in its maximum shear deformation with cycles, caused the sliding displacement of the interface to increase and, therefore, mobilize the peak shear. These coupling effects were clearly demonstrated in Figs. 5.21 and 5.22.

(2) Reduction in normal effective stress due to a change in normal displacement: Ooi and Carter (1987) developed a constant normal stiffness direct shear device for static and cyclic loading of interfaces and presented some results for the joints between sandstone-concrete and calcarenite interfaces, both in static and cyclic loading conditions. They attributed the shear strength degradation to constant stiffness condition in the direction normal to the interface shearing plane. This phenomenon was described in more detail by Poulos (1989) who attributed the degradation in shaft resistance to the compressibility of the soil, which results in a large reduction in soil volume near the pile shaft due to cyclic loading. This volume reduction leads to a reduction in normal stress, and consequently to a reduction or degradation of the shaft resistance. Airey *et al.* (1992) also confirmed experimentally the above idea by conducting sand-to-sand two-way cyclic displacement controlled tests under constant normal stiffness condition by using a direct shear device. No experimental study has been reported for cyclic constant normal stiffness testing on *interfaces* between *soils* and *construction materials*. Moreover, the available studies were mostly concentrated on the calcareous sediments because of their greater compressibility.

As described in Chapter 3, the capabilities of C3DSSI include cyclic tests at interfaces between soil and structural materials, under the condition of constant normal stiffness, by using a simple shear soil container. With these capabilities, C3DSSI seems to be a very useful device to further investigate the degradation of shaft resistance problem. In fact the use of the simple shear soil container, and also the simulation of the condition of constant normal stiffness, allow the examination of the combined effects of both factors described above on the shear strength degradation in Silica sand-steel interfaces.

The results of a typical test are presented first in Figs. 7.5 through 7.14, to identify the main characteristics of the behaviour of a sand-steel interface under constant normal stiffness condition in two-way total tangential displacement controlled tests. The test was performed on an interface between the No. 2 sand at an initial relative density of 88%, and the sand blasted steel plate (R_{max} = 25 µm for L = 0.8 mm). The testing procedure was the same as those presented in Section 5.3 (2-D cyclic tests under constant normal stress conditions) except that a constant normal stiffness condition was imposed in the direction normal to the interface plane. The initial normal stress, σ_{no}, was 300 kPa and constant normal stiffness, K, was set at 400 kPa/mm. The specimen was cycled at a total tangential displacement amplitude of 0.75 mm at a frequency of 1/200 Hz up to 50 cycles.

Several other test results are presented later to illustrate the effects of magnitudes of displacement amplitude (Figs. 7.15 to 7.18) and constant stiffness (Figs. 7.19 to 7.21) on the behaviour of the sand-steel interface.

Figure 7.5 shows that the mobilized shear stress reduced with increase in number of cycles so that the rate of reduction was higher within the first few cycles. Figure 7.6 illustrates the plots for cycles 1, 12, and 50. A substantial reduction is observed in the shear stress with increase in cycles such that the mobilized shear stress which was 170 kPa at the displacement amplitude of 0.75 mm during the first cycle, dropped to 50 kPa in the 50th cycle.

The shear stress was normalized by the corresponding normal stress and was plotted against tangential displacements as demonstrated in Figs. 7.7 and 7.8. The variations of stress ratio, τ / σ_n, with total tangential displacement, sliding displacement, and shear deformation of sand exhibited both qualitatively and quantitatively the same trend as the results of tests under constant normal stress (Fig. 5.19). The mobilized stress ratio, τ / σ_n, which was 0.61 at the maximum tangential displacement during first cycle, increased to 0.8 at cycle 12, and subsequently decreased and reached a residual value of 0.6. Despite the fact that the mobilized shear stress decreased from beginning of cycles, the stress ratio followed exactly the same patterns of a typical 2-D displacement controlled cyclic behaviour of the sand-steel interface presented in Chapter 5.

The results also indicate that the sliding displacement and shear deformation of the sand mass underwent the same variations as in the case of constant normal stress tests. With increase in the number of cycles, the amplitude of shear deformation of sand decreased while the sliding displacement amplitude increased. These variations are illustrated in detail in Fig. 7.9 in which u_{xa}, u_{xb}, and u_x are plotted against time. The variations of shear stress, stress ratio, and normal stress with time are also shown in Fig. 7.10. The rapid reduction in shear and normal stresses continued up to about 30 cycles (time 6000 Sec.) after which these stresses approached their respective residual values. The peak stress ratio, $(\tau / \sigma_n)_{peak}$ was reached at cycle 12 equivalent to 2400 seconds (Fig. 7.10 *b*). This graph is identical to the one shown in Fig. 5.21, which was obtained from a displacement controlled cyclic test under the condition of constant normal stress.

Figures 7.11*a*, *b* demonstrate the variations of normal displacement and normal stress with total tangential displacement, respectively. Due to compressive behaviour of sand under cyclic loads, the normal stress had to decrease eventually in parallel with the normal displacement, to maintain the normal stiffness, *K*, at the designated value of 400 kPa/mm throughout cycles. Similar results at cycles 1, 12, and 50 are shown in Fig. 7.12. The rapid reduction of the normal stress with cycles contributed to the rapid reduction of the mobilized shear stress, which is the so-called degradation of shear stress with cycles.

The stress path, illustrated in Fig. 7.13*a*, demonstrates the gradual decrease in both shear stress and normal stress with cycles. The complete loops for cycles 1, 12, and 50 are plotted in Fig. 7.13*b*. The envelopes of both peak and residual strengths are plotted in those figures. The stress path cycles are within the peak envelope before failure. At failure (cycle 12) the stress path touched the failure envelope and consequently bounced back inward until it stabilized on the residual envelope. The failure occurred at a normal stress of 134 kPa and a shear stress of 106 kPa. After 50 cycles the normal stress and shear stress dropped to 79 kPa and 51 kPa, respectively.

Similar plots based on the normalized shear stress, τ / σ_n are shown in Fig. 7.14. Despite the drop in both normal stress and the maximum shear stress with cycles, the maximum stress ratio increased and reached a peak strength ratio of 0.8, as clearly observed at a normal stress, σ_n, of 134 kPa, after which the stress ratio decreased to reach a residual strength ratio of 0.61.

The results of the test under a constant stiffness of 400 kPa/mm, clearly demonstrated the phenomenon of shear stress degradation for a sand-steel interface and its relation to the degradation of shaft resistance of axially loaded piles, subjected to two-way displacement controlled cyclic shearing. Both factors contributing to the shear stress degradation, are shown to be applicable simultaneously. The first category, proposed by Uesugi *et al.* (1989) and Uesugi and Kishida (1991), attributed the reduction in maximum stress ratio, τ / σ_n, to the the sliding displacement at the interface, and stated that it was the dominant factor. That idea was true within the framework of their experimental results, which was limited to one-way and two-way cyclic displacement controlled tests under the condition of *constant normal stress*. The second factor was attributed to the reduction in normal effective stress due to the change in normal displacement. Using the calcareous sediments, with high potential of compressibility due to crushing of the particles during shearing, was one reason to conclude that this was the dominant factor. Moreover, since the direct shear box as the soil container would not permit to distinguish between the sliding displacement and shear deformation of the sand mass, therefore it would not be possible to capture the first factor.

The stress ratio variations, τ / σ_n, shown in Figures 7.7 and 7.10*b*, resemble the shear stress variations in similar tests under *constant normal stress* conditions. This is in favour of the first factor that the sliding displacement is a dominant factor. Figures 7.5, 7.10*a*, and 7.10*c*, illustrating the decrease in both maximum shear stress and normal stress with increase in cycles, provide support for the second factor. In order to determine the degree to which each of the two factors is contributing to the strength degradation, two parametric studies were performed. The first one was about the effect of the displacement amplitude which is described in 7.3.1. The effect of the magnitude of constant normal stiffness is described in 7.3.2.

7.3.1 Effect of displacement amplitude

Two tests were conducted under the same conditions, but at low tangential displacement amplitudes. The first one had a total tangential displacement amplitude of 0.25 mm. The variations of shear stress, stress ratio, and normal stress with cycles are presented in Fig. 7.15. Although the normal stress dropped substantially during cycles (from 300 to 110 kPa), the maximum shear stress decreased only slightly (from 138 kPa in the 1st cycle to about 90 kPa in the 50th cycle). The stress ratio variations in Fig. 7.15*b* showed gradual increase with cycles but no failure was observed. The second test was conducted under a total tangential displacement amplitude of 0.5 mm. As demonstrated in Fig. 7.16, no failure occurred during the test. However, the normal stress and hence the shear stress reduced at a higher rate compared to the test with 0.25 mm amplitude.

The rate of shear stress degradation for different values of total tangential displacement are given in Fig. 7.17. The shear stress degradation occurred at a faster rate for higher displacement amplitudes. For a better representation, the mean normal stress and maximum shear stress after 30 cycles, at which a large portion of degradation had already taken place, were plotted against the total tangential displacement amplitudes of 0.25, 0.50, and 0.75 mm for all three tests (Fig. 7.18). There is no substantial difference between 0.25 and 0.5 mm amplitudes. This is attributed to the fact that no failure occurred at those amplitudes at the interface. A major reduction in both stresses, however, is related to the failure of the interface at cycle 12 for the displacement amplitude of 0.75 mm.

These results provided information about how the amplitude of the total tangential displacement affect the degradation phenomenon. Under very low displacement amplitudes (0.25 and 0.5 mm), during which no failure occurred, the degradation in shear stresses were substantially lower than the degradation of shear stress in the case during which the failure occurred (the test with 0.75 mm amplitude). This parametric study demonstrated the importance of the first factor. As described previously, if the maximum sliding displacement did not accumulate with cycles, no degradation would occur in the stress ratio. Maximum shear stresses, however, reduced even when failure did not occur, which was the result of a decrease in the normal stress due to compression of sand.

7.3.2 Effect of the magnitude of normal stiffness

The results of four constant normal stiffness tests are presented in Figs. 7.19 and 7.20. The total tangential displacement amplitude was 0.75 mm in all tests. The values of K were 200, 400, 800, and 1200 kPa/mm. The variations in shear stress with cycles, shown in Fig. 7.19, indicate that shear stress degradation occurred faster, and maximum shear stresses were much lower after the same number of cycles, for higher normal stiffness values. All four tests had an initial normal stress of 300 kPa. At higher K values, the normal stress also dropped rapidly (Fig. 7.20). The reduction in mean normal stress and maximum shear stresses as a function of normal stiffness are plotted in Fig. 7.21 which represents the results after 30 cycles. It is observed that the mean normal stress and maximum shear stresses decreased with increasing K values.

7.4 One-Way Shear Stress Controlled Cyclic Tests

It is of interest to study the behaviour of interfaces which are subjected to repeated application of shear stresses of a magnitude less than the monotonic shear strength. This type of loading condition is relevant, for example, to the shaft resistance of piles used in the foundations of ship-landing platforms. The loading-unloading process of the cargo on the platform results in one-way cyclic shear stress along the shaft of the supporting piles.

Ooi and Carter (1987) conducted such tests on the interface between rock blocks of calcareous sediments. The tangential displacement accumulated with increase in cycles and a failure occurred after 570 cycles. Therefore, failure may occur under conditions of cyclic loading, even when the maximum shear stress applied in all cycles is below the peak strength of the material. The normal displacement and as a result the normal stress decreased with cycles and caused the failure under condition of constant normal stiffness. Similar results were reported by Mouchaorab and Benmokrane (1994) on interfaces between granite rock blocks. The failure occurred after 79 cycles, at which the accumulated tangential displacement was 16.25 mm, under a shear load equivalent to 50% of the monotonic shear strength. The normal displacement and therefore, normal stress increased with cycles in their study, however, and they dropped rapidly after failure.

In this section, the results of two stress-controlled tests under one-way cyclic shearing are presented. The interface was subjected to a shear stress lower than the peak strength. Then the shear stress was lowered to zero. This process was repeated up to a certain number of cycles during which the variations of sliding displacement, shear deformation of sand mass, normal displacement, and normal stress were recorded.

The first cyclic test was conducted under a constant normal stress of 300 kPa, i.e. $K = 0$. The shear stress on the interface was first cycled between zero and a maximum shear stress of 120 kPa up to 75 cycles at a frequency of 1/100 Hz. Afterwards the shear stress amplitude was increased to 180 kPa for the rest of 125 cycles. The shear strength of this interface under monotonic loading measured 225 kPa (Fig. 5.5). Therefore, the applied shear stresses in the cyclic test were lower than the shear strength in monotonic loading tests. The shear stress-tangential displacements and normal displacement results are presented in Fig. 7.22. The variations of tangential displacements and stresses with cycles are presented in Figs. 7.23 and 7.24, respectively. The sliding displacement and shear deformation of sand mass increased with increase in the number of cycles up to about 120 cycles (Time 12000 Sec.) after which there were no significant changes in the displacements. No failure occurred until the end of the 200 cycles.

In the second test a normal stiffness of 800 kPa/mm was imposed on the interface. The shear stress on the interface was first cycled between zero and 120 kPa for 66 cycles. Subsequently the shear stress was cycled between zero and 150 kPa for another 76 cycles. The total number of cycles was 142. At the end of the cycles, the interface was monotonically sheared up to a total tangential displacement of 5 mm. The results are presented in Figs. 7.25 through 7.30. Unlike the previous test under constant normal stress, large amounts of tangential displacement, shear deformation, and sliding displacement were accumulated with cycles in this test. At the total tangential displacement of 5 mm at which the monotonic test was terminated, the shear stress had reached a value of 230 kPa which was close to a horizontal asymptote. The peak shear strength of this interface under the condition of constant normal stress of 300 kPa was 225 kPa. Unfortunately, there is no test data available at present for a similar test under the condition of constant normal *stiffness*. However, due to the increase in the normal stress as a result of dilation during monotonic shearing, it can be anticipated that the mobilized shear strength in a constant normal stiffness test would be much larger. Therefore, it can be inferred that one-way cyclic shearing may cause a substantial degradation in the shear resistance of the interface.

The variations of stress ratio shown in Fig. 7.26 indicate that the interface was very close to failure at the end of the cycles. A peak strength ratio of 0.8 was reached at the very early stages of the monotonic shearing and subsequently it moved toward its residual value of 0.6. This pattern was the same in all the tests in this study. The variations of tangential displacements with shear stress cycles are presented in Fig. 7.27. Both shear deformation of sand mass and sliding displacement at the interface were still accumulating until the very end of all the cycles before the monotonic test was conducted.

Simultaneous variations in normal displacement and normal stresses, as illustrated in Fig. 7.28, show that they both reduced during cyclic shearing. A jump is observed at the time when the shear stress amplitude was increased form 120 to 150 kPa at cycle 66. The interface dilated during the monotonic shearing, and therefore normal stress increased accordingly, to maintain the constant normal stiffness of 800 kPa/mm. However, since the normal stress at the end of the cycles had already dropped below 200 kPa, which was less than 2/3 of the initial normal stress of 300 kPa, it was not possible to reach to the load level of a monotonically sheared interface under the same constant normal stiffness condition. Therefore, the mobilized shear stress at peak, which under any loading condition was proved to be directly dependent on the magnitude of the normal stress at that instant, would not reach the shear strength of a monotonically sheared interface. This is the main reason for the degradation of the shear strength of the interface subjected to cyclic shearing under a constant normal stiffness condition.

Figure 7.29 illustrates the variations of shear stress, stress ratio, and normal stress with cycles. The comparison between Figs. 7.29*a* and 7.29*b* clearly demonstrates the gradual increase in maximum stress ratio with cycles, although the maximum shear stress had the same specified values of 120 and 150 kPa. This is due to the gradual decrease in normal stress with cycles as shown in Fig. 7.29*c*.

For completeness, the stress paths in τ-σ_n and τ/σ_n-σ_n spaces are shown in Figs. 7.30*a* and 7.30*b*, respectively.

Similar to the test results presented for the calcareous rock blocks by Ooi and Carter (1987), the normal displacement was compressive in the behaviour of sand-steel interface. This is due to the densification of the sand mass with cycles. In calcareous rock blocks, however, the reductions in the normal displacement, and as a result, the reduction in normal stress, were attributed to the high compressibility and crushing of the calcareous sediments.

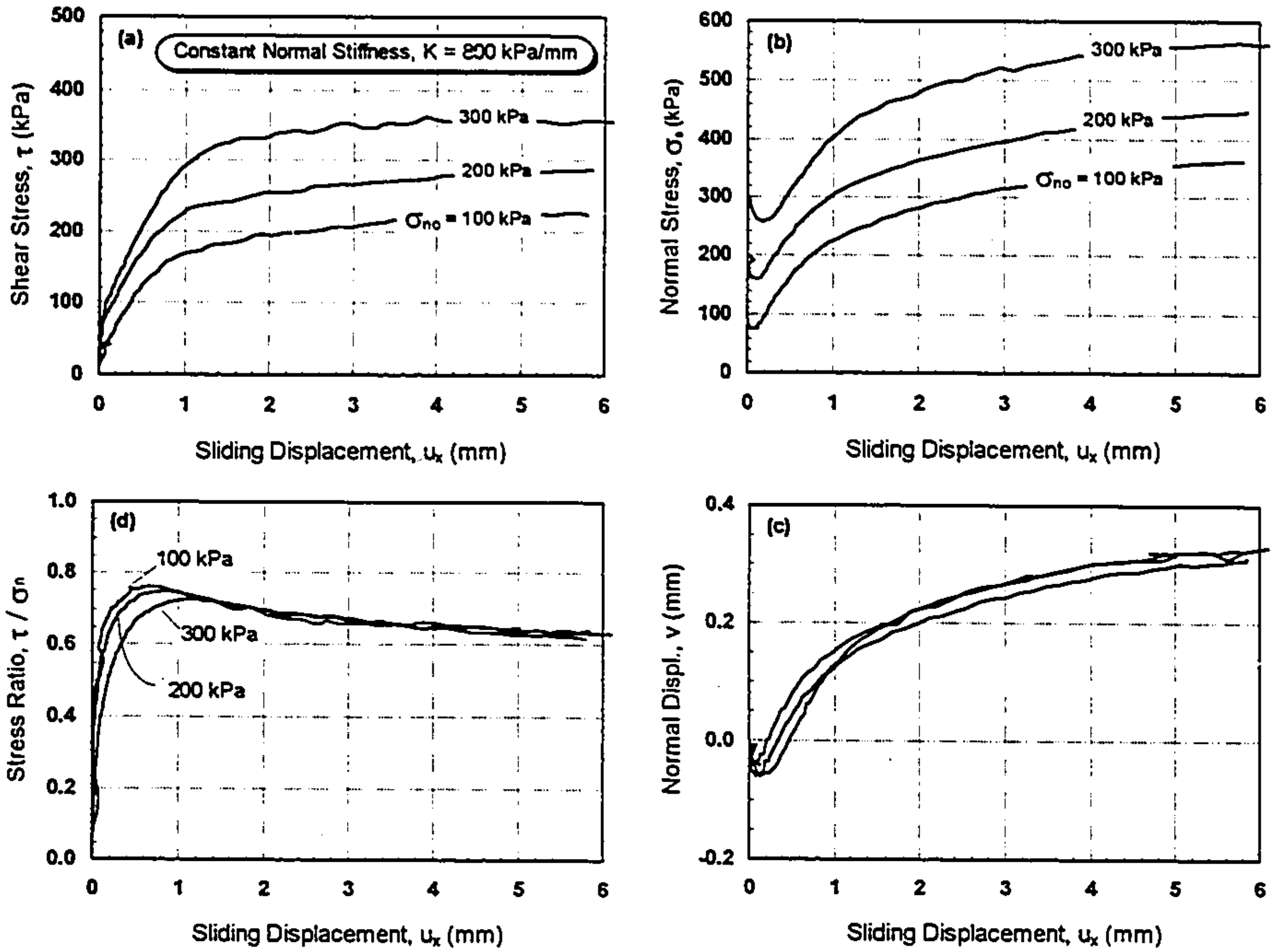

FIG. 7.1. 2-D monotonic test results under constant normal *stiffness* of 800 kPa/mm.

σ_{no} = 100, 200, and 300 kPa

Surface: Sand blasted steel plate (R_{max} = 25 μm for L = 0.8 mm)

Sand: No. 2; Dense (D_r = 88%)

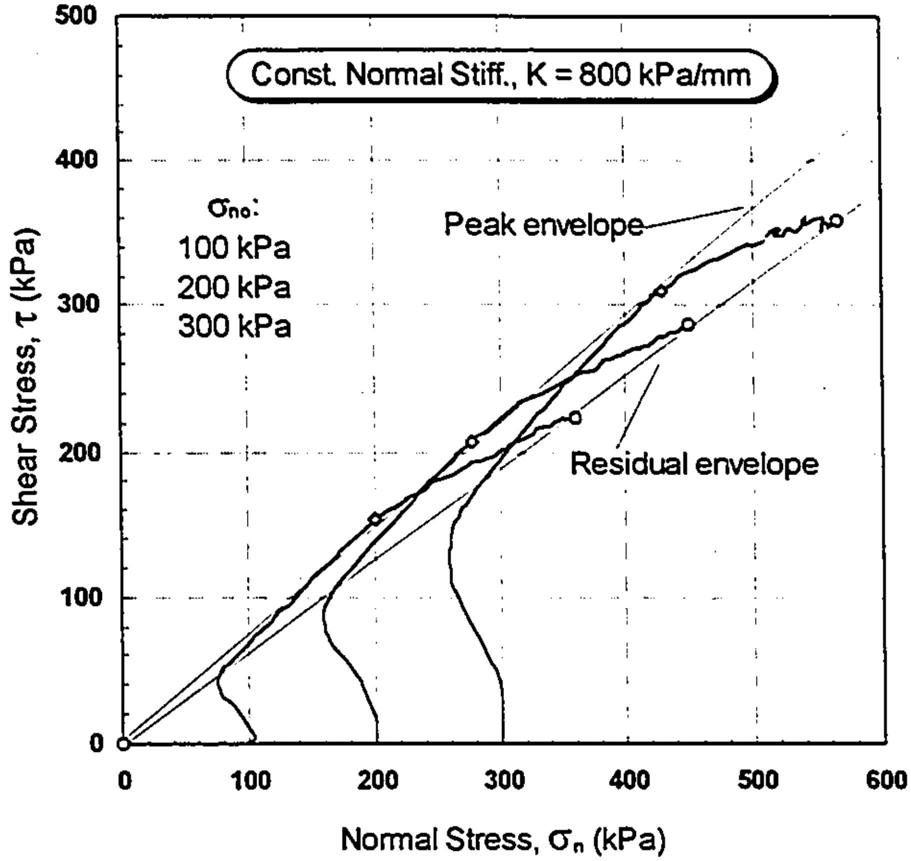

FIG. 7.2. Stress paths in 2-D constant normal stiffness tests corresponding to Fig. 7.1.

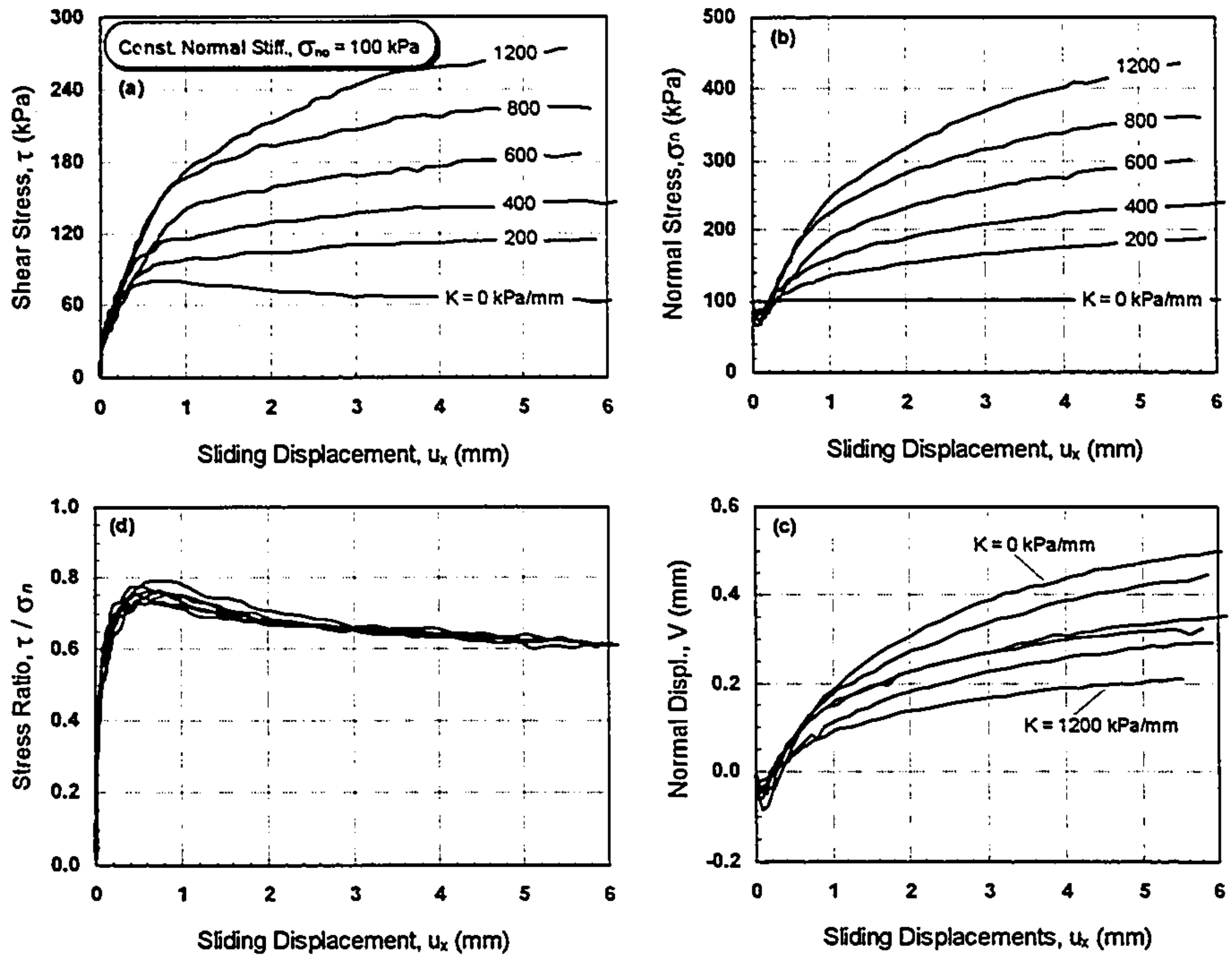

FIG. 7.3. 2-D monotonic test results under constant normal *stiffness* of 0 through 1200 kPa/mm. σ_{no} = 100 kPa

Surface: Sand blasted steel plate (R_{max} = 25 μm for L = 0.8 mm)

Sand: No. 2; Dense (D_r = 88%)

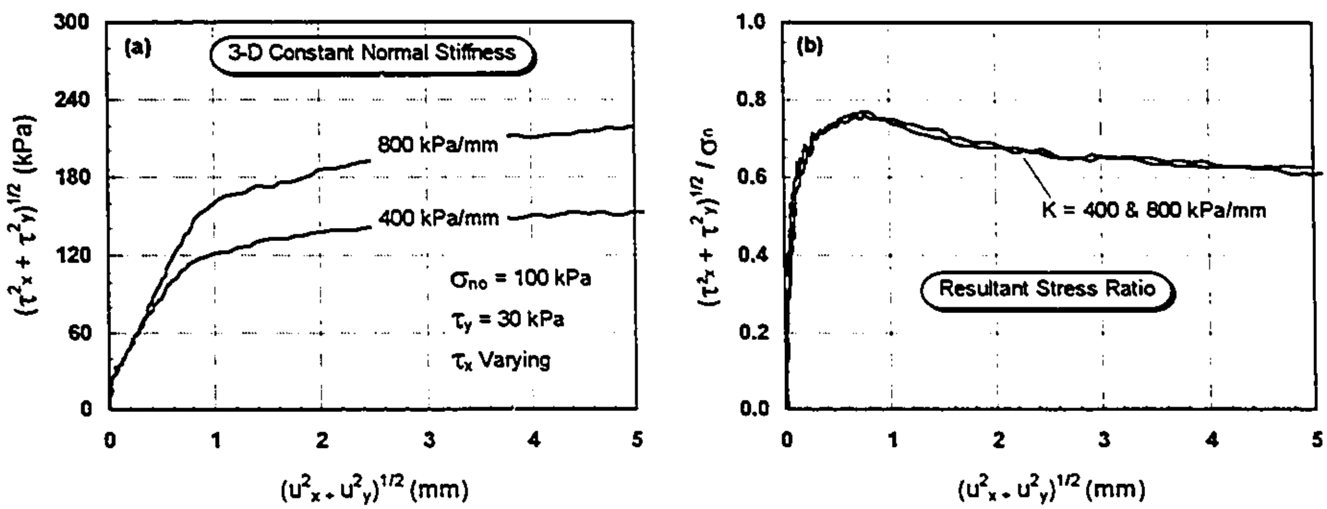

FIG. 7.4. 3-D monotonic test results for constant normal *stiffness* tests with K = 400 and 800 kPa/mm.

σ_{no} = 100 kPa; τ_y = 30 kPa

Surface: Sand blasted steel plate (R_{max} = 25 μm for L = 0.8 mm)

Sand: No. 2; Dense (D_r = 88%)

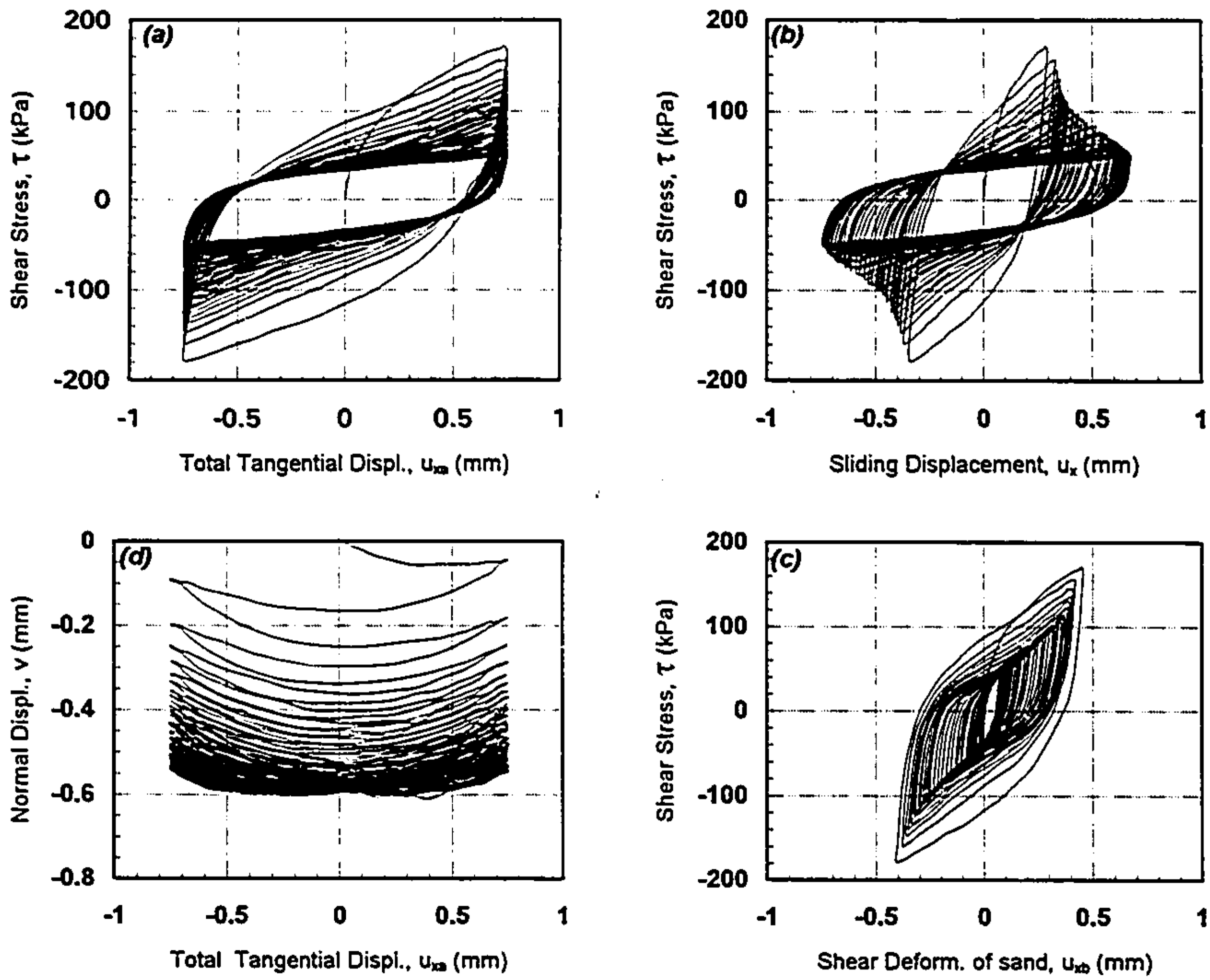

FIG. 7.5. 2-way total tangential displacement controlled test results under constant normal stiffness.

$\sigma_{no} = 300$ kPa; $K = 400$ kPa/mm

Surface: Sand blasted steel plate ($R_{max} = 25$ mm for $L = 0.8$ mm)
Sand: No. 2; Dense ($D_r = 88\%$)

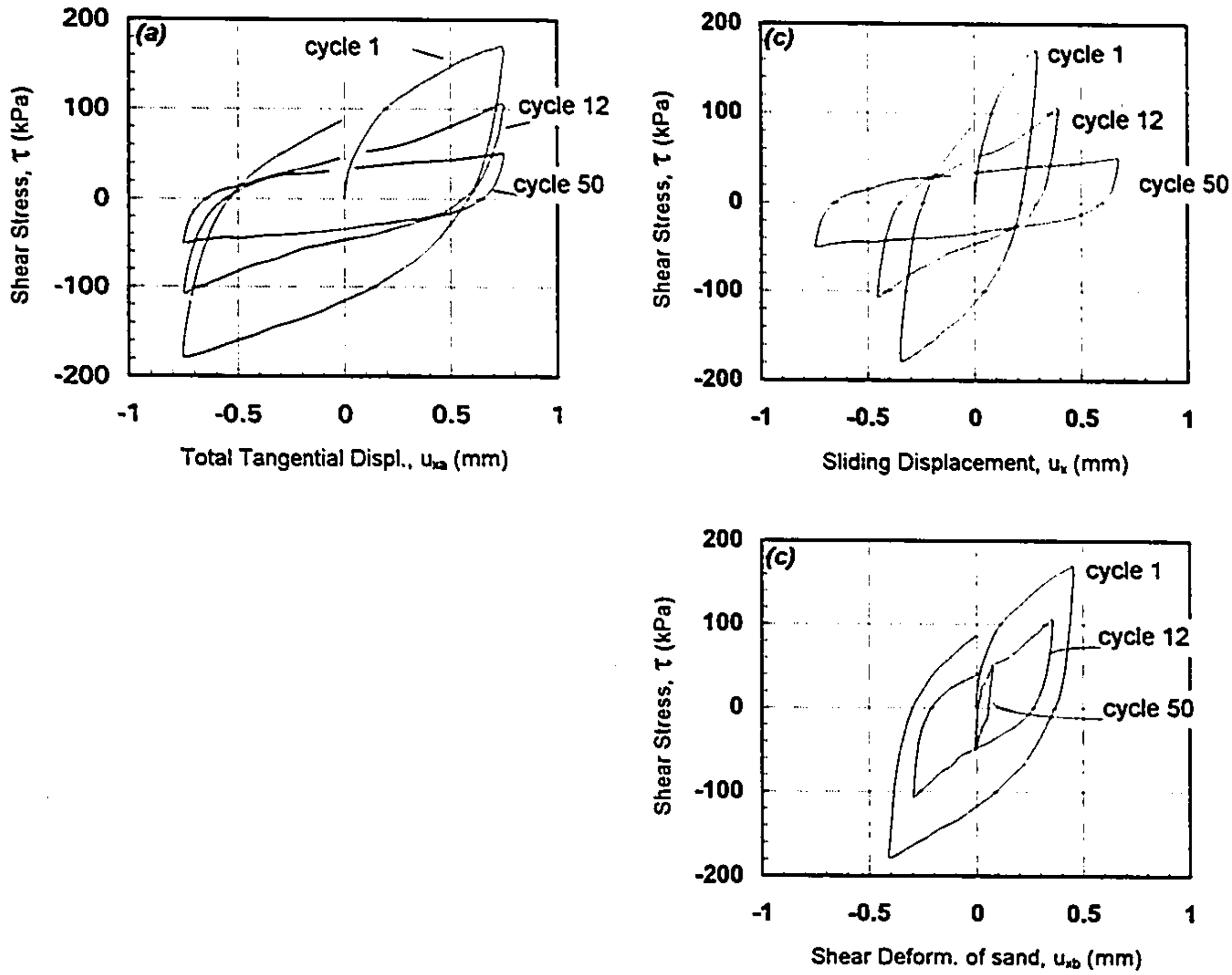

FIG. 7.6. Shear stress variations at cycles 1, 12, and 50 for results of Fig. 7.5.

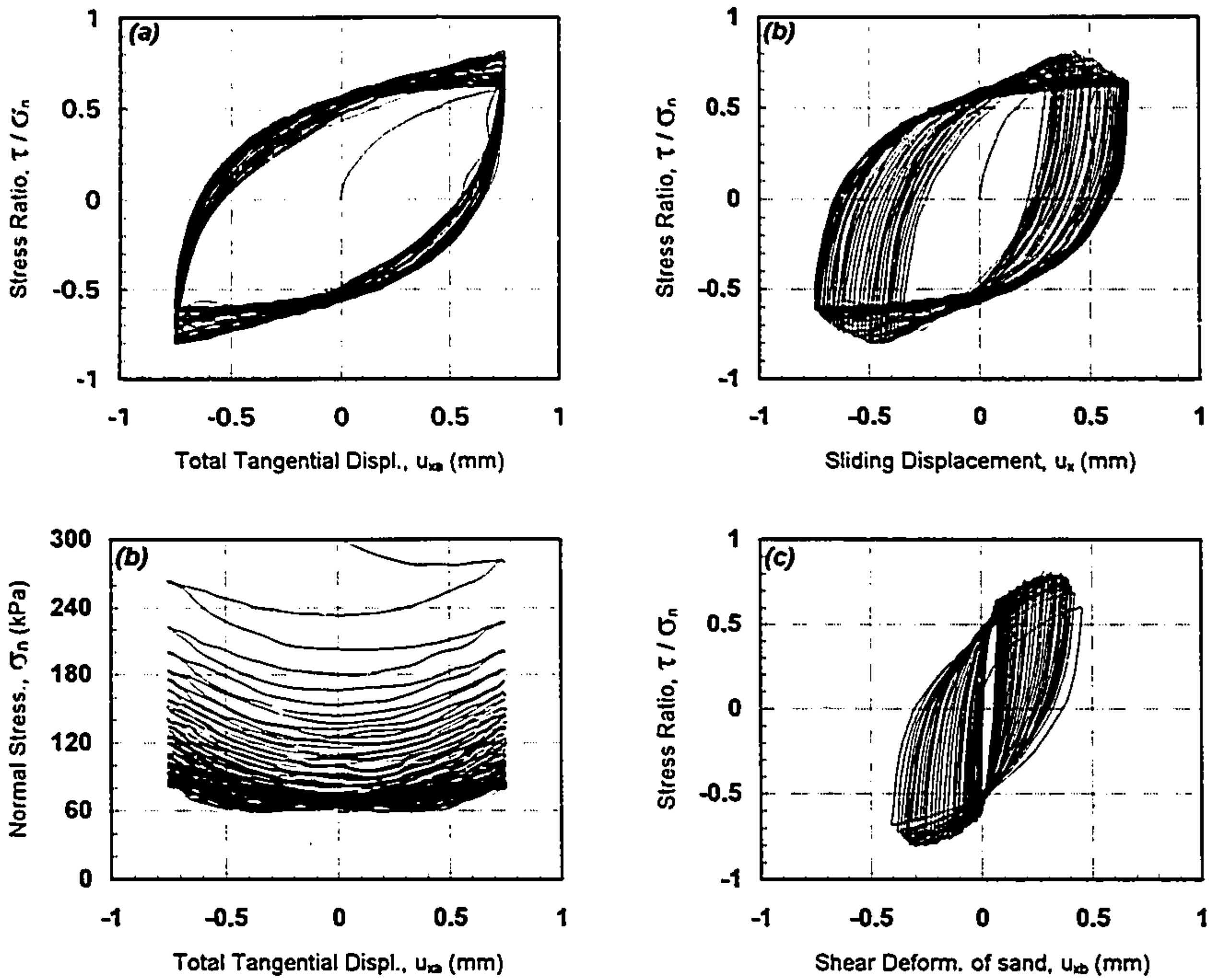

FIG. 7.7. 2-way total tangential displacement controlled test results under constant normal stiffness.
(normalized results of Fig. 7.5)

σ_{no} = 300 kPa; K = 400 kPa/mm; Initial D_r = 84%

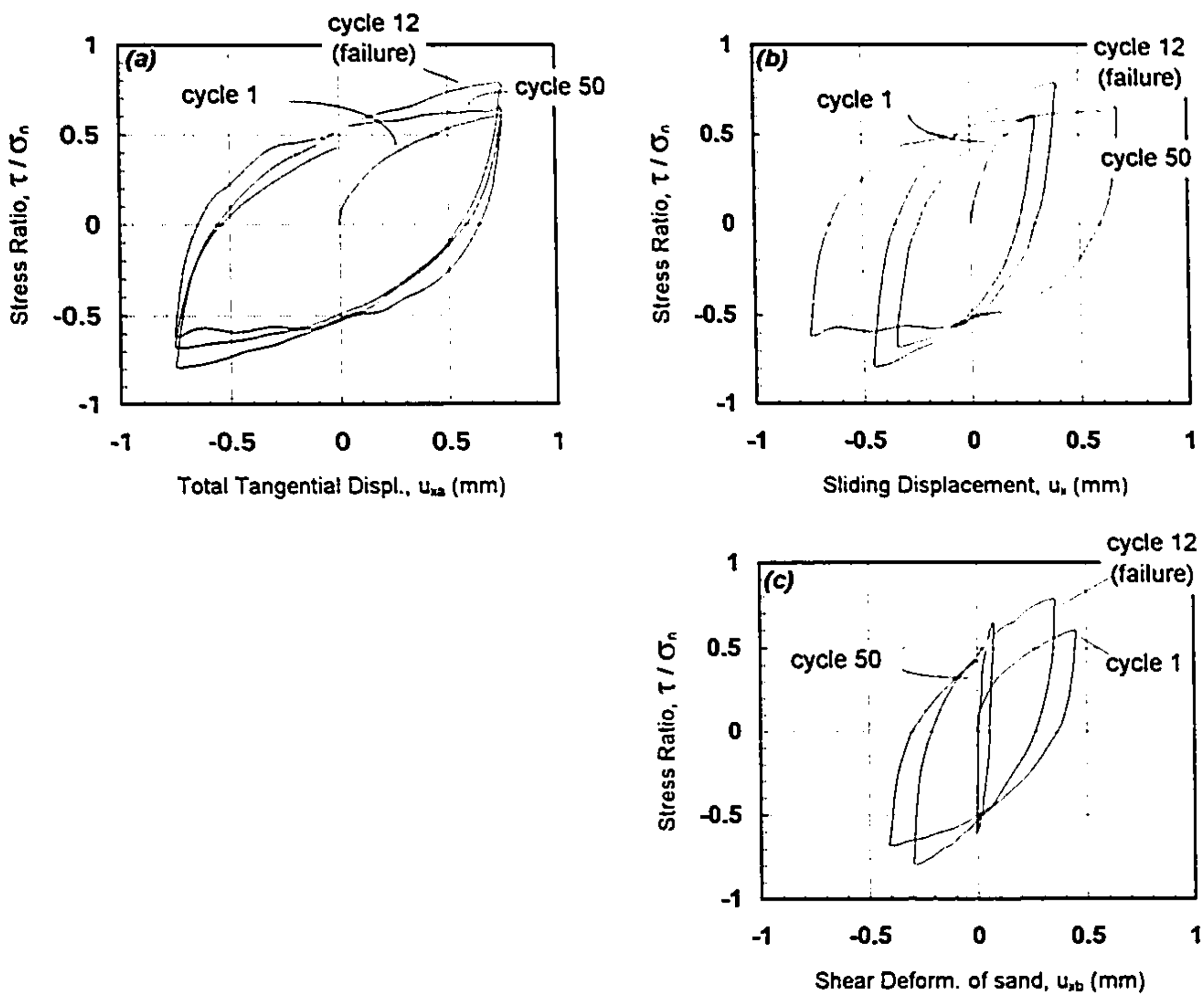

FIG. 7.8. Stress ratio variaions at cycles 1, 12 (failure), and 50 for results of Fig. 7.7.

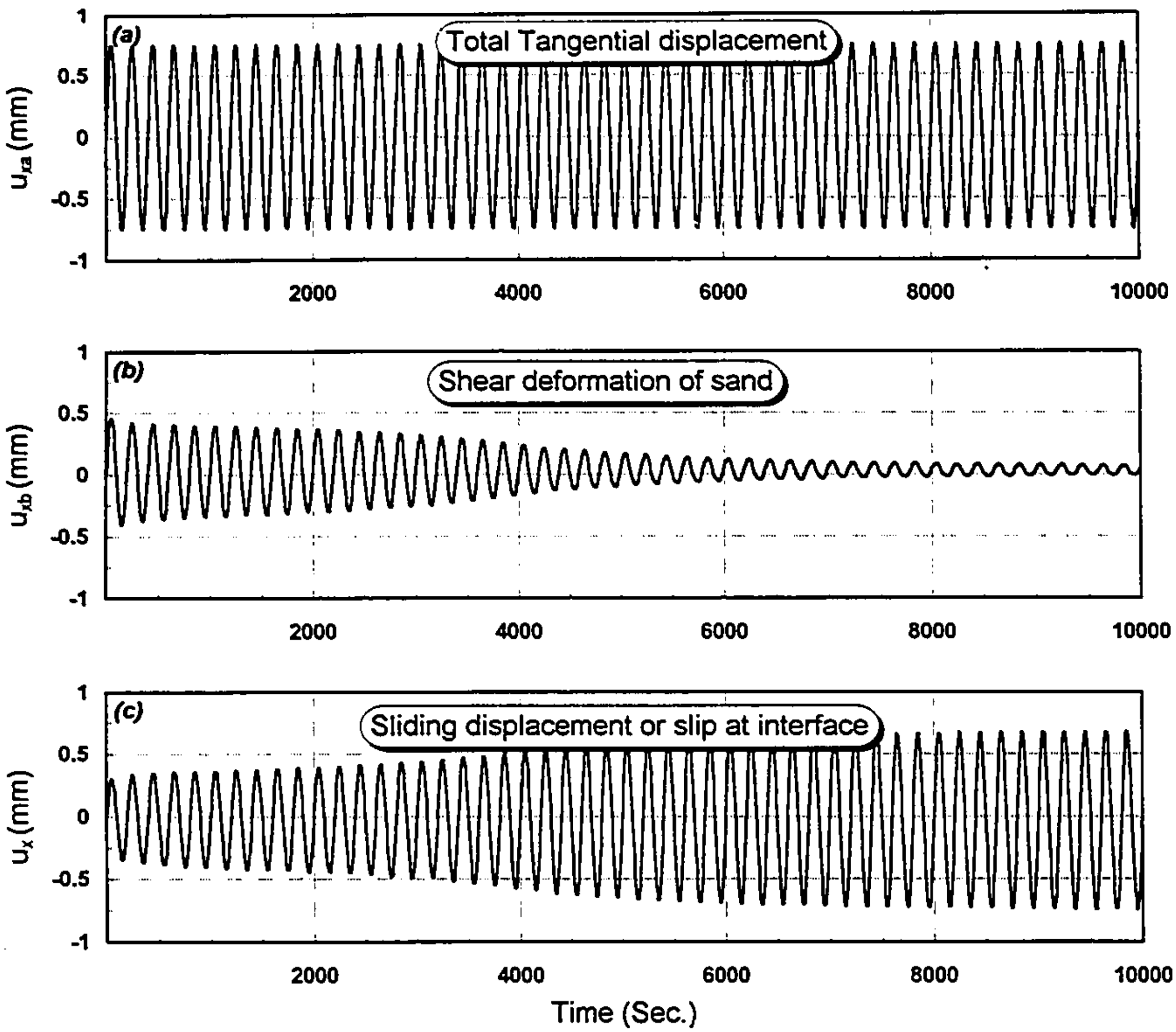

FIG. 7.9. Variations of tangential displacements with time.

Two-way tangential displacement controlled

σ_{no} = 300 kPa; K = 400 kPa/mm; Initial D_r = 84%

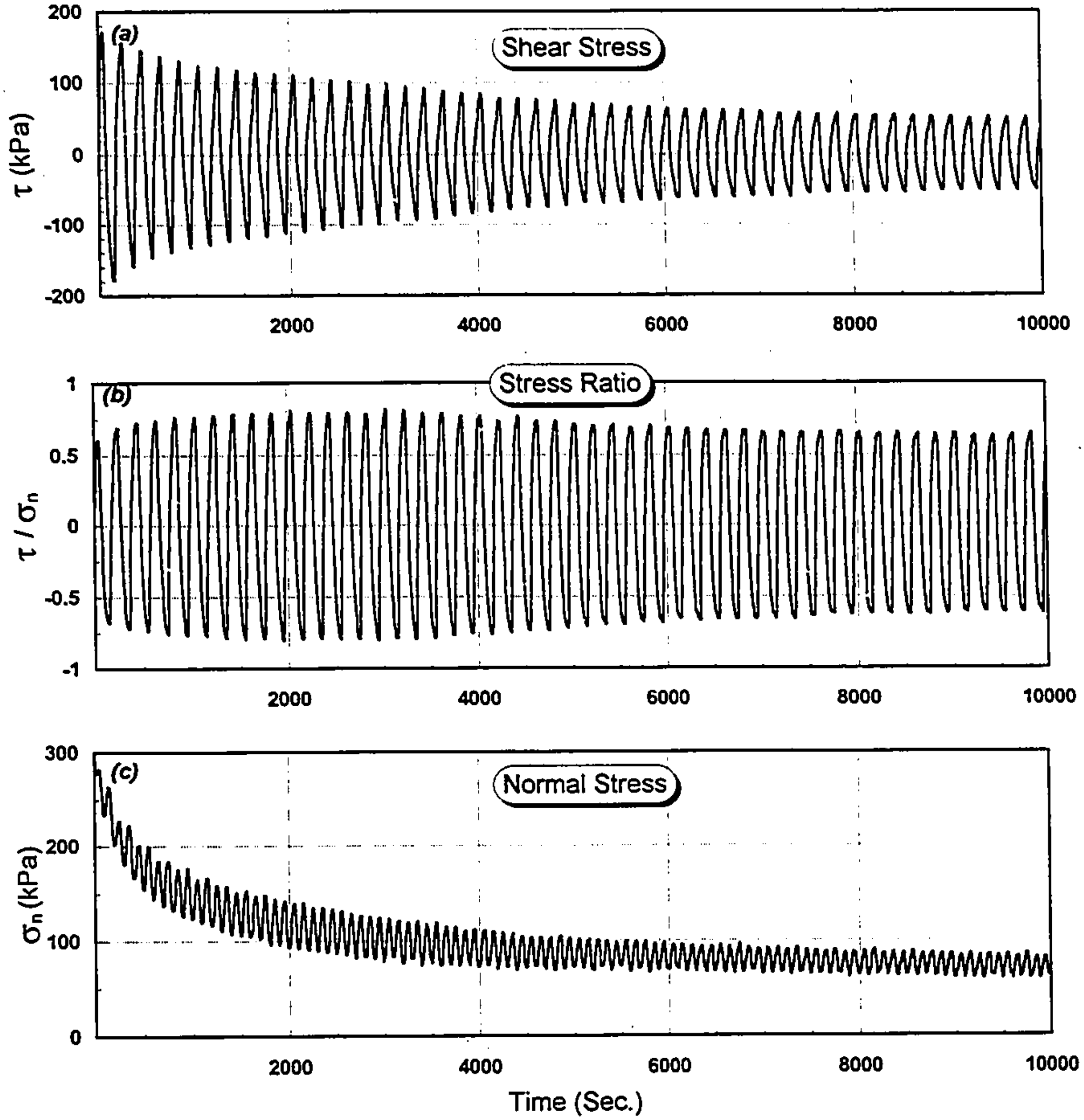

FIG. 7.10. Variations of shear stress, stess ratio, and normal stress with time.

σ_{no} = 300 kPa; K = 400 kPa/mm; Initial D_r = 84%

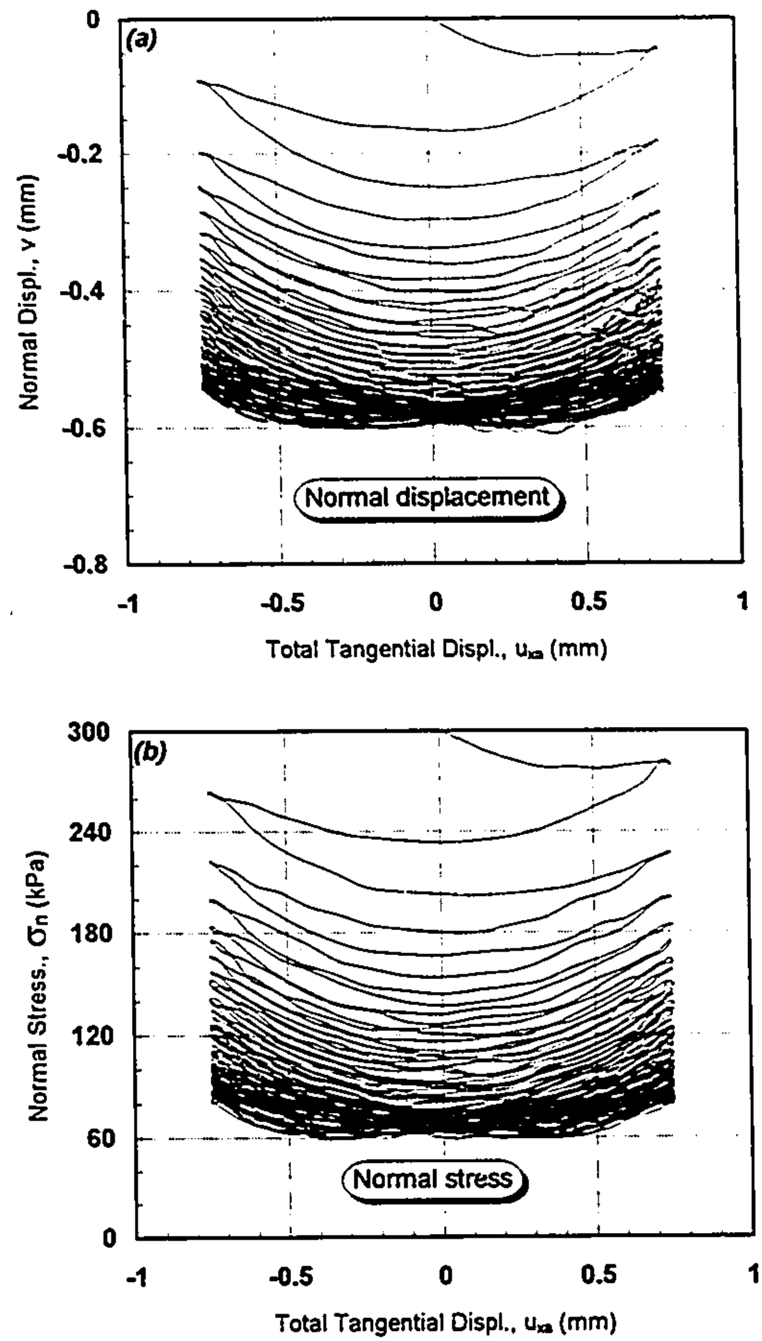

FIG. 7.11. Variations of normal displacement and normal stress with total tangential displacemnt.

σ_{no} = 300 kPa; K = 400 kPa/mm; Initial D_r = 84%

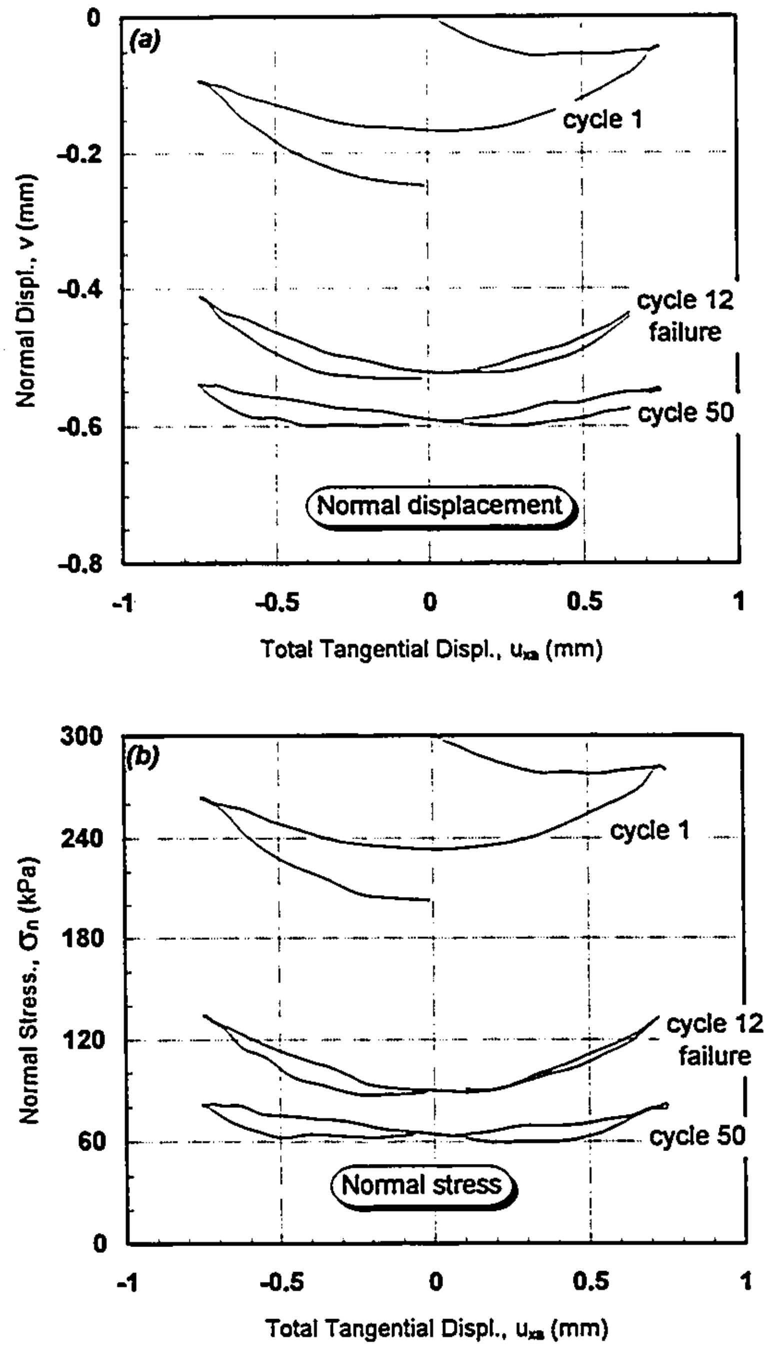

FIG. 7.12. Variations of normal displacement and normal stress with total tangential displacemnt. at cycles 1, 12, 50.

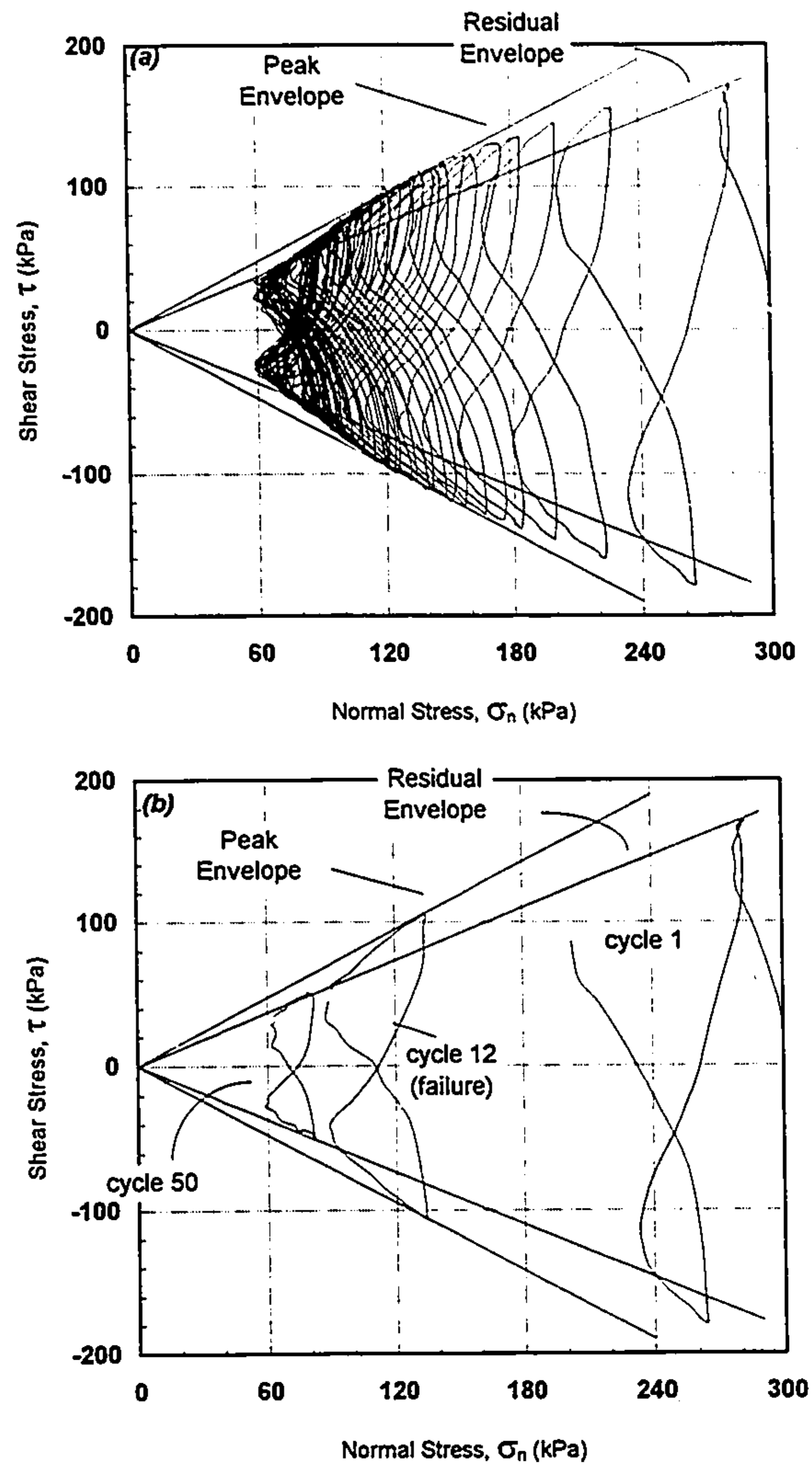

FIG. 7.13. Stress paths in τ-σ_n space.

σ_{no} = 300 kPa; K = 400 kPa/mm; Initial D_r = 84%

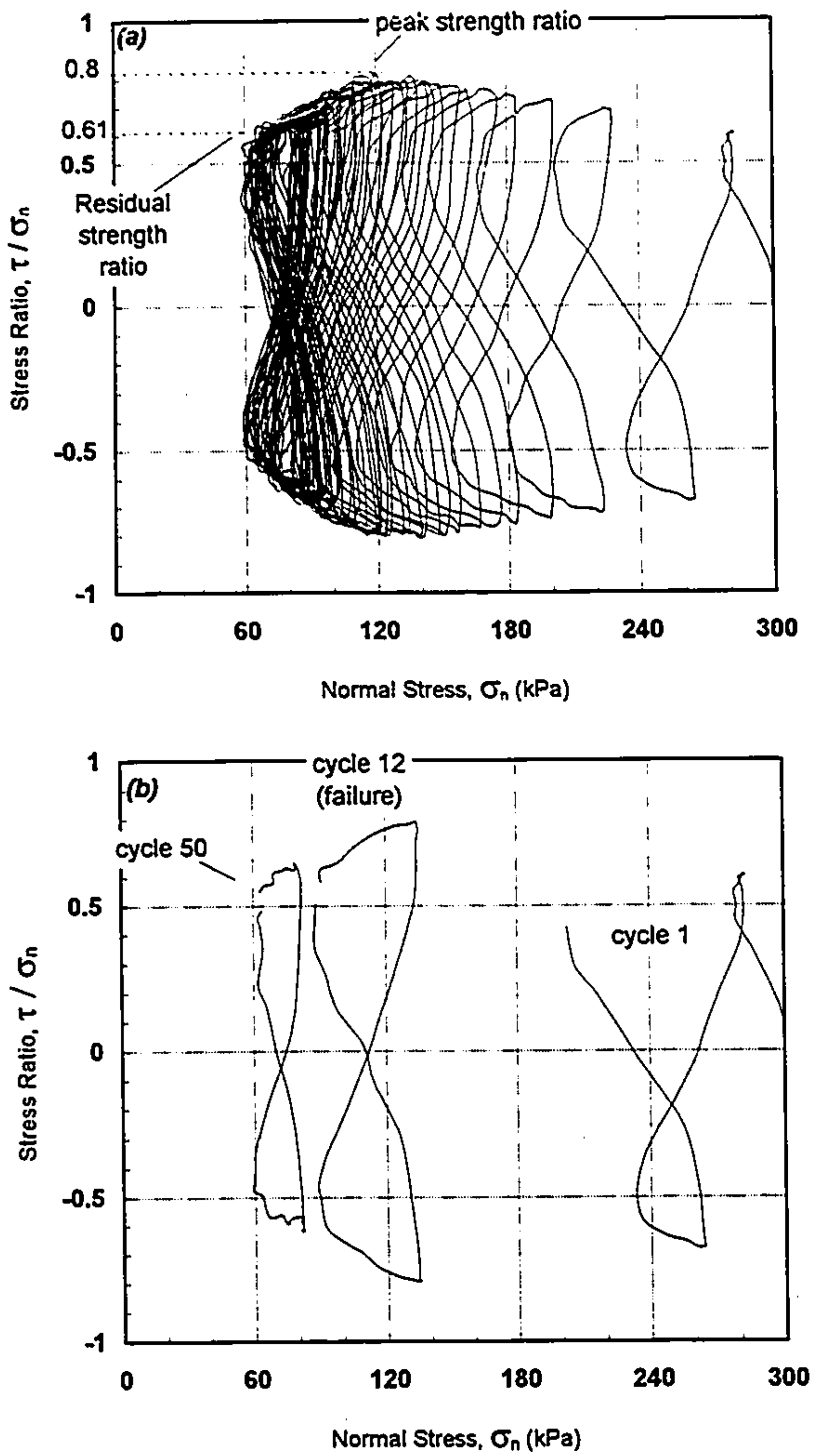

FIG. 7.14. Stress paths in τ/σ_n-σ_n space.
σ_{no} = 300 kPa; K = 400 kPa/mm; Initial D_r = 84%

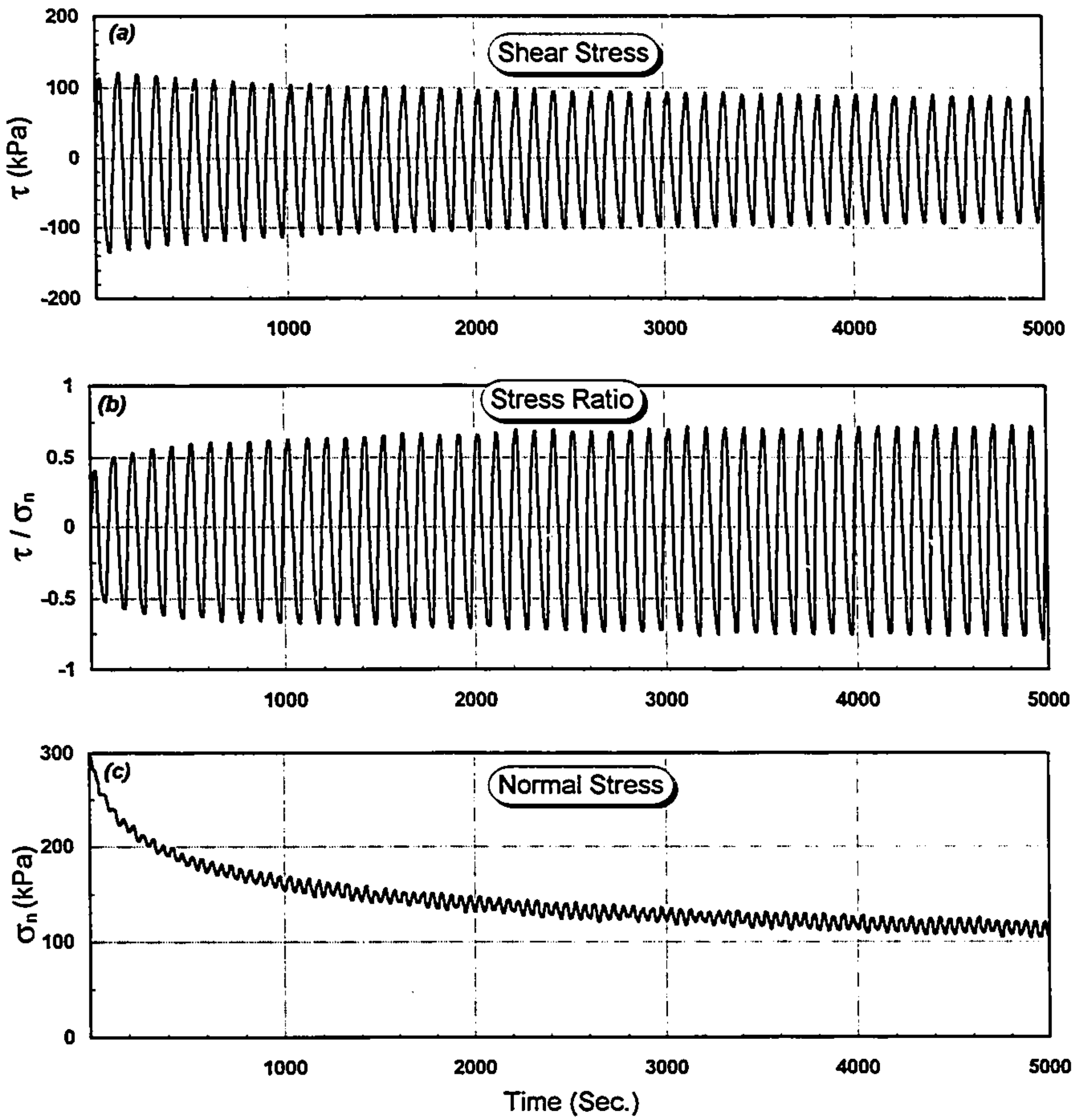

FIG. 7.15. Variations of shear stress, stress ratio, and normal stress with time.

Total displacement amplitude = 0.25 mm

σ_{no} = 300 kPa; K = 400 kPa/mm; Initial D_r = 84%

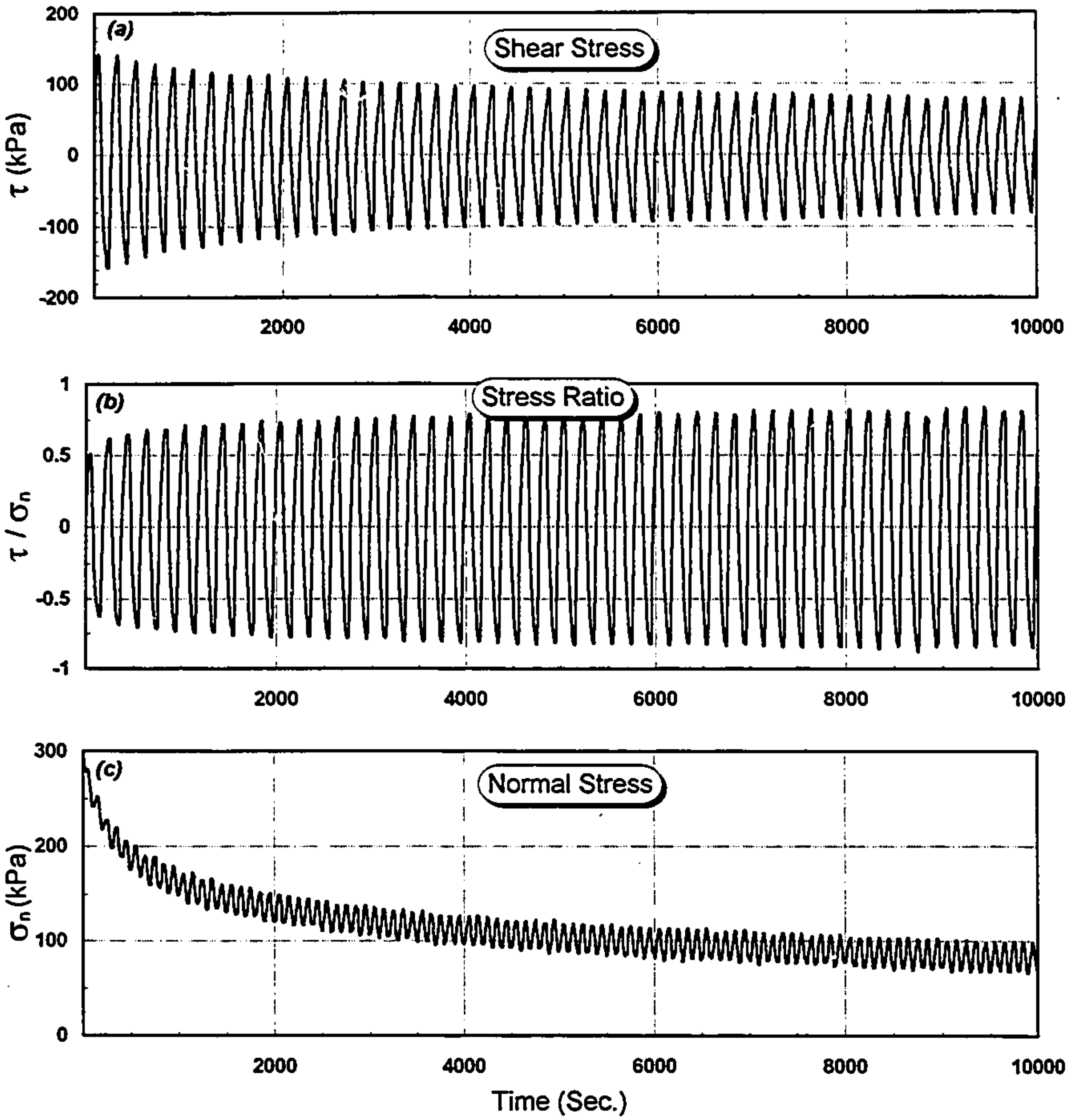

FIG. 7.16. Variations of shear stress, stress ratio, and normal stress with time;

Total displacement amplitude = 0.50 mm

σ_{no} = 300 kPa; K = 400 kPa/mm; Initial D_r = 84%

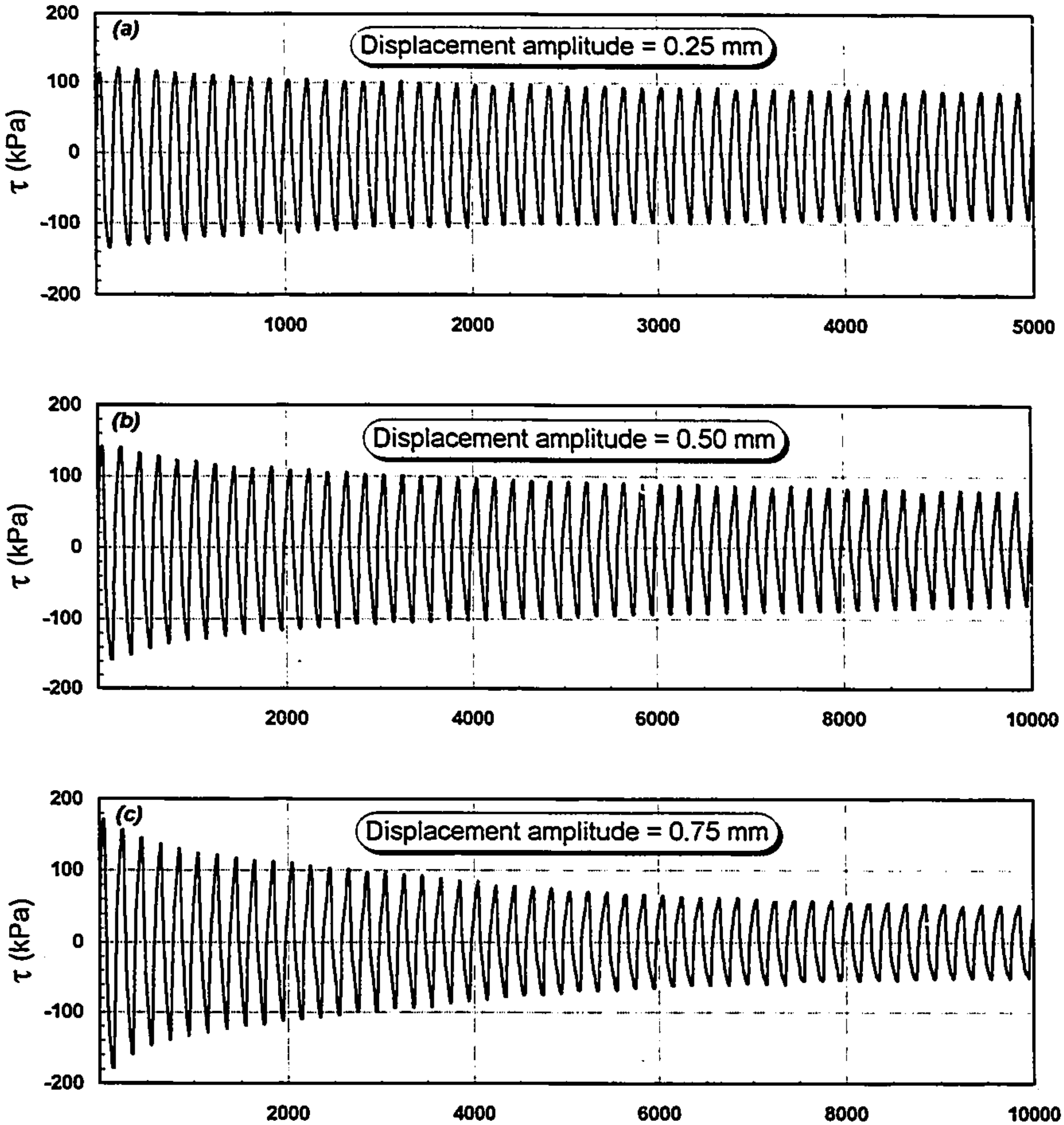

FIG. 7.17. Shear stress variations with cycles at different values of total tangential displacement amplitude.

σ_{no} = 300 kPa; K = 400 kPa/mm; Initial D_r = 84%

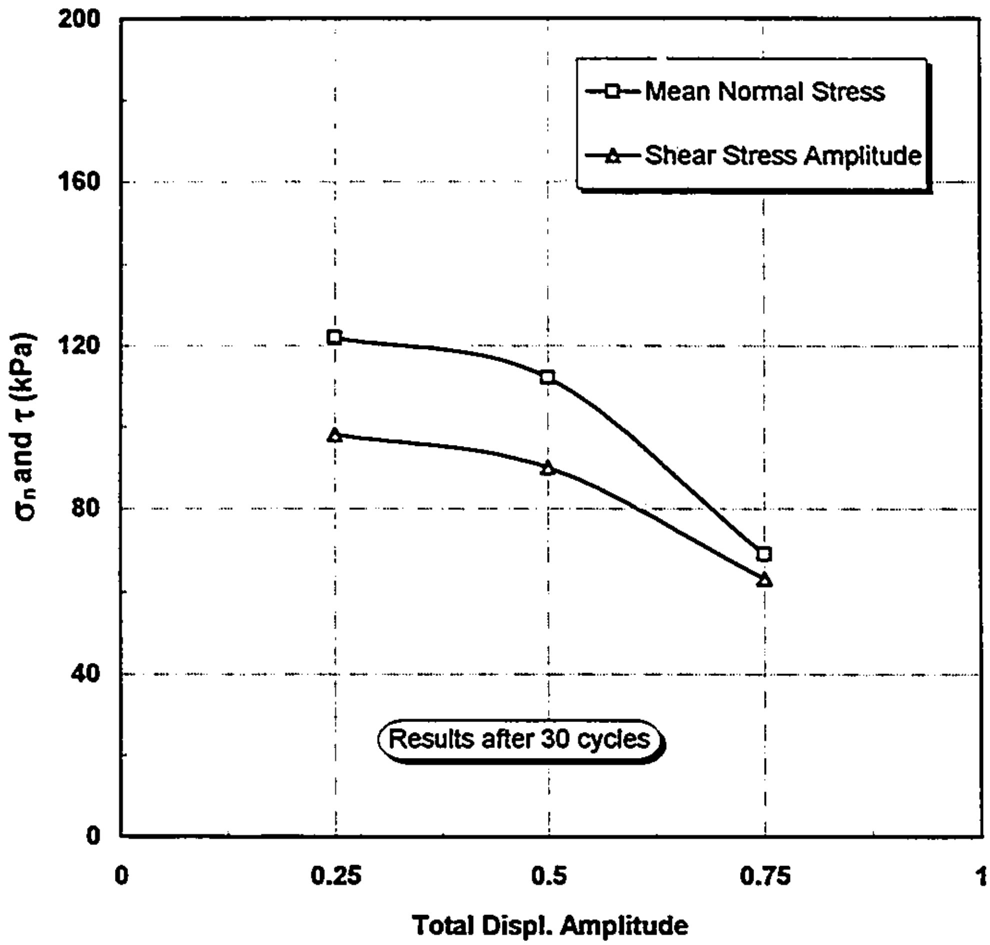

FIG. 7.18. Variations of mean normal stress and shear stress amplitude with total tangential displacement amplitude after 30 cycles.

σ_{no} = 300 kPa; K = 400 kPa/mm; Initial D_r = 84%

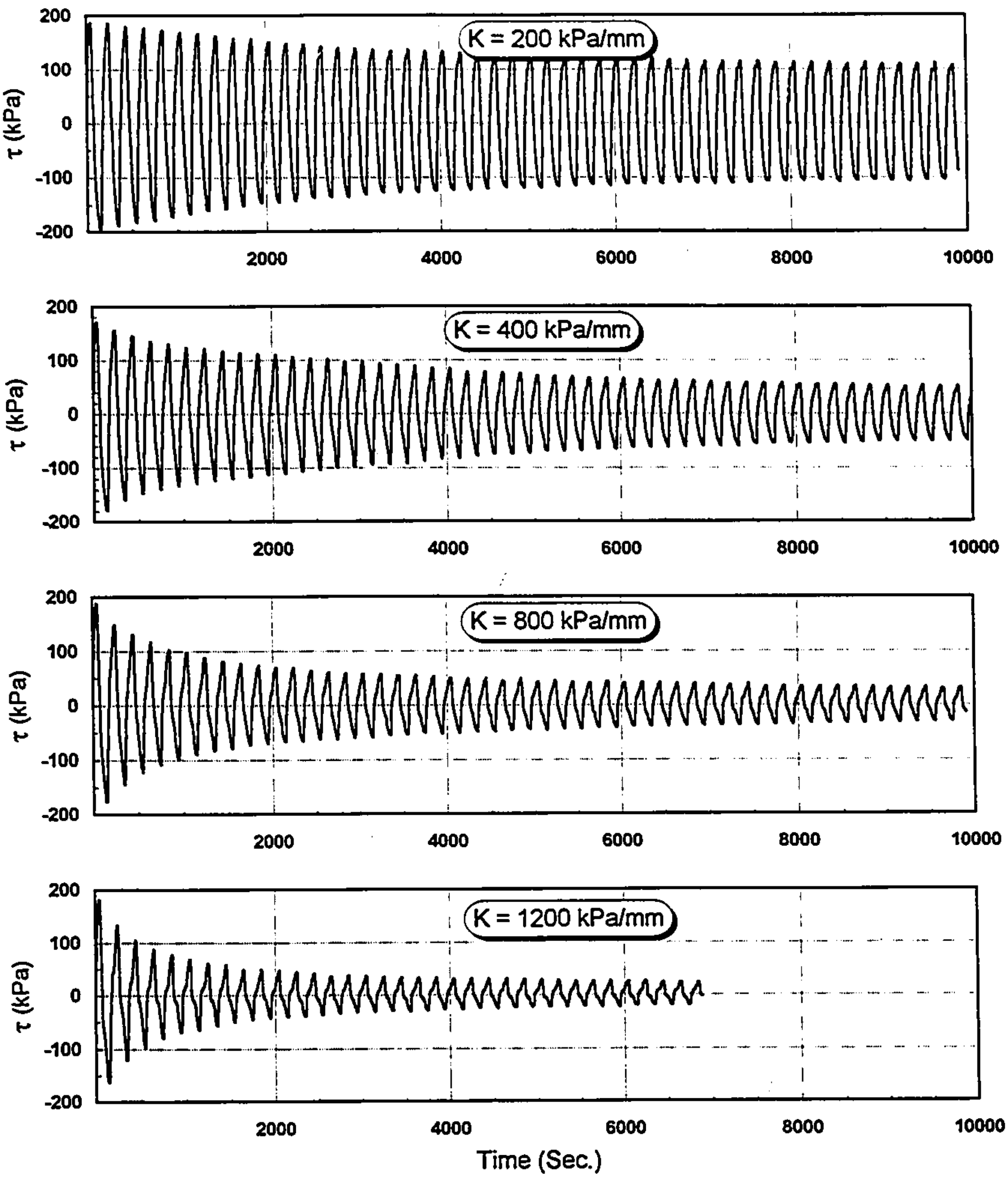

FIG. 7.19. Variation of shear stress with cycles for different values of K.

$\sigma_{no} = 300$ kPa; Initial $D_r = 84\%$

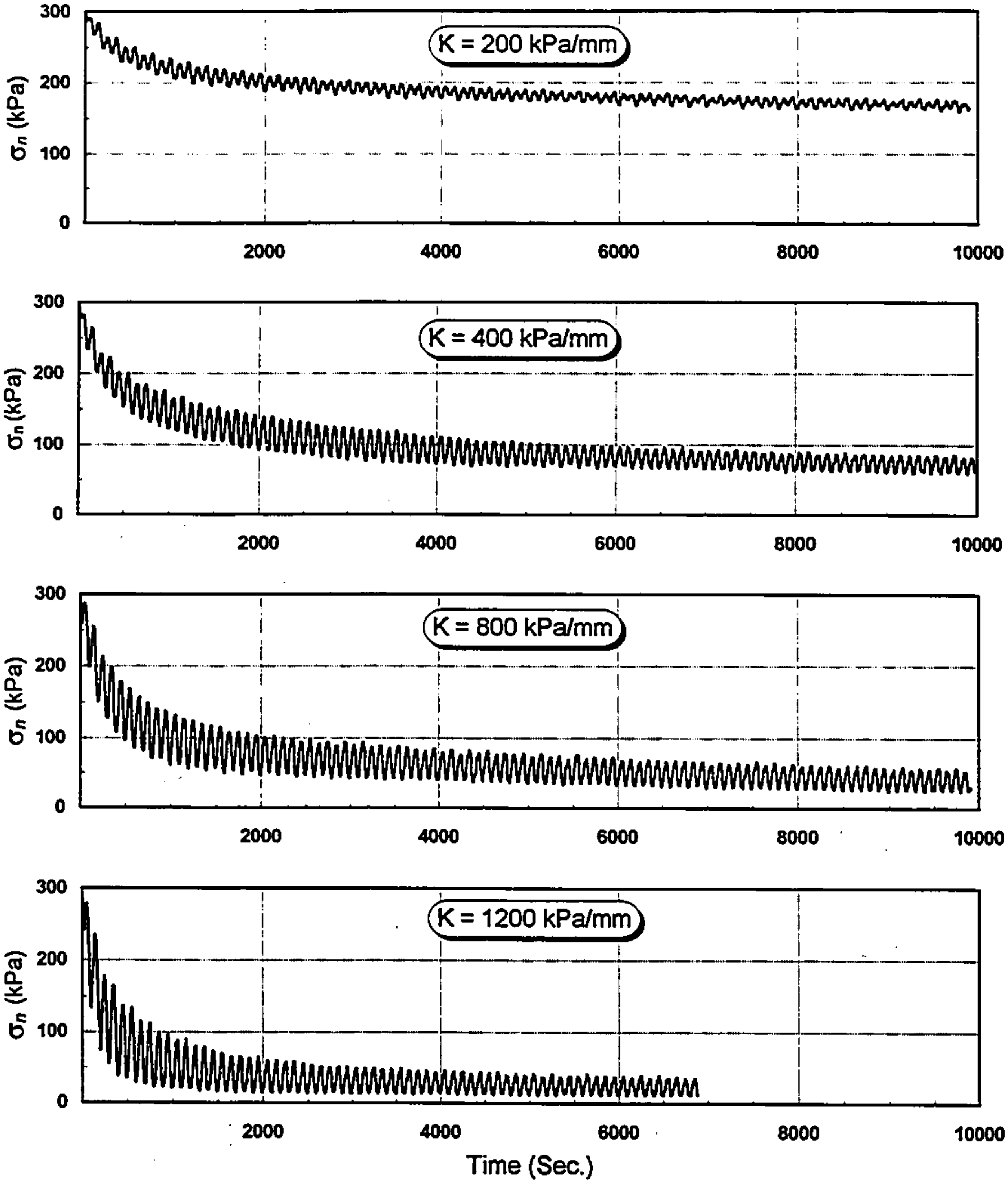

FIG. 7.20. Variation of normal stress with cycles for different values of K.

$\sigma_{no} = 300$ kPa; Initial $D_r = 84\%$

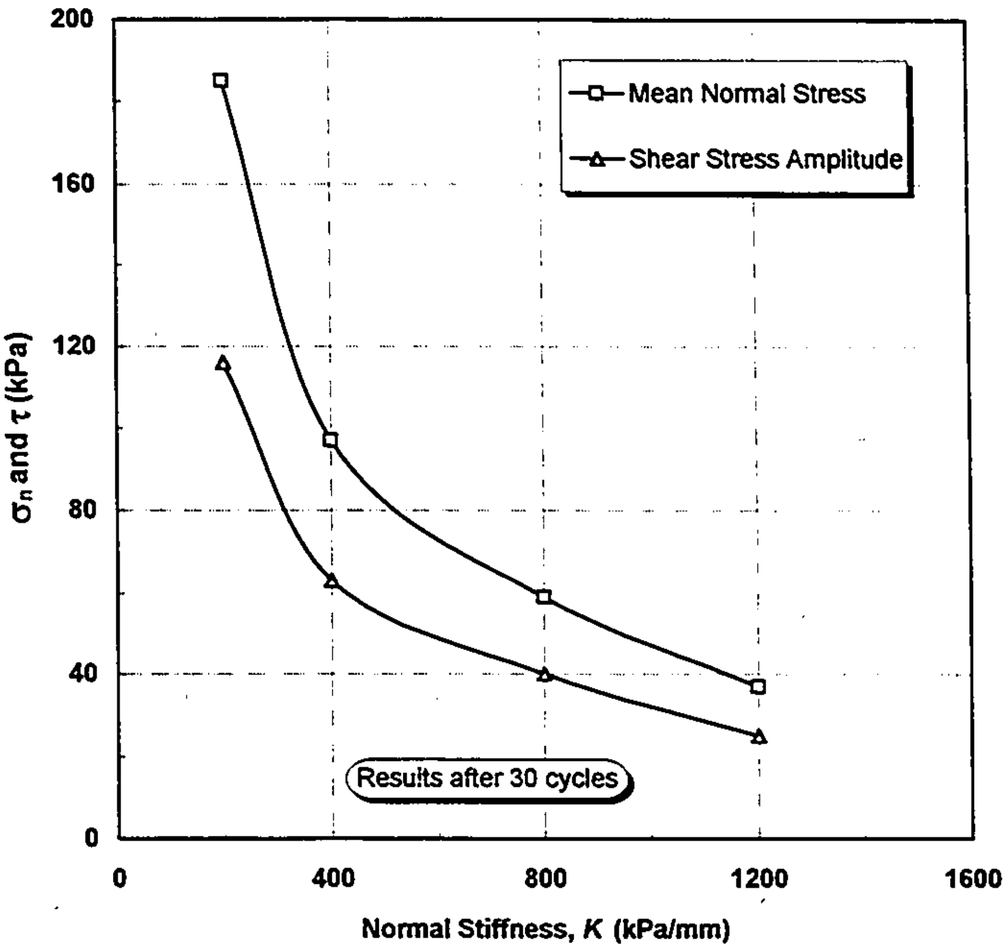

FIG. 7.21. Variations of mean normal stress and shear stress amplitude with magnitude of normal stiffness after 30 cycles.

σ_{no} = 300 kPa; Initial D_r = 84%

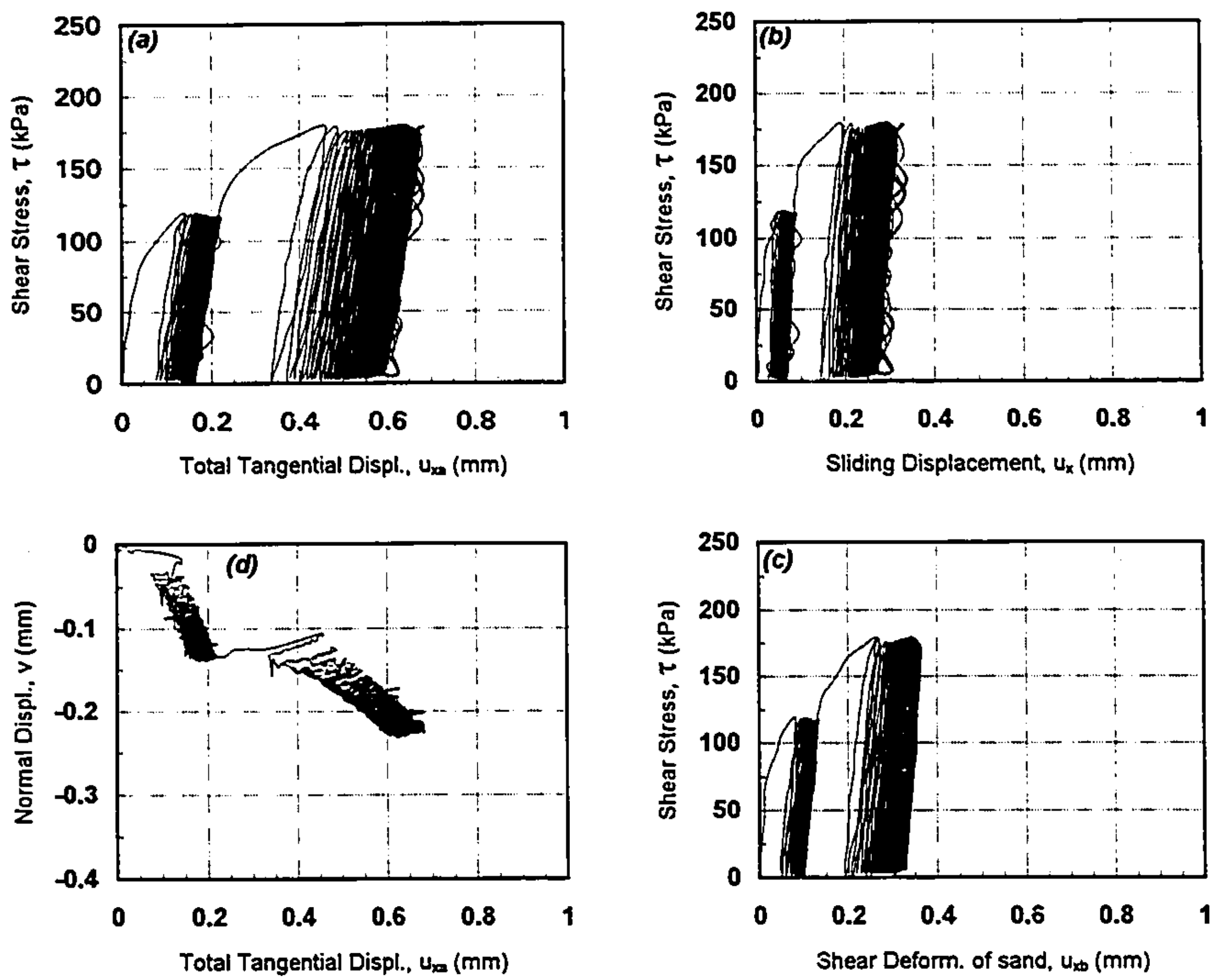

FIG. 7.22. One-way shear stress controlled test results under constant normal stress;

$\sigma_{no} = 300$ kPa; $K = 0$

Surface: Sand blasted steel plate ($R_{max} = 25$ mm for $L = 0.8$ mm)
Sand: No. 2; Dense ($D_r = 88\%$)

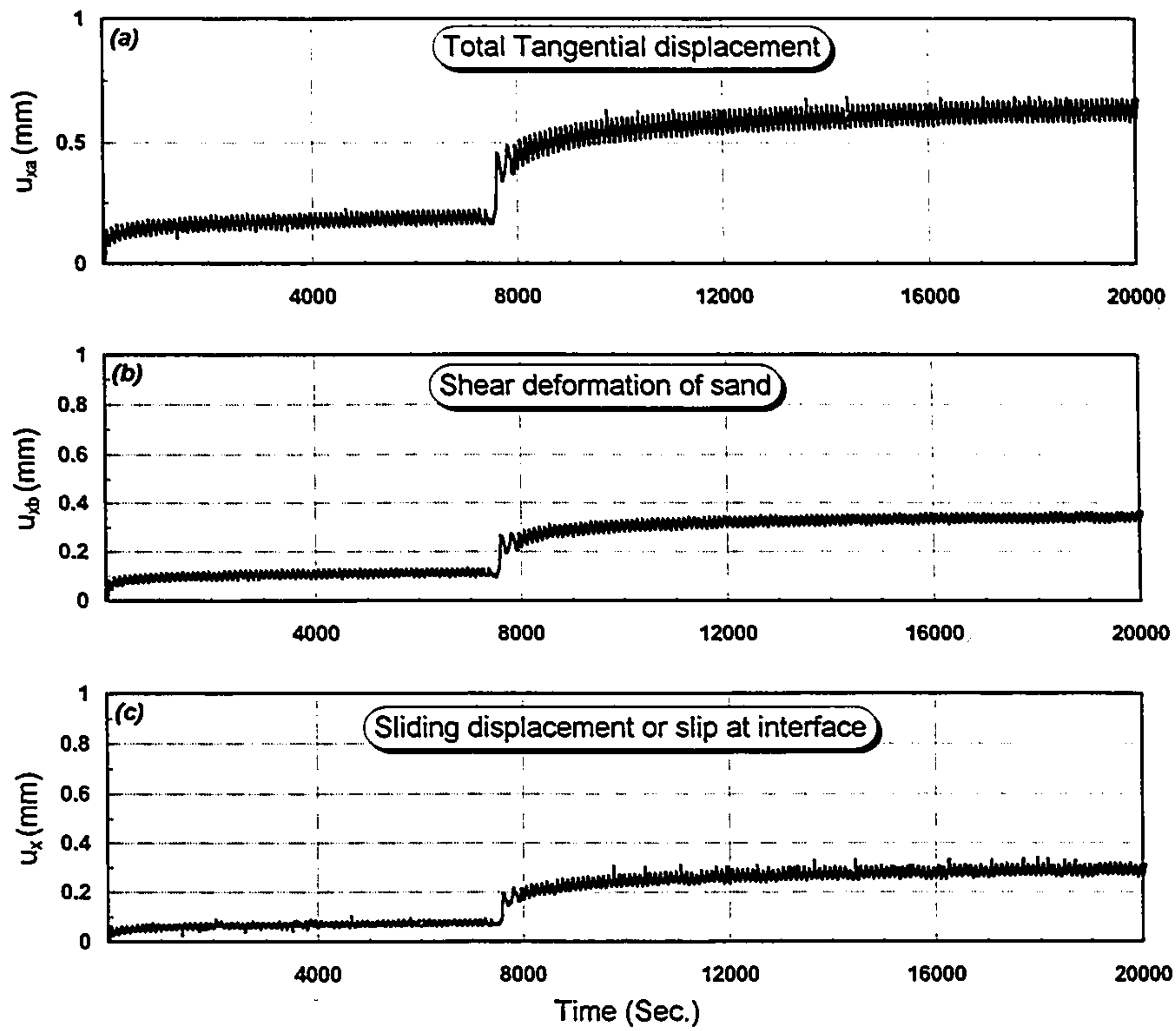

FIG. 7.23. Variations of tangential displacements with time.

σ_{no} = 300 kPa; K = 0; Initial D_r = 88%

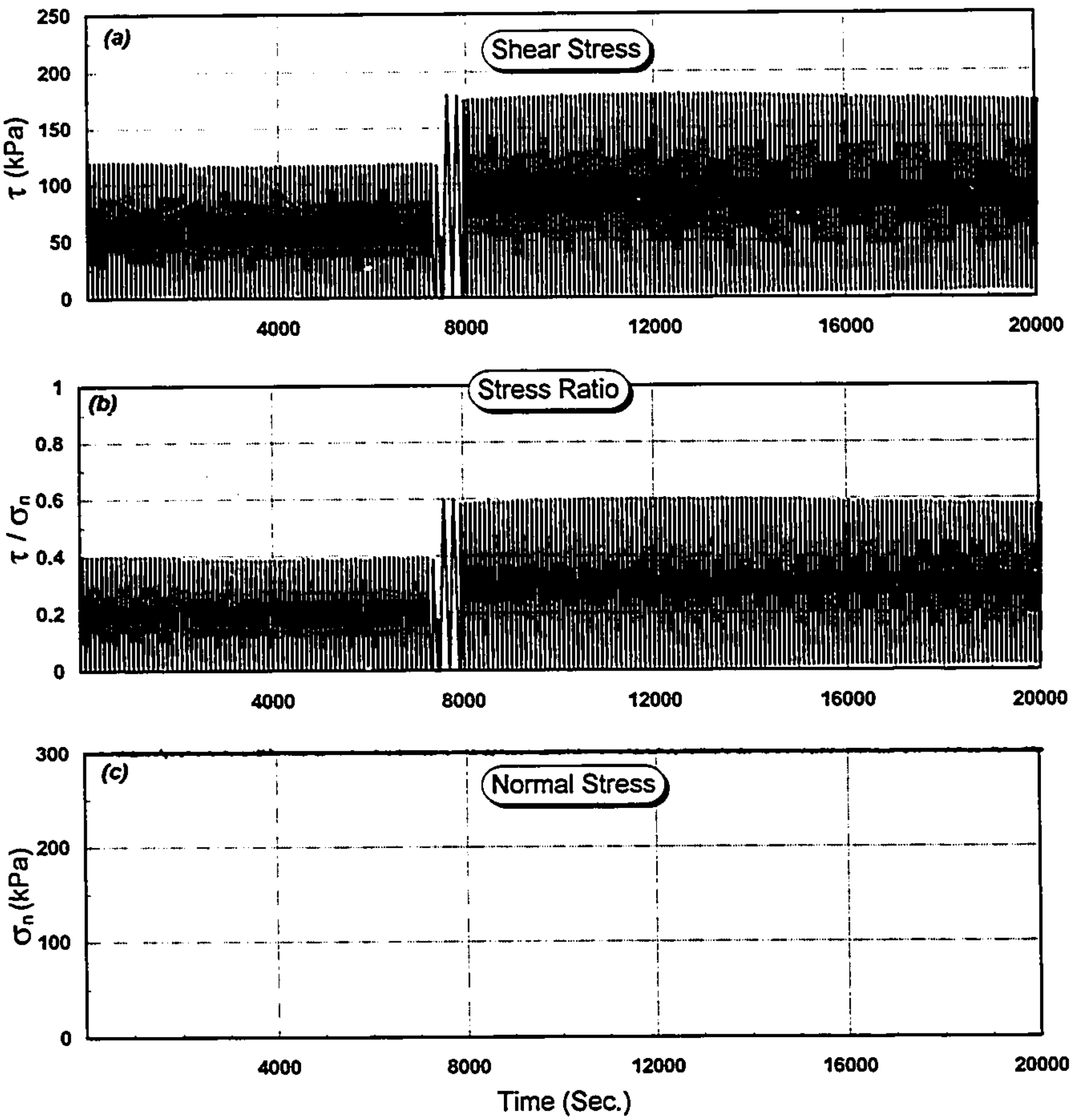

FIG. 7.24. Variations of shear stress, stress ratio, and normal stress with time.

$\sigma_{no} = 300$ kPa; $K = 0$; Initial $D_r = 88\%$

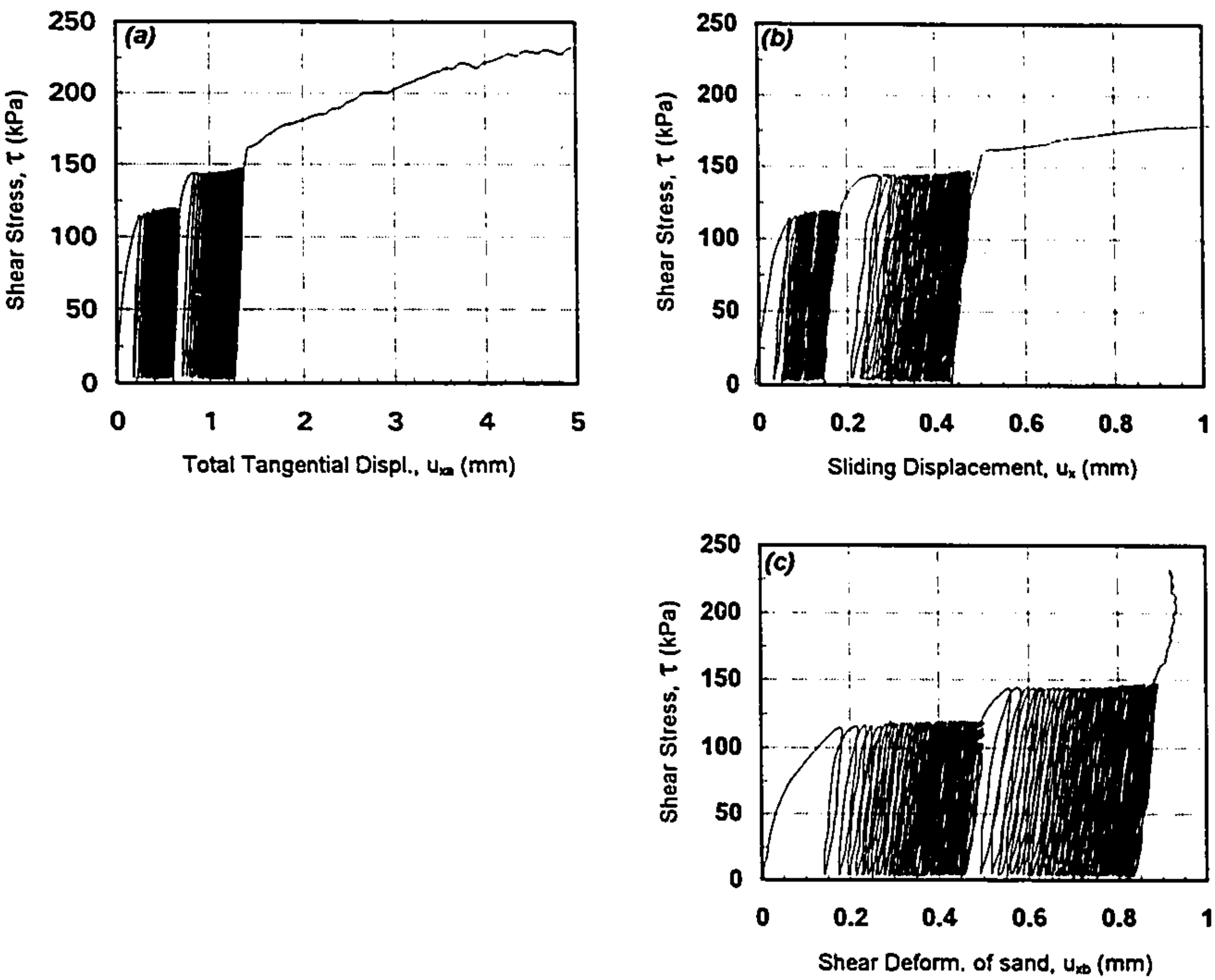

FIG. 7.25. One-way shear stress controlled cyclic test results under constant normal stiffness;

$\sigma_{no} = 300$ kPa; $K = 800$ kPa/mm

Surface: Sand blasted steel plate ($R_{max} = 25$ mm for $L = 0.8$ mm)
Sand: No. 2; Dense ($D_r = 88\%$)

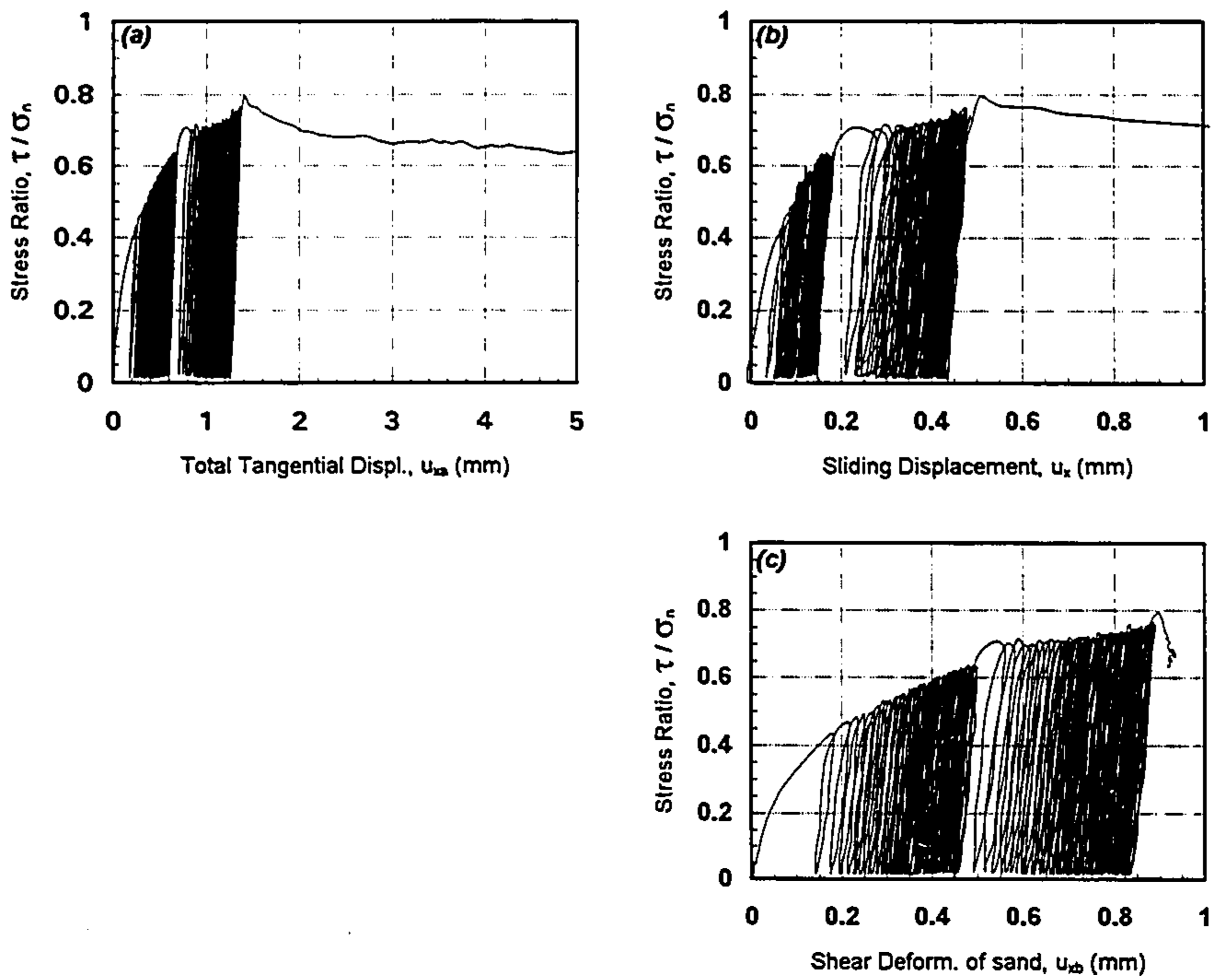

FIG. 7.26. One-way shear stress controlled cyclic test results under constant normal stiffness; (normalized results of Fig. 7.)

σ_{no} = 300 kPa; K = 800 kPa/mm; Initial D_r = 88%

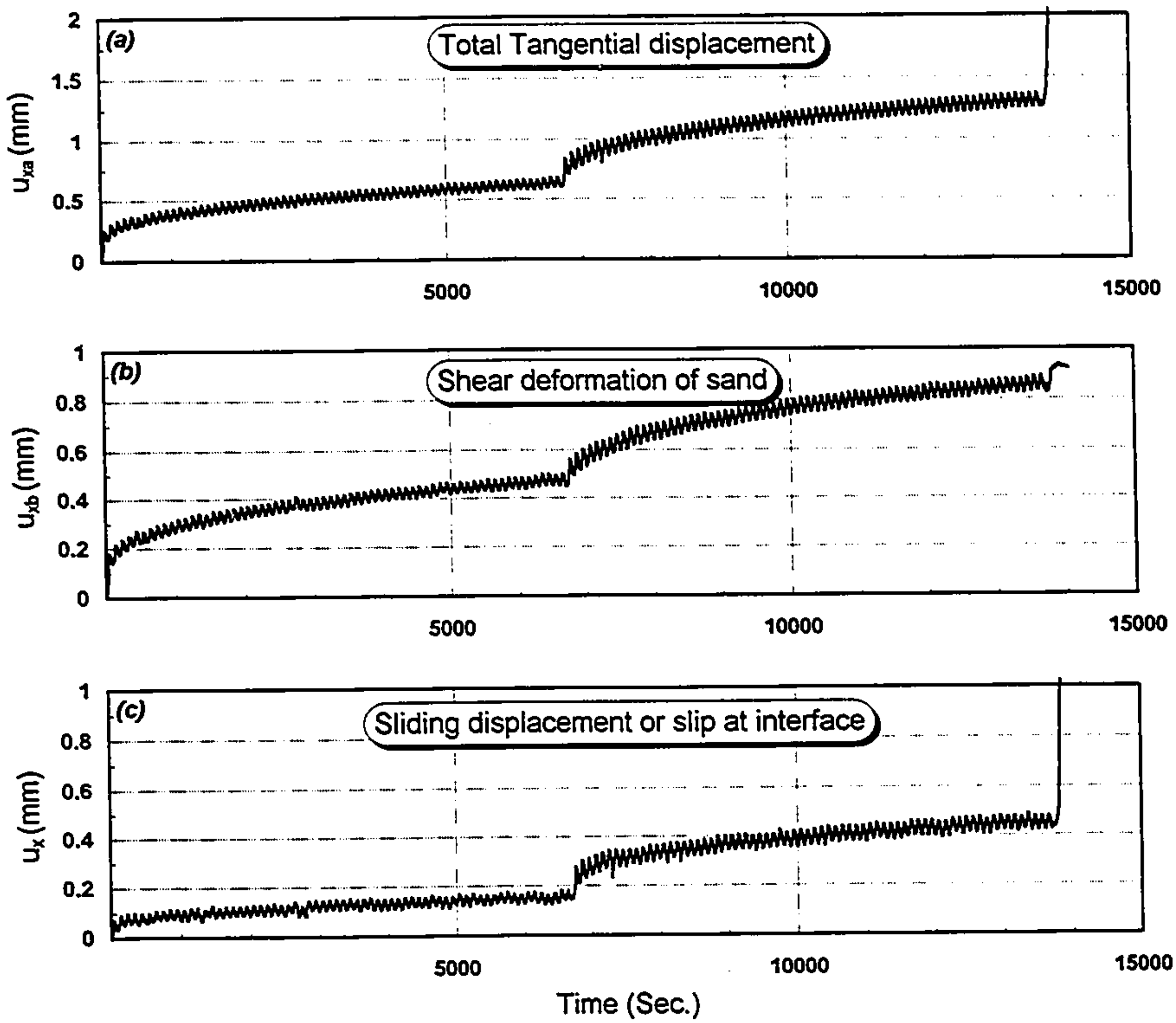

FIG. 7.27. Variations of tangential displacements with time.

σ_{no} = 300 kPa; K = 800 kPa/mm; Initial D_r = 88%

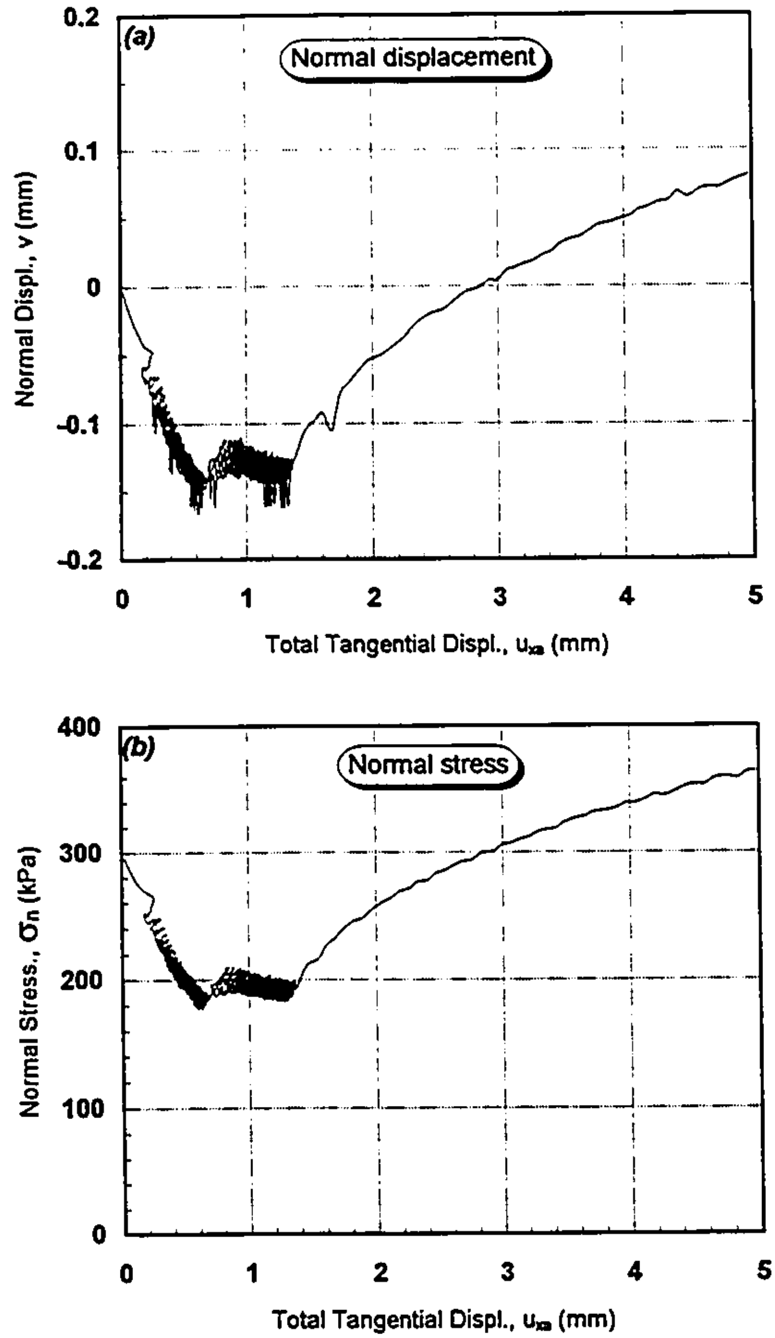

FIG. 7.28. Variations of normal displacement and normal stress with total tangential displacement.

$\sigma_{no} = 300$ kPa; $K = 800$ kPa/mm; Initial $D_r = 88\%$

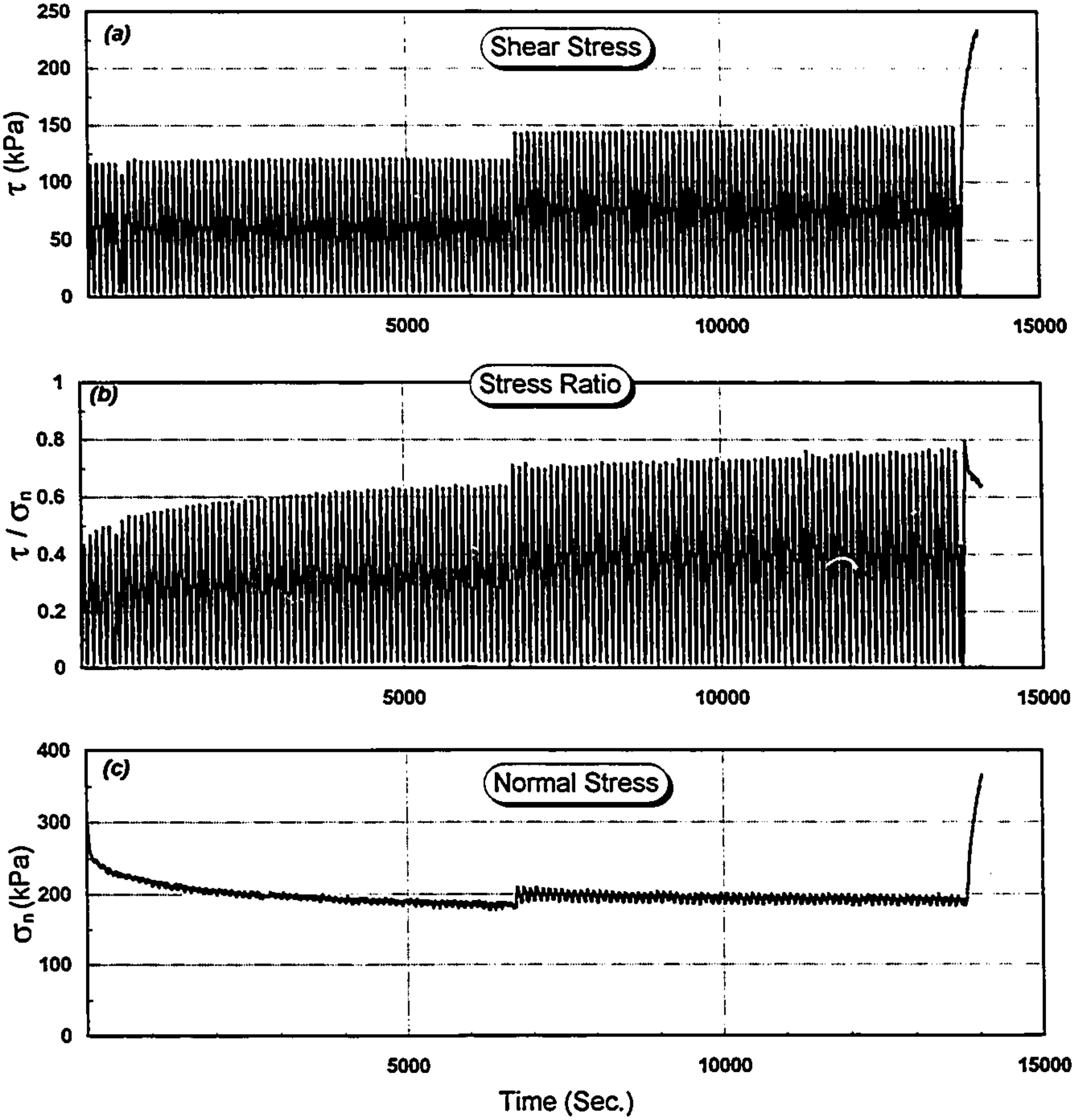

FIG. 7.29. Variations of shear stress, stess ratio, and normal stress with time.

σ_{no} = 300 kPa; K = 800 kPa/mm; Initial D_r = 88%

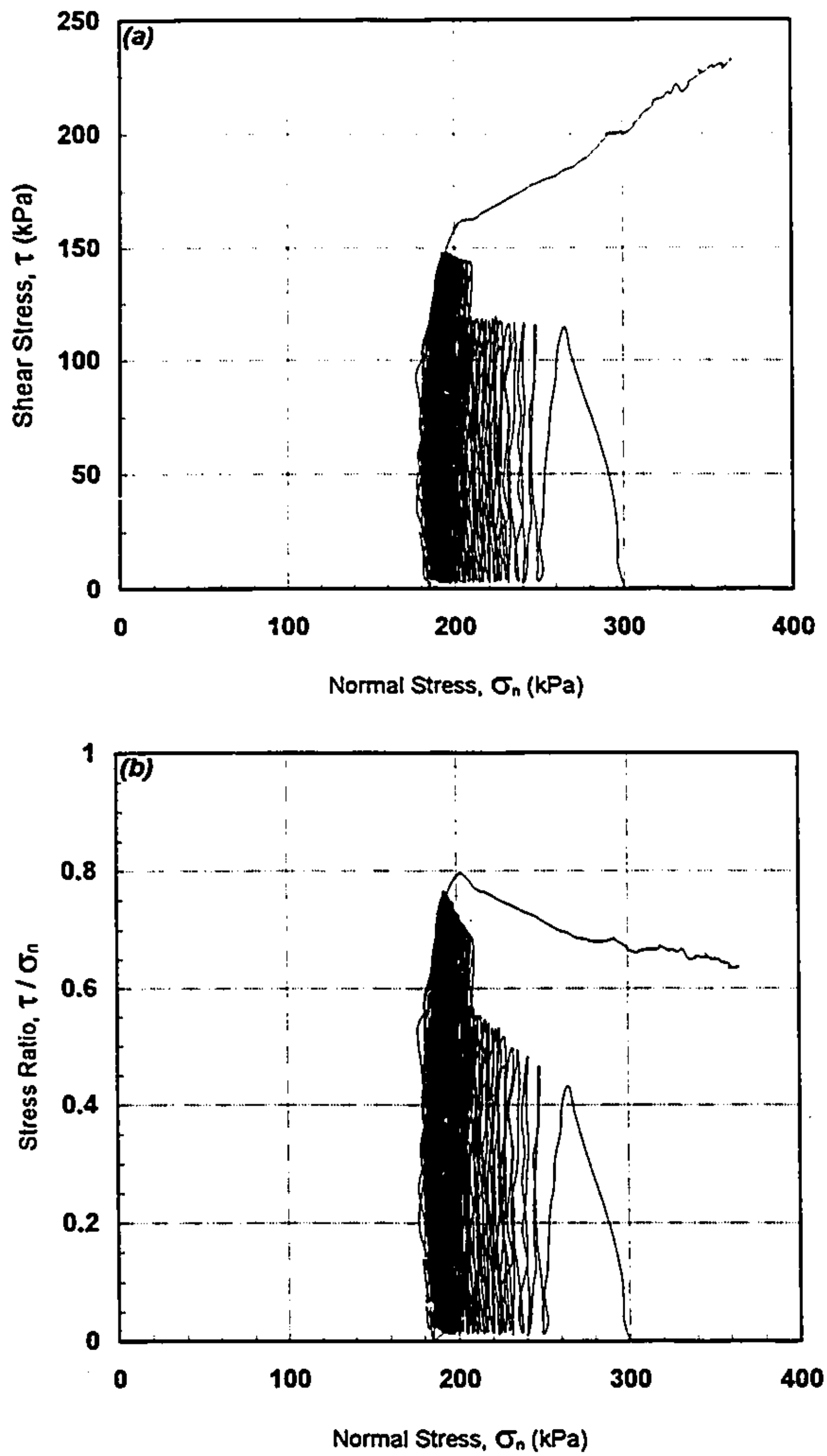

FIG. 7.30. Stress paths in: (a) τ–σ_n space; (b) τ/σ_n-σ_n space

$\sigma_{no} = 300$ kPa; $K = 800$ kPa/mm; Initial $D_r = 88\%$

CHAPTER 8

ELASTO-PLASTIC CONSTITUTIVE MODELLING

8.1 Introduction

A brief review of elasto-plasticity based models for interface behaviour was presented in Subsection 2.3.4. The modified model by Navayogarajah *et al.* (1992) was selected to be expanded and applied for simulating the 2-D and 3-D monotonic test results presented in this study. The model was originally developed for simulating the behaviour of frictional materials by Desai and co-workers (Desai 1980; Desai and Faruque 1984; and Desai *et al.* 1986). Authors refer to this model as hierarchical approach in the sense that progressively refined versions can be developed to allow for various behavioural characteristics, i.e. a simple version of the model (associative model with isotropic hardening) can be modified to obtain a model having non-associativeness, strain-softening effect, and cyclic loading capability.

The so-called hierarchical approach was specialized by Fishman and Desai (1987) and Desai and Fishman (1991) for modelling the behaviour of rock joints. Navayogarajah *et al.* (1992) employed the same model for idealization of the interface between sand-steel and sand-concrete, based on the comprehensive experimental results using a simple shear type interface device by Uesugi and Kishida (1986*b*, 1987) and Uesugi *et al.* (1989, 1990). The model was modified to simulate the strain-softening and cyclic loading behaviour of interfaces between sand and steel or concrete.

Navayogarajah's model was selected in this study to be modified and be employed for modelling the behaviour of interface under 3-D monotonic as well as various boundary conditions in the direction normal to the interface. This choice was based on the following considerations:

- The model has been formulated based upon the general framework of the theory of plasticity, thus has a strong and meaningful theoretical basis.

- The model has been modified by Navayogarajah *et al.* (1992) based on the experimental results from a simple shear type apparatus between sand and structural materials, therefore, it is capable of capturing the general characteristics of the experimental results produced in this study.

- The model is capable of simulating non-associativeness, strain softening, and cyclic loading.

Navayogarajah's 2-D model is described in detail in Appendix A.

Analogies between the behaviour of soil mass and interface behaviour are presented in Section 8.2. The model validation is presented in Section 8.3 by reproducing some of the predictions presented by Navayagarajah (1990), for the monotonic behaviour of an interface between Toyoura sand and steel. The model was then used to predict some of the 2-D monotonic test results presented in Chapter 5, for which the determination of the required parameters are described in Appendix *A*. The procedure for expanding the model to 3-D is described in Section 8.4. Some 3-D predictions for monotonic loading are compared with the corresponding test results presented in Chapter 6. Section 8.5 describes the formulation of the model for incorporating the various normal boundary conditions like constant volume and constant normal stiffness, in addition to constant normal stress. Some predictions are compared with experimental results.

8.2 Analogies Between Soil Behaviour and Interface Behaviour

The idea of application of the theory of plasticity to the behaviour of interfaces was introduced by Ghaboussi *et al.* (1973). They used a perfectly plastic yield surface to limit shear stresses and a strain hardening cap to control dilatancy and contraction (Fig. 8.1). The normal and shear components of strain increments, ε_n and ε_s, were divided into elastic and plastic parts:

$$d\varepsilon_n = d\varepsilon_n^e + d\varepsilon_n^p$$
$$d\varepsilon_s = d\varepsilon_s^e + d\varepsilon_s^p \qquad 8.1$$

in which *e* and *p* denote elastic and plastic components. Since the exact thickness of the interface zone is not known, displacement increments are often employed instead of strains:

$$dv = dv^e + dv^p$$
$$du = du^e + du^p \qquad 8.2$$

in which *dv* and *du* are increments of normal and tangential displacements, respectively.

The elastic components of displacements were considered uncoupled and were obtained from the following equation:

$$\begin{pmatrix} d\sigma_n \\ d\tau \end{pmatrix} = \begin{bmatrix} K_n & 0 \\ 0 & K_s \end{bmatrix} \begin{pmatrix} dv^e \\ du^e \end{pmatrix} = [C^e](dU^e) \qquad 8.3$$

where K_n= normal elastic stiffness, K_s= tangent elastic stiffness, and $[C^e]$ is the elastic constitutive matrix. Incremental plastic displacements were computed by using a flow rule based on the plastic potential as follows:

$$dv^p = \lambda \frac{\partial Q}{\partial \sigma_n}$$
$$du^p = \lambda \frac{\partial Q}{\partial \tau} \qquad 8.4$$

in which λ = a scalar factor of proportionality
Q = plastic potential function

If the plastic potential function, Q, assumed to be the same as the yield function, F, then the interface behaviour follows the associative flow rule of plasticity. Otherwise the interface is following the non-associative flow rule. λ can be obtained from Eq. 8.4 and also consistency condition, $dF = 0$.

Finally, the stress-displacement relation can be written as:

$$(d\sigma) = \left([C^e] - [C^p]\right)(dU) = [C^{ep}](dU) \qquad 8.5$$

in which $[C^p]$ and $[C^{ep}]$ are the plastic and elasto-plastic constitutive matrices, respectively.

Boulon and Nova (1990) provided an analogy based on the similarities of drained and undrained triaxial test results for sand, and constant normal load and constant volume interface test results, respectively. Figure 8.2 represents typical experimental results for an interface between sand and steel, which were obtained from a direct shear type device. Shear stress- tangential displacement and normal displacement-tangential displacement under constant normal stress are shown in Fig. 8.2*a*. Figure 8.2*b* presents the results from tests performed under constant volume condition.

Drained and undrained triaxial test results on sand are presented in Figs. 8.3*a* and 8.3*b*, respectively. P' is the effective mean pressure, q is the deviator stress, and ε_v and ε_s are volumetric and deviatoric strains as expressed below:

$$p' = \frac{\sigma_1' + 2\sigma_3'}{3}$$
$$q = \sigma_1 - \sigma_3 \qquad 8.6$$

$$\varepsilon_v = \varepsilon_1 + 2\varepsilon_3$$
$$\varepsilon_s = \tfrac{2}{3}(\varepsilon_1 - \varepsilon_3) \qquad 8.7$$

Similarity exists between constant normal load results of Fig. 8.2*a* and drained triaxial test results of Fig. 8.3*a* as well as constant volume test results of Fig. 8.2*b* and undrained triaxial test results of Fig. 8.3*b*, respectively.

In drained triaxial tests, the deviatoric stress, q, increases to a peak and then the soil strain softens till a residual stress state is reached, after which soil deforms without noticeable change in stresses and volume. Volumetric strain, ε_v, is initially compressive, then well before peak the sample starts dilating. Eventually, the dilation rate becomes very small and the stress-strain curve becomes horizontal. Obviously, one can describe the constant normal stress test results for interface, Fig. 8.2*a*, by means of the same expressions, except that the deviatoric stress, q, is substituted by the term shear stress, τ, the deviatoric strain, ε_s, is substituted by the tangential relative displacement, u, and finally, the role of confining pressure is played by the normal stress, σ_n.

Similarly, one can establish a comparison between the undrained triaxial and the constant volume direct shear type test results, presented in Figs. 8.3*b* and 8.2*b*, respectively.

The analogous quantities for triaxial tests and interfaces are presented in Table 8.1.

Table 8.1. Analogous quantities for soil and interface

Soil	**Interface**
q	τ
p'	σ_n
ε_v	v
ε	u

Using these analogies between the behaviour of soils and interfaces (or joints), one can develop the general framework of a plastic model for the interface behaviour.

8.3 Validation of the Model

8.3.1 Toyoura sand-steel interface

In this study, a computer code was written for the elasto-plastic model which is described in Appendix *A*. The computer code was first used with the model parameters determined by Navayogarajah (1990), to simulate the behaviour of the interface between Toyoura sand (D_r = 90%) and steel plate. The results of four predictions are shown in Fig. 8.6. The predictions were made for the stress ratio, τ / σ_n, versus sliding displacement, u_x, and the normal displacement versus sliding displacement relations for four surface roughnesses of 40, 19, 9.6, and 3.8 μm. The parameters were exactly the same as those determined by Navayogarajah (1990) and they are listed in Table 8.2. Stress ratio-sliding displacement results match those predicted in Fig. 5.9 in Navayogarajah (1990). The volume change predictions were good for surface roughnesses of 3.8, 9.6, and 18 μm whereas the volume change for the surface with roughness 40 μm was underestimated as compared with his predictions. These comparisons indicate that the model has been correctly formulated and programmed.

8.3.2 Simulation for 2-D monotonic test results

The results of three predictions for 2-D monotonic sand-steel interface are presented together with the corresponding experimental results, in Fig. 8.7. The results include the No. 2 sand at a relative density of 88% and steel plates with surface roughnesses of 4, 15, and 25 μm, which cover from very smooth to rough surfaces. The experimental results are only available for surface roughnesses of 4 and 25 μm. The normal stress, was 100 kPa for all presented results. The determination of parameters are described in Appendix *A* and their values are shown in Table 8.2. Some discrepancy exists between the parameters determined by Navayogarajah (1990) for the Toyoura sand-steel and those determined in this study, Particularly in elastic normal stiffness, K_n, and elastic shear elastic, K_s. The results of Fig. 8.4*b* indicates that K_n varies with stress level. Three values were determined at average normal stress levels of 100, 200, and 300 kPa at 5800, 8500, and 1800 kPa/mm, respectively. A K_n of 6000 kPa/mm was selected since it was close to the stress level of 100 kPa for the predicted results. The parameters can be obtained using the results of 2-D monotonic tests under constant normal stress condition. The test results presented in Fig. 8.7 and some other results using the No. 1 sand were used for the determination of the parameters. The parameters were then used to predict the test results related to different stress paths such as constant normal stiffness and 3-D loading as will be presented in the subsequent sections.

The predictions shown in Fig. 8.7 seems to be in good agreement with the experimental results. The shear stress-sliding displacement results indicate that both peak and residual stresses were predicted adequately. Most of the model parameters are dependent on the interface roughness ratio, R, as defined in Appendix *A*. Therefore, the effect of surface roughness on peak and residual strengths are well captured in predictions. The dilative response of the interface is also well-predicted by the model, however, the compressive mode is not simulated well. For example Fig. 8.7*b* shows that for smooth surfaces the predicted normal displacement is zero whereas the experimental results show compression. Also the initial compression portion for the rough surface is not predicted. The compressive mode is controlled by the phase change parameter n as described in the Appendix *A*. Compression is occurring in the soil mass in the vicinity of the interface, and the dilation is the result of particle movements in the interface in the direction normal to the interface plane. Therefore, it was discussed by Navayogarajah (1990) that interface cannot undergo compaction, but it can dilate or remain in steady state, during monotonic loading. In such a case the shear stress at phase change point, τ_{ph}, is very small or equal zero leading to a value $n = 2.0$. He adopted a value of 2.001 for n.

The model requires 12 parameters as listed in Table 8.2. This is regardless of the point that some parameters like κ and ξ_D^* have two components each. However, all the parameters can be determined based on 2-D monotonic test results under various surface roughnesses. Effect of normal stress, relative density, and made of structural materials are not incorporated in the model. Different set of parameters are required to include such effects. The normal stress and relative density affect the peak strength as well as the normal displacement response as described in Chapter 5.

Table 8.2. Model Parameters

Model Parameters		Toyoura Sand-steel Navayogarajah (1990)	Silica Sand-steel (This Study)
(1)	(2)	$\sigma_n = 98\ kPa$ $D_r = 90\%$	$\sigma_n = 100\ kPa$ $D_r = 88\%$
R_n^{cr}	-	0.184	0.053
γ	μ_{p1}	0.081	0.275
-	μ_{p2}	0.1509	0.695
n	-	2.001	2.005
$\dot{\xi}_D$ (mm)	$\dot{\xi}_{D1}$	0.035	0.09
-	$\dot{\xi}_{D2}$	0.1679	0.559
a	-	20.5	22.5
b	-	1.5	2.2
κ	κ_1	-1.94	-1.26
-	κ_2	0.97	0.63
r_u	μ_{o1}	0.0648	0.257
-	μ_{o2}	0.1167	0.443
A	-	2.0	0.5
K_n	-	80000 kPa/mm	6000
K_τ	-	4000 kPa/mm	1000

8.4 Expansion of Model to 3-D

As explained in Appendix A, the elasto-plastic model developed by Navayogarajah *et al.* (1992) is a special type of a general constitutive model for material behaviour. The model has been expanded to 3-D in this study and used to make predictions for the behaviour of a sand-steel interface under monotonic, 3-D loading conditions. For this purpose, the yield surface was expanded from 2-D to 3-D first, and the formulation of the elasto-plastic constitutive matrix was modified accordingly.

8.4.1 Yield Surface

The general equation of a yield surface for 3-D solid materials (Eq. *A*.3) was specialized for 2-D interfaces (Eq. *A*.4). For the case of 3-D interface element, the specialized equation applies, except that the second invariant of deviatoric stress tensor, J_{2D}, is:

$$J_{2D} = \frac{1}{6}[(\sigma_{11} - \sigma_{22})^2 + (\sigma_{22} - \sigma_{33})^2 + (\sigma_{11} - \sigma_{33})^2] + \sigma_{12}^2 + \sigma_{23}^2 + \sigma_{13}^2 \qquad 8.8$$

for 3-D interface elements:

$$\sigma_{33} = \sigma_n$$
$$\sigma_{13} = \tau_x$$
$$\sigma_{23} = \tau_y$$
$$\sigma_{11} = \sigma_{22} = \sigma_{12} = 0$$

therefore,

$$J_{2D} = \frac{1}{3}\sigma_n^2 + \tau_x^2 + \tau_y^2 \qquad 8.9$$

The yield surface equation (*A*.3) can thus be written as:

$$F = \tau_x^2 + \tau_y^2 + \alpha\sigma_n^n - \gamma\sigma_n^2 = 0 \qquad 8.10$$

Similar to 3-D solid materials, where the yield surface is plotted in $J_1 - \sqrt{J_{2D}}$ plane, the yield surface for 3-D interface element can be plotted in $\sigma_n - \sqrt{\tau_x^2 + \tau_y^2}$ plane as presented in Fig. 8.4.

In order to consider the coupling effects between the orthogonal shear stress components, τ_x and τ_y, it is proposed to represent the yield surface in a 3-D space as shown in Fig. 8.5.

Another advantage of presenting the yield surface in a 3-D space is the possibility of modelling any kind of anisotropy in the shear plane, i.e. the different shear strength or stress-displacement relations in *x*- and *y*-directions.

8.4.3 3-D Constitutive Relations

The $[C^e]$ and $[C^p]$ are 3 × 3 matrices. The elasto-plastic matrix, $[C^{ep}]$can be obtained:

$$[C^{ep}]=[C^e]-[C^p]$$

$$=\begin{bmatrix} K_n & 0 & 0 \\ 0 & K_{sx} & 0 \\ 0 & 0 & K_{sy} \end{bmatrix}-\begin{bmatrix} C_{11}{}^p & C_{12}{}^p & C_{13}{}^p \\ C_{21}{}^p & C_{22}{}^p & C_{23}{}^p \\ C_{31}{}^p & C_{32}{}^p & C_{33}{}^p \end{bmatrix}$$

$$=\begin{bmatrix} K_n-C_{11}{}^p & -C_{12}{}^p & -C_{13}{}^p \\ -C_{21}{}^p & K_{sx}-C_{22}{}^p & -C_{23}{}^p \\ -C_{31}{}^p & -C_{32}{}^p & K_{sy}-C_{33}{}^p \end{bmatrix} \quad 8.11$$

in which K_n, K_{sx}, and K_{sy} are the elastic normal and shear stiffnesses in the x-direction, and the shear stiffness in the y-direction of the interface, respectively. Similar to 2-D, it is assumed that elastic normal and shear behaviour are uncoupled. For the simulation of test results of this study, it is assumed that:

$$K_{sx} = K_{sy} \quad 8.12$$

because of the isotropic condition in the x- and y-directions. Thus K_{sy} = 1000 kPa/mm.

$C_{ij}{}^p$ are components of the plastic constitutive matrix. The procedure for derivation of $C_{ij}{}^p$ is described in Appendix A, Section A.3, which is the same as the derivation of $C_{ij}{}^p$ for 2-D stress space.

Three stress and displacement components are involved in 3-D space as described previously. The general stress-displacement relation in the 3-D space is:

$$\begin{pmatrix} d\sigma_n \\ d\tau_x \\ d\tau_y \end{pmatrix} = \begin{bmatrix} K_n - C_{11}^{\ p} & -C_{12}^{\ p} & -C_{13}^{\ p} \\ -C_{21}^{\ p} & K_{sx} - C_{22}^{\ p} & -C_{23}^{\ p} \\ -C_{31}^{\ p} & -C_{32}^{\ p} & K_{sy} - C_{33}^{\ p} \end{bmatrix} \begin{pmatrix} dv \\ du_x \\ du_y \end{pmatrix} \qquad 8.13$$

where $d\sigma_n$, $d\tau_x$, and $d\tau_y$ are the components of stress increments in the normal, x- and y-directions, respectively. The corresponding displacement components are dv, du_x, and du_y.

The relationship between the elastic displacement increments and stress increments is:

$$\{dU^e\} = [C^e]^{-1}\{d\sigma\} \qquad 8.14$$

The plastic components can be then obtained as:

$$\{du^p\} = \{du\} - \{du^e\} \qquad 8.15$$

8.4.4 Sample Predictions

The experimental results presented in Figs. 6.2 and 6.3, for 3-D monotonic tests under a constant normal stress of 100 kPa were simulated by the expanded model. The same parameters obtained from 2-D test results, as presented in Table 8.2, were used. The test procedure for those results was that a shear stress was applied first in the y-direction up to a target value such as 20, 40, and 60 kPa. Subsequently, the interface was sheared in the x-direction while the normal stress and the shear stress in the y-direction were maintained.

The comparison between the predictions and experiments are presented in Figs. 8.8 and 8.9. The predictions and experimental results are in good agreement. The computational steps for predictions followed the loading steps in experiments. The initial normal stress, σ_{no}, was specified as 100 kPa. Initially, shear stresses, τ_x and τ_y, were specified as zero. Subsequently, a shear stress increment in the y-direction, $\Delta\tau_y$, was specified while the increments of normal stress $\Delta\sigma_n$, and shear stress in the x-direction, $\Delta\tau_x$, were specified as zero. The prediction stopped at the target value of τ_y, after which the $\Delta\tau_y$ was specified as zero and a tangential displacement increment in the x-direction, Δu_x was specified. The model is applicable for the prediction of displacement as well as stress controlled test results or even combination of both, as was used in this case. The shearing in the y-direction was stress controlled whereas it was displacement controlled in the x-direction.

Comparisons between the results of Figs. 8.8*a* and 8.8*c* indicate that the peak strengths in the x-direction are slightly over-estimated. This is because the parameters were obtained based on average values between the experimental results of the No. 1 and the No. 2 sands. Thus the peak strength for the No. 2 sand, which is predicted here, is higher than the corresponding experimental results, because the peak strength between the No. 1 sand and the rough steel plate was slightly higher than that of the interface between the No. 2 sand and the same plate. For the case of $\tau_y = 60$ kPa, the shear stress in the x-direction, τ_x, dropped rapidly and stabilized at about 18 kPa. Whereas in the experimental results it went down to 44 kPa only. This difference is due to the fact that the τ_y dropped after peak during the test as illustrated in Fig. 8.8*a* between points *g* and *h*. During predictions, however, the shear stress, τ_y, was kept at the constant value of 60 kPa until the end of shearing in the x-direction. The reason for drop in the τ_y during testing was explained in Chapter 6. The predictions and experimental data for the normal displacement variations with the sliding displacement, u_x, compare well as demonstrated in Figs. 8.8*b* and 8.8*d*.

The shear stress paths and sliding displacement paths are illustrated in Fig. 8.9. All shear stress paths, except for the τ_y = 60 kPa case, are identical in both experimented and predicted results. The siding displacement paths are also in very good agreement. This illustrates how well the elasto-plastic model simulates the coupling effects between the shear stress and tangential displacements in the x- and y-directions on the x-y plane.

The comparisons presented so far showed that the model is capable of capturing all important aspects of the interface behaviour between sand and steel.

8.5 Normal Boundary Conditions

Three boundary conditions may be applied in the normal direction to the interface as described in the previous chapters:

1. $K = 0$ or constant normal stress
2. $K \neq 0$ or constant normal stiffness
3. $K = \infty$ or constant volume

where K is the stiffness of the soil in the direction normal to the interface plane:

$$K = \frac{d\sigma_n}{dv} \qquad 8.16$$

in which σ_n and v are normal stress and normal displacement increments, respectively. The application of such boundary conditions in the described elasto-plastic model is as follows:

The constitutive equation is:

$$\{d\sigma\} = \left[C^{ep}\right]\{dU\} \qquad 8.17$$

or

$$\{dU\} = \left[D^{ep}\right]\{d\sigma\} \qquad 8.18$$

where

$$\left[D^{ep}\right] = \left[C^{ep}\right]^{-1} \qquad 8.19$$

Expanding Eq. 8.18 for the 2-D case gives:

$$\begin{aligned} dv &= D_{11}{}^{ep} d\sigma_n + D_{12}{}^{ep} d\tau \\ du &= D_{21}{}^{ep} d\sigma_n + D_{22}{}^{ep} d\tau \end{aligned} \qquad 8.20$$

For Condition 1, i.e. $K = d\sigma_n / dv = 0$, the variations in normal stress is zero, therefore: $d\sigma_n = 0$. Condition 2 implies that the ratio between $d\sigma_n$ and dv has a constant value, K. For each increment, can be substituted in Eq. 8.20 by $K_{n}dv$, and then solve the linear equations. Finally, for Condition 3, i.e., $K = d\sigma_n / dv = \infty$ can be set as zero during increments.

This technique was used to make predictions for the results of experiments under constant normal stiffness conditions, similar to those presented in Fig. 7.3 in Chapter 7. The results of three predictions are presented and compared with their corresponding experimental results, as illustrated in Figs. 8.10 through 8.12. They correspond to the tests with constant normal stiffnesses of 400, 800, and 1200 kPa/mm. The initial normal stress was 100 kPa. The same parameters as described for the 2-D monotonic results listed in Table 2 were used for predictions.

The predicted results are qualitatively in good agreement with the experimental results. There are some discrepancies in the peak strength ratios such that the predictions are about 15% less than measured values. This is attributed to the fact that the model does not incorporate the effect of the normal stress on the peak strengths. The predicted peak strength ratios are the same as those in the constant normal stress test results. However, the experiments give lower values because of the increase in normal stress during shearing. It was shown in the parametric study provided in Chapter 5 that the peak strengths are lower at higher normal stresses. The magnitudes of the mobilized shear stress and increase in normal stress are generally predicted well. Therefore, in can be concluded that the model is capable of simulating the behaviour of interfaces under various boundary conditions and stress paths.

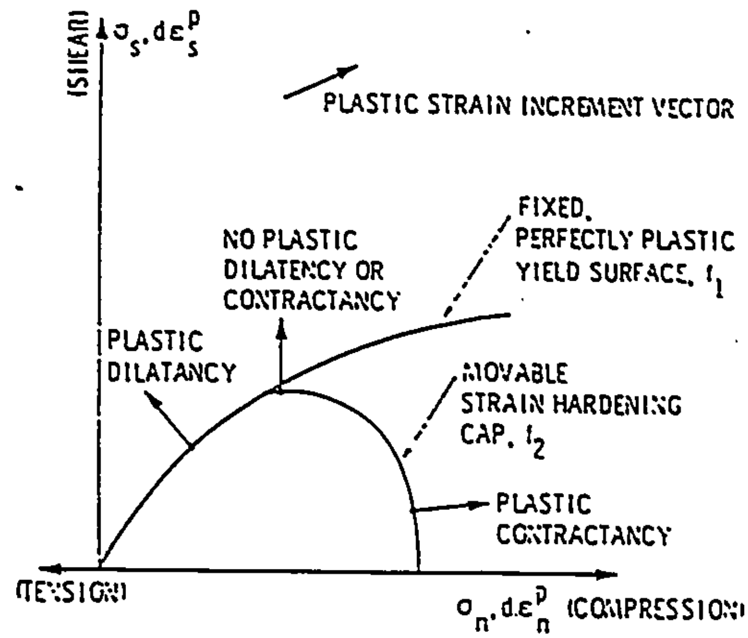

FIG. 8.1. Application of capped plasticity model to rock joints (After Ghaboussi *et al.* 1973)

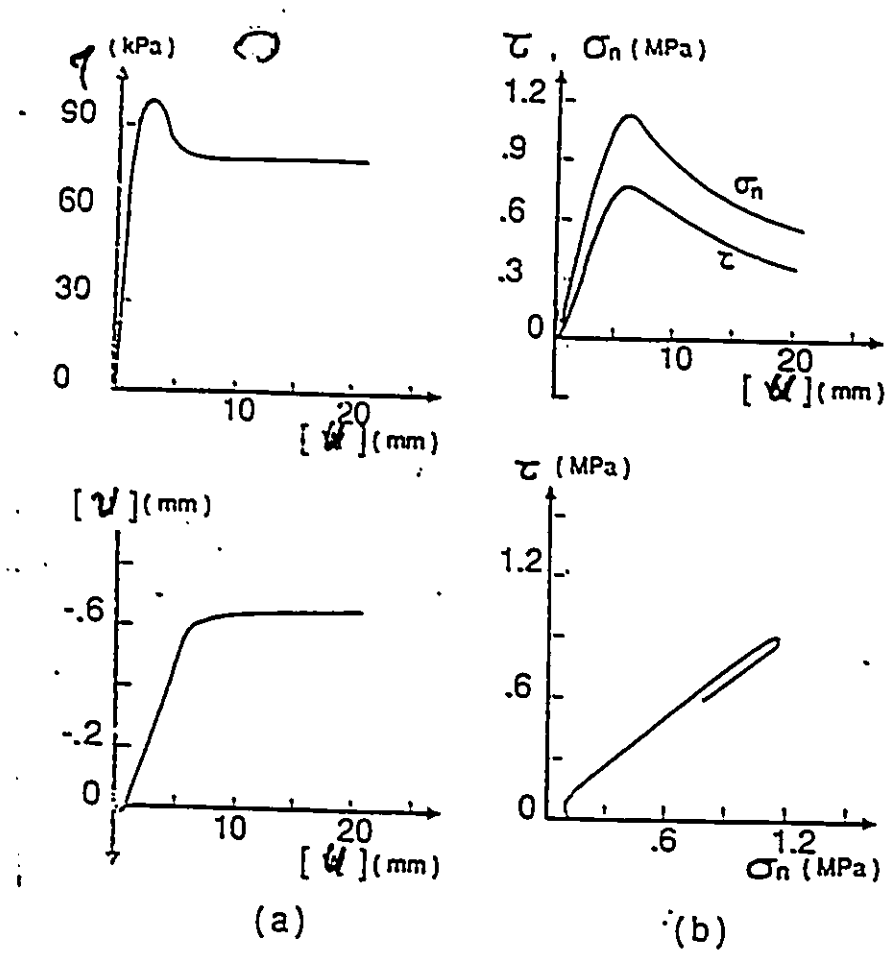

FIG. 8.2. Direct shear tests on dense coarse Hostun sand, σ_{no} = 122 kPa (After Boulon and Nova, 1990)
(a) Constant normal stress *(b)* Constant volume

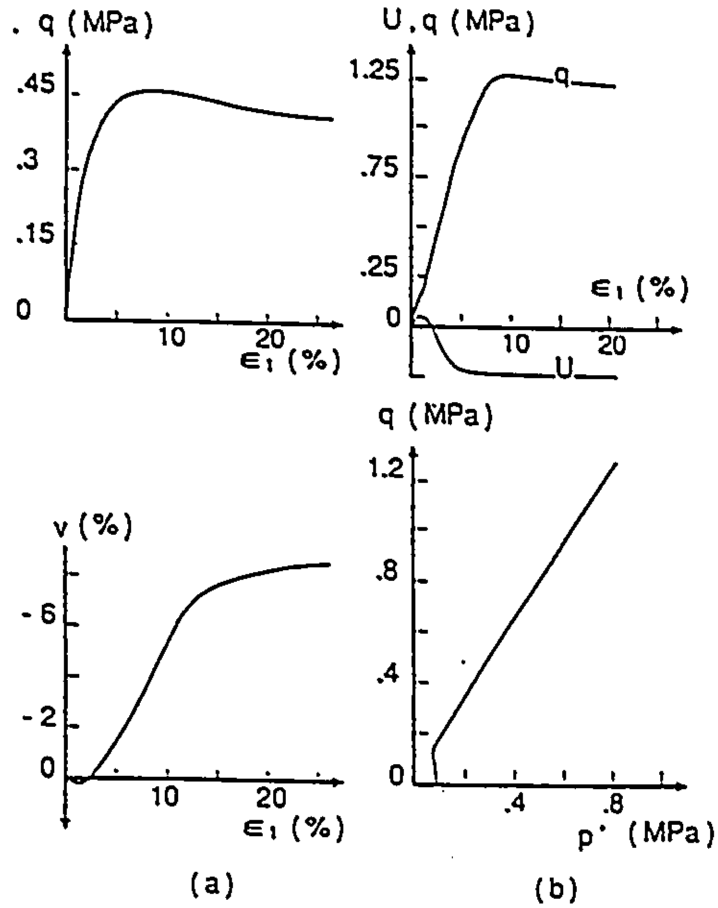

FIG. 8.3. Triaxial tests on dense coarse Hostun sand, $\sigma_3 = 100$ kPa (After Boulon and Nova, 1990)
(a) Drained *(b)* Undrained

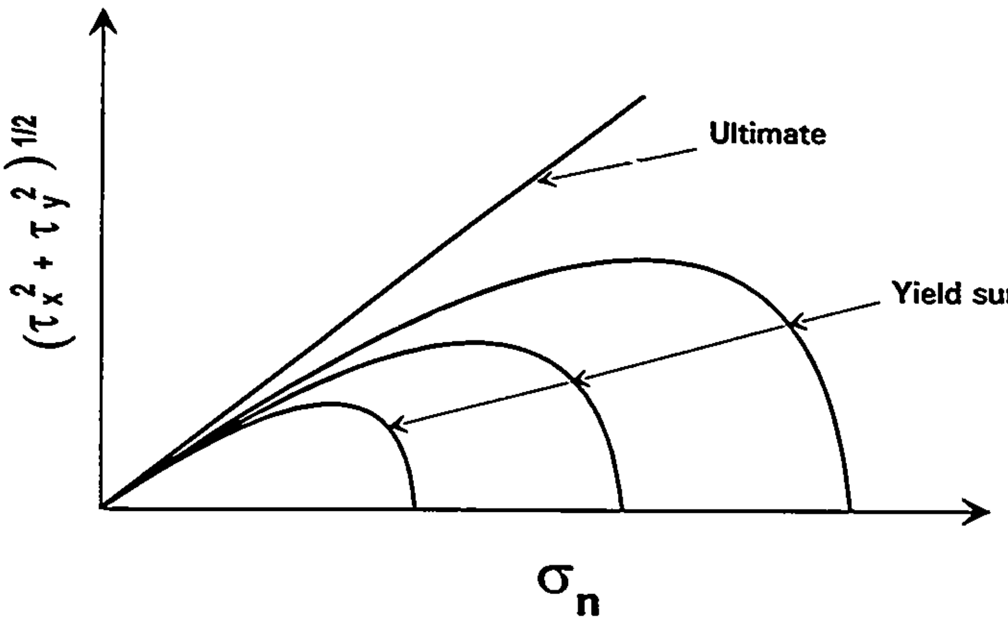

FIG. 8.4. 3-D yield surface in $\sigma_n - \sqrt{\tau_x^2 + \tau_y^2}$ space

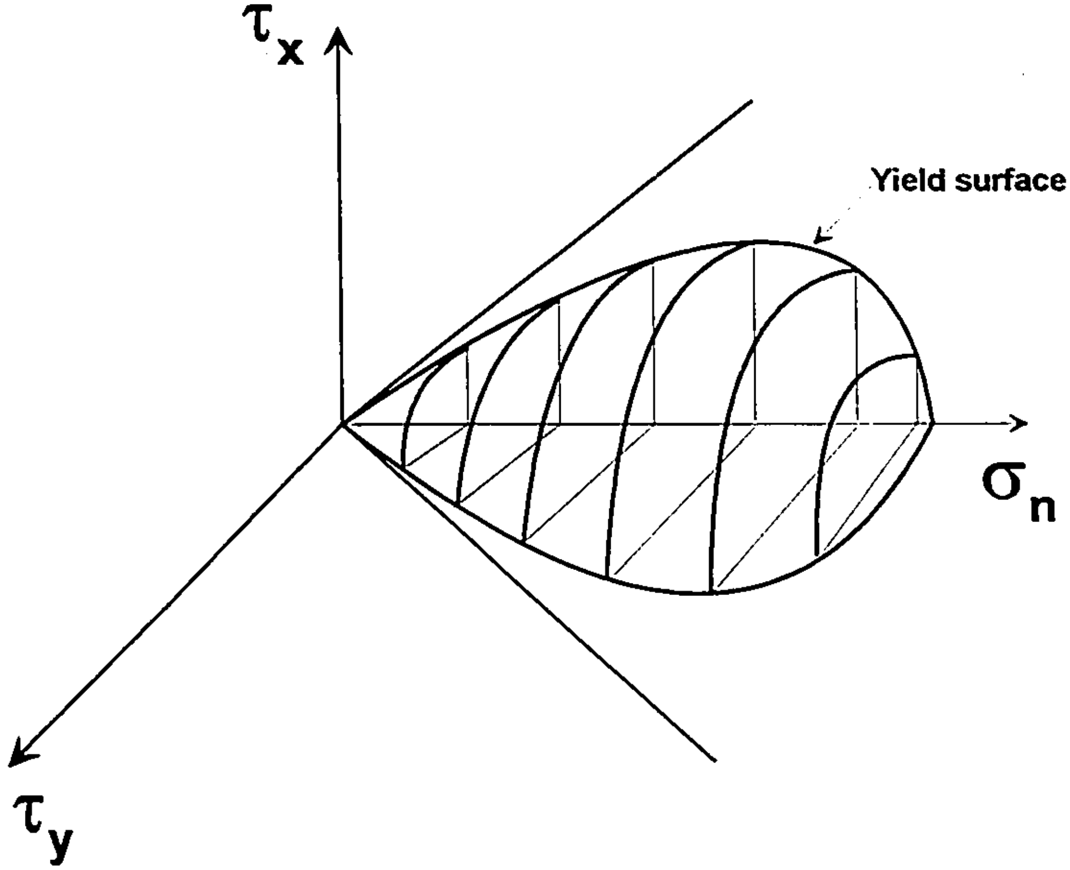

FIG. 8.5. 3-D yield surface in $\sigma_n - \tau_x - \tau_y$ space

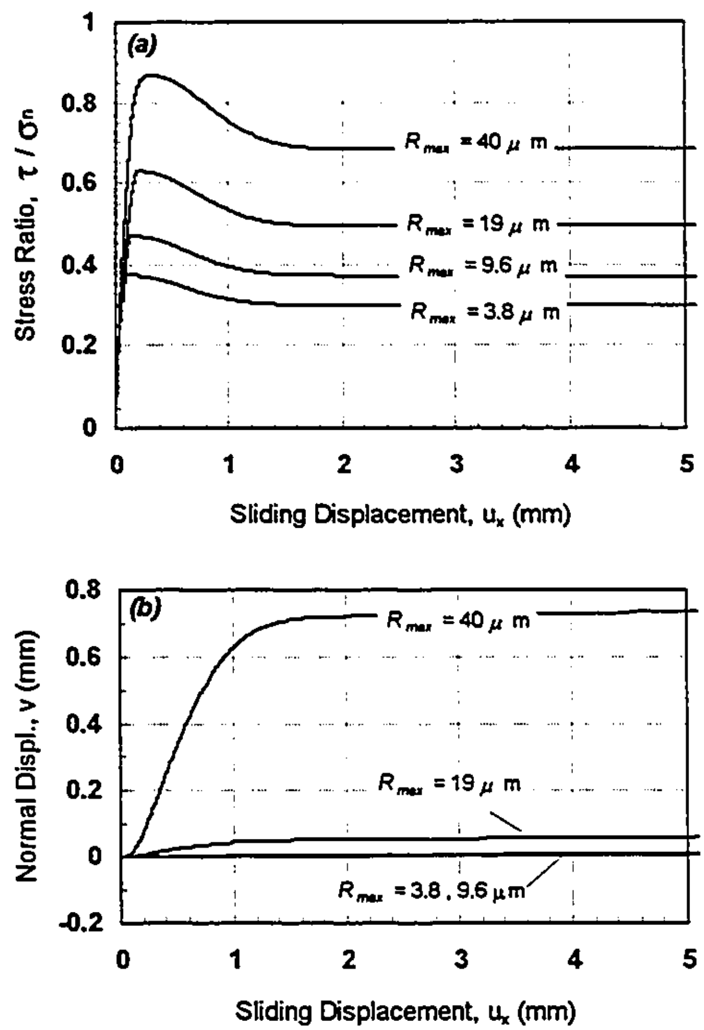

FIG. 8.6. Predicted results by the Desai's Hierarchical Single-Surface Model: 2-D constant normal stress. (Validation of the programmed model based on the predicted results by Navayogarajah (1990))

Steel-Toyoura sand (D_r = 90%) interface; σ_n = 98 kPa

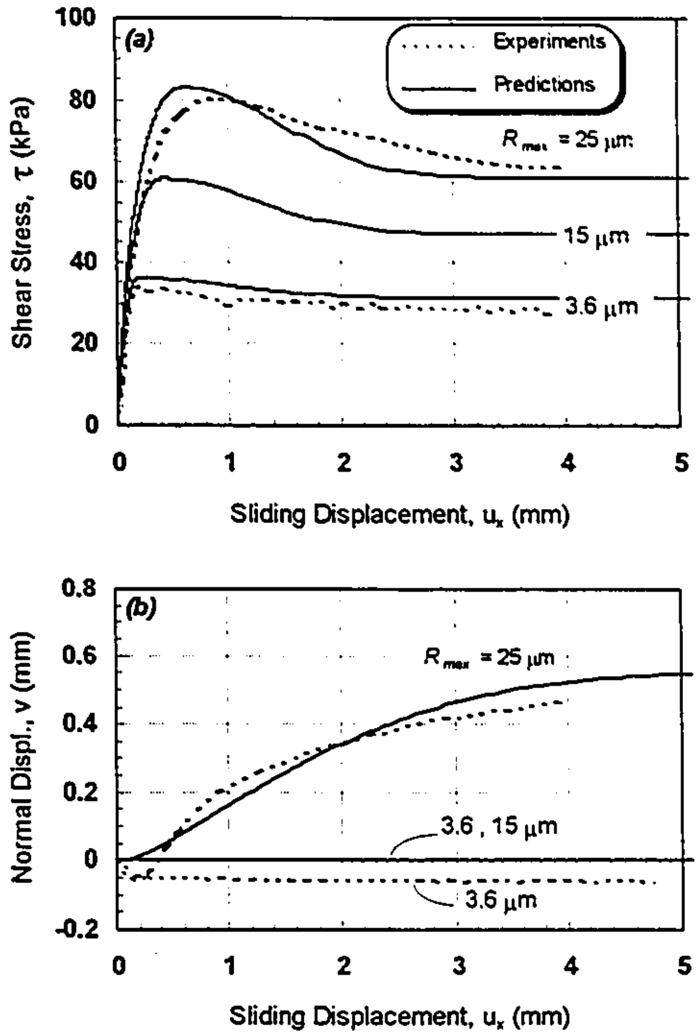

FIG. 8.7. Comparison between *predicted* and *experimental* results for various surface roughnesses: 2-D constant normal stress.

Surface: Steel plate (R_{max} = 25, 15 (predicted only), and 3.6 μm for L = 0.8 mm)
Sand: No. 2, D_r = 88 %
σ_n = 100 kPa

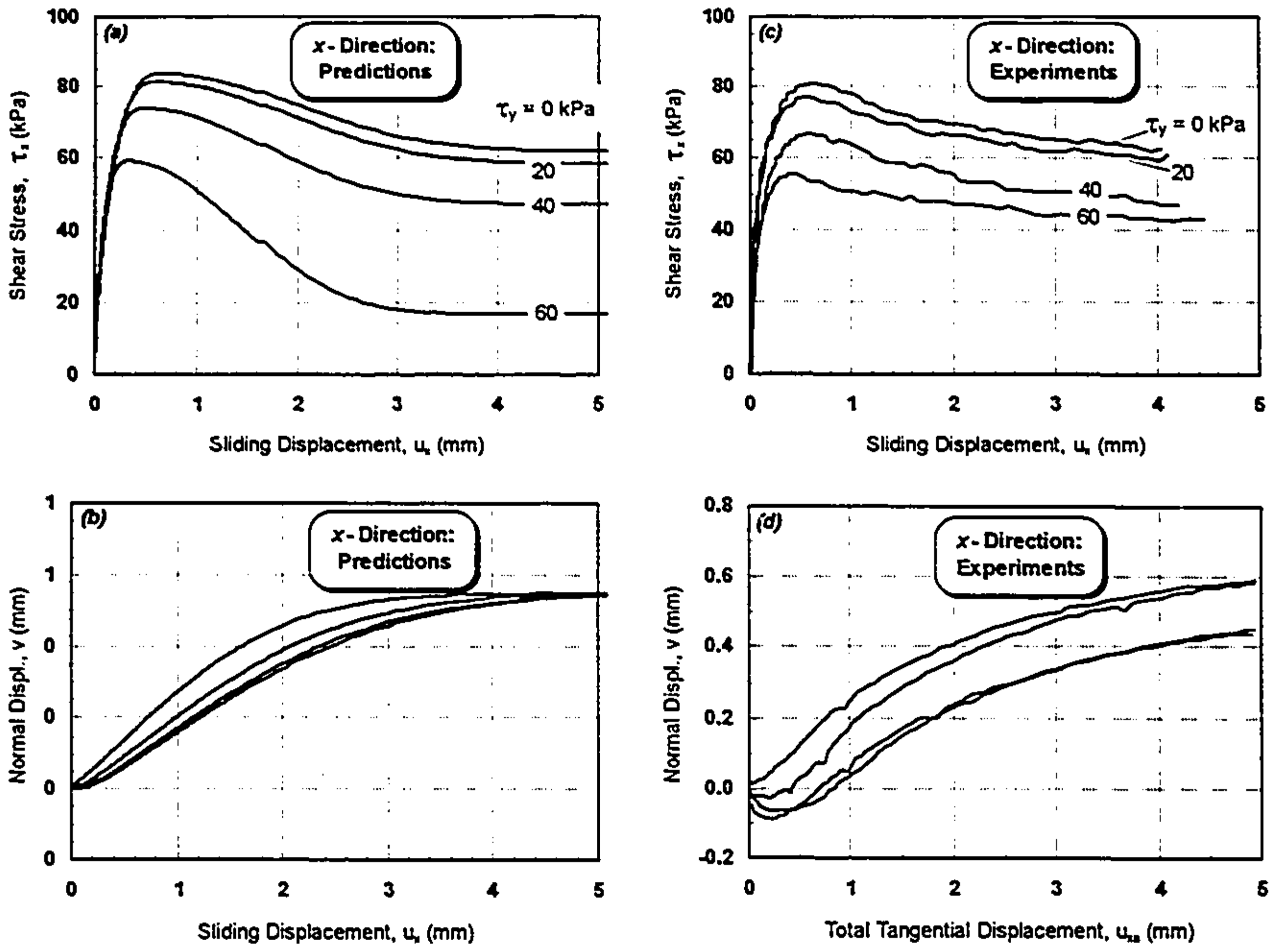

FIG. 8.8. Comparison between *predicted* and *experimental* results for various values of τ_y: **3-D** constant normal stress; τ_y = 0, 20, 40, 60 kPa

Surface: Steel plate (R_{max} = 25 μm for L = 0.8 mm)
Sand: No. 2, D_r = 88 %
σ_n = 100 kPa

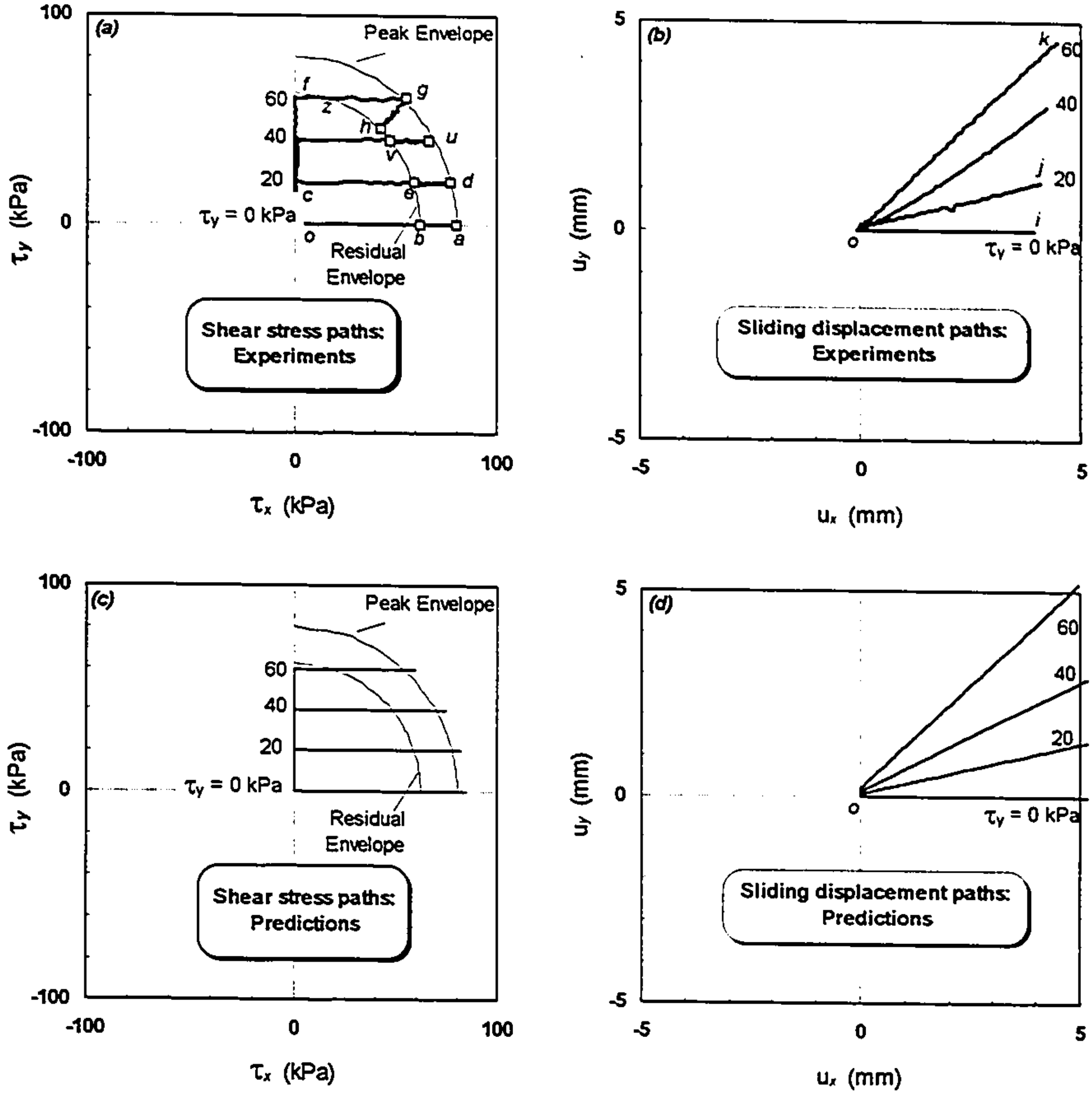

FIG. 8.9. Comparison between stress and displacement paths for *predicted* and *experimental* results: **3-D** constant normal stress; $\tau_y = 0, 20, 40, 60$ kPa; $\sigma_n = 100$ kPa

Surface: Steel plate ($R_{max} = 25$ µm for L = 0.8 mm)
Sand: No. 2, $D_r = 88$ %

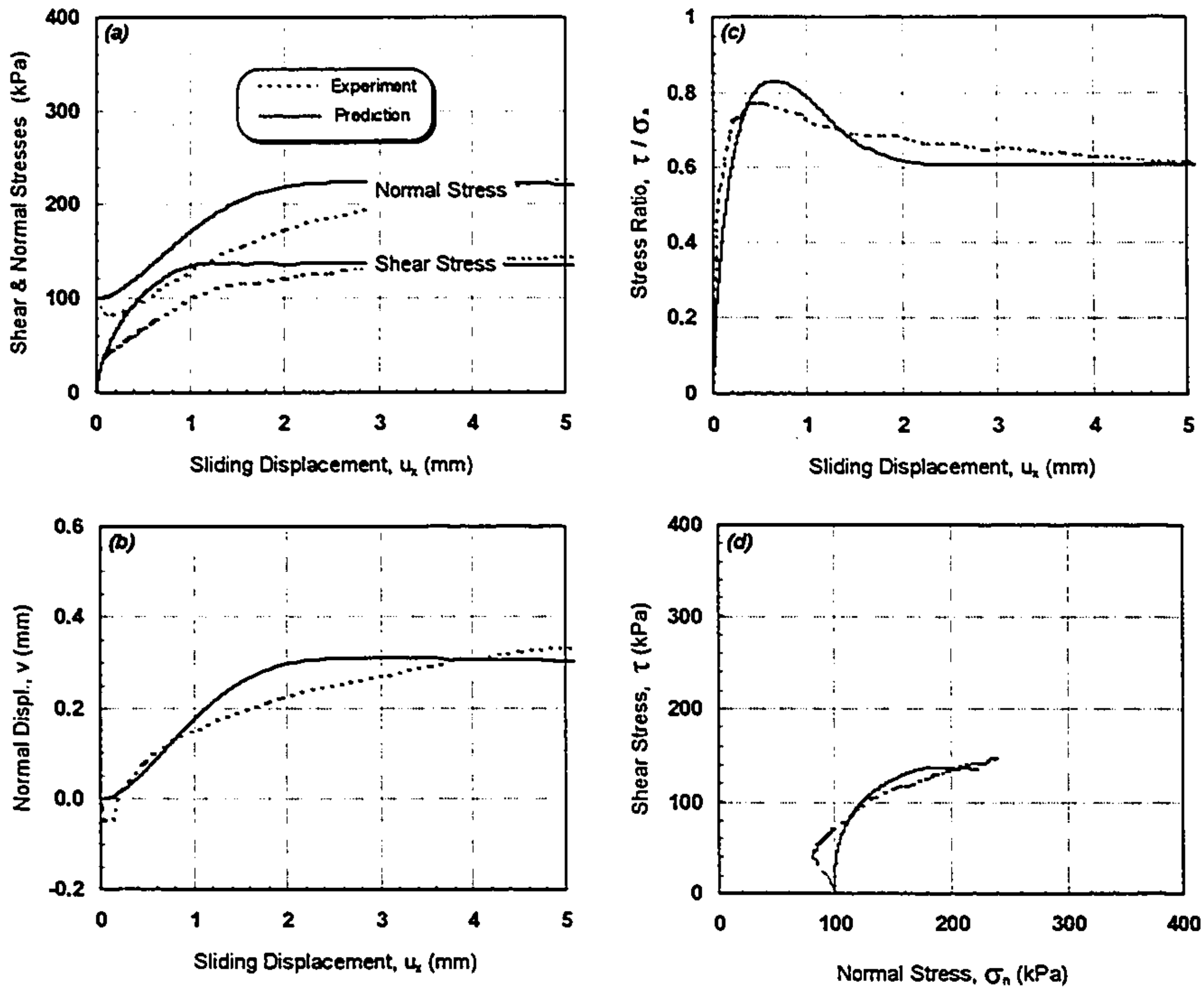

FIG. 8.10. Comparison between *predicted* and *experimental* results for 2-D constant normal *stiffness*: **K = 400 kPa** ; σ_{no} = 100 kPa

Surface: Steel plate (R_{max} = 25 μm for L = 0.8 mm)

Sand: No. 2, D_r = 88 %

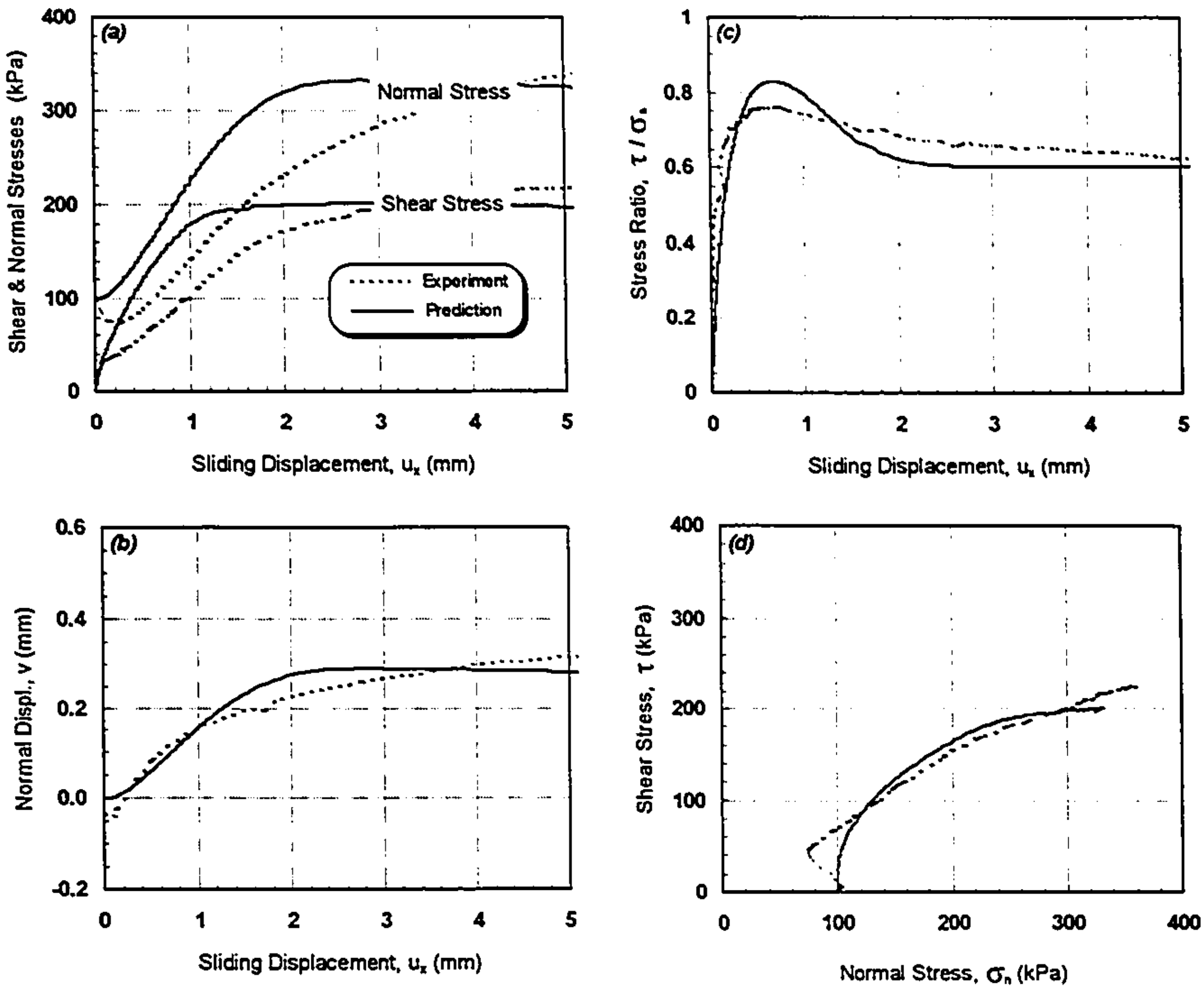

FIG. 8.11. Comparison between *predicted* and *experimental* results for 2-D constant normal *stiffness*: <u>**K = 800 kPa**</u> ; σ_{no} = 100 kPa

Surface: Steel plate (R_{max} = 25 μm for L = 0.8 mm)

Sand: No. 2, D_r = 88 %

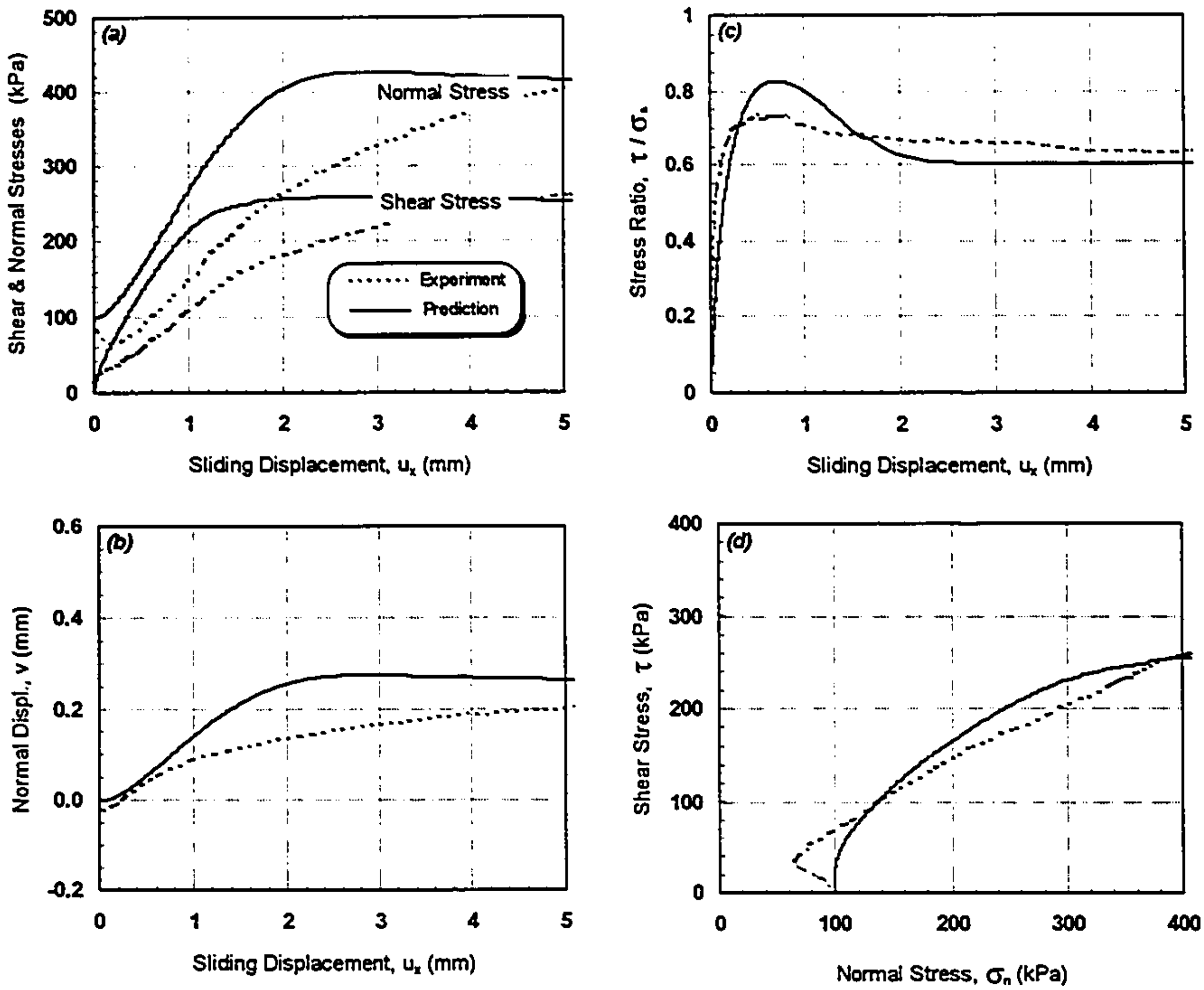

FIG. 8.12. Comparison between *predicted* and *experimental* results for 2-D constant normal *stiffness*: **K = 1200 kPa** ; σ_{no} = 100 kPa

Surface: Steel plate (R_{max} = 25 μm for L = 0.8 mm)

Sand: No. 2, D_r = 88 %

CHAPTER 9

SUMMARY AND CONCLUSIONS

9.1 Summary

The main objective of this research was to study the effects of various monotonic and cyclic stress and displacement paths on the shear strength, residual strength, stress-displacement relations, and volume change behaviour of sand-steel interfaces. A new automated interface testing apparatus was developed for performing the experimental program to achieve the described objectives. Direct shear as well as simple shear type soil containers can be used in this interface apparatus. The interface apparatus is referred to as C3DI whenever the direct shear box is used as the soil container, or C3DSSI, if the simple shear box is employed. The majority of the presented results were obtained by using C3DSSI.

The new apparatus is capable of applying simultaneous monotonic and cyclic forces in three perpendicular directions, x, y, and z. Test can be displacement or load controlled. The boundary conditions in the direction normal to the interface plane are imposed by using a pneumatic actuator which is operated by the computer-controlled system. The boundary conditions include constant normal stress, constant volume, and constant normal stiffness. The simultaneous operation of two computer controlled stepper motors, which are installed perpendicular to each other, allows the application of shear loads simultaneously in the *x*- and *y*-directions. With this loading arrangement, any desired type of tangential load or displacement paths, such as rotational stress or displacement paths (circular or elliptical) can be generated on the interface plane. The coupling effects of sliding displacement or slip at the interface, and simple shear deformation of soil mass can be studied in both *x*- and *y*-directions, when the simple shear box is used as the soil container.

An extensive experimental program was performed to study the behaviour of Silica sand-steel interfaces, and the test results were presented and discussed in Chapters 5, 6, and 7. The various types of presented experimental results are as follows:

- *2-D monotonic constant normal stress tests*: The results of two sample test were presented first. These results were obtained by using C3DI and C3DSSI. The data obtained from these two tests provide a framework for presenting and discussing the results of subsequent tests. A series of results were presented next to study the effects of the following parameters: normal stress, initial relative density of sand, surface roughness, shape of sand particles, and rate of shearing.

- *2-D cyclic constant normal stress tests*: The results of five cyclic tests were presented. These tests were conducted under two-way cyclic tangential displacement controlled and constant normal stress conditions. Small displacement amplitudes were selected to investigate the possibility of failure of the interface in such conditions.

- *3-D monotonic constant normal stress tests*: Two series of experiments were conducted: (1) stepwise shearing in which interface was sheared and failed in the *x*-direction first, and subsequently it was sheared in the *y*-direction. The results of two tests were presented. One of the tests was performed with dense and the second test with loose sands. The interface surface was rough; (2) simultaneous shearing during which interface was sheared and failed in the *x*-direction while a constant shear stress was maintained at a constant level in the *y*-direction. The results of four tests were presented to show the effect of the magnitude of the shear stress in the *y*-direction on the behaviour of the interface.

- *3-D cyclic tests under constant normal stress*: Two groups of tests were performed: (1) two-way cyclic tangential displacement controlled in the x-direction, while a constant shear stress in the y-direction was maintained at a constant level. The results of four tests were presented to investigate the effects of magnitude of shear stress in the y-direction on the cyclic behaviour of the interface in the x-direction; (2) the interface was sheared along a circular or elliptical path on the interface plane. The results of four tests were presented to demonstrate the effects of the *cyclic tangential displacement amplitude ratio*, u_{yao} / u_{xao}, on the stress displacement relations and volume change behaviour of the sand-steel interface.

- *2-D monotonic tests under constant normal stiffness*: The results of eight tests were presented to investigate the effects of magnitude of the initial normal stress, as well as magnitude of the constant normal stiffness.

- *3-D monotonic constant normal stiffness tests*: The results of two tests were presented to investigate the combined effects of constant normal stiffness boundary condition as well as simultaneous shear stresses on the x-y plane, on the resultant peak shear strength, residual shear strength, and the resultant strength ratios.

- *2-D cyclic constant normal stiffness tests*: A group of cyclic two-way tangential displacement controlled tests were conducted under the condition of constant normal stiffness. the results of seven tests were presented to study the effect of the magnitude of the tangential displacement amplitude, and also the effect of the magnitude of the constant normal stiffness, on the shear stress degradation at the interface plane with cycles.

An elasto-plastic single surface constitutive model was used to simulate the behaviour of interfaces tested in this study. The model was originally developed by Desai and coworkers for frictional materials, and subsequently modified by Fishman and Desai (1987), and Desai and Fishman (1991) for idealization of rock joints, and also by Navayogarajah (1990), and Navayogarajah *et al.* (1992) for idealization of sand-steel interfaces. The model modified by Navayogarajah requires a total of 12 parameters. It is capable of predicting the non-associativeness behaviour of the interface, strain-softening, and the behaviour of interface under cyclic loading conditions. The contribution of this research study to the modelling part is as follows:

- A computer code was developed for the model modified by Navayogarajah to predict the stress-displacement and volume change behaviour of the sand-steel interface. The model parameters determined by Navayogarajah were used first. Four comparisons were made with Navayogarajah's results to verify the correctness of the computer code written in this study.

- The model parameters for the interfaces between Silica sands No. 1 and No. 2, and a steel plate were determined for dense samples. Then the results of predictions for three tests under 2-D constant normal stress and monotonic conditions were shown together with their corresponding experimental results.

- The formulation of the model was expanded to be used in 3-D stress space. The parameters determined in the previous step were adopted to predict the behaviour of an interface under monotonic 3-D conditions. Predictions for four tests were presented together with their corresponding experimental results.

- A special method was used in the model to simulate the constant normal stiffness and constant volume conditions. Predictions for three tests were presented to show the effect of the magnitude of the constant normal stiffness. The results were compared with their corresponding experimental results.

9.2 Conclusions

1. Among the various parameters affecting the behaviour of the sand-steel interface, the surface roughness of steel has the most significant influence on both peak and residual shear strengths of the interface. For example, the peak and residual shear strength ratios of the interface between the dense No. 2 sand (D_r = 88%) and the sand blasted steel plate (R_{max} = 25 μm) were 0.80 and 0.62, respectively. They were only 0.34 and 0.29 for the interface between the same sand and the smooth steel plate (R_{max} = 4 μm).

2. The magnitude of initial normal stress affects the peak shear strength in such a way that the peak shear strength is high at low normal stresses. The peak stress ratio varied between 0.76 and 0.80 for normal stresses ranging form 500 to 100 kPa. This variation may not be significant for practical purposes. The residual shear strength is not affected by normal stress.

3. Initial relative density of sand affects the peak shear strength in such a way that a higher peak is mobilized at higher densities. The peak strength ratio varied between 0.6 to 0.8, for initial relative densities ranging from 15 to 88%. The residual strength, however, was not affected by the initial relative density of sand.

4. Higher peak and residual strengths are observed for the crushed angular sands compared to Ottawa sand which has rounded particles. The peak strength ratios were 0.76 and 0.63 for the No. 2 sand and the Ottawa sand, respectively, for the interfaces between each sand and the rough steel plate. The residual strength ratio was 0.65 for the No. 2 sand and 0.52 for the Ottawa sand. Higher dilation was observed for the interface between the Ottawa sand and the rough surface compared to the crushed quartz sand No. 2.

5. Rate of shearing had no effect on the stress-displacement relations and volume change behaviour of the sand-steel interfaces, for the examined rates between 0.1 to 10 mm/min. Both rough and smooth surfaces as well as dense and loose sands were considered in this study.

6. The results of two-way displacement controlled cyclic tests indicated that the interface may fail and strength softening may occur, even at tangential displacement amplitudes less than that required to mobilize the peak strength in a monotonic test. This phenomenon is explained clearly by using the simple shear box. This observation agrees very well with those presented by Uesugi and Kishida (1987*b*) and Uesugi *et al.* (1989).

7. As far as peak and residual shear strengths are concerned, both direct shear box and simple shear box would produce the same strengths. However, the stiffness of the interface, i.e. the relations between the shear stress and sliding displacement at the

interface is higher in the simple shear box than the direct shear box, which is more precise.

8. 3-D monotonic and cyclic experimental results indicated that the sliding displacement at the interface and the shear deformation of sand mass are plastic in nature. The paths followed by the sliding displacement of the interface and the shear deformation of the sand mass are different from shear stress paths.

9. The 3-D simultaneous monotonic and cyclic test results, indicated that the magnitudes of the resultant peak stress ratio and residual stress ratio are independent of the stress paths.

10. The magnitude of the *cyclic tangential displacement amplitude ratio*, u_{yao} / u_{xao}, affected the compression response of the sand mass, variations of shear stress, and resultant peak and residual strengths, in 3-D cyclic rotational tests. The increase in u_{yao} / u_{xao} from 0 to 1, i.e. approaching a full circular rotational path, increased the average compression of the sand for the same number of cycles, reduced the variations of the shear stress during each cycle, and decreased the peak and residual strengths.

11. The shear stress variations are affected significantly if a *constant stiffness* is specified as the boundary condition in the normal direction to the interface plane. In monotonic tests between the dense sands and rough surfaces, normal stress and, therefore, mobilized shear stress increase with sliding displacement due to the tendency of the interface to dilate. The peak and residual shear strength ratios are, however, independent of the constant stiffness condition. Mobilized shear stress is higher at higher constant stiffness values in the normal direction.

12. The 2-way displacement controlled cyclic tests under the condition of *constant normal stiffness* indicated that the maximum shear stress decreases with increase in cycles irrespective of the magnitude of tangential displacement amplitude. The maximum shear stress begins to decrease right after cycling starts. This is an indication that the degradation of the maximum shear stress depends on the compressibility of the sand mass with cycles, and as a result drop in the normal stress with cycles. The rate of the decrease in maximum shear stress, however, was significantly affected by the

magnitude of the tangential displacement amplitude. If the tangential displacement amplitude is large enough, then the stress ratio, τ / σ_n, reaches its peak value after several cycles. After the peak (failure), the stress ratio would approach a residual value, then the shear stress, τ, would reduce at a faster rate than when the stress ratio would simply increase with cycles. These are indications that the shear stress degradation is influenced not only by the compression of sand with cycles, but also it is significantly dependent on the mobilized sliding displacement. In addition, the degradation of maximum shear stress is significantly affected by the magnitude of the constant stiffness in the normal direction. Normal stress and, as a result, maximum shear stress reduce rapidly under higher normal stiffness values.

13. The one-way cyclic shear stress controlled results indicated that the degradation in shear stress occurred under the condition of *constant normal stiffness*. The peak shear strength $(\tau / \sigma_n)_{peak}$, and residual shear strength, $(\tau / \sigma_n)_{residual}$, were the same as those in monotonic tests.

14. For the interface between the No. 2 sand at an initial relative density of 88%, and the sand blasted steel plate (R_{max} = 25 μm for L = 0.8 mm), the resultant peak stress ratio varied between 0.8 to 0.83, and the resultant residual stress ratio varied between 0.60 and 0.62, regardless of the applied stress or displacement path on the interface plane. This was the case for all presented monotonic and cyclic, 2-D and 3-D, constant normal stress and constant normal stiffness tests, except in the cyclic rotational tests in which lower values were observed for an unexplained reason.

15. Predictions of the employed elasto-plastic constitutive model in this study for the monotonic 2-D and 3-D tests under constant normal stiffness as well as constant normal stress, agreed well with the experimental results. The same parameters determined from the conventional 2-D monotonic tests were used to predict the results of tests in various stress paths.

9.3 Recommendations for Future Research

The majority of experiments were performed to determine the effects of various stress and displacement paths on the interface behaviour and they were restricted to an interface between a dense Silica sand and a rough sand blasted steel plate. For future research, it is recommended:

1. To study cyclic behaviour of interfaces using loose and medium dense sands. It is of practical importance to determine whether the same phenomenon of experiencing peak, and then post-peak behaviour at small amplitudes observed for dense sands, would also occur for loose and medium dense sands.

2. To study the behaviour of calcareous sands. Calcareous sands are highly compressible. Shear behaviour of such materials, and also interface behaviour between this type of sand and structural materials are important in practice.

3. To study the behaviour of interfaces between structural materials and clay.

4. To study the behaviour of interfaces between soils and geosynthetics.

5. To extend the capabilities of the computer code written for the constitutive model to simulate the behaviour of interfaces under cyclic loading conditions and compare the predictions with the experimental results given in this study.

6. To implement the interface constitutive model in a finite element code and to analyse the load-deformation response and the stability of the soil-structure systems.

REFERENCES

ACAR, Y. B., DURGUNOGLU, H. T., and TUMAY, M. T., 1982. Interface properties of sand. Journal of Geotechnical Engineering, ASCE, 108(GT4), 648-654.

AIREY, D. W., AL-DOURI, R. H., and POULOS, H. G., 1992. Estimation of pile friction degradation from shearbox tests. Technical Note, Geotechnical Testing Journal, GTJODJ, 15(4), 388-392.

BEER, G., 1985. An isoparametric joint/interface element for finite element analysis. International Journal for Numerical Methods in Engineering, Vol. 21, 585-600.

BOULON, M. and FORAY, p., 1986. Physical and numerical simulation of lateral shaft friction along offshore piles in sand. Proceedings, 3rd International Conference in Numerical Methods in Offshore piling, Nantes, pp. 127-147.

BOULON, M. and NOVA, R., 1990. Modeling of soil-structure interface behaviour-A comparison between elastoplastic and rate type laws. Computers and Geotechnics, Vol. 9, 21-46.

BOULON, M. and PLYTAS, C., 1986. Soil structure directionally dependent interface constitutive equations-Application to the prediction of shaft friction along piles. Proceedings, 2nd International Symposium on numerical Models in Geomechanics, 43-54.

BRIAUD, J. L., SMITH, T. D., and MEYER, B., 1982. Design of laterally loaded piles using pressuremeter test results. Symposium of the Pressuremeter and its Marine Application, Paris.

BRUMUND, W. F. and LEONARDS, G. A., 1973. Experimental study of static and dynamic friction between sand and typical construction materials. Journal of Testing and Evaluation, JTEVA, 1(2), 162-165.

BUDHU, M., 1988. The mechanism of failure under cyclic simple shear strain. Soils and Foundations, 28(4), 119-129.

CHAN, S. F. and HANNA, T. H., 1980. Repeated loading on single piles in sand. Journal of Geotechnical Engineering, ASCE, 106(2), 171-188.

DEGROOT, D. J., GERMAINE, J. T., and LADD, C. C., 1993. The multidirecrional direct simple shear apparatus. Geotechnical Testing Journal, GTJODJ, 16(3), 283-295.

DESAI, C. S., 1980. A general basis for yield, failure and potential functions in plasticity. Int. J. Numer. and Analyt. Methods in Geomech., Vol. 4, 361-375.

DESAI, C. S., 1981. Behaviour of interfaces between structural and geologic media. Proceedings, International Conference on Recent Advances in Geotechnical Earthquake Engineering and Soil Dynamics, Vol. 2, 619-638.

DESAI, C. S. and APPEL, G. C., 1976. 3-D analysis of laterally loaded structures. International Conference on Numerical Methods in Geomechanics, 2d, Blacksburg, Va., Vol. 1, 405-418.

DESAI, C. S., DRUMM, E. C., and ZAMAN, M. M., 1985. Cyclic testing and modeling of interfaces. ASCE, Journal of Geotechnical Engineering, 111(6), 793-815.

DESAI, C. S. and FARUQUE, M. O., 1984. Constitutive model for (geological) materials. Journal of Engineering Mechanics Division, ASCE, Vol. 110.

DESIA, C. S. and FISHMAN, K. L., 1991. Plasticity-based constitutive model with associated testing for joints. Int. J. Rock Mech. and Min. Sci., 28(1), 15-26.

DESAI, C. S. and HASHMI, Q. S. E., 1989. Analysis, evaluation, and implementation of a non-associative model for geologic materials. International Journal of Plasticity, Vol. 5, 397-420.

DESIA, C. S., PHAN, H. V., and PERUMPRAL, J. V., 1982. Mechanics of three-dimensional soil-structure interaction. Journal of Engineering Mechanics, ASCE, 108(EM5), 731-747.

DESAI, C. S. and MA, Y., 1992. Modelling of joints and interfaces using the disturbed-state concept. International Journal for Numerical and Analytical Methods in Geomechanics, Vol. 16, 623-653.

DESAI, C. S., SOMASUNDARAM, S., and FRANTZISKONIS, G., 1986. A hierarchical approach for constitutive modelling of geologic materials. International Journal for Numerical and Analytical Methods in Geomechanics, Vol. 10, 225-257.

DESAI, C. S., ZAMAN, M. M., LIGHTNER, J. G., and SIRIWARDANE, H. J., 1984. Thin-layer element for interfaces and joints. International Journal for Numerical and Analytical Methods in Geomechanics, Vol. 8, 19-43.

EVGIN, E. and FAKHARIAN, K., 1995. Three-dimensional cyclic behaviour of interfaces. Proc., 3rd Int. Conf. on Recent Advances in Geot. Earth. Eng. & Soil Dyn., April 2-7, 1995, Vol. 1, 9-12, St. Louis, Missouri, USA.

FAKHARIAN, K. and EVGIN, E., 1993. A three dimensional apparatus for cyclic testing of interfaces. Proceedings, 46th Annual Canadian Geotechnical Conference, Saskatoon, Canada, pp. 485-493.

FAKHARIAN, K. and EVGIN, E., 1995. Simple shear versus direct shear tests on interfaces during cyclic loading. Proc., 3rd Int. Conf. on Recent Advances in Geot. Earth. Eng. & Soil Dyn., April 2-7, 1995, Vol. 1, 13-16, St. Louis, Missouri, USA.

FAKHARIAN, K. and EVGIN, E., 1996. An automated apparatus for three-dimensional monotonic and cyclic testing of interfaces. Geotechnical Testing Journal, GTJODJ, 19(1), 22-31.

FIGUEROA, L., YAMAMOTO, T., and NAGAI, T., 1985. Inverted shear modulus from wave-induced soil motion. Journal of Geotechnical Engineering, ASCE, 111(1), 115-132.

FISHMAN, K. L. and DESAI, C. S., 1987. A constitutive model for hardening behaviour of rock joints. Desai *et al.*, Editors, Constitutive Laws for Engineering Materials: Theory and Applications, 1043-1050.

FUJII, S., IWANO, M., TANIZAWA, F., and MURAMATSU, M., 1986. Studies on the sliding of structures during earthquakes. Proc. of 7th Japan Earthquake Engineering Symposium, Tokyo, 1075-1080.

GHABOUSSI, J. and WILSON, E. L., 1973. Finite element for rock joints and interfaces. Journal of the Soil Mechanics and Foundations Division, ASCE, 99(SM10), 833-848.

GOODMAN, R. E., TAYLOR, R. L., and BREKKE, T. R., 1968. A model for the mechanics of jointed rock. Journal of the Soil Mechanics and Foundations Division, ASCE, 94(SM3), 637-659.

HERRMANN, L. R., 1978. Finite element analysis of contact problems. Journal of the Engineering Mechanics Division, 104(EM5), 1043-1057.

IDRISS, I. M., DOBRY, R., and SINGH, R. D., 1978. Nonlinear behaviour of soft clays during cyclic loading. Journal of the Geotechnical Engineering Division, ASCE, 104(GT12), 1427-1447.

ISHIHARA, K., SHIMIZU, K., and YAMADA, Y., 1981. Pore water pressure measured in sand deposits during an earthquake, Soils and Foundations, 21(4), 85-100.

ISHIHARA, K. and YAMAZAKI, F., 1980. Cyclic simple shear tests on saturated sand in multi-directional loading. Soils and Foundations, 20(1), 45-59.

KATONA, M. G., 1981. A simple contact-friction interface element with application to buried culvert. Proceedings, Symposium on Implementation of Computer Procedures and Stress-Strain Laws in Geotechnical Engineering, Desai and Saxena (Eds.), Chicago, Illinois, Vol. 1, 45-63.

KISHIDA, H. and UESUGI, M., 1987. Tests of interface between sand and steel in the simple shear apparatus. Geotechnique, 37(1), 45-52.

KUERBIS, R. and VAID, Y. P., 1988. Sand sample preparation- The slurry deposition method. Soils and Foundations, 28(4), 107-118.

KULHAWY, F. H., TRAUTMANN, C. H., BEECH, J. F., O'ROURKE, T. D., MCGUIRE, W. A., WOOD, W. A., and CAPANO, C., 1983. Transmission line structure foundations for uplift-compression loading, Rpt EL-2870, Elec. Power Res. Inst., Palo Alto, 412 P.

KURIMOTO, M. and MATSUDA, A., 1986. Estimation of sliding displacement of rigid body by model vibration test, Proc. of 7th Japan Earthquake Engineering Symposium, Tokyo, 871-876.

LAM, T. S. K. and JOHNSTON, I. W., 1982. A constant normal stiffness direct shear machine. Proceedings, 7th Southeast Asian Geotechnical Conference, Hong Kong, China, pp. 805-820.

LEICHNITZ, W., 1985. Mechanical properties of rock joints. Int. J. Rock Mech. Min. Sci. and Geomech., 22(5), 313-321.

MAHTAB, M. A. and GOODMAN, R. E., 1970. Three dimensional finite element analysis of jointed rock slopes. Proceedings, Second Congress of the International Society of Rock Mechanics, Belgrade, Yugoslavia, 353-360.

MIURA, S. and TOKI, S., 1982. A sample preparation method and its effect on static and cyclic deformation-strength properties of sand. Soils and Foundations, 22(2), 61-77.

MOUCHAORAB, K.S. and BENMORANE, B., 1994. A new combined servo-controlled loading frame/direct-shear apparatus for the study of concrete or rock joint behaviour under different boundary and loading conditions. Geotechnical Testing Journal, GTJODJ, 17(2), 233-242.

MUQTADIR, A., DESAI, C. S., and SCHEELE, F., 1985. Three-dimensional analysis of pile group foundation and anchor-soil system. Fifth International Conference on Numerical Methods in Geomechanics, Nagoya, Japan, 755-763.

NAVAYOGARAJAH, N., 1990. Constitutive modeling of static and cyclic behavior of intefaces and implementation in boundary value problems. Ph.D. Dissertation, Department of Civil and Engineering Mechanics, University of Arizona, USA.

NAVAYOGARAJAH, N., DESAI, C. S., and KIOUSIS, P. D., 1992. Hierarchical single-surface model for static and cyclic behaviour of interfaces. Journal of Engineering Mechanics, ASCE, 118(5), 990-1011.

OBERT, L., BRADY, B. T., and SCHMECHEL, F. W., 1976. The effect of normal stiffness on the shear resistance of rock. Rock Mechanics, Wien, Austria, Vol. 8, pp. 57-72.

OOI, L. H. and CARTER, J. P., 1987. A constant normal stiffness direct shear device for static and cyclic loading. Geotechnical Testing Journal, GTJODJ, 10(1), 3-12.

PANDE, G. N. and SHARMA, K. G., 1979. On joint/interface elements and associated problems of numerical ill-conditioning. International Journal for Numerical and Analytical Methods in Geomechanics, Vol. 3, 293-300.

POULOS, H. G., 1989. Cyclic axial loading analysis of piles in sand, Journal of Geotechnical Engineering, ASCE, 115(6), 836-852.

POTYONDY, J. G., 1961. Skin friction between various soils and construction materials. Geotechnique, 11(4), 831-353.

RAMBERG, W. and OSGOOD, W. R., 1943. Description of stress-strain curves by three parameters. Technical Note 902, National Advisory Committee for Aeronautics, Washington, D.C..

SAEB, S. and AMADEI, B., 1992. Modelling rock joints under shear and normal loading. Int. Journal Rock Mech. Min. Sci. and Geomech. Abstr., 29(3), 267-278.

STREETER, V. L., WYLIE, E. B., and RICHART, F. E., 1974. Soil motion computations by characteristics method. Journal of Geotechnical Engineering Division, ASCE, 100(GT3), 247-263.

SMITH, T. R. and RAY, B., 1986. Shear mobilization on laterally loaded shafts. Geotechnical Aspects of Stiff and Hard Clays, Ed. Khera and Lovell, ASCE, Newyork, 60-68.

TURNER, J. P. and KULHAWY, F. H., 1989. Issues in evaluating conbined repeated loading of deep foundations. Foundation Engineering: Current Principles and Practices, Proc. of the Congress, Evanston, Illinois, June 25-29, Vol. 2.

UESUGI, M. and KISHIDA, H., 1986*a*. Influential factors between steel and dry sand. Soils and Foundations, 26(2), 33-46.

UESUGI, M. and KISHIDA, H., 1986*b*. Frictional resistance at yield between dry sand and mild steel. Soils and Foundations, 26(4), 139-149.

UESUGI, M. and KISHIDA, H., 1987, Cyclic testing and modeling of interfaces. (Discussion) Journal of Geotechnical Engineering, ASCE, 113(9), 1086-1087.

UESUGI, M., KISHIDA, H., and TSUBAKIHARA, Y., 1989. Friction between sand and steel under repeated loading. Soils and Foundations, 29(3), 127-137.

UESUGI, M., KISHIDA, H., and UCHIKAWA, Y., 1990. Friction between dry sand and concrete under monotonic and repeated loading. Soils and Foundations, 30(1), 115-128.

UESUGI, M., KISHIDA, H., 1991. Cyclic axial loading analysis of piles in sand. (Discussion), Journal of Geotechnical Engineering, ASCE, 115(6), 1435-1437.

WANG, Z. L., DAFALIAS, Y. F., and SHEN, C. K., 1990. Bounding surface hypoplasticity model for sand. Journal of Engineering Mechanics, ASCE, 116(5), 983-1001.

WONG, P. C.-W., KULHAWY, F. H., and INGRAFFEA, A.R., 1989. Numerical modelling of interface behaviour for drilled shaft foundations under generalized loading. Proceedings of the Congress, Foundation Engineering, Current Principles and Practices, Vol. 1, 565-579.

YOSHIMI, Y. and KISHIDA, T., 1981. Friction between sand and metal surface. Proceedings, 10th International Conference on Soils Mechanics and Foundation Engineering, Vol. 1, 831-834.

ZIENKIEWICZ, O. C., BEST, B., DULLAGE, C., and STAGG, K. G., 1970. Analysis of non linear problems in rock mechanics with particular reference to jointed rock systems. Proceedings, Second Congress of the International Society of Rock Mechanics, Belgrade, Yugoslavia, 501-509.

APPENDIX A

ELASTOPLASTIC SINGLE-SURFACE MODEL OF DESAI

This Appendix describes a constitutive model which was proposed by Navayogarajah *et al.* (1992) for simulating the monotonic and cyclic behaviour of interfaces between sand and structural materials. The model is based on the hierarchical single surface approach and elastoplasticity theory, formerly proposed by Desai (1980), Desai and Faruque (1984), and Desai *et al.* (1986), for simulating the behaviour of the geomaterials. It can simulate associative, non-associative, and strain-softening behaviour during monotonic as well as cyclic loading. The test data reported by Uesugi and Kishida (1986a, b), Uesugi (1987), and Kishida and Uesugi (1987), were adopted to develop the elastoplastic constitutive model. The test data were obtained from a simple shear device for testing soil-structural material interfaces. The model was developed as part of a Ph.D. thesis by Navayogarajah (1990) under the supervision of Professor C. S. Desai.

The idealization for an interface between two contacting bodies *A* and *B* is shown in Fig. A.1 (Navayogarajah *et al.* 1992). During the load transfer between body *A* and body *B*, forces develop in the tangential or normal directions on the interface plane.

The interface zone is subjected to a simple-shear stress state (Fig. A.1*b*), and is idealized as a 2-D body considering in-plane deformations. Unlike the modelling of the stress-strain behaviour of solids, in which 3-D states of stress and strain at a single point are considered, the modelling of interfaces is often based on the consideration of traction forces (*N* and *T*) and displacements (v and u) on the interface plane. Normal (σ) and shear (τ) stresses on the interface plane are obtained by normalizing the normal (*N*) and shear (*T*) forces using the interface length (*B*).

The constitutive relation of interface behaviour relates the increments of normal and shear stresses ($d\sigma_n$ and $d\tau$) to the increments of normal and shear displacements (dv and du) written as:

$$d\sigma = C^{ep} dU \qquad \text{A.1}$$

where $d\sigma^T = (d\sigma_n\,,\ \tau)$; $dU^T = (dv\,,\ du)$; and C^{ep} = elasto-plastic constitutive matrix (2 × 2 for 2-D interface elements). The objective is to define the constitutive matrix C^{ep} using the proposed model by Navayogarajah *et al.* (1992) for monotonic loading condition.

A.1 Model Description

A.1.1 Elastic Behaviour

The incremental elastic behaviour of an interface is expressed as:

$$\begin{pmatrix} d\sigma_n \\ d\tau \end{pmatrix} = \begin{bmatrix} K_n & 0 \\ 0 & K_s \end{bmatrix} \begin{pmatrix} dv^e \\ du^e \end{pmatrix}$$

or $$d\sigma = C^e dU \qquad \text{A.2}$$

where C^e = elastic constitutive matrix of interface; and K_n and K_s = elastic normal and shear stiffness of the interface, respectively. It is assumed that elastic normal and shear behaviour are uncoupled.

A.1.2 Plastic behaviour-Yield surface

A general 3-D yield function written in terms of stress invariants was proposed for soils by Desai (1980), Desai and Faruque (1984), and Desai *et al.* (1986):

$$F = J_{2D} - \left(\frac{-\alpha J_1}{\alpha_0} + \gamma J_1^2\right)(1 - \beta S_r)^m = J_{2D} - F_b F_s = 0 \qquad \text{A.3}$$

where J_1 is the first invariant of the stress tensor and J_{2D} is the second invariant of the deviatoric stress tensor S_{ij}. The parameters α, n, γ, β, and m are the response functions, and S_r equals stress ratio such as $J_{3D}^{1/3} / J_{2D}^{1/2}$, where J_{3D} is the third invariant of S_{ij}. F_b and F_s are referred to as basic and shape functions and are related to the shape of F in $J_1 - \sqrt{J_{2D}}$ (Fig. A.2*a*) stress space.

Using the analogies between the behaviour of solids and interfaces, the Eq. A.3 has been specialized for 2-D interface elements (Fig. A.2*b*) by Fishman and Desai (1987):

$$F = \tau^2 + \alpha\sigma_n^n - \gamma\sigma_n^2 = 0 \qquad \text{A.4}$$

where γ and n = interface parameters; and α = hardening function, which defines evolution of the yield surface during the deformation. To simulate the occurrence of peak shear stress (τ_p) at small shear displacements, the following relation was proposed for α by Navayogarajah *et al.* (1992):

$$\alpha = \gamma \exp(-a\xi_v)\left(\frac{\xi_D^* - \xi_D}{\xi_D^*}\right)^b \quad \text{for} \quad \xi_D \phi \xi_D^*$$

$$\alpha = 0 \qquad \text{for} \quad \xi_D \geq \xi_D^* \qquad \text{A.5}$$

where γ = ultimate (or failure) parameter; a and b = interface parameters; $\xi_v = \int |dv^p|$ and $\xi_D = \int |du^p|$ = volumetric and shear plastic displacement trajectories, respectively. $\xi_D^* = \xi_D$ when τ reaches τ_p. It is found that ξ_D^* is predominantly a function of the parameter R which is defined as:

$$R = \begin{cases} R_n / R_n^{cr} & if \quad R_n^{cr} \phi \; R_n \\ 1 & if \quad R_n^{cr} \le R_n \end{cases} \qquad \text{A.6}$$

where R_n is normalized roughness:

$$R_n = \frac{R_{max}(L = D_{50})}{D_{50}} \qquad \text{A.7}$$

and R_n^{cr} is the critical normalized roughness beyond which shear failure occurs in soil rather than the interface. Numerically, R varies from *0* to *1*, and it is a non-dimensional quantity.

Based on the experimental evidence, the parameters τ_p and ξ_D^* are related to R as :

$$\mu_p = \frac{\tau_p}{\sigma} = \frac{1}{\overline{R}}\left[\mu_{p1} + \mu_{p2} R\right] \qquad \text{A.8}$$

$$\gamma = \mu_p^2$$

$$\xi_D^* = (\xi_{D1}^* + \xi_{D2}^* R) \qquad \text{A.9}$$

Here, μ_p = ultimate (or peak) stress ratio; $\overline{R}$ denotes the roundness of sand particles; and μ_{p1}, μ_{p2}, ξ_{D1}^*, and ξ_{D2}^* = interface parameters.

A.1.3 Non-Associative flow rule for interface

The plastic potential function, Q, given in Eq. A.10 was employed for considering the non-associative flow rule.

$$Q = \tau^2 + \alpha_Q \sigma^n - \gamma \sigma^2 \qquad \text{A.10}$$

The following equation was proposed for α_Q:

$$\alpha_Q = \alpha + \alpha_{ph}\left(1 - \frac{\alpha}{\alpha_i}\right)\left[1 - \kappa\left(1 - \frac{r}{r_u}\right)\right] \qquad \text{A.11}$$

where κ = a material parameter that defines the slope of the normal displacement versus shear displacement curve at the point where shear stress τ reaches its peak value τ_p. The damage parameters r and r_u in Eq. A.11 are defined later. The value of α at the phase-change point (the point where the change in normal displacement is zero) for the associative flow case ($F \equiv Q = 0$) is defined as α_{ph} in Eq. A.11; α_i is defined as the value of α at the initiation of non-associativeness, which usually starts on the application of the shear stress; κ is related to R as:

$$\kappa = \left\{\kappa_1 + \kappa_2\left[\exp\left(R^2\right) + \exp\left(-R^2\right)\right]\right\} \qquad \text{A.12}$$

A.1.4 Strain softening behaviour

The concept of decomposition of material behaviour (Fig. A.3) is adopted to model the strain-softening behaviour of interfaces.

The observed or average response (stress) of an interface is assumed to be the sum of the response of the two parts, namely: (1) The intact (or topical) part; and (2) the damaged part, as shown in Fig. A.3. During the shear loading, the intact part is progressively transformed into the damaged part due to the accumulation of plastic strains. Characterization of the intact and damaged parts is achieved by elasto-plasticity and rigid plasticity, respectively. The non-associative model presented before is used for the intact part. It is assumed that the shear strength of the damaged part is zero, but it can sustain normal stress. The normal stress is assumed to be compressive. With these assumptions, the observed or average interface stresses τ and σ_n can be written as:

$$\begin{Bmatrix} \sigma_n \\ \tau \end{Bmatrix} = (1-r)\begin{Bmatrix} \sigma_n^t \\ \tau^t \end{Bmatrix} + r\begin{Bmatrix} \sigma_n^t \\ 0 \end{Bmatrix} \qquad \text{A.13}$$

The parameter $r = (A_0 / A)$ is a scalar quantifying the damage; A_0 = the area of damaged part; and A = total area. The state of stress vectors {σ_n ,τ }, {σ_n^t , τ^t }, and {σ_n^t , 0 } relate to average, intact part, and damaged part of the interface, respectively.

The following relation is proposed for the damage function r as follows:

$$r = 0 \qquad \text{for} \quad \xi_D \; \mathrm{P} \; \xi_D^*$$

$$r = r_u - r_u \exp\left[-A\left(\xi_D - \xi_D^*\right)^2\right] \qquad \text{for} \quad \xi_D \; \phi \; \xi_D^* \qquad \text{A.14}$$

where

$$r_u = \frac{\tau_p - \tau_r}{\tau_p} \qquad \text{A.15}$$

A = a parameter that depends on the roughness ratio R of the interface. The residual stress ratio, μ_0 is related to R as:

$$\mu_o = \frac{\tau_r}{\sigma_n} = \frac{1}{\overline{R}}[\mu_{01} + \mu_{02} R] \qquad \text{A.16}$$

Here, μ_{01} and μ_{o2} = interface parameters.

A.2 Evaluation and Determination of Model Parameters

The two major classes of parameters required to define interface behaviour are elastic and plastic. The elastic behaviour of interface defined by Eq. A.2, requires the elastic normal stiffness K_n and elastic shear stiffness K_s. The plastic part of interface behaviour can be categorized into three components as (1) associative, (2) non-associative, and (3) strain-softening.

- Elastic parameters: $K_s K_n$,
- Plastic parameters:

1. Associative model: n, γ, ξ_D, a, b
2. Non-associative model: κ
3. Strain-softening: A, r_u

All these 12 parameters are related to the surface roughness ratio R. Therefore, most of these parameters are explicitly related to R in the corresponding equations.

In the following sections, the procedures for determining the parameters are described. In addition, the model parameters are determined for the No. 2 sand at the relative density of 88% and the steel plate used in the testing programs described in Chapters 5 through 7.

A.2.1 Elastic parameters K_n and K_s

Elastic parameters can be obtained from the unloading-reloading portions of the σ_n versus v and τ versus u curves, as indicated in Figs. A.4 and A.5, respectively. Figure A.4*a* shows the normal compliance of the interface apparatus by plotting the normal stress versus normal displacement when a stiff solid material is placed in the soil container instead of the soil sample. Figure A.4*b* shows the normal stress-normal displacement relation for the sand-steel interface before the corrections are made for the machine compliance. Fig. A.4*c* presents the corrected results of the normal stress plotted against the normal displacement. Parameter K_n is the slope of the unloading curve in Fig. A.4*c*. An average of 6000 kN/mm would be appropriate for the test result presented.

The loading-unloading results for normalized shear stress *vs.* sliding displacement are illustrated in Fig. A.5. An average of 1000 kN/mm was obtained for K_s.

A.2.2 Ultimate (or Failure) parameter γ:

Ultimate shear stress condition of interface is given by $\alpha = 0$ in yield function *f*, Eq. A.4:

$$\frac{\tau_p}{\sigma} = \mu_p = \gamma^{1/2} \qquad \text{A.17}$$

Slope of τ_p versus σ curve will give $\gamma^{1/2}$ for a given interface roughness. The experimental data together with Eqs. A.8 and A.17 results in Fig. A.6 where the variation of μ_p with R is given. The μ_{p1} is the intercept of the line with the μ_p axis and μ_{p2} is the slope of the line. μ_{p1} and μ_{p2} were measured 0.275 and 0.695, respectively, for the interface between the No. 2 sand at a relative density of 88% and the steel plate.

A.2.3 Phase change parameter *n* :

Phase change parameter n is evaluated by considering the phase change point. Let the shear stress corresponding to the phase change point be denoted by τ_{ph}. Since incremental plastic volumetric strain is zero at the phase change point, by setting $\partial Q/\partial\sigma = 0$ in Eq. A.10:

$$\frac{\partial Q}{\partial \sigma} = (n\sigma^{n-1}\alpha_Q - 2\gamma\sigma) = 0 \qquad \text{A.18}$$

For the interface, phase change point usually occurs soon after the start of shear for all ranges of interface roughness. Thus assuming $\alpha_Q = \alpha$ at phase change point and combining Eqs. A.17 and 4 gives:

$$\tau_{ph}^2 = \gamma(1-\frac{2}{n})\sigma^2 \qquad \text{A.19}$$

Knowing the value of γ, the parameter n can be computed from the slope of the best fit of τ^2_{ph} *vs.* σ^2. Experimental results indicate that compaction is observed at the beginning of shear, which is occurring in the soil mass in the vicinity of the interface. Subsequent dilation (rough interface), or steady state (smooth interface) volumetric behaviour is due to the interface action only, and at this state soil mass does not contribute to the volumetric behaviour. Using the above statement, it is assumed that the interface cannot undergo compaction but it can dilate or remain in steady state (neither compaction nor dilation) during monotonic loading. In such case τ_{ph} is very small or equal to zero leading to a value $n = 2.0$. Here the phase change parameter $n = 2.01$ is adopted.

A.2.4 Hardening parameters ξ^*_D, a, b:

When $\tau = \tau_p$ the value of ξ_D is equal to ξ^*_D. Therefore, ξ^*_D can be computed for a given interface roughness. Figure A.7 shows ξ^*_D versus R for data points. The line predicted by least square fit procedure gives ξ^*_{D1} and ξ^*_{D2} of Eq. A.9. ξ^*_{D1} and ξ^*_{D2} are the intercept with the vertical axis and slope of the line, respectively, and were obtained as 0.09 and 0.559 from the line of Fig. A.7. Select a set of data points (σ , τ), and the corresponding plastic displacement trajectories ξ_V and ξ_D from the test curves τ versus u, and v versus u, under constant normal stress. Knowing (σ , τ), α can be computed using $f = 0$, Eq. A.4, at all data points. Now the hardening function α, Eq. A.5, can be written in the following linear form:

$$\left\langle \xi_V \quad \ln\left(\frac{\xi_D^* - \xi_D}{\xi_D^*}\right)\right\rangle \begin{Bmatrix} a \\ b \end{Bmatrix} = (\ln\gamma - \ln\alpha) \qquad \text{A.20}$$

A least square method is suitable in this case to calculate a and b as shown in Figs. A.8*a* and 8*b* respectiveiy. a and b were obtained as 22.5 and 2.2, respectively, for the presented data presented in Fig. A.8.

A.2.5 Non-Associative flow parameter κ:

The parameter κ is computed using the slope of volumetric curve at $\tau = \tau_p$ (or at $\xi_D = \xi^*_D$). The slope is given by:

$$\left.\frac{dv^p}{du^p}\right|_{\xi_D=\xi_D^*} \approx \left.\frac{dv^p}{du}\right|_{\xi_D=\xi_D^*} = \left[\frac{n\alpha_Q\sigma^{n-1} - 2\gamma\sigma}{Q\tau_p}\right] \qquad \text{A.21}$$

Using $\alpha = 0$ and $r = 0$ at $\xi_D = \xi^*_D$ in α_Q (Eq. A.11), Eq. A.21 will reduce to

$$\kappa = -\gamma^{(-1/2)} \left.\frac{dv^p}{du}\right|_{\xi_D=\xi_D^*} \qquad \text{A.22}$$

For a given interface roughness ratio R, parameter κ can be computed using Eq. A.22. κ_1 and κ_2 were determined by least square fit based on Eq. A.12 as -1.26 and 0.63.

A.2.6 Strain-Softening parameters r_u and A:

For a given interface roughness ratio R, τ_p and τ_r can be obtained from τ versus u curve, thus r_u can be computed using Eq. A.15. The μ_0 versus R curve is shown in Fig. A.9 from which the μ_{01} and μ_{02} were determined as 0.257 and 0.443, respectively. Knowing μ_0, r_u can be computed using Eq. A.16.

In the softening region, $\xi_D \geq \xi^*_D$, the damage function r (Eq. A.13) can be written as:

$$\ln\left(\frac{r_u - r}{r_u}\right) = A\left[-(\xi_D - \xi_D^*)^2\right] \qquad \text{A.23}$$

The slope of straight line relation of Eq. A.34 gives values of A. Calculation of parameter A is shown in Fig. A.10 which is the slope of the line and was determined as 0.5.

A.3 Derivation of C^{ep}

The Eq. A.1 can be written as:

$$\{d\sigma\} = \left([C^e] - [C^p]\right)\{dU\} \qquad \text{A.24}$$

where $$[C^{ep}] = [C^e] - [C^p]$$

subscripts e and p denote elastic and plastic parts of $[C^{ep}]$, respectively. $[C^e]$ was given in Eq. A.2 as:

$$[C^e] = \begin{bmatrix} K_n & 0 \\ 0 & K_s \end{bmatrix}$$

$$\{d\sigma\} = [C^e]\{dU^e\} \qquad \text{A.25}$$

The $\{dU\}$ can be decomposed into elastic and plastic components as:

$$\{dU\} = \{dU^e\} + \{dU^p\} \qquad \text{A.26}$$

Then Eq. A.25 can be written as:

$$\{d\sigma\} = [C^e]\left(\{dU\} - \{dU^p\}\right) \qquad \text{A.27}$$

with non-associative plasticity, the flow rule is given by:

$$\{dU^p\} = \lambda \frac{\partial Q}{\partial\{\sigma\}} = \lambda\{B\} \qquad \text{A.28}$$

where λ = a scalar factor of proportionality. The consistency condition gives:

$$dF = \left(\frac{\partial F}{\partial\{\sigma\}}\right)^T \{d\sigma\} + \frac{\partial F}{\partial \xi} d\xi = 0$$

$$= \{A\}^T \{d\sigma\} + \frac{\partial F}{\partial \xi} d\xi = 0 \qquad \text{A.29}$$

Equation A. 28 and $d\xi = \left(\{d\varepsilon^p\}^T \{d\varepsilon^p\}\right)^{1/2}$ leads to:

$$d\xi = \lambda\left(\{B\}^T \{B\}\right)^{1/2}$$

or $$d\xi = \lambda \gamma_F \qquad \text{A.30}$$

Substitution of $\{d\sigma\}$ from Eq. A.27 and $d\xi$ from Eq. A.30 in Eq. A.29 gives:

$$\lambda = \frac{\{A\}^T [C^e]\{dU\}}{\{A\}^T [C^e]\{B\} - \frac{\partial F}{\partial \xi}\gamma_F} \qquad \text{A.31}$$

Finally, substituting λ in Eq. A.27 with use of Eq. A.28 leads to:

$$\{d\sigma\} = [C^e]\left(1 - \frac{\{A\}^T [C^e]\{B\}}{\{A\}^T [C^e]\{B\} - \frac{\partial F}{\partial \xi}\gamma_F}\right)\{dU\} \qquad \text{A.32}$$

which can be written as:

$$\{d\sigma\} = \left([C^e] - [C^p]\right)\{dU\} = [C^{ep}]\{dU\} \qquad \text{A.33}$$

where

$$[C^p] = \frac{[C^e]\{B\}\{A\}^T}{\{A\}^T[C^e]\{B\} - \frac{\partial F}{\partial \xi}\gamma_F} \qquad \text{A.34}$$

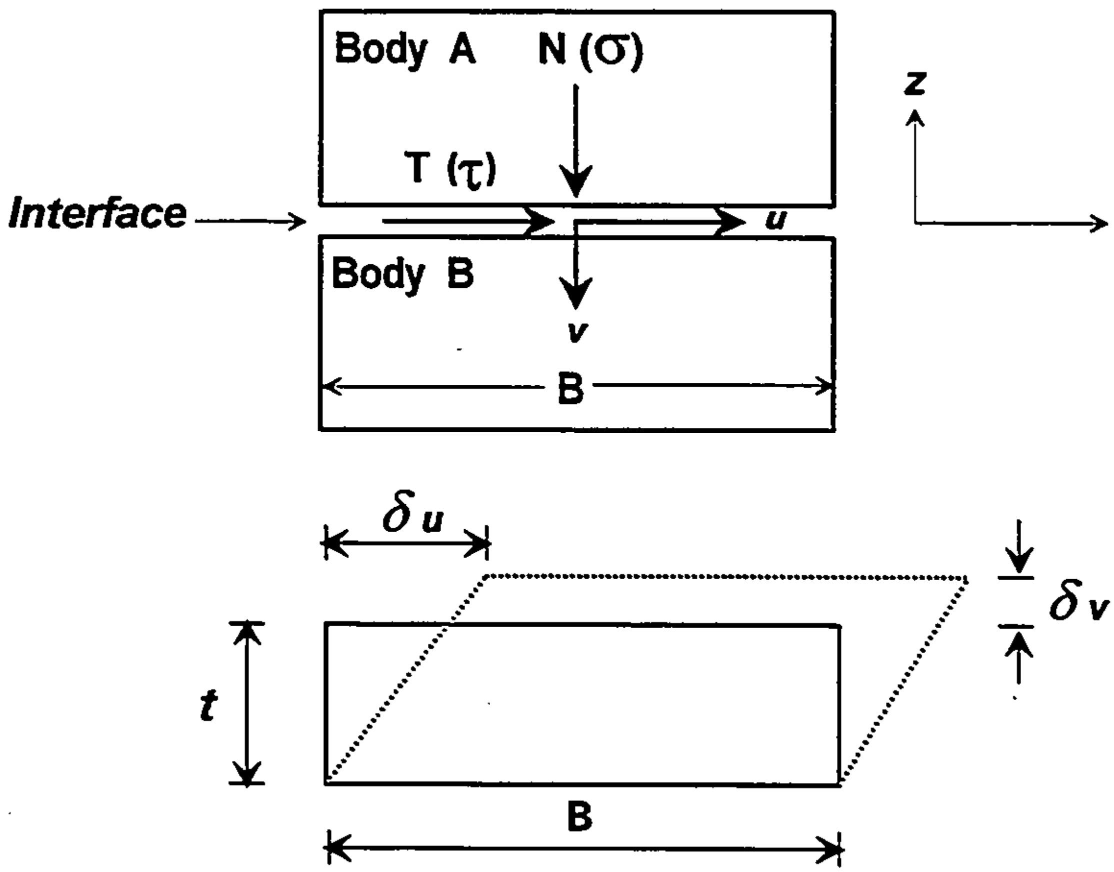

FIG. A.1. *(a)* Idealization of interface; *(b)* Deformation at interface, simple shear condition

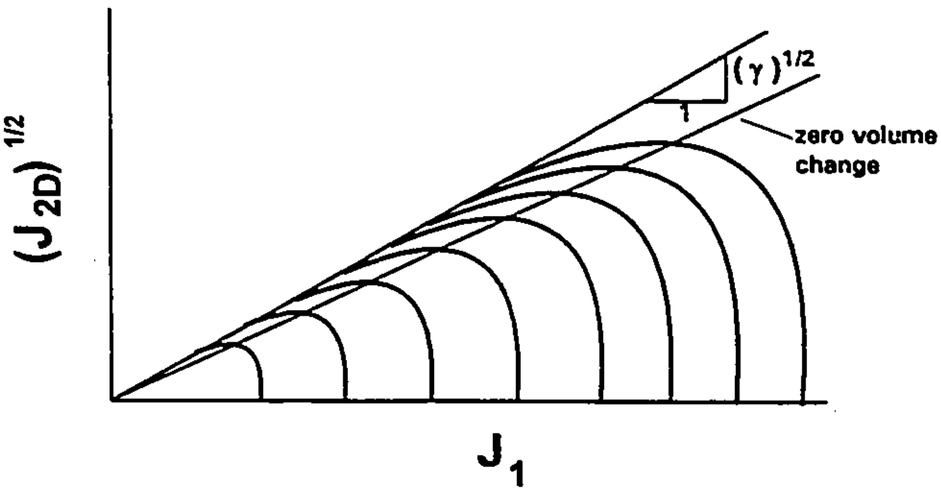

(a)

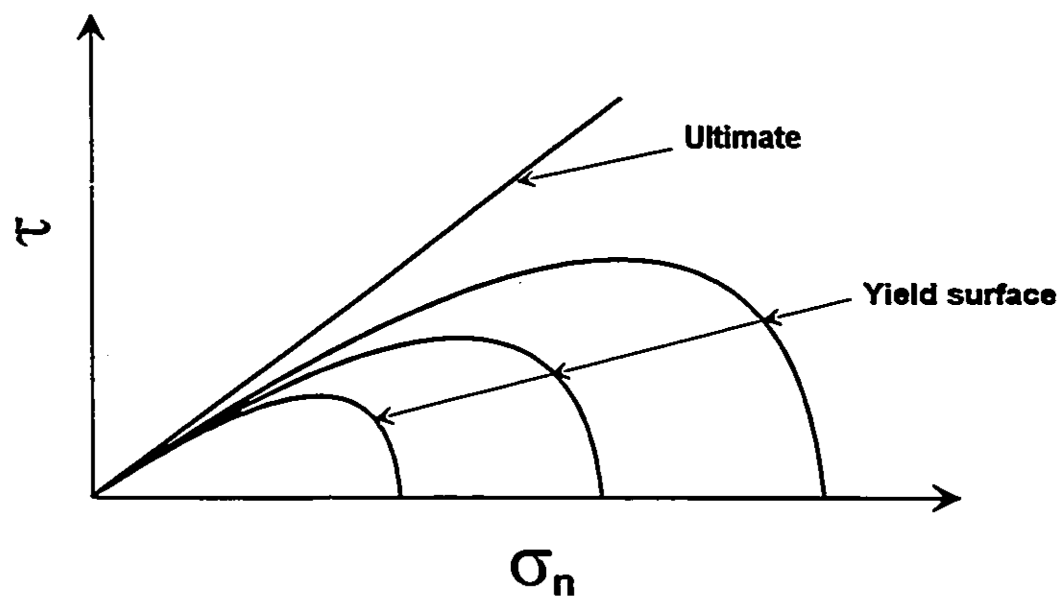

(b)

FIG. A.2. Plots of yield function F in stress spaces for: *(a)* solid materials; (b)Interfaces

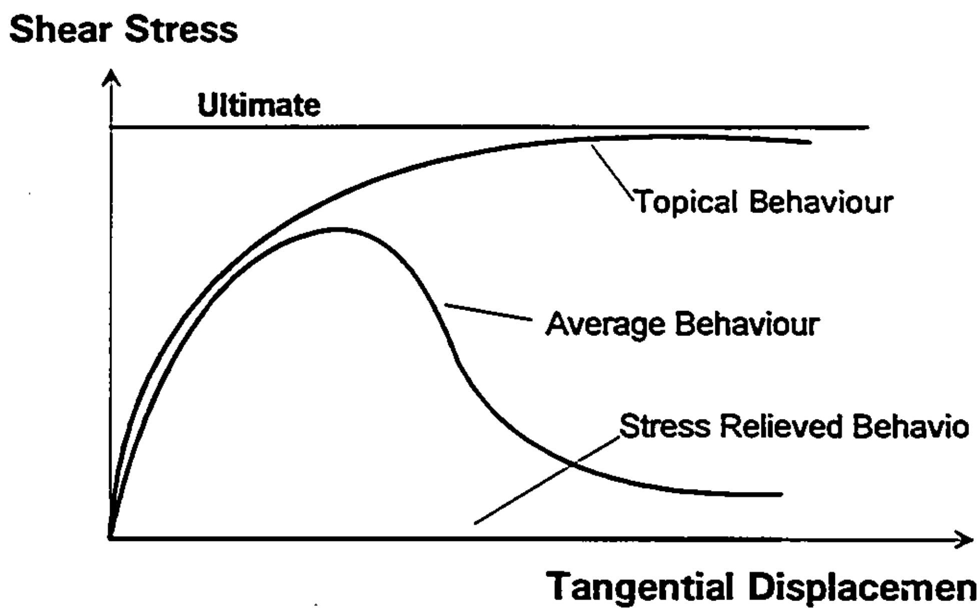

FIG. A.3. Strain softening behaviour

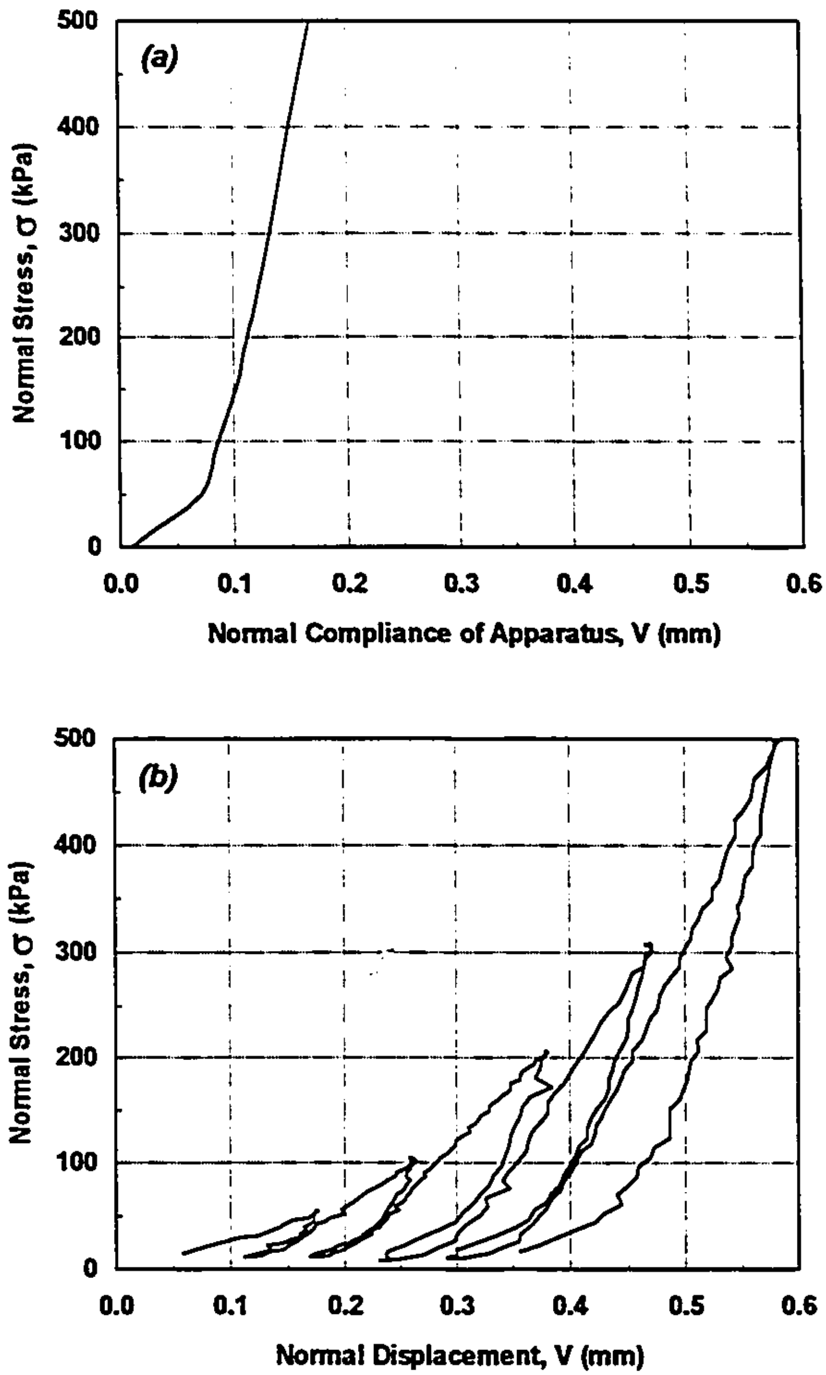

FIG. A.4. *(a)* Normal compliance of the interface apparatus; *(b)* Normal stress-normal displacement; *(c)* Corrected results of *b* to determine K_n

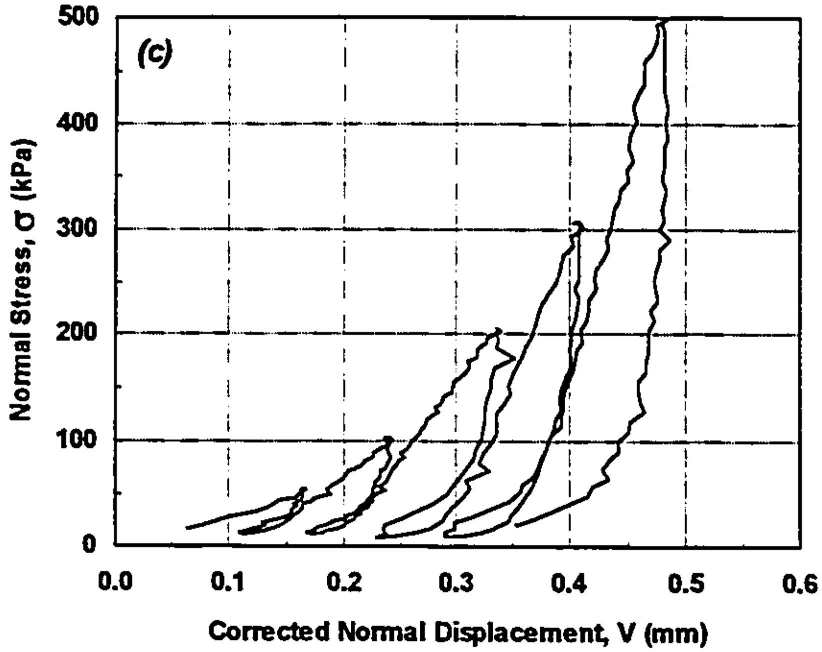

FIG. A.4. (Continue)

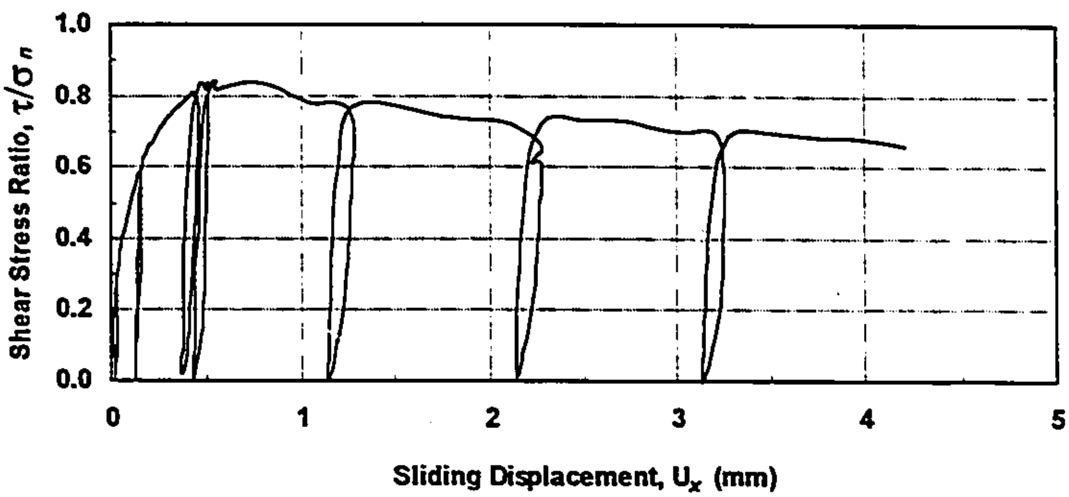

FIG. A.5. Loading-unloading results for normalized shear stress *vs.* sliding displacement to determine K_s

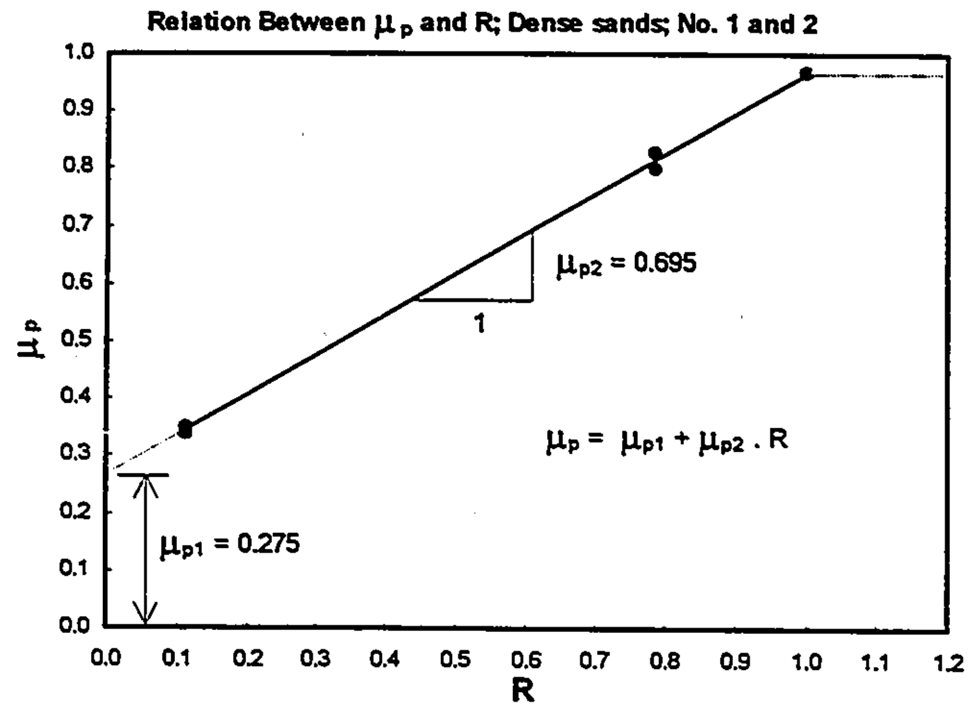

FIG. A.6. Parameter μ_p; (μ_{p1} and μ_{p2})

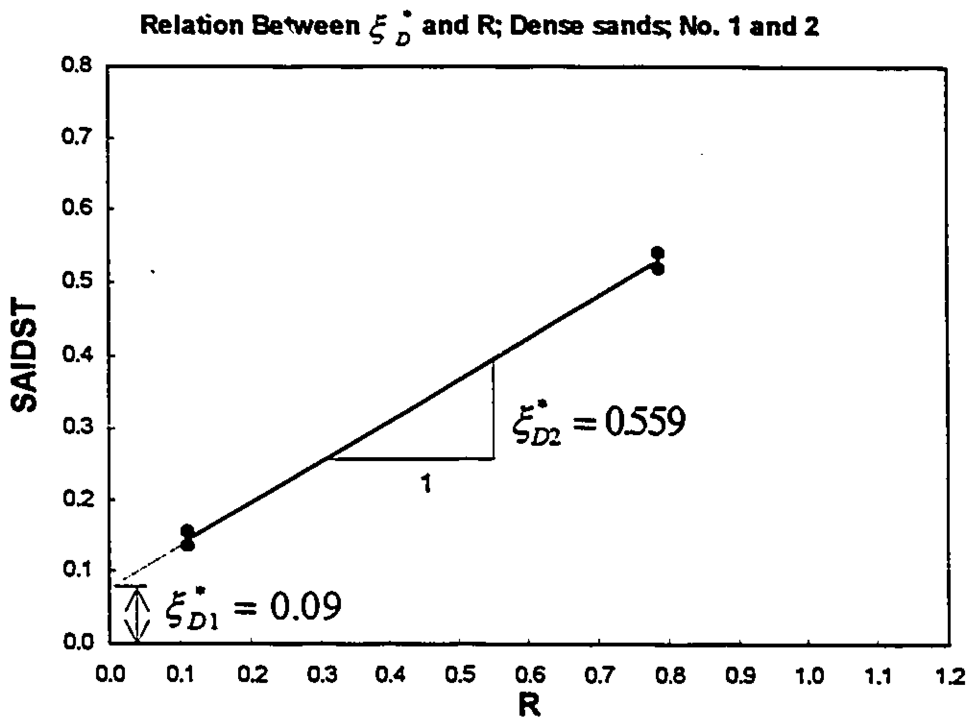

FIG. A.7. Parameter ξ^*_D; (ξ^*_{D1} and ξ^*_{D2})

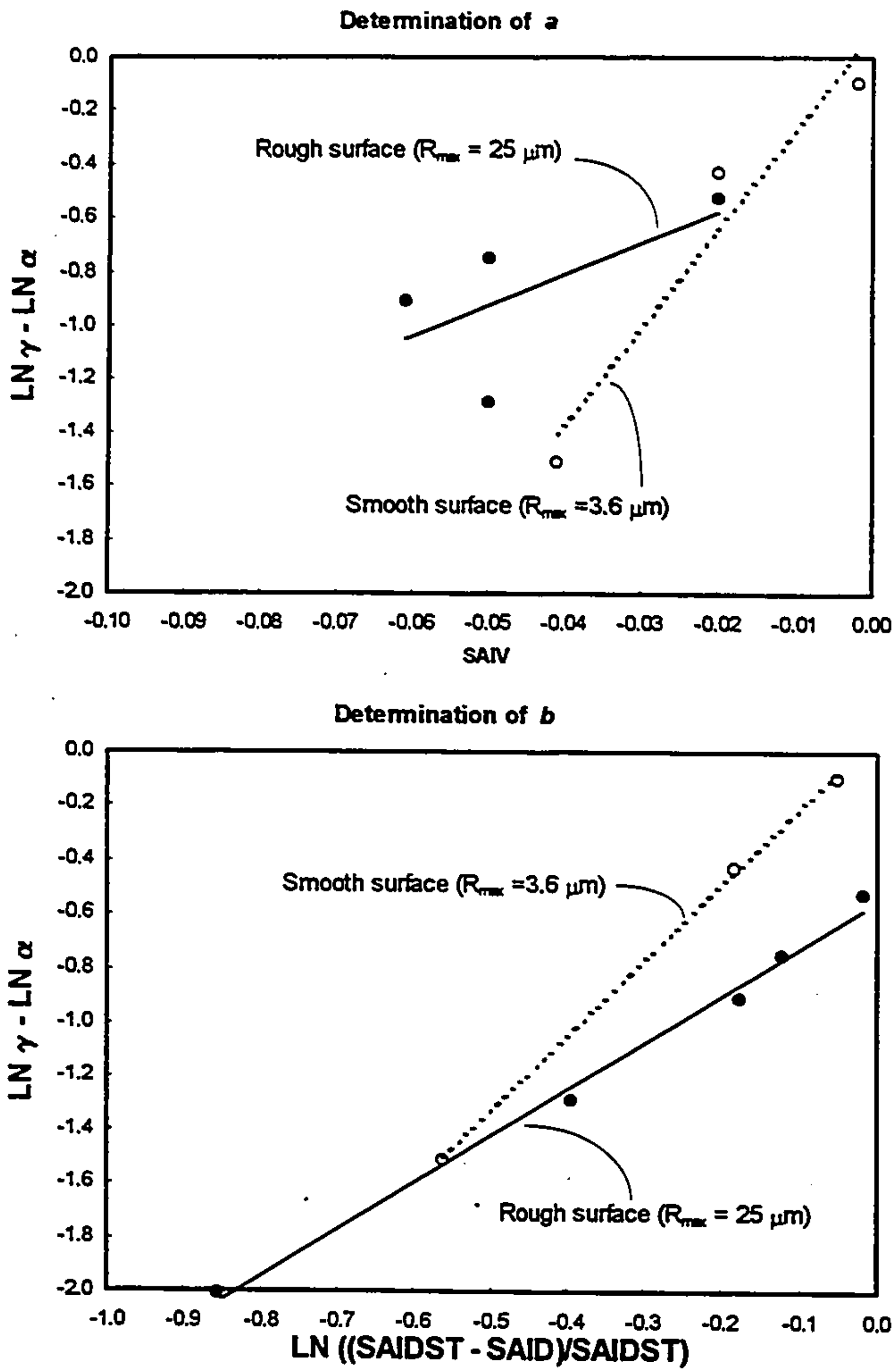

FIG. A.8. Parameters of a and b

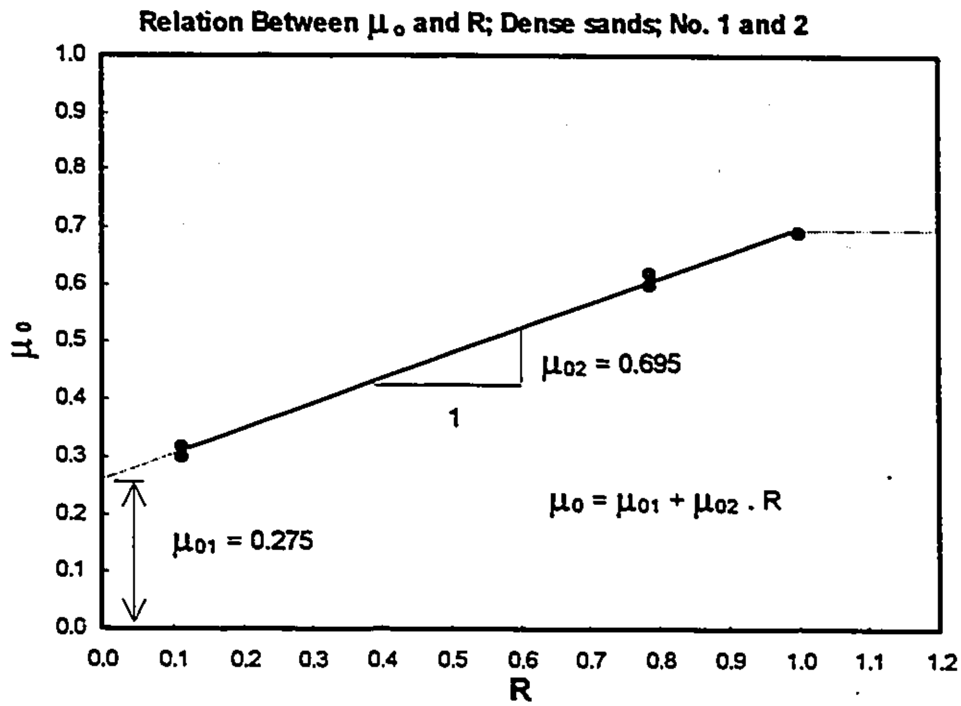

FIG. A.9. Parameter μ_0; (μ_{01} and μ_{02})

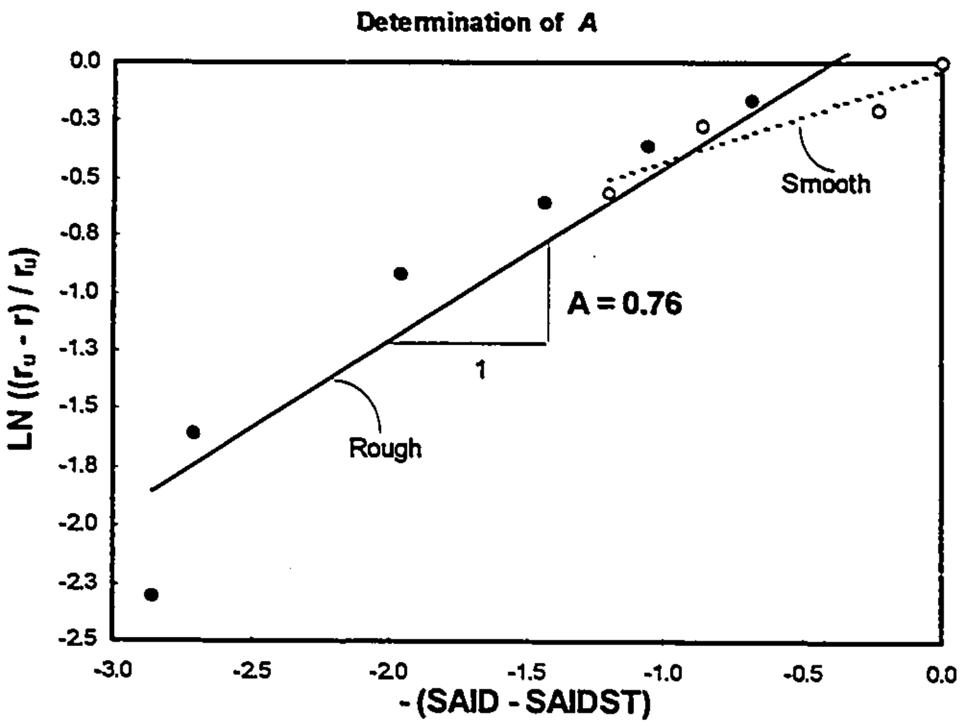

FIG. A.10. Parameter *A*

APPENDIX B

LIST OF EXPERIMENTS

This Appendix presents a complete list of experiments conducted in this study. They are classified as:

• M2DCNL: Monotonic 2-D under Constant Normal Load	83 tests
• M3DCNL: Monotonic 3-D under Constant Normal Load	27 tests
• M2DCNS: Monotonic 2-D under Constant Normal Stiffness	15 tests
• C2DCNL: Cyclic 2-D under Constant Normal Load	19 tests
• C3DCNL: Cyclic 3-D under Constant Normal Load	28 tests
• C2DCNS: Cyclic 2-D under Constant Normal Stiffness	15 tests
	183 TESTS

B.1 Monotonic 2-D under Constant Normal Load

M: Monotonic, C: Cyclic, 2-D: two-dimensional, 3-D: three-dimensional
D: Direct Shear Box, S: Simple Shear Box
CL: Constant Normal Load, CS: Constant Normal Stiffness
Sand No. 1: Crushed Silica (D_{50} = 1.2 mm)
Sand No. 2: Crushed Silica (D_{50} = 0.6 mm)
Sand No. 3: Ottawa Sand (D_{50} = 0.6 mm)
Plate Type: SB = Sand Blasted, SM = Smooth, ALO = Aluminium Oxide, ec = emery cloth
RUST: Rusted

Test No.	M / C	2D/3D	D / S	CL/CS	σ_n (kPa)	Sand #	Dr (%)	Plate	Rate (mm/min)
m2dbn101	M	2-D	D	CL	100	1	82	ec 150	1
m2dbn114	M	2-D	D	CL	100	2	88	SB	1
m2dbn115	M	2-D	D	CL	100	2	88	SB, 3	1
m2dbn116	M	2-D	D	CL	100	2	88	ALO 500	1
m2dbn117	M	2-D	D	CL	100	2	88	ALO 600	1
m2dbn118	M	2-D	D	CL	100	2	88	SB, 5	1
m2dsn51	M	2-D	S	CL	50	2	88	ALO 600	1
m2dsn151	M	2-D	S	CL	100	2	88	SM	1
m2dsn153	M	2-D	S	CL	100	2	88	SM	1
m2dsn154	M	2-D	S	CL	100	2	88	SM	1
m2dsn155	M	2-D	S	CL	100	2	17	SM	1
m2dsn158	M	2-D	S	CL	100	2	88	SM	10
m2dsn159	M	2-D	S	CL	100	2	17	SM	10
m2dsn163	M	2-D	S	CL	100	1	82	SM	1
m2dsn164	M	2-D	S	CL	100	2	88	ec 150	1
m2dsn165	M	2-D	S	CL	100	2	88	ec 150	1
m2dsn166	M	2-D	S	CL	100	2	88	ec 150	2
m2dsn167	M	2-D	S	CL	100	2	88	SB	1
m2dsn168	M	2-D	S	CL	100	2	88	SB	1
m2dsn169	M	2-D	S	CL	100	2	17	SB, 3	1
m2dsn170	M	2-D	S	CL	100	2	17	SB, 2	1
m2dsn171	M	2-D	S	CL	100	2	88	SB, 2	1
m2dsn172	M	2-D	S	CL	100	3	84	SM	1
m2dsn173	M	2-D	S	CL	100	3	17	SM	1
m2dsn174	M	2-D	S	CL	100	2	88	ALO 500	1
m2dsn175	M	2-D	S	CL	100	2	88	ALO 500	10
m2dsn176	M	2-D	S	CL	100	2	88	ALO 240	1
m2dsn177	M	2-D	S	CL	100	2	88	ALO 220	1
m2dsn178	M	2-D	S	CL	100	2	88	SB, 4	1
m2dsn179	M	2-D	S	CL	100	2	88	SB, 6	1

Test No.	M / C	2D/3D	D / S	CL/CS	σ_n (kPa)	Sand #	Dr (%)	Plate	Rate (mm/min)
m2dsn180	M	2-D	S	CL	100	2	88	ALO 400, 2	1
m2dsn181	M	2-D	S	CL	100	2	88	ALO 400	1
m2dsn182	M	2-D	S	CL	100	2	88	ALO 400	1
m2dsn183	M	2-D	S	CL	100	2	88	ALO 600	1
m2dsn134	M	2-D	S	CL	100	2	88	ALO 600, 2	1
m2dsn185	M	2-D	S	CL	100	2	88	ALO 600	1
m2dsn186	M	2-D	S	CL	100	2	88	ALO 600	1
m2dsn187	M	2-D	S	CL	100	3	84	ALO 600	1
m2dsn188	M	2-D	S	CL	100	1	82	ALO 600	1
m2dsn189	M	2-D	S	CL	100	2	88	ALO 600	1
m2dsn190	M	2-D	S	CL	100	2	88	ALO 600	10
m2dsn191	M	2-D	S	CL	100	2	88	ALO 600	0.1
m2dsn192	M	2-D	S	CL	100	2	60	ALO 600	1
m2dsn193	M	2-D	S	CL	100	2	30	ALO 600	1
m2dsn194	M	2-D	S	CL	100	2	12	ALO 600	1
m2dsn195	M	2-D	S	CL	100	2	30	SB	2
m2dsn196	M	2-D	S	CL	100	2	30	SB	1
m2dsn197	M	2-D	S	CL	100	2	88	SB	L/U
m2dsn198	M	2-D	S	CL	100	2	88	RUST	1
m2dsn199	M	2-D	S	CL	100	2	88	SB	N L/U
m2dsn200	M	2-D	S	CL	100	2	45	ALO 600	1
m2dsn251	M	2-D	S	CL	200	2	88	ALO 600	1
m2dsn252	M	2-D	S	CL	200	2	88	ALO 600	1
m2dsn351	M	2-D	S	CL	300	2	88	SM	1
m2dsn353	M	2-D	S	CL	300	2	12	SM	1
m2dsn354	M	2-D	S	CL	300	2	88	SM	10
m2dsn355	M	2-D	S	CL	300	2	12	SM	10
m2dsn357	M	2-D	S	CL	300	1	82	SM	1
m2dsn358	M	2-D	S	CL	300	2	88	SB	1
m2dsn359	M	2-D	S	CL	300	2	12	SB, 4	1
m2dsn360	M	2-D	S	CL	300	3	88	SM, 2	1
m2dsn361	M	2-D	S	CL	300	3	88	SM	1
m2dsn362	M	2-D	S	CL	300	2	84	ALO 600	1
m2dsn363	M	2-D	S	CL	300	3	84	ALO 600, 2	1
m2dsn364	M	2-D	S	CL	300	3	84	ALO 600	1
m2dsn365	M	2-D	S	CL	300	1	82	ALO 600	1
m2dbn513	M	2-D	D	CL	500	2	82	SB, 3	1
m2dbn514	M	2-D	D	CL	500	2	8	SB, 2	1
m2dsn551	M	2-D	S	CL	500	2	88	SM	1
m2dsn552	M	2-D	S	CL	500	2	8	SM	1

Test No.	M / C	2D/3D	D / S	CL/CS	σ_n (kPa)	Sand #	Dr (%)	Plate	Rate (mm/min)
m2dsn553	M	2-D	S	CL	500	2	88	SM	10
m2dsn554	M	2-D	S	CL	500	2	8	SM	10
m2dsn557	M	2-D	S	CL	500	1	82	SM	1
m2dsn560	M	2-D	S	CL	500	2	8	SM	1
m2dsn561`	M	2-D	S	CL	500	2	88	SB, 3	10
m2dsn562	M	2-D	S	CL	500	3	88	SM	1
m2dsn563	M	2-D	S	CL	500	3	6	SM	1
m2dsn564	M	2-D	S	CL	500	2	88	ALO 600	1
m2dsn565	M	2-D	S	CL	500	2	88	ALO 600	1
m2dsn566	M	2-D	S	CL	500	3	75	SB, n	1
m2dsn567	M	2-D	S	CL	500	3	84	ALO 600	1
m2dsn568	M	2-D	S	CL	500	1	82	ALO 600	1
m2dsn569	M	2-D	S	CL	500	1	82	ALO 600	1

B.2 Monotonic 3-D under Constant Normal Load

M: Monotonic, C: Cyclic, 2-D: two-dimensional, 3-D: three-dimensional
D: Direct Shear Box, S: Simple Shear Box
CL: Constant Normal Load, CS: Constant Normal Stiffness
Sand No. 1: Crushed Silica (D_{50} = 1.2 mm)
Sand No. 2: Crushed Silica (D_{50} = 0.6 mm)
Sand No. 3: Ottawa Sand (D_{50} = 0.6 mm)
Plate Type: SB = Sand Blasted, SM = Smooth, ALO = Aluminium Oxide, ec = emery cloth
RUST: Rusted

Test No.	M / C	2D/3D	D / S	CL/CS	σ_n (kPa)	Sand #	Dr (%)	Plate	τ_y (kPa)
m3dbn107	M	3-D	D	CL	100	2	88	ALO 500	0
m3dbn108	M	3-D	D	CL	100	2	88	ALO 500	20
m3dbn110	M	3-D	D	CL	100	2	88	ALO 500	60
m3dbn111	M	3-D	D	CL	100	2	88	ALO 500	40
m3dbn112	M	3-D	D	CL	100	2	88	ALO 500	60
m3dbn113	M	3-D	D	CL	100	1	82	ALO 150	0
m3dbn114	M	3-D	D	CL	100	1	82	ALO 150	23
m3dbn115	M	3-D	D	CL	100	1	82	ALO 150	44
m3dbn116	M	3-D	D	CL	100	1	82	ALO 150	44
m3dbn117	M	3-D	D	CL	100	1	82	ALO 150	44
m3dbn118	M	3-D	D	CL	100	1	82	ALO 150	63
m3dbn119	M	3-D	D	CL	100	2	88	ALO 500	40
m3dbn120	M	3-D	D	CL	100	2	88	ALO 500	60
m3dbn121	M	3-D	D	CL	100	2	88	ALO 500	60
m3dbn122	M	3-D	D	CL	100	2	88	ALO 500	40
m3dbn123	M	3-D	D	CL	100	2	88	ALO 150	63
m3dsn151	M	3-D	S	CL	100	3	84	ALO 600	x-y
m3dsn152	M	3-D	S	CL	100	2	84	ALO 600	0
m3dsn153	M	3-D	S	CL	100	2	84	ALO 600	20
m3dsn154	M	3-D	S	CL	100	2	84	ALO 600	40
m3dsn155	M	3-D	S	CL	100	2	84	ALO 600	60
m3dsn156	M	3-D	S	CS(K=400	100	2	84	ALO 600	30
m3dsn157	M	3-D	S	CS(K=800	100	2	84	ALO 600	30
m3dsn351	M	3-D	S	CL	300	3	84	ALO 600	x-y
m3dbn507	M	3-D	S	CL	500	2	88	SB, n	cx-x
m3dbn508	M	3-D	S	CL	500	2	88	SB, n	cx-x
m3dsn551	M	3-D	S	CL	500	2	88	ALO 600	x-y

B.3 Monotonic 2-D under Constant Normal Stiffness

M: Monotonic, C: Cyclic, 2-D: two-dimensional, 3-D: three-dimensional
D: Direct Shear Box, S: Simple Shear Box
CL: Constant Normal Load, CS: Constant Normal Stiffness
Sand No. 1: Crushed Silica (D_{50} = 1.2 mm)
Sand No. 2: Crushed Silica (D_{50} = 0.6 mm)
Sand No. 3: Ottawa Sand (D_{50} = 0.6 mm)
Plate Type: SB = Sand Blasted, SM = Smooth, ALO = Aluminium Oxide, ec = emery cloth
RUST: Rusted

K: Normal Stiffness ($d\sigma_n$ / dv)

Test No.	M / C	2D/3D	D / S	CL/CS	σ_{no} (kPa)	K (kPa/mm)	Sand #	Dr (%)	Plate
m2dcn001	M	2-D	S	CS	50	800	2	88	ALO 600
m2dcn002	M	2-D	S	CS	100	800	2	88	ALO 600
m2dcn003	M	2-D	S	CS	200	800	2	88	ALO 600
m2dcn004	M	2-D	S	CS	300	800	2	88	ALO 600
m2dcn005	M	2-D	S	CS	100	1000	2	88	ALO 600
m2dcn006	M	2-D	S	CS	100	0	2	88	ALO 600
m2dcn007	M	2-D	S	CS	100	200	2	88	ALO 600
m2dcn008	M	2-D	S	CS	100	400	2	88	ALO 600
m2dcn010	M	2-D	S	CS	100	1600	2	88	ALO 600
m2dcn011	M	2-D	S	CS	100	800	2	88	ALO 600
m2dcn012	M	2-D	S	CS	100	400	2	88	SB
m2dcn013	M	2-D	S	CS	100	0	2	88	ALO 600
m2dcn015	M	2-D	S	CS	100	800	2	88	ALO 600
m2dcn016	M	2-D	S	CS	100	800	2	88	ALO 600, 4
m2dcn017	M	2-D	S	CS	100	800	2	88	ALO 600

B.4 Cyclic 2-D under Constant Normal Load

M: Monotonic, C: Cyclic, 2-D: two-dimensional, 3-D: three-dimensional
D: Direct Shear Box, S: Simple Shear Box
CL: Constant Normal Load, CS: Constant Normal Stiffness
Sand No. 1: Crushed Silica (D_{50} = 1.2 mm)
Sand No. 2: Crushed Silica (D_{50} = 0.6 mm)
Sand No. 3: Ottawa Sand (D_{50} = 0.6 mm)
Plate Type: SB = Sand Blasted, SM = Smooth, ALO = Aluminium Oxide, ec = emery cloth
RUST: Rusted
Amp. = Total Tangential Displacement Amplitude

Test No.	M / C	2D/3D	D / S	CL/CS	σ_n (kPa)	Sand #	Dr (%)	Plate	Amp. (mm)
c2dbn102	C	2-D	D	CL	100	2	88	ALO 600	0.75
c2dbn104	C	2-D	D	CL	100	2	88	ALO 600	0.5
c2dbn105	C	2-D	D	CL	100	2	88	ALO 600	0.5
c2dsn150	C	2-D	S	CL	100	1	82	ALO 150	0.5
c2dsn151	C	2-D	S	CL	100	1	82	ALO 150	2
c2dsn152	C	2-D	S	CL	100	1	82	ALO 150	1.4
c2dsn153	C	2-D	S	CL	100	1	82	ALO 150	1
c2dsn154	C	2-D	S	CL	100	2	88	SB, 4	0.75
c2dsn155	C	2-D	S	CL	100	2	88	SB, 4	0.5
c2dsn164	C	2-D	S	CL	100	2	88	ALO 600	0.75
c2dsn166	C	2-D	S	CL	100	2	88	LO 600,	0.75
c2dsn167	C	2-D	S	CL	100	3	84	ALO 600	0.5
c2dsn168	C	2-D	S	CL	100	1	82	ALO 600	0.5
c2dsn169	C	2-D	S	CL	100	2	88	RUST	1.25
c2dsn170	C	2-D	S	CL	100	2	88	RUST, 3	1
c2dsn302	C	2-D	S	CL	300	2	88	ALO 600	0.75
c2dsn501	C	2-D	S	CL	500	2	88	ALO 600	1
c2dsn503	C	2-D	S	CL	500	2	88	SB	1
c2dsn504	C	2-D	S	CL	500	2	88	SB	1.25

B.5 Cyclic 3-D under Constant Normal Load

M: Monotonic, C: Cyclic, 2-D: two-dimensional, 3-D: three-dimensional
D: Direct Shear Box, S: Simple Shear Box
CL: Constant Normal Load, CS: Constant Normal Stiffness
Plate Type: SB = Sand Blasted, SM = Smooth, ALO = Aluminium Oxide, ec = emery cloth
RUST: Rusted
Amp(x) = Total Tangential Displacement Amplitude in the x-direction
Amp(y) = Total Tangential Displacement Amplitude in the y-direction

Test No.	M / C	2D/3D	D / S	Type	σ_n (kPa)	Plate	Amp(x) (mm)	Amp(y) (mm)	τ_y (kPa)
c3dsn153	C	3-D	S	Cons τ_y	100	ALO 600	0.75	0	20
c3dsn154	C	3-D	S	Cons τ_y	100	ALO 600	0.75	0	40
c3dsn156	C	3-D	S	Cons τ_y	100	ALO 600	0.75	0	30
c3dsn157	C	3-D	S	Cons τ_y	100	ALO 600	0.75	0	60
c3dsn158	C	3-D	S	Cons τ_y	100	ALO 600	0.5	0	30
c3dsn159	C	3-D	S	Cons τ_y	100	ALO 600	0.5	0	40
c3dsn160	C	3-D	S	Cons τ_y	100	ALO 600	0.5	0	20
c3dsn161	C	3-D	S	Rot.	100	ALO 600	0.75	0	0
c3dsn163	C	3-D	S	Rot.	100	ALO 600	0.75	0.25	0
c3dsn164	C	3-D	S	Rot.	100	ALO 600	0.75	0.5	0
c3dsn165	C	3-D	S	Rot.	100	ALO 600	0.75	0.75	0
c3dsn166	C	3-D	S	Rot.	100	ALO 600	0.5	0	0
c3dsn167	C	3-D	S	Rot.	100	ALO 600	0.5	0.2	0
c3dsn170	C	3-D	S	Rot.	100	ALO 600	0.5	0.5	0
c3dsn171	C	3-D	S	Rot.	100	ALO 600	0.6	0	0
c3dsn173	C	3-D	S	Rot.	100	SB, 3	0.75	0.75	0
c3dsn174	C	3-D	S	Rot.	100	ALO 600	0.75	0.75	0
c3dsn173	C	3-D	S	Rot.	100	SB, 3	0.75	0.75	0
c3dsn173	C	3-D	S	Rot.	100	SB, 3	0.75	0.75	0
c3dsn173	C	3-D	S	ALT	100	SB, 3	0.75	0.75	0
c3dsn173	C	3-D	S	ALT	100	SB, 3	0.75	0.75	0
c3dsn174	C	3-D	S	ALT	100	ALO 600	0.75	0.75	0
c3dsn175	C	3-D	S	ALT	100	ALO 600	0.75	0.5	0
c3dsn176	C	3-D	S	ALT	100	ALO 600	0.75	0.25	0
c3dsn177	C	3-D	S	ALT	100	SB	0.5	0.5	0
c3dsn351	C	3-D	S	Cons τ_y	300	ALO 600	1	0	60
c3dsn353	C	3-D	S	Cons τ_y	300	ALO 600	1	0	120
c3dsn551	C	3-D	S	Cons τ_y	500	SB	1	0	100

B.6 Cyclic 2-D under Constant Normal Stiffness

M: Monotonic, C: Cyclic, 2-D: two-dimensional, 3-D: three-dimensional
D: Direct Shear Box, S: Simple Shear Box
CL: Constant Normal Load, CS: Constant Normal Stiffness
Plate Type: SB = Sand Blasted, SM = Smooth, ALO = Aluminium Oxide, ec = emery cloth
RUST: Rusted

***K*: Normal Stiffness ($d\sigma_n$ / dv)**

Test No.	M / C	2D/3D	D / S	CL/CS	Type	σ_{no} (kPa)	K (kPa/mm)	Stress A. (kPa)	Dis A. (mm)	Plate
c2dcn001	C	2-D	S	CS	2-way	300	400		0.75	ALO 600
c2dcn002	C	2-D	S	CS	2-way	300	400		0.25	ALO 600
c2dcn003	C	2-D	S	CS	2-way	300	400		0.5	ALO 600
c2dcn004	C	2-D	S	CS	1-way	300	0	120-180		ALO 600
c2dcn005	C	2-D	S	CS	1-way	300	400	120-180		ALO 600
c2dcn006	C	2-D	S	CS	1-way	300	800	120-150		ALO 600
c2dcn007	C	2-D	S	CS	1-way	300	1200	120-150		ALO 600
c2dcn008	C	2-D	S	CS	2-way	300	400		0.75	SB
c2dcn009	C	2-D	S	CS	1-way	300	1200	120-150		SB
c2dcn010	C	2-D	S	CS	2-way	300	800		0.75	ALO 600
c2dcn011	C	2-D	S	CS	2-way	300	200		0.75	SB
c2dcn012	C	2-D	S	CS	2-way	300	1600		0.75	SB
c2dcn013	C	2-D	S	CS	2-way	300	400		0.75	ALO 600
c2dcn014	C	2-D	S	CS	2-way	300	400		1	RUST, 1
c2dcn012	C	2-D	S	CS	2-way	300	400		1.25	RUST, 2